DOCTOR OF PHILOSOPHY

Advanced Vehicle Electrical Power Supply System

Boulos, Alkiviadis

Award date:
2021

Awarding institution:
Coventry University

Advanced Vehicle Electrical Power Supply System

By

Alkiviadis Boulos

PhD

June 2020

Advanced Vehicle Electrical Power Supply System

By

Alkiviadis Boulos

June 2020

A thesis submitted in partial fulfilment of the University's requirements for the Degree of Doctor of Philosophy

Faculty of Engineering, Environment and Computing in collaboration with Jaguar Land Rover Limited

Certificate of Ethical Approval

Applicant:

Alkiviadis Boulos

Project Title:

Advance Vehicle Electrical Power Supply System

This is to certify that the above named applicant has completed the Coventry University Ethical Approval process and their project has been confirmed and approved as Low Risk

Date of approval:

17 June 2020

Project Reference Number:

P108448

Abstract

Jaguar Land Rover is focusing on improving fuel economy across the complete vehicle product portfolio. It has invested in new technologies to increase efficiency in all areas including weight, aerodynamics, tyres, friction, powertrain, hybridization and finally electrical systems.

This work focuses on the management of electrical energy, including comfort loads, for internal combustion engine vehicle. The aim of this work is to meet the increasing demand for electrical power and meet the customers' expectations in terms of performance whilst minimising their negative impact on fuel economy and emissions.

The experimental work with the Low Emissions Vehicle (LEV) demonstrator, initiated, designed and carried out by the author, provided the required understanding of the impact of electrical loads on fuel economy and potential mitigating effects from the use of ultracapacitors, solar panels and high efficiency alternators. The data, collected in environmental dynamometer chamber as well as on UK roads under real world conditions, were used for modelling, calibration and verification.

A statistical approach was adopted to derive, from the experimental data, a relationship between CO_2 emissions and the electrical power resulting from the alternator loading. It forms the fuel consumption index (FCI) [$g.km^{-1}.A^{-1}$].

A complete simulation tool for electrical load management was realised in MATLAB®/Simulink™. It includes batteries, alternators, ultracapacitors, solar panels and all electrical features/loads found on a high-end luxury vehicle. The validated, industry standard, model was used to evaluate a novel fuzzy logic electrical energy management control strategy.

The proposed controller exploits traditional information such as measured electrical power demand, cabin features usage, driving conditions, battery state of charge and the vehicle's system electrical stability. In addition it proposes the adoption of the FCI and a customer's 'feel factor', expressed as the customer satisfaction index to manage the trade-off between reducing fuel emission and satisfying customer demand.

The overall approach was evaluated using extensive simulation studies for a range of realistic test cases representing real world vehicle operation. It was found that the proposed controller can significantly reduce CO_2 emissions by reducing comfort loads without noticeable effect on the customer's satisfaction. Best savings were obtained by reducing the load during idling and by reducing the alternator use when the battery can meet the load demand when it operates at a high SoC.

Acknowledgements

I would like to herewith express my gratitude to all the people who have supported me during this research.

I would like to thank my supervisors Dr. Olivier Haas and Prof. Dobrila Petrovic for their continuous support, guidance and motivation that helped me to restart and complete this research.

The research undertaken in this thesis would not have been possible without a close collaboration with Jaguar Land Rover. I would like to thank all the people whose financial and technical assistance, was a milestone in the completion of this research, including the Senior Board of Electrification Department and my line managers during my professional career.

I would like to specially thank my partner Neraida Klemou for her patience, relentless support, constructive advice and kindness throughout those years of my research.

Finally, I acknowledge with a deep sense of reverence, my gratitude towards my parents Michael and Vasilia Boulou and my sisters Catherine and Johanna Boulou who have always supported me, financially and morally throughout this research journey and without whom I would never have enjoyed so many opportunities.

Contents

List of Tables

List of Figures

Nomenclature

A/C	Air Conditioning
ABS	Anti-lock Braking System
AC	Alternator Current
ACC	Li-Ion Autonomous Cruise Control
AFS	Active Front System
AGM	Absorbent Glass Matt
ANN	Artificial neural network
A-PMP	Adaptive Pontryagin's Minimum Principle
BEV	Battery Electric Vehicle
BLW	Blowers
BMS	Battery Management System
C	Cell capacitance
CAN	Controller Area Network
CC	Combined Cycle
CCA	Cold Cranking Current
COA	Centre of Area
COG	Centre of Gravity
COS	Centre of Sums
CP	Confirmation Prototype
CPE	Constant Phase Element
CPU	Central Processing Unit
CSCT	Combined Suburban and City Traffic Cycle
CSI	Customer Satisfaction Index
CT	City Traffic
Dc	Direct Current
DID	Drive-Idle-Drive
EC	Electrochemical Capacitor
ECE15	Economic Commission Europe
ECMS	Equivalent Consumption Minimisation Strategy
ECU	Electronic Control Unit
EEM	Electrical Energy Management
EEMS	Electrical Energy Management System
EHB	Electric Hydraulic Brake
EMS	Energy Management System
ENR	Engine Not Running
EPA	Environmental Protection Agency
EU	European Union
EV	Electric Vehicle
EVA	Electrical Valve Actuation
EVR	Electrical Voltage Regulation
FC	Fuel Consumption
FCI	Fuel Consumption Index
FEAD	Front End Ancillary Drive
FET	Field Effect Transistor

FLC	Fuzzy Logic Control
FOM	First of Maxima
FS	Front Seats
FTP75	Federal Test Procedure
HED	High Efficiency Diodes
HEV	Hybrid Electric Vehicle
HFS	Heated Front Screen
HMI	Human Machine Interface
HMR	Heated Mirrors
HRPSOC	High-rate Partial State of Charge
HRS	Heated Rear Screen
HVAC	Heating, ventilation and Air Conditioning
HWFET	Highway Fuel Economy Test
HWP	Heated Wiper Park
ICE	Internal Combustion Engine
ISEA	Institute of Current Rectification and Electrical Drives
ISET	Institute of Solar and Renewable Energy
ISG	Integrated Starter Generator
ISO	International Organization for Standardization
JLR	Jaguar Land Rover
KCL	Kirchhoff's Current Law
KERS	Kinetic Energy Recovery Systems
LEV	Low Emissions Vehicle
LIN	Local Interconnect Network
LOM	Last of Maxima
MF	Membership Function
MHEV	Mild Hybrid Electric Vehicle
MIT	Massachusetts Institute of Technology
MOM	Mean of Maxima
MOSFETs	Metal Oxide Semiconductor Field-Effect Transistors
MPC	Model Predictive Control
MPPT	Max Power Point Tracking device
MY	Model Year
NEDC	New European Driving Cycle
NN	Neural Networks
OCV	Open Circuit Voltage
OEM	Original Equipment Manufacturer
OPD	Optimal Power Distribution
PFLC	Predictive Fuzzy Logic Control
PHEV	Plug-In Hybrid Electric Vehicle
PI	Proportional-Integral
PMP	Pontryagin's Minimum Principle
PSO	Particle Swarm Optimisation
PTC	Positive Temperature Co-efficient
PV	Photo-Voltaic
PWM	Pulse Width Modulation
R&D	Research and Development
RAM	Random-Access Memory
RS	Rear Seats
S.A.V.E	Solar Assisted Vehicle Electrical
S/C	Supercharged
SAR	Synchronous Active Rectification
SLI	Starting Lighting and Ignition
SOC	State of Charge
SOH	State of Health
SUV	Sport utility vehicle

TSS	Tandem Solenoid Starter motor
VRLA	Valve Regulated Lead Acid
WLTP	Worldwide Harmonised Light Vehicle Test Procedure
μC	Microcontroller

Chapter 1

1.1 Introduction

When something is important enough you do it
even if the odds are not in your favour.'
Elon Musk

This chapter presents the fundamental research topic and the approach followed to address it. The aim and objectives of the research and the methodology followed are then described. Finally, the original contributions from this research and the outline of the thesis are presented.

The motivation of this research is based on two factors. A primary factor is originated from the continuous effort by the majority of automotive vehicle manufacturers to develop a range of design, system integration and control solutions for increasing the electrical energy efficiency of powertrain systems while maintaining vehicle performance and customer satisfaction. A secondary factor is based on the necessity to achieve continuously low fleet average emissions as required to meet stringent targets set by most of the countries across the world. As an example, CO_2 emissions target set by European Union by 2021 is at $95gr.km^{-1}$ (Council of European Union, European Parliament, 2014). The majority of automotive stakeholders are aware that actions focusing solely on enhancing the efficiency of the Integral Combustion Engine (ICE) will not be sufficient. Additional measures on a vehicle level are necessary to meet such low emission targets as proposed by EU. To satisfy both challenges, vehicle system electrification has gained the interest of the automotive industry. Electrical energy used by automobiles have been rapidly increased by either the replacement of traditional mechanical systems into electrical more efficient ones, as well as by the increase of electrical comfort cabin features that luxury automotive manufacturers offer within their product portfolio. Electrical energy efficiency is no longer an option, but a prerequisite when defining and developing new automobiles, in the form of either traditional 12V ICE vehicle architectures or non-conventional such as full Battery Electric Vehicle (BEVs), Plug-in Hybrid Electric Vehicles (PHEVs) or Mild Hybrid Electric Vehicles (MHEVs).

Most of the automotive electrical power supply systems are sized for the ultimate load conditions and not necessarily optimised for the region of power consumption which the vehicle will spend for the majority of its operational life. The key factor here is the balance between the appropriate energy consumption within the vehicle while achieving customer attribute performance on all levels including driveability, comfort, convenience, safety and fuel economy. The latter is one of the most important key attributes which every vehicle manufacturer has focused to achieve through continuous technology improvement.

The research addressed in this thesis is focused on the impact of electrical energy to the vehicle's overall fuel consumption levels. This includes the development of a control strategy which by monitoring and altering vehicle's electrical energy consumption levels, based on certain design criteria, achieves high fuel economy levels on typical commuting driving cycles. Although this research is focused on conventional (non-electrified) ICE vehicles typically fitted with an alternator or an electric motor acting as the main power generation device, it is also applicable to non-conventional vehicles (i.e. BEV, PHEV) with 12V electrical systems incorporated as part of the vehicle's overall electrical power supply system.

Despite certain improvements made in modern vehicles and the hybridization of more conventional configurations, a significant amount of energy is still wasted due to the lack of overall onboard electrical energy management strategies which could minimise the impact of electrical energy usage on the overall efficiency of the automobile. Furthermore, electrification of auxiliary systems promises energy efficiency gains but there is an additional need for a coordinated approach to the electrical power generation, energy distribution, use and storage of energy (Beher et al. 2009; Koklj et al. 2013; Asada et al. 2008). The collaborating company has also shifted its focus on fuel efficiency and economy across the whole vehicle product portfolio. It has been recognised that the company has invested heavily in technologies to increase efficiency in all areas including weight, aerodynamics, tyres, friction, powertrain, hybridization and finally electrical systems. Two key areas, electrical system efficiency and parasitic electrical loading have been extensively investigated as main contributors with a significant impact on fuel consumption for traditional ICE vehicles.

During vehicle operation, the electrical system supplies the electrical power required for multiple operating subsystems, components and actuators including lighting, infotainment, heated glazing, climatic seats, cabin blowers, engine cooling fans and other supporting vehicle's primary and engine functions. The ancillary loads of the vehicle represent a considerable source of energy dissipation. Existing methodologies to manage the energy consumption of the vehicle electrical loads have been investigated as a direction towards vehicle fuel economy (Silva et al. 2009; Chiara et al. 2013; Lyu et al. 2007, Couch et al. 2013). Ancillary load reduction including optimisations of the alternator and a reduction of the front-end accessory drive systems have been explored and discussed in Xu et al. (2004)

and Macka (2013). Additional contributions have been proposed on the electrical energy analysis of vehicle's auxiliary loads by Rumbolz et al. (2011).

In particular, as concluded by Rumbolz et al. (2011), fuel energy used by auxiliary electrical loading was estimated at 8% from a wide range of vehicle fleet. Experimental studies analysed the impact of parasitic loading on the fuel economy with reference to a hybrid electric bus by (Campbell et al. 2011; Muncrief et al. 2012). Pang et al. (2004), focused on the power consumption related to the cooling system as electric cooling fans power wattage levels reach up to 1.5kW, a considerable high-power electrical load which is applicable on both conventional ICE and non-conventional xEV vehicle configurations. However, the real effects of electrical energy and the contribution of it to an ICE vehicle's real-world fuel consumption levels have not been fully quantified up to date.

There has been several studies and developments in the area of vehicle energy management techniques and control strategies aiming to optimise energy usage and power distribution as well as improve fuel economy and emissions. In particular, Kessels et al. (2004) and (2007), conducted simulation studies as part of an overall energy management strategy. The developed control strategy included battery, alternator, electrical loading models correlated under particular CO_2 driving cycles. Based on optimisation techniques an optimal offline as well as a causal online strategy was proposed. Other approaches (Eymman et al. 2011; Williams et al. 2011), presented a holistic implementation of a vehicle energy management strategy focused on recuperation, minimising energy loss and monitoring energy flow for the entire vehicle architecture network system. In Monalto et al. (2015), smart alternator control strategy was deployed to improve CO_2 emissions. This was realised by reducing alternator duty cycle depending on battery and driving conditions. Additional studies in Wang et al. (2015) followed similar energy management approach by controlling the output power of the battery and the alternator within a battery state of charge range depending on driving conditions

Based on (Zhang et al. 2016; Saleh et al. 2015; Haifeng et al. 2015), artificial intelligence control approaches can be classified in three categories. First, rule based control is based on human knowledge and expertise using mathematical and heuristic information. It is convenient to adopt in industry due to existing in depth systems knowledge. Second, fuzzy logic based control, offers a robust approach and structure, can handle nonlinearities and gives flexibility to the controller to deal with nonlinear problems such as managing power from different sources of controller. Third, Neuro-fuzzy, a combination of fuzzy logic and Artificial Neuro-fuzzy control enables to add online adaption and some predictive elements to fuzzy logic. Fuzzy logic based controllers have been used to optimise energy management estimators on hybrid vehicles and manage feed energy flow between battery and supercapacitor. Currently hybrid electric vehicles are at the epicentre of research and development in fuzzy logic systems. Early research has introduced fuzzy logic energy management control strategies for electric vehicles responsible for efficient powertrain control Cerruto et al. (1994) while a more recent studies in

Kheir et al. (2015) developed a generalised fuzzy logic controller (FLC) to optimise fuel economy and reduce emissions on a parallel hybrid configuration.

FLC schemes are used lately in automotive applications as become popular for on-line vehicle implementation. A possibility to overcome complex nonlinear models by using intuitive rules makes FLC and fuzzy identification procedures user friendly tools by rapid system prototyping. FLC can efficiently handle real time applications with its pre-emptive control under strong presence of data and model uncertainty (Ivanov 2015).

Therefore, the work presented in this thesis is proposing a Fuzzy Logic Control strategy as a practical solution to improve vehicle's fuel consumption and emissions while preserving customer convenience and comfort within the cabin. It considers both static and dynamic behaviours and adapts to the vehicle condition (on operation, locked, armed or standstill). Key design criteria include: i) electrical loading demand, ii) customer satisfaction index, iii) available electrical power and energy generation sources, iv) battery conditions (i.e. state of charge levels) and v) vehicle driving conditions.

Whilst many electrical energy management strategies have been investigated, these are generally evaluated on short simulation that do not always consider dynamic response (Qiao et al., 2016) or on a limited number of driving cycles (see Chapter 2, section 2.6) It is the author's belief that real world driving assessment and performance are essential to fully evaluate electrical management system. An experimental approach is therefore proposed in this thesis to provide greater understanding and critical analysis of the impact of electrical energy to the overall real world fuel consumption of a vehicle. Extensive vehicle testing was carried out to evaluate the impact of auxiliary electrical loading associated with vehicle subsystems on the vehicle's overall fuel consumption. The investigation was conducted using environmental dynamometer chambers, including both types of vehicles (i.e. saloons and SUVs) under a proposed experimental driving cycle. In addition to the dynamometer chamber vehicle testing, real world measurements were conducted under typical commuting driving cycle scenarios and fuel consumption measurements were analysed under various customer electrical loading scenarios (i.e. selecting multiple cabin/comfort electrical features during testing). A unique feature of this research is therefore the large amount of data collected to both validate the developed models and controllers but also to critically analyse the proposed solution under realistic conditions.

1.2 Research Questions

Having introduced the topic and the motivation of this research as described in Section 1.1, the research questions of this study are now defined as follows:

1. Will electrification have an impact on energy losses and electrical systems' efficiency?
2. Can alternative cost effective technologies be used on conventional ICE vehicles to increase energy efficiency, recuperation and regeneration?
3. Does electrical energy consumption affect a vehicle's fuel consumption and emissions? Can this effect be experimentally derived and expressed as a mathematical relationship?
4. Can an integrated software-based solution reduce energy usage and result in fuel economy for conventional vehicles and increase the range for hybrid powertrain configurations?

1.3 Aim and objectives

The overall aim of this work is to develop an Electrical Energy Management strategy that controls the operation of vehicle's electrical comfort features in order to minimise the effect on fuel consumption under various vehicle real world operating conditions. The developed electrical energy management strategy is based on Fuzzy Logic. To achieve this aim, several key objectives were addressed:

- Review existing Electrical Energy Management concepts, identify requirements, assumptions and approaches which could be used to design, formulate and implement a Fuzzy Logic Control (FLC) for the purpose of the work addressed in this thesis.
- Use vehicle prototype (Low Emissions Vehicle Demonstrator (LEV)) to gather data for the modelling phase and deduce a relationship between electrical load and fuel consumption.
- Develop and validate simulation models of an electrical power supply system against experimentally measured data for different loading profiles and drive cycles. The model calibration and validation provided confidence in exploiting the model for the control strategy development.
- Design, formulate, implement and demonstrate the effectiveness of the proposed FLC.
    - Develop an Electrical Energy Management exploiting the validated model to form a complete simulation suite
    - Implement Fuzzy Logic Control strategies including predictive concepts
    - Integrate the complete FLC into MATLAB®/Simulink™ environment. Assess the performance of the proposed Electrical Energy Management strategy to vehicle's overall fuel emissions.

1.3 Research methodology

The overall objective of the research is to develop a methodology to reduce the impact of electrical energy towards fuel consumption, usually translated as $gr.km^{-1}$ for ICE vehicles or mileage range for Battery Electrical vehicles (BEV). The approach adopted is to develop a non-linear model of a vehicle's typical power supply system including all main components such as battery model, alternator model and all related electrical features used by customers. In addition, a supercapacitor and a PV solar panel were added to the overall simulation platform to enhance the capability of the overall charging system. The model was validated against a range of experimental data as obtained from actual measurements from various testing activities including prototype vehicle testing and virtual simulations. This original and fully validated simulation tool was then used for model-based control system design. Subsequently, an experimental method was developed to model the effect of electrical energy on a vehicle's overall fuel consumption and emissions. This testing method involved actual vehicle testing using environmental dynamic chambers as well as data collected from real world driving based on a typical commuter route. Statistical analysis was then conducted based on the population data collected, helping to relate fuel consumption and electrical energy in a simple interpretation of fuel emissions achieved vs electrical energy usage pattern. Finally, using this experimentally developed relationship, the Fuzzy Logic Control based Electrical Energy Management System (FLC EEMS) was realised and linked to the overall MATLAB®/Simulink™ model. An evaluation and a comparative analysis were conducted using simulation scenarios based on realistic customer use cases and typical driving scenarios.

1.4 Contributions

The overall study carried out during this project has led to several contributions and adaptations of pre-existing approaches.

- **Design and implementation of FLC EEMS:** Previous FLC based energy management strategies (Kheir et al. 2004; Zhou et al. 2011; Lu et al. 2012; Tareq et al. 2015) mainly regulated the operation of vehicle's power supply system under certain operating modes without customer interaction. The proposed Fuzzy Logic Control based Electrical Energy Management System (EEMS) originality stems from both the introduction of the customer satisfaction index (CSI) and the fuel consumption index (FCI) to deliver a customer-selected trade-off between the comfort level within the cabin and fuel economy.

- **FLC based alternator strategy:** The aim of an alternator is to support electrical load demand during vehicle operation. In the past, several methodologies have been developed to benefit fuel economy by applying electrical power balancing techniques (Swanand et al. 2014) or balancing recuperation under specific driving cycles (Brabetz et al. 2009; Lakshminarasimhan et al. 2013). By contrast, in this thesis, the alternator's operation is regulated by taking into consideration the battery's charging levels as well as the vehicle's mode of operation. This increases efficiency, as it limits charging operation on high battery SoC levels to improve aging, reduce heat losses, whilst reducing fuel consumption.

- **Experimental analysis of the effect of electrical energy upon vehicle's fuel consumption and emissions:** Several studies have introduced different electrical energy recuperation schemes to benefit fuel economy and assessed them on a test-bench basis or using specific emission driving cycles (i.e. FTP, NEDC, Artemis) (Brabetz et al. (2009); Lakshminarasimhan et al. 2013; Noyori et al. 2013; Yun et al. 2015). In this thesis, extensive vehicle testing was carried out to evaluate the impact of different alternator electrical loading levels on vehicle fuel consumption. A critical statistical analysis of the recorded data was conducted to formulate the relationship between electrical energy and fuel emissions into $g.km^{-1}A^{-1}$. The approach obtained is incorporated into the developed FLC EEMS as the fuel consumption index.

- **Low Emissions Vehicle Project (LEV):** A novel aspect of this work is the significant amount of experimental work conducted and critically evaluated by the author under the LEV project. This provided an ideal real world vehicle platform to evaluate innovative technologies such as high efficient alternators, ultracapacitors and solar panels connected to an existing power supply system configuration. Several learnings of this project were incorporated into the developed system-level simulation models whilst experimental data were used to validate the model.

- **Fully validated power supply system simulation model implemented in MATLAB®/Simulink™:** The contribution of the author is the development and integration of several developed simulation models into a system-level design approach. The developed simulation platform included a battery model, an alternator model, an ultracapacitor model, a solar panel model and several electrical features/loads as part of the vehicle's electrical systems. Rigorous validation of the power supply system model was done by subjecting it to specified loads and environments via different driving cycles. A good correlation between real systems and simulation models was achieved using experimental data from various vehicle tests.

1.5 Outline of thesis

Having introduced the research theme, aims, objectives and the methodology followed, this section presents the remainder of the thesis structure. Figure 1 presents in a structural flow diagram the Ph.D. thesis structure:

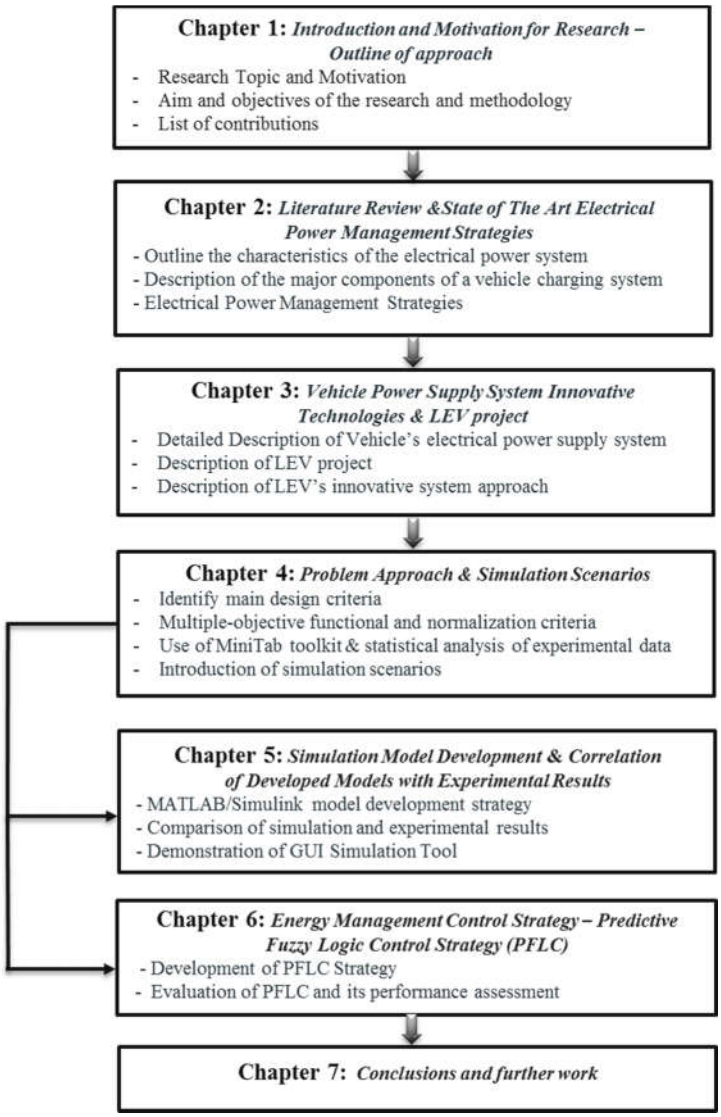

Figure 1.1. Logical Flow representation of thesis development

The remainder of this thesis is structured as follows.

Chapter 2: *Literature Review & State of The Art Electrical Power Management Techniques*

This chapter starts with the literature review of vehicle's electrical systems and simulation techniques with regards batteries and power electronics including alternators, batteries, DcDc converters, ultracapacitors and automotive solar panels. In addition, the chapter includes i) a review of

vehicle electrical power management strategies, (i.e. including battery management control strategies: thermal, SoC), ii) a review of modelling techniques and different approaches to assessing the impact of electrical energy on vehicle's emissions, iii) a review of control approaches for vehicle electrical power management techniques and finally iv) a review statistical approaches to quantify the effect of electrical energy to vehicle's fuel emissions. The literature review has resulted in the identification of some research gaps and a justification of the approach adopted in this work.

Chapter 3: Vehicle Power Supply System Innovative technologies & Low Emissions Vehicle (LEV) project

Chapter 3 provides a description of detailed understanding of the characteristics of the electrical power system; load demands and power generation capacities of vehicle's alternator and battery size are determined for a vehicle. The potential for ultracapacitors and automotive solar panels was investigated as part of the Low Emissions Vehicle (LEV) JLR project. The project has been led and managed by the author as a new proposed approach to investigate innovative technologies that could be implemented in existing ICE vehicles and help to reduce fuel consumption and vehicle's emissions. LEV's vehicle power supply topology consists of the basis of our simulation approach as used by Chapters 5 and 6.

Chapter 4: Problem Approach & Simulation Scenarios

The research problem highlighted in Chapter 3 is formulated and discussed in detail in Chapter 4. Chapter 4 includes an investigation and analysis made to measure the impact of electrical energy (i.e. alternator loading) on the vehicle's overall fuel consumption in $g.km^{-1}.A^{-1}$. An understanding of the impact of different alternator electrical loading levels associated with vehicle subsystems towards fuel consumption has been measured and analysed against certain design criteria. Using the Minitab tool a variability analysis of electrical loading, alternator toque, fuel flow rate and consumption has been conducted using the standard deviation method and statistically quantifies the effect of electrical energy on the overall vehicle fuel emissions.

In addition, this chapter identifies the main design criteria and weighing factors that need to be controlled and formulated to minimise the impact of electrical energy on a vehicle's fuel consumption. Speed profiles of two legislative drive cycles, real world driving cycles and annual solar activity were analysed to identify simulation scenarios and test cases for the simulation studies reported in Chapter 5 and Chapter 6.

Chapter 5: Simulation Model Development & Correlation of Developed Models with Experimental Results

Chapter 5 includes the overall simulation strategy and its correlation with experimental data. First, the complete vehicle power supply plant modelling is demonstrated. The simulation model includes the

development of a lead-acid battery model, an alternator model and two types of Ultracapacitors models to enhance the performance of the overall charging system and the life-cycle of a lead-acid battery. In addition, the overall developed simulation model included a solar panel representation. Secondly, it describes the method of collecting experimental data from vehicle tests and using the data to evaluate the candidate simulation system. Simulink connections and the conversion of experimental data for use in MATLAB®/Simulink™ are explained. The simulation studies combine the developed models and engineering knowledge to create a realistic vehicle charging system. Parameters such as battery currents and voltage, alternator current outputs, ultracapacitor voltage and currents, battery electrolyte temperature and state of charge rates have been compared and analysed with experimental data, analysed and the absolute error values have been calculated demonstrating the overall validity of the simulation platform.

Chapter 6: Electrical Energy Management System – Fuzzy Logic Control based strategy

Chapter 6 includes the implementation of the energy management control strategy into the developed overall simulation model in MATLAB®/Simulink™. The implemented Simulink model in Chapter 5 is merged with the FLC into a single simulation model. The overall developed control strategy is evaluated against simulation scenarios discussed and presented in Chapter 4. Finally, using the developed FLC scheme, it is shown how to adjust certain trades-off/criteria between electrical energy consumption and fulfillment of the overall low fuel consumption

Chapter 7: Conclusions and Further Work

Chapter 7 contains research conclusions, key contributions made and areas of further work are suggested.

Chapter 2

Literature review

2.1 Introduction

This chapter reviews conventional[1] automotive electrical power supply system topologies and related automotive Electrical Energy Management strategies. The literature review is focused on methodologies that improve vehicle's electrical energy efficiency and therefore fuel consumption and emissions, which constitute a basis of this research. The review of the control strategies adopted in the literature is focused on *'electrical energy efficiency'*, *'recuperation'* and *'fuel economy'*. All of these fields have extensive literature and wide application coverage, including non-conventional vehicle powertrains such as Mild Hybrid Electric Vehicles (MHEVs), Plug-In Hybrid Electric Vehicles (PHEVs) and Battery Electric Vehicle (BEVs). These three fields are considered as they constitute target applications of this research.

This chapter is organised as follows; Section 2.2 reviews the means to improve vehicle efficiency with consideration given to the range of conventional, hybrid and electric powertrains available today. Section 2.3 reviews Energy Recuperation and Regeneration as a solution to increase fuel economy and the efficiency of all types of electrical vehicles. Section 2.4 presents the electrical load requirements that need to be satisfied as well as associated losses and how they affect fuel economy and range. Section 2.5 reviews the different modelling approaches adopted to model automotive electrical systems including energy storage and harvesting. This section is used to justify the modelling approaches adopted in Chapter 5. Section 2.6 reviews the electrical energy management strategies that led to the selection of fuzzy logic for the solution proposed in this thesis.

[1] conventional electrical power supply configurations defined as non-hybrid ICE configurations

2.2 Electrical energy efficiency

The primary objective when designing an energy-efficient vehicle system is to minimise energy losses. However, the efficiency of the vehicle and its energy consumption over particular driving conditions (i.e. over a specified driving cycle) is a result of many different factors including i) the appropriate selection of power supply components for a specific vehicle powertrain application; ii) the use of energy recovery/recuperation strategies integrated as part of vehicle's energy recovery capability; iii) the efficient operation of electrified auxiliary loads during a vehicle's stop/start and on move conditions; iv) the effectiveness of energy management and power control strategies to minimise the impact of electrical energy usage to the vehicle's fuel consumption on ICE configuration and EV range on BEV configurations, and finally, v) driver's driving patterns as the effectiveness of energy consumption of the vehicle over a designated time is often limited by the performance of the driver (Liu et al. 2016).

With a continuous increase in vehicle functions for functional safety, comfort and fuel economy, future automobiles will consume more electrical power. Continuous electrification of auxiliary vehicle systems offers energy and efficiency benefits however there is still a need for a coordinated approach to the generation, distribution and use of energy. To efficiently meet this demand, higher voltage systems or improving existing electrical system efficiencies are considered during the design process of today's automobile. Higher voltage systems are introduced with the development of MHEVs, PHEVs and BEVs. Figure 2.1 illustrates a volume prediction of vehicles with electrified powertrain by 2025 (Jean-Luc Mate, 2013).

Figure 2.1. Powertrain 2025 – Prediction of global electrified powertrain
(source: Jean-Luc Mate, VP Continental Engineering Services France)

During the 90s, various Research and Development (R&D) centres of major automotive companies started evaluating the advantages of higher-voltage systems. MIT in USA, was the primary R&D centre

for Mercedes Benz developing new electrical systems. Part of this research was the investigation of new voltage level to increase fuel efficiency. A working group of automotive OEMs and suppliers, in total 7 companies, met regularly on a yearly basis to discuss issues of efficiency, safety, reliability and transition costs. This effort initiated the development of the 42-volt consortium group, a forum expanded to 34 companies with the responsibility of redefining engineering recommendations and turning them into ISO standards (da Silva et al. 2002). 42-volt was chosen to meet new automotive requirements of high power consumption levels (i.e. well over 1.5kW) and increased electrical loading demand from various 'x-by-wire' technologies such as ride control, brake-by-wire, steer-by-wire active suspension, electromagnetic valve actuation and stop-start technologies. The effects of such electrical loads implemented on 42-volt or 12-volt/42-volt dual voltage configurations and the benefits gained by improving fuel economy, reducing emissions, increasing system performance and safety were explored and quantified by Lukic et al. (2003). However, the automotive industry was skeptical regarding the technology, the reason being more economic than technological (Keim 2004; Stence 2004). The 42-volt debate was replaced with the 48-volt which took off in 2011. 48-volt onboard power supply systems now supplement existing 12-volt power supply systems rather than replace them. The opportunity to develop stop-start systems using 48-volt increased dramatically vehicle's fuel economy potentials with remarkable recuperation, boost and coast features. The new 48-volt voltage level is currently defined as an intermediate step towards electrical energy efficiency, reduction of CO_2 emissions and ability of increased recuperation compared to a conventional 12V, thus resulting in a potential cost-effective fuel-saving enabler (German J. 2015; Romanato et al. 2018; Bao et al. 2017; Tate et al. 2009).

MHEV powertrain configurations are usually realised as 12-volt/48-volt dual voltage power supply system configurations. Details on a typical MHEV configuration as having recently been developed from various OEMs can be found in Appendix B, section B.2. Jaguar Land Rover recently announced the development of a 48-volt powertrain configuration to enable fuel economy and achieve reduced CO_2 emissions across all vehicle models. Figure 2.2 illustrates Range Rover Evoque's newly developed 12-volt/48-volt MHEV system:

Figure 2.2. New Range Rover's 12-volt/48-volt system vehicle topology (source:https://www.autocar.co.uk/car-news/new-cars/radical-jaguar-saloon-plotted-ev-shake)

Even though 48V systems will progressively consist of the main electrical system of a vehicle, 12V conventional bus will continue to power most of the electrical systems of the vehicles including ignition, lighting, cabin comfort features, infotainment and audio systems. Despite multiple improvements incorporated in today's vehicles, a considerable amount of energy wastage is still evident due to the lack of an online energy management strategy therefore significantly impacting electrical efficiency and fuel economy respectively.

PHEV and BEV are other forms of hybridization that most automotive OEMs have adopted and developed within their complete product range. With the development of advanced battery technologies, the energy storage capacity of batteries has significantly improved (Masjosthusmann et al 2013). The increased electrification of propulsion and auxiliary mechanical systems with optimised operation promises high energy efficiency gains. This can be achieved by optimising and adapting energy generation and distribution to vehicle's driving conditions and power demands on a continuous basis. Details of all hybrid configurations used currently by automotive manufacturers can be found in Appendix B.

2.3 Energy recuperation & regeneration

Energy recovery is one of the key elements in modern vehicles that allows for increased fuel economy and high electrical system efficiency. The primary objective when designing an energy-efficient system is to minimise energy losses. However, in real world driving scenarios, the reduction of energy losses is not the sole objective that needs to be satisfied. Energy harvesting and recuperation is another objective that contributes to fuel economy. A good balance of recuperated energy and the

consumed energy by a vehicle's electrical system can improve fuel economy at minimal additional cost (Yun et al. 2015).

Regeneration can be achieved in multiple ways depending on vehicle electrical system architecture. For hybrid vehicles including MHEV, PHEV and BEV applications, energy recuperation is dependent on the power of the traction motor and the capacity of the main energy storage device they use. Regenerative braking and Kinetic Energy Recovery Systems (KERS) both offer high energy recuperation and are widely used in the automotive industry (Moro et al. 2010).

Regenerative braking uses the vehicle's electric motor as a generator to convert much of the kinetic energy lost when decelerating back into electric energy in the vehicle's energy storage device. When the vehicle accelerates, it uses much of the energy previously stored from regenerative braking instead of using its energy reserves. Regenerative braking has been extensively studied in the literature, by Yeo et al. (2004); von Albrichsfeld et al. (2009); Zhou et al. (2011); Koecher et al. (2012); Rask et al. (2013); Lu et al. (2014).

KERS, electrical or mechanical, are systems used most in Formula 1 sector to improve energy efficiency by recovering vehicles kinetic when the vehicle decelerates into electrical energy which is stored into an energy storage device such as a battery or supercapacitor. KERS systems advantages include high efficiency, low fuel consumption, and low cost compared to electric hybrids (Cross et al. 2008; Barr et al. 2008; Cross et al. 2009; Moro et al. 2010; Matthews et al. 2013). Conventional powertrain configurations have seen significant developments that could contribute to energy recuperation and regeneration. Recuperation control algorithms have been developed based on the conventional alternator and battery systems to recuperate brake energy to supply the vehicle's electrical loading.

Asada et al. (2008), demonstrated a charging management system with regeneration control to improve efficiency and fuel economy. The proposed regeneration control strategy monitored battery's State of Charge (SoC) levels and control charging by calculating both voltage and current. The developed algorithm includes a vehicle motion estimator which calculates and judges the vehicle motion by alternator speed and detects vehicle motion. The charging voltage control strategy sends the target voltage set-point to the alternator thus controlling the regenerating power in the battery based on vehicle motion conditions. During the acceleration phase, it minimises the voltage set-point to reduce the alternator drag torque but maintaining appropriate SoC levels. During vehicle deceleration, it increases the alternator output. The developed charging management system improved a passenger car's fuel economy over the EU driving cycle (i.e. NEDC) by 1%. This was possible without significant changes to the vehicle's powertrain configuration.

Brabetz et al. (2009), proposed a voltage-controlled alternator in combination with a battery, supercapacitors and a corresponding energy management system. The corresponding energy

management strategy took into account driving conditions during a particular cycle, the electrical power consumption of the vehicle and the thermal characteristics of the alternator to maximise recuperated power and minimise the impact on the battery's lifecycle. However, the approach and the development of this study were only being demonstrated against a particular driving emission cycle (i.e. FTP-75). The experiment and installation were based on a test bench set up with real world benefits planned for future study.

To estimate the improvement of fuel economy of the vehicle by recuperation system, Lakshminarasimhan et al. (2013) studied an intelligent alternator control mechanism for energy recuperation by using a new battery sensor attached to the battery tab. Based on this study, the improvement due to the developed algorithm on the fuel economy was between 3% and 7% depending on the driving cycle.

Noyori et al. (2013), proposed a dual battery system with a combination of a Li-Ion and a lead-acid battery in parallel for an idling start-stop application while using regenerative braking energy to maximise fuel economy and increase fuel efficiency for the K-car Japanese vehicle category. The proposed system incorporated two Metal Oxide Semiconductor Field-Effect Transistors (MOSFETs) to switch between the two energy storage devices or connect them both based on the vehicle's operation modes (i.e. acceleration, deceleration). The developed regenerative braking control strategy was assessed against the JC08 driving cycle, a test cycle in Japan to measure tail-pipe emissions and fuel economy. The results showed that the new strategy could store 110% of the energy into both batteries during deceleration whilst the original configuration (i.e. only lead-acid battery) could recover 55% with the energy shortage required to be met by the alternator thus resulting in increased fuel consumption. However, adding another battery to an existing configuration adds weight, cost and complexity. In addition, the capability of this recuperation system is yet to be proven under real world driving conditions.

Yun et al. (2015), presented a design optimization process of the alternator and battery system equipped with recuperation control algorithms for a mid-sized sedan based on the fuel economy and system cost. The experimental study included recuperation systems with flooded lead-acid, Absorbent Glass Matt (AGM), and Li-Ion batteries. Different design optimization processes were presented depending on the battery types and system architectures. The results showed that 100% of the energy consumption of electric loads can be supplied by energy recuperation over the FTP75 driving cycle with a suitable alternator and battery system using a recuperation algorithm. A total of 4.3% of fuel economy improvement was reported compared to base alternator configurations without recuperation control algorithms. However, the study was limited to the FTP75 driving cycle with no further assessment of the proposed strategy under real world driving conditions.

Energy harvesting and generation can also be achieved by solar activity via a solar panel or cell. In Sonchal et al. (2012), a solar panel has been integrated on a roof of a popular hatchback. The study demonstrated a solar-assisted vehicle electrical system (S.A.V.E) consisted of a microcontroller that senses the instantaneous electrical loading and based on a developed algorithm controlled alternator's operation thus improving CO_2 emissions by a declared of 6% improvement in vehicle fuel efficiency. The developed concept has been proved out in real world driving under city traffic conditions. This approach has been considered by the authors due to its integration simplicity of modifying an existing vehicle system architecture by adding a Photovoltaic (PV) panel and controlling alternator excitation field output via software algorithm. This approach avoids adding complexity to the Front End Ancillary Drive (FEAD) system by either using an electromagnetic clutch or switching relays at its main feed.

Several Automotive OEMs have reported using onboard PV panels in their vehicles. Toyota with its Prius HEV 2012 reported using about a 67 W solar panel to operate an active cabin ventilation system (Abdelhamid et al. 2018). Another example is Prius Prime PHEV 2017 which also reported using a 180W solar panel to support extended electric driving range. Nissan with its model Leaf (BEV) reported using a small solar panel located at the rear spoiler to help charge the 12 V battery (Abdelhamid et al. 2018). In addition, the luxury hybrid sports car Fisker Karma also reported using a solar roof from Asola Technologies to power various interior accessories. Jaguar Land Rover competitors, Audi and Lexus appear to offer solar panels in the foreseeable future. Audi has been offering solar roof variants for over 20 years and as such have sunk investment costs. There is no specific intelligence that suggests that Lexus will offer a solar roof option, but this is noted as a possibility as they could carry the technology over from the Toyota Prius (Latimer 2012).

The PV panels can provide energy to all vehicles via an onboard method. In the onboard applications, PV modules are vehicle integrated either to assist in propulsion or to run a specific vehicle application. An internal investigation within the collaborative company had also investigated the potential benefits of such technology (Latimer 2012). The solar panel integration research project (JLR1509) was initiated to respond to a perceived increasing demand from Consumers for innovative and 'green' technologies. A business case was conducted across vehicle programme lines to study the potential of integrating solar panels on certain Range Rover vehicles. Concepts considered were to use the energy provided by the solar panel for (i) running the HVAC blower when the vehicle is stationery and shutdown, (ii) charging the 12V battery, and (iii) providing an additional cigar lighter socket. The chosen concept was to run the HVAC blower and to provide a contribution to battery charging. However due to various reasons such as perceived benefit for the customer, take rate on selected models, substantial loss of transparency on panoramic roofs and its potential loss of profit through substitution if PV panels fitted, the project was placed on hold as all facts led to the conclusion not to pursue or investigate further the implementation of PV panels to the top of the range SUV vehicles.

The interest in solar panels and their use on automotive vehicles however continue to increase. Asola Technologies announced the development of integrated semi-transparent solar panels that could be fitted on a panoramic roof of a vehicle, therefore providing both the benefits of a panoramic view and a solar panel that could provide additional energy to the vehicle's electrical system. Kia Motors and Hyundai Motor have also announced plans to introduce solar panels to the roof or bonnet of selected internal combustion, hybrid and battery electric vehicles, increasing fuel efficiency and range. The technology will involve a semi-transparent solar roof that will be applied to traditional petrol and diesel vehicles, replacing a traditional panoramic sunroof.

The proposed approach in this thesis is to use such technology to complement vehicle's power and energy generation while in parallel reduce the impact of alternator loading on vehicle's fuel consumption levels. Integrating a PV panel as part of the supervisory energy management strategy should fulfill the following requirements:

Requirement	Rationale
Battery fully charged during vehicle operation	With the vehicle switched on, and the battery fully charged, the alternator will be switched off to maximise fuel economy, therefore the electrical features of the vehicle will be supported by the main battery and the solar panel. Solar panel will contribute to this support, prolong the period of time the alternator is deactivated.
Battery partially charged during vehicle operation	With the vehicle switched on, the electrical system requires current that is generated by the engine via the alternator. The solar panel can supply part of it therefore reduce alternator load applied to the engine.
Battery charged during park (sleep mode[2])	With the vehicle switched off, and most of the electrical systems on sleep mode, quiescent current drain continuously discharging the main battery of the vehicle.
Comfort features/loads activation during park (sleep mode)	With the vehicle switched off, the solar panel is used to activate some features offered such as preconditioning vehicle's cabin. This feature allows the operation of the blowers to circulate fresh air in hot ambient conditions or use the vehicle's fuel to heat engine coolant (via fuel-burning heater) and circulate hot air to warm up the cabin. The added benefit is that the solar panel's capability could be used to provide the complete feature without using the main battery.

Table 2.1. List of PV panel functional requirements

[2] Sleep mode is defined as vehicle's lowest energy consumption mode

2.4 Electrical power demand and losses

The demand for electric power consistently increases as the number of electric components in the ICE and xEV vehicles grow. The discussed powertrain configurations take all power for operating low-voltage electronic hardware from a high voltage input. The electrical power is generated with very little knowledge or control of the actual loads in conventional and even those regarded as state of the art vehicles. Most traditional ICE vehicles utilize 12V battery systems which require 14V charging systems to maintain the system in good working order. Recently such systems have experienced increased demands from new power consumers (e.g. mechanical loads that have become electrically driven, comfort related loads, future x-by-wire safety systems).

In general, the energy required for auxiliary systems (i.e. lighting, electrical actuation, heated glazing, heated seating) is generated and consumed continuously, regardless of the actual demand. Since many electrical and electronic systems are continuously added to a vehicle to meet various regulations and customer demands over the last decade, the demand for electrical power has been substantially increased. Figure 2.3 illustrates the energy flow on traditional ICE configurations in comparison to full electrical vehicle configurations:

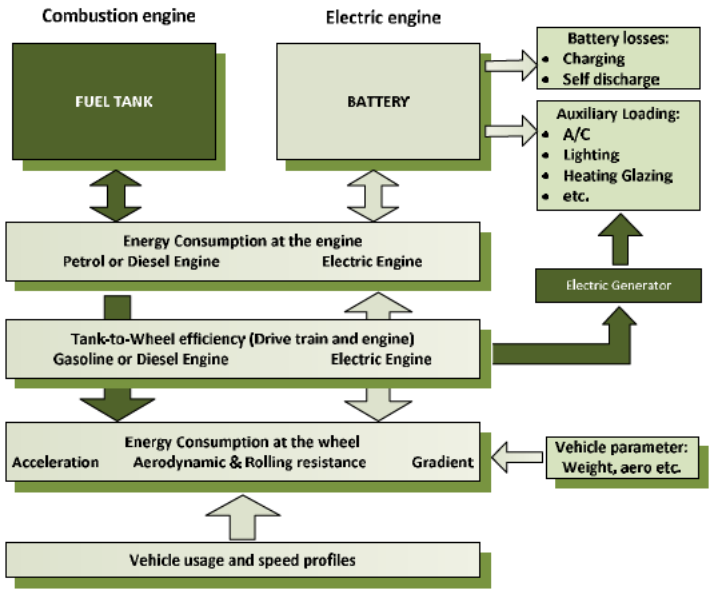

Figure 2.3. Energy flow comparison between ICE and full electric drivetrain concepts

In ICE vehicles, the power flow in the vehicle starts with the fuel that enters the combustion engine. An alternator is mechanically attached to the engine and rotates with a crankshaft by a pulley. The alternator generates electric energy through rotational motion of the crankshaft. In this process, the operation of the alternator affects the operating point of the engine (Bosch 2013). In effect, this causes

an increase in fuel consumption when supplying the electric energy for electric power systems. In addition, driver usage and driving cycle profiles also contribute to the overall energy flow of a vehicle.

A breakdown of the energy losses on various vehicle configurations has been presented in section 2.1. Figure 2.4 illustrates typical energy losses based on ICE configurations including engine losses, T
hi
vetrain losses, auxiliary electrical losses, parasitic losses and finally power to wheel losses:

Figure 2.4. Typical energy losses in an ICE configuration on a combined cycle (source: U.S Department of Energy, JLR vehicle used for reference only)

The energy loss percentage breakdown illustrated in Figure 2.4 with regards to the losses which occur from each part of the vehicle is subject to the type of the vehicle and its selected powertrain (source: EPA). As illustrated in Figure 2.4, electrical losses reach 4% - 10%, a significant number considering other parts of the vehicle architecture. Vehicle's electrical load demand includes auxiliary and parasitic losses and its operation impacts alternator loading and consequently vehicle's fuel consumption. Parasitic losses are associated with the engine's auxiliary loads, such as the air conditioning (AC) compressor, the engine cooling system including cooling fans and any other components directly driven by the engine. Since those systems are generally driven direct by the engine via a belt-drive, constant losses occur during operation as drawing power from the engine in operating conditions where the engine itself operates in far-from-optimal conditions. Few contributions have been proposed recently by Rumbolz et al. (2011), Campbell et al. (2012) and Muncrief et al. (2012) with regards to the impact of parasitic loading on fuel economy of a vehicle or a hybrid electric bus. Campbell et al. (2012), studied the effect of dependency of the input power to the major mechanically driven accessories on a modern parallel hybrid city bus. This study included the replacement of mechanically driven accessories with electrically driven components and analyse the performance of the new system over a certain period of time on various routes. It was calculated that the electrification of those

accessory loads would reduce the accessory power demand by 34% (AC Off) and 31% (AC On). The overall result on fuel economy was a reduction of 13% (AC Off) and 15% (AC On). This approach was considered by the author, as it demonstrates AC system contribution to vehicle's fuel consumption.

Similar studies were conducted by Page et al. (2006), where electrical cooling fans and electric coolant pump fitted on a 'mini-hybrid' bus, demonstrating a 10.5% fuel economy improvement over a four-month period. Mackay (2012), studied different alternator drive concepts based on a four-cylinder 2.5L engine. The study included four alternator arrangements including two different capacity of alternators (i.e.150A and 120A), a 120A alternator driven by a twin-belt dual ratio pulley and finally a 120A alternator driven by a dual-speed gearbox. The twin-belt dual ratio alternator drive demonstrated a reduction in parasitic loads of 300W to 400W with a 60A alternator load and between 300W and 450W at a 20A alternator load. The study was limited to a bench-type dyno set up including a modified engine with reduced FEAD associated engine systems to reduce background friction levels. From that perspective, the approach is yet needed to be proven on real world driving conditions. The additional noise factors due to various temperature conditions could eliminate the benefits demonstrated in this experimental analysis. Hence, utilisation of such an approach could not be adopted by the author of this thesis.

2.5 Vehicle's power supply system model approach

The literature review has identified several approaches focusing on the reduction of vehicle's fuel consumption by either replacing mechanical systems with electrical more efficient systems or by controlling the operation of the parasitic loads to benefit vehicle's fuel economy. However, most of these approaches are not without restrictions and limitations. The main restrictions are that most of the approaches have been evaluated either on an experimental basis using a simulated environment (i.e. test bench) or proven on a vehicle level assessing its performance over an emissions cycle (i.e. NEDC, WLTP). The deployment of such a type of solution on production vehicles requires thorough testing for typical vehicle configurations, especially under realistic real world driving conditions. It also requires accurate models of all the features and their impact on fuel consumption for a representative range of the vehicle fleet.

2.5.1 Energy storage modelling approach

As described in section 2.1.1, efficiency is one of the key objectives in the automotive industry for all ICE, HEV, PHEV or full BEV powertrain configurations. Common to all vehicle configurations is the adoption of the traditional 12-volt power supply system as the main electrical system. Continuous electrification of auxiliary mechanical systems to electrical dictates the need to integrate such systems in the vehicle's architecture. Major efforts are invested in the development and experimentation of high energy density batteries with low internal resistance such as the Valve Regulated Lead Acid (VRLA) batteries and most recently 12V lithium-ion batteries. By combining those battery cells with ultracapacitors, the combined power pack is able to provide high power and energy levels, deep cycling and extended life-cycle operation at a reasonable cost. The ultracapacitor's capability to regenerate high energy during braking increases the vehicle's energy efficiency levels with minimum maintenance needed. Extensive use of ultracapacitors has been demonstrated in Schupbach et al. (2003); Ortuzar et al. (2007); Burke et al. (2007); Brabetz et al. (2009); Stević et al. (2011); Trovao et al. (2013); Kulkarmi et al. (2015); Tareq et al. (2015) and Qiao et al. (2016). This thesis will demonstrate the use of ultracapacitors combined in parallel with the vehicle's primary Valve Regulated Lead Acid (VRLA) battery on a traditional ICE configuration. The combined powerpack VRLA battery/ultracapacitor combines high and low frequency power levels, high capacitance and lower internal resistance and therefore high electrical efficiency as a power and energy storage subsystem.

Since the energy storage devices significantly affect the performance of the entire vehicle electrical power system ideal or black box models are not suitable as simulation models.

Depending on the aim of the simulation tool, models with different levels of complexity or different simulation approach can be employed (Myoungho et al. 2001; Wootaik et al. 2000). The choice of such models compromises simulation accuracy, computation time and initial parameterisation effort. When batteries are used as energy storage devices in automotive power systems, a few factors can be considered (Myoungho et al. 2001; Wootaik et al. 2000):

- Batteries are highly non-linear, i.e. their non-linearity during charging/discharging currents is significant for every operating condition.
- Batteries are not ideal devices, i.e. their behaviour depends on several parameters such as the charging/discharging current level, ambient and internal temperature, state of charge (SoC) and the internal resistance. Batteries behave differently in real world conditions than in laboratories or test-bench tests.

In order to choose an appropriate way to develop an adequate battery model for the need of the project, several simulation choices were investigated. The choices were as follow:

Ideal models: In the case of batteries, an ideal battery consists of an ideal voltage source that offers limitless power. If the behaviour of the energy storage device is not of interest, then this kind of modelling can easily be adopted.

Black box models: These kinds of models simulate the behaviour of energy devices without rebuilding the physical processes. These models are based on measured data and these data are fed into look-up tables. One of the best-known examples of such kind of modelling in the field of batteries is Peukert's law. This model describes the dependence of the capacity of lead-acid batteries on the discharge current.

Equivalent-circuit or physical-based models: These models include the most important physico-chemical processes that determine an energy storage device. The computation effort is greater than black-boxing modelling. An important advantage of the equivalent-circuit models is that they can easily be adapted to any kind of battery or capacitor technology (Karden 2000; Karden 2001 and Karden et al. 2002).

Finally, *physico-chemical models*. These models include the physico-chemical processes into an energy storage device by using partial differential equations. The disadvantage of such models is the large computational effort and the parameterization effort. With appropriate assumptions and simplifications, both problems can be eliminated.

2.5.2 Energy harvesting and recuperation approach

Energy harvesting and recuperation have also been extensively discussed in section 2.1.2. Recuperation control strategies have been demonstrated on several studies as described by Asada et al. (2008); Brabetz et al. (2009); Lakshminarasimhan et al. (2013); Noyori et al. (2013) and Yun et al. (2015). The proposed regeneration control strategies are focused on monitoring battery's SoC, alternator's duty cycle based on electrical demand and vehicle's motion condition (i.e. acceleration/deceleration). Based on certain acceptance criteria, the supervisory control strategies are either regulating alternator output and its duty cycle or the power flow between the power and energy storage devices. Regulating the alternator's current output minimises the impact of the alternator to the vehicle's fuel consumption levels while increasing electrical energy efficiency due to continuous power monitoring and distribution.

2.5.3 PhotoVoltaic panel model approach

Energy harvesting is achieved in this thesis by adding PV panels or solar array to the vehicle's power supply architecture. PV panel experimentation was part of the vehicle project initiated by the author, the LEV project. Use of PV panels on an experimental basis has also been demonstrated by Sonchal et al. (2012); Abdelhamid et al. (2018), EU funding projects and various automotive manufacturers (i.e. Kia, Hyundai, Toyota, Audi, Fisker Karma) including Jaguar Land Rover. The rationale behind the decision to use PV panels has been explained in Table 2.1, including the following functional requirements:

- When the vehicle operates with the engine running, PV panel will provide additional power to support the vehicle's electrical demand, decreasing the alternator's duty cycle and current output.
- Provide continuous charging to the vehicle's main battery and ultracapacitor module while the vehicle is standstill/switched Off. This results to minimise the vehicle's quiescent current drain (i.e. 15-20mA) while charging the combined power pack (i.e. battery and ultracapacitors).
- Upon certain vehicle conditions, support auxiliary systems related to customer comfort such as park climate functionality. Park climate includes features such as cabin preheat, cabin venting and engine preheat based on temperature conditions.

2.6 Electrical energy management strategies

2.6.1 Background concepts

The preliminary objective of the developed control strategy is to satisfy vehicle's power electrical demand with minimum fuel consumption and emissions but with optimum vehicle performance. Moreover, fuel economy and emissions minimization are conflicting objectives, a state-of-the-art control strategy should satisfy a trade-off between them.

Various control strategies have been proposed for optimal performance on various powertrain configurations. All these strategies are compared in terms of structural complexity, computation time, type of solution (real, global, and local), and a priori knowledge of driving pattern. According to Panday et al. (2014), structural complexity deals with complexity classes a set of problems of related source-based complexity. Complexity classes can be characterised in terms of mathematical logic needed to express them. Nevertheless, based on the type of control solution, real, global or local of an optimisation

problem, control strategies are classified into two main types, *rule-based* and *optimisation-based.* A classification of these control strategies and all their other subcategories is illustrated in Figure 2.5:

Figure 2.5. Classification of control strategies (Panday et al. 2014)

Rule-based control strategies are fundamentally depending on mode of operation. Mostly, the rules are determined based on human intelligence, heuristics or mathematical models. Rule-based are further subdivided into *deterministic rule-based* and *fuzzy rule-based* (Panday et al. 2014).

Rule-based controllers are realised without prior knowledge of a drive cycle and classed as static controllers since the operating point of the components of a system is chosen using rule tables or flowcharts and the decisions are related to instantaneous inputs. They can be easily implemented with real-time supervisory control to manage the power flow within a certain powertrain topology (i.e. HEV, ICE).

Eymann et al. (2011) proposed vehicle energy management techniques based on the complete vehicle architecture network and its PowerNet with the main focus to optimise energy usage of the entire system. In this study, an appropriate simulation model of the entire in-vehicle energy flow was developed as a closed-loop system including three main functions: storage, generation and consumption. The proposed vehicle energy management strategy was concentrated to control/regulate energy flow by using actuators and energy conversion devices. The combination of freewheeling-function, brake energy recuperation and start-stop operation resulted in 10%-15% fuel consumption reduction. However, the evaluation of the proposed control strategy was carried out using the driving profile of the US driving cycle FTP-75 and the EPA Highway Fuel Economy Cycle (HWFET). This

approach will be considered to this thesis, as the elements of energy recuperation, fuel cut off in the overrun and the holistic approach of reducing electrical energy towards fuel consumption conform to the objectives of this research while extending it by including real world driving conditions.

Alternative approaches were developed in the past to control the power flow between battery and ultracapacitor by Trovao et al. (2013) and Kulkarmi et al. (2015). Trovao et al. (2013), integrated a rule-based meta-heuristic optimization approach to share energy and power between two sources, battery and ultracapacitors, namely one with high specific energy (battery) and the other with high specific power (ultracapacitors). Embedding strategic and tactical decisions on a set of rules, the optimal power sharing problem was used to generate the power references for a lower (operational) level DcDc converters controller. The proposed scheme was simulated in MATLAB®/Simulink™, with models of energy sources for several driving cycles. The approach provided a quality solution for sharing energy between two energy sources on an electric vehicle, with improved performance on source usage and lower installed capacities.

Kulkarmi et al. (2015) proposed an energy management system (EMS) on an MHEV configuration, to control the power flow between the two sources, battery and ultracapacitor using a DcDc converter. The study demonstrated an effective utilisation of ultracapacitor and the battery in circuit, and an effective capture mechanism of regenerative power. The study though was focused on battery lifecycle and proven using a test bench set up without any evidence of vehicle validation. This approach will not be considered for this thesis, due to the fact that the main objective of the study is to minimise the random charging and discharging effects on battery lifecycle rather than any effects on vehicle's fuel consumption. Furthermore, the lack of evidence (i.e. computational power requirements, speed processing memory requirements) assessing it under real world driving conditions, make it more theoretical than possible candidate for real world implementation.

Fuzzy rule-based control strategy is based on fuzzy logic which was introduced by L.A Zadeh. L.A. Zadeh described the mathematics of fuzzy set theory. In fuzzy logic, the truth of any statement is a matter of degree. It includes designer's experience to define rules directly. An intelligent control strategy can be performed using fuzzy logic as a tool since it enables the development of rule-based behaviour that can be used in decision making. Fuzzy logic control (FLC) has certain advantages such as easy to implement, strong robustness, can be tuned based on the problem objectives or become adaptive based adjustable parameterisation mechanisms, therefore, enhancing the degree of freedom of control. Since its non-linear structure is very useful in a complex system such as automotive powertrains, it is currently used in many automotive applications. In addition, FLC can accommodate model uncertainties and very robust against environmental noises. It requires fast processing and fast execution of the inference algorithm but conventional microcontrollers (μC) with large memory can

accommodate such type of controllers. FLC is sub-categorised in conventional, adaptive and predictive control depending on the application and the information can be available as a priori knowledge.

FLC has been widely used on energy management control strategies particularly for HEV configurations. Kheir et al. (2004) used FLC to optimise fuel economy and reduce emissions on parallel HEV. The approach demonstrated an effective power split between the electric motor and the ICE while optimised fuel flow and reduced emissions (i.e. NO_x). Zhou et al. (2011) proposed an FLC for torque demand and battery SoC (as input) and required torque (as output) based on particle swarm optimisation (PSO) for energy management for a parallel HEV. Lu et al. (2012) also implemented FLC for torque distribution between the engine and the motor on a PHEV configuration. Using ADVISOR software programme, they simulated the proposed FLC strategy demonstrating significant benefits on fuel economy for different driving/road conditions.

Tareq et al. (2015) demonstrated the benefits of using fuzzy logic control in a developed energy management strategy to distribute the energy between the battery and ultracapacitor on a hybrid electric vehicle. Due to fuzzy logic and its intuitive nature, results demonstrated in this study showed improvement in the operation of the combined power source as the electric load demand was supported from both modules. However, the approach demonstrated was validated using driving cycles and it did not consider dynamic response during various driving conditions.

Qiao et al. (2016) proposed an energy management system of an electric vehicle ensuring power distribution between battery and ultracapacitor to meet loading demand. In this study, the developed power management control strategy optimised system efficiency and battery lifetime by using terrain information. In order to avoid rapid changes in power demand and achieve high efficiency, a Haar wavelet transform algorithm was proposed to decompose different frequencies components of the load power demand. The results demonstrated that low frequency loading was supported mainly by the battery while the remainder higher frequency electrical loading was provided by the ultracapacitor. Due to the vehicle's velocity dependency of the ultracapacitor's voltage set-point, terrain information was used in advance into the decision matrix to guide power distribution. Limitations of this study amongst others were limited simulation time (i.e. 800secs) as well as lack of dynamic responses taken into consideration. The approach described will not be considered in this thesis since it is only focused on the power flow control between two energy devices (i.e. battery and ultracapacitor) while the main objectives of our energy management strategy will focus on vehicle's electrical loading demand including consumers and energy sources.

Optimisation-based control strategies are divided into two main groups, namely, *Global Optimisation* and *Real-Time Optimisation*. *Global optimization control* techniques require the knowledge of the entire driving pattern (i.e. driving route) including vehicle or system information such as battery SoC levels and driving conditions. Due to the computational complexity, they are not easy to

be implemented for real-time applications. In this category, linear programming, dynamic programming, (i.e. Equivalent Consumption Minimisation Strategy ECMS), Model Predictive Control (MPC) and genetic algorithms are used to resolve vehicle energy management issues.

Real-Time Optimisation-based control methods include amongst others Neural Networks (NN), Model Predictive Control (MPC) and Pontryagin's Minimum Principle (PMP).

NN's designed by McCuloh and Pitts in 1943 and Hebb in 1949 developed the first learning rule, proposing when two neurons fire together and its activity. Artificial neural network (ANN) is a network of artificial neurons and is a parallel computation consisting of many processing blocks connected in a specific way to perform a specific task. ANN is using the principle of function approximation to learn and generalise from training data. The output of a neuron is a function of the weighted sum of the inputs and a bias. The computation of the outputs of all the neurons is the function of the entire NN. NN's adaptive structure makes it suitable for any control applications. Baumman et al. (1998) and Rajagopalan et al. (2003), demonstrated the use of NN and fuzzy logic to implement a load levelling strategy. The proposed supervisory controllers coordinated powertrain components and adapted to different drivers and driving cycles resulting to fuel economy and reduced emissions. More recently, Asher et al. (2018) demonstrated the use of ANN's for a hydraulic hybrid truck to predict fuel consumption (FC) and emissions. The control strategy was evaluated using real world data. The results demonstrated errors of 0.1% on FC prediction and 3% on emissions proving that the use of ANN's in predicting FC and emissions is significantly beneficial and easier to implement than other simulation methods and could significantly reduce physical vehicle testing and improve the understanding of real world fuel impacts.

Among the global optimisation-based strategies, MPC is a good method for dynamic model of the process which is obtained by system identification. MPC can handle a large number of controlled and manipulated variables while predicting future plant dynamics (Sengupta et al. 2017). MPC provides an optimal solution to the predefined cost function over a fixed future horizon using prediction algorithms. The cost function can be effectively tuned based on multiple weights on inputs, outputs or states. Best examples of using MPC on energy management strategies to improve fuel economy were demonstrated by Feng et al. (2015); Borhan et al. (2010); Ripaccioli et al. (2010); Poramapojana et al. (2012) and Yan et al. (2012).

PMP is originally formulated in 1956 by the Russian mathematician Lev Semenovich. PMP is a special case of Euler-Lagrange equation of calculus of variations. The number of non-linear second-order differential equations linearly increases with the dimension, so the control based on PMP takes less computational time for getting an optimal local trajectory rather than global (International Journal of Vehicular Technology). Waldman et al. (2015); Wang et al. (2016) and Hou et al. (2014) used PMP as the basis of their energy management strategy proposals.

Waldman et al. (2015) developed an energy management strategy for a 12V vehicle electrical system. The proposed simulation model included a battery model, an alternator model and an Electrical Voltage Regulation (EVR) control strategy which controlled the battery terminal voltage close to a temperature dependent reference voltage based on a gain-scheduled PI (Proportional-Integral) control. The simulation model has been validated against vehicle data and numerous driving cycles (i.e. FTP, NEDC, Artemis, and Indian Urban), the PMP solution provided a fuel economy improvement of up to 2.2%. However, adding the variability of the electrical loading as per real world driving conditions, the need for a 'forward-looking' control strategy in the form of an adaptive PMP approach was identified. An adaptive PMP (A-PMP) was implemented including SoC and time factors as the main control strategy parameters. The benefit of this adaptive approach was the development of a control strategy that could benefit fuel economy up to 1.4% without prior knowledge of electrical loading or vehicle/engine speed conditions.

Wang et al. (2016) also used the PMP approach to control the alternator duty cycle and the state of the battery charge to provide an optimal real-time solution to reduce fuel consumption on a 12 V traditional powertrain configuration. The energy management strategy followed in this study aimed to control the output power of the battery and the alternator and to maintain the battery SoC within a working mode. By receiving information from various sensors of the electrical system, such as On/Off state of electrical loads, vehicle/engine speed and engine torque, optimised the alternator as well as the battery power output to maintain fuel consumption. The proposed optimal power distribution (OPD) strategy lead to fuel economy improvements of 1.7%. The improved fuel economy effects compared to that of the A-PMP strategy proposed in Waldman et al. (2015) indicate that based on the complexity between the two approaches, the OPD strategy is pragmatically a preferred option on a real world vehicle application.

Hou et al (2014) used the PMP method to develop real-time optimal electrical energy management strategies for plug-in hybrids. The research focused on reducing simulation time by applying a linear approximation strategy for Hamiltonian optimization on driving cycles known in advance. The approach followed by Hou et al (2014), will be considered as part of our study due to particular interest in ICE configuration and the approach followed of the intelligent distribution of output power from alternator and battery according to vehicle's electrical load.

Table 2.3 summarizes all approaches described in this section, categorised into different control methodologies and its main model plant criteria and objective:

Begin of Table 2.3

Authors	Controller Structure	Model plant properties	Criteria/Objectives
Eymann et al. (2011)	Rule-based, control/regulate energy flow by using actuators and energy conversion devices	Freewheeling-function Brake energy recuperation	- Energy recuperation - Start-Stop - Fuel consumption
Trovao et al. (2013)	Rule-based, meta-heuristic optimisation approach First long-term management: Strategic decisions Second short-term management: Tactical decisions	Battery model Ultracapacitors model	- Sharing energy between two sources (battery and ultracapacitor)
Kulkarmi et al. (2015)	Rule-based, Energy management system	Battery model Ultracapacitors model	- Sharing energy between two sources (battery and ultracapacitor) - Torque assist - Battery lifecycle
Kheir et al. (2004)	Fuzzy Logic Control	Battery model Parallel HEV model	- Power split between electric motor and ICE - Optimisation of fuel economy - Reduce emissions
Lu et al. (2012)	Fuzzy Logic Control	ADVISOR model PHEV model	- Torque distribution between electric motor and ICE - Fuel economy
Zhou et al. (2011)	Fuzzy Logic Control, Particle swarm optimisation	Battery model Parallel HEV model	- Torque distribution between electric motor and ICE - Battery SoC
Tareq et al. (2015)	Fuzzy Logic Control,	Battery model Ultracapacitors model Parallel HEV model	- Sharing energy between two sources (battery and ultracapacitor)
Kulkarmi et al. (2015)	Rule-based, Energy management system	Battery model Ultracapacitors model	- Sharing energy between two sources (battery and ultracapacitor) - Torque assist - Battery lifecycle

Continuation of Table 2.2			
Kheir et al. (2004)	Fuzzy Logic Control	Battery model Parallel HEV model	- Power split between electric motor and ICE - Optimisation of fuel economy - Reduce emissions
Lu et al. (2012)	Fuzzy Logic Control	ADVISOR model PHEV model	- Torque distribution between electric motor and ICE - Fuel economy
Zhou et al. (2011)	Fuzzy Logic Control, Particle swarm optimisation	Battery model Parallel HEV model	- Torque distribution between electric motor and ICE - Battery SoC
Tareq et al. (2015)	Fuzzy Logic Control,	Battery model Ultracapacitors model Parallel HEV model	- Sharing energy between two sources (battery and ultracapacitor)
Qiao et al. (2016)	Predictive Fuzzy Logic Control, Haar wavelet transform algorithm	Battery model Ultracapacitors model Parallel HEV model Terrain information	- Power distribution between two sources (battery and ultracapacitor) - System efficiency - Battery lifetime
Baumman et al. (1998)	Artificial Neural Networks, Fuzzy Logic	Parallel HEV model	- Power distribution between components (i.e. transmission, clutch) - Load levelling
Rajagopalan et al. (2003)	Artificial Neural Networks, Fuzzy Logic	ADVISOR 3.2	- Torque split between ICE and Electric Motor
Suzuki et al. (2008)	Artificial Neural Networks, Fuzzy Logic	Battery model Ultracapacitors model Parallel HEV model	- Torque distribution between ICE and Electric Motor - Battery SoC
Asher et al. (2018)	Artificial Neural Networks, Fuzzy Logic	Battery model Ultracapacitors model Parallel HEV model	- Torque distribution between ICE and Electric Motor - Battery SoC

Sengupta et al. (2017)	Model Predictive Control, Equivalent Consumption Minimization Strategy (ECMS)	Battery Model Parallel HEV model	- Fuel Consumption - Battery SoC - Motor Energy consumption
Feng et al. (2015)	Model Predictive Control, Rule-Based Control	Battery Model Power-split HEV model	- Fuel Consumption - Battery SoC - Vehicle speed
Hou et al. (2014)	Optimisation based, Pontryagin's Minimum Principle Hamiltonian Optimisation	Battery model Alternator model	- Power distribution between battery and alternator
Waldman et al. (2015)	Optimisation based, Adaptive Pontryagin's Minimum Principle	Battery model Alternator model Electrical Voltage Regulation (EVR)	- Power distribution between battery and alternator - Fuel economy
Wang et al. (2016)	Optimisation based, Adaptive Pontryagin's Minimum Principle	Battery model Alternator model Electrical Voltage Regulation (EVR)	- Power distribution between battery and alternator - Battery SoC - Fuel economy

Table 2.2. Summary of the approaches and assumptions from literature to design and develop an adaptive electrical energy management control strategy on an ICE vehicle powertrain configuration.

2.6.2 Discussion on electrical energy management approach

After considering the optimization-based methods described in section 2.6, the following observations have been made. Firstly, many optimization techniques suffer from complex calculations which are undesirable for online vehicle implementation. Due to the fact that there is a desire to implement the proposed approach in a real vehicle application, careful consideration is taken to the complexity of the control strategy and the implementation technique followed within the vehicle's Electronic Control Unit (ECU). An ECU incorporates at least one microcontroller (μC) which is used to execute multitasking and parallel processing. High performance microcontrollers with complex periphery systems and sensors are the base of today's vehicle systems. Computation power and memory sizes of automotive embedded systems are the key critical characteristics. 'Flash Memory' is the current

established memory technology for microcontrollers to store executable operation code. Flash memory is organised in pages or blocks of several kilobytes. Microcontroller flash memories are ranged from 1kB to 4MB, also depending on RAM and CPU clock frequency. Figure 2.6 shows a comparison of 3 selected microcontrollers:

Microcontroller	Programming performance		Source
INFINEON TC1796	51.2 kByte/s	(256 Byte / 5 ms)	[TC1796]
NEC V850 Ex3	91 kByte/s	(4,096 Byte / 45 ms)	[V850-Ex3]
TMS470	128 kByte/s	(256 kByte / 2 s)	[TMS470]

Figure 2.6. Comparison of μC programming performance

A second observation is that strategies as described in Qiao et al. (2016); Baumman et al. (1998); Sengupta et al. (2017); Feng et al. (2015); Hou et al. (2014); Debert et al. (2010), require accurate information about the future driving cycle, terrain information, vehicle/engine speed or battery SoC levels. The computational time required for such dynamic programming algorithms makes them unsuitable for automotive real-time implementation.

Use of fuzzy logic and neural networks on control schemes to benefit vehicle's fuel economy have been demonstrated, as described in section 2.6.1, in Baumman et al. (1998); Rajagopalan et al. (2003); Sengupta et al. (2017); Feng et al. (2015); Hou et al. (2014) and Debert et al. (2010). However, implementing NNs in a real automotive application is often too complex or too difficult to parameterise across multiple vehicle applications. Computational power requirement is another element that limits the use of NNs for high volume vehicle applications as this will impact the overall cost of the processing capability of an internal ECU. Compared to other control schemes, NNs require much more data hence memory together with a significant period of training prior to its use. In addition, re-training is often recommended, making it challenging to deploy in a rapid development environment such as vehicle development and manufacturing.

In addition, the man-hour effort that will be required to integrate such control schemes on a rapid development framework that usually automotive industry operates in, it could be economically not feasible to be met by any automotive company.

Using a fuzzy logic approach for the proposed Electrical Energy Management System (EEMS) on a real vehicle application could be beneficial for several reasons:

- Fuzzy logic is flexible, it enables fuzzy structures to be applied to vehicles' features by applying new information to established rules.
- Fuzzy logic is tolerant to imprecise data and errors. It provides a more effective solution to complex issues. In our application, most of a vehicle's electrical features and its power

consumption are based on voltage system level and harness impedance that varies based on environmental conditions. Fuzzy logic can handle those variations within its fuzzification process.

- Fuzzy logic exploits human language and can be tuned and calibrated based on user experience. This allowed the author to calibrate the performance of the controller output taking into consideration factors such as vehicle usage experience and customer feature operation as recorded under real world driving conditions.

Table 2.3 shows a summary of the advantages and disadvantages between Fuzzy Logic and Neural Networks as described in Baumman et al. (1998) as well as Model Predictive Control strategy:

	Fuzzy Logic Systems	Neural Networks	Model Predictive Control (MPC)
Advantages	- No plant mathematical model required - Knowledge representation - Fault tolerance - Simple design of systems and rule bases - Expert knowledge - Real-time operation - Nonlinearity	- No plant mathematical model required - Generalization and association ability - Fault tolerance - Various models and parametric approach - Nonlinearity	- Flexible and intuitive formulation in time domain - Solving problems with linear and non-linear systems without changing the control formulation. - Can be proactive due to its ability to exploit model knowledge to predict future behaviour.
Disadvantages	- No learning ability - Problems with changing an existing system - No optimization methods	- No knowledge representation - No expert knowledge - Real-time operation - Hardware and software requirements - Training prior to use	- Robustness problems when prediction model is not accurate due to system noises or unmodelled dynamics. - High computational cost, high memory microcontroller required - High level of expertise required to implement and maintain for industrial applications

Table 2.3. Comparison between Fuzzy Logic Systems,Neural Networks and MPC

This thesis proposes a causal online FLC based Electrical Energy Management System (EEMS) which puts aside many of the drawbacks mentioned above. The proposed system remains free from complex optimization algorithms and does not rely on prediction information. The aim of the proposed strategy is to manage individual electrical loads/features to achieve a reduction in fuel consumption and emission problem while maintaining customer satisfaction within the cabin. Two novel design criteria will be introduced within the proposed control strategy, the fuel consumption index (FCI) and the

customer satisfaction index (CSI). FCI will indicate the effect of electrical energy on vehicle's fuel emissions while CSI will introduce a Human Machine Interface (HMI) element which will allow the customer to select the levels of convenience and comfort as a trade-off on fuel economy.

Based on LEV's experimental data results and analysis on the effect of electrical loading on vehicle's fuel consumption, the proposed EEMS strategy should provide an improved performance fuel economy on real world vehicle conditions. The choice of the technique is based on two important factors, the complexity of the problem, as well as the application purpose (i.e. a real-time implementation) and application constraints (i.e. memory storage capacity).

2.7 Summary

This chapter has presented the background to this research and the literature that has affected the methodology adopted in this thesis. Sections 2.2 to 2.4 provided an overview of different approaches followed on electrical energy efficiency, recuperation and fuel economy. Different model approaches and energy management control strategies have also been discussed in detail in Sections 2.5 to 2.6.

Having identified the potential use of alternative power supply components such as different battery technologies, ultracapacitors, high efficiency alternators and solar panels, the *Low Emissions Vehicle* (LEV) project was initiated by the author to evaluate such alternative technologies, see Chapter 3.

The literature review conducted, provided the need to create a Jaguar Land Rover specific 'Energy Cost' to evaluate the impact of electrical energy, associated with delivering customer level functions and features, on vehicle's fuel consumption. Chapter 4 presents the experimental methodology followed during vehicle testing to establish the relationship between fuel consumption and electrical energy in $g.km^{-1}.A^{-1}$.

The literature review included alternative modelling approaches for power supply components. In this work equivalent-circuit or physical-based models have been selected due to the availability of experimental data extracted from actual components (Karden 2000; Karden 2001 and Karden et al. 2002). Such models provide a good trade-off between computational effort and accuracy. Details of the overall simulation model are given in Chapter 5.

The literature review comparing most suitable control schemes for the purpose of Electrical Energy Management as used for Automotive applications has identified the use of Fuzzy Logic to realise an online strategy, able to monitor vehicle's electrical energy consumption based on the operation of its electrical loads/features under real world conditions, see Chapter 6.

Whilst the literature review was an ongoing and integral part of the work, the initial review was beneficial in focusing on the research directions. It became clear that the approach followed in this thesis offers the right level of complexity and challenging work which could well lead to a realistic and practical solution easy for real world automotive application. While it is shown that the proposed concept is suitable for ICE applications with conventional drivetrain, it is also applicable for all hybrid and full electric vehicle applications since 12-volt electrical bus is considered an integral part of vehicle architecture.

Chapter 3

Low Emissions Vehicle (LEV) research platform

3.1 Introduction

Chapters 1 and 2 identified the need to use realistic real world data to calibrate and validate the model used to design the proposed electrical energy management strategy. This chapter describes the development, experimental work and findings from the Low Emissions Vehicle (LEV) project initiated and carried out by the author. This is the main experimental contribution of this thesis. The LEV demonstration vehicle has provided data for the overall system modelling and enabled to derive a new relationship between the vehicle's electrical load and fuel consumption.

This chapter is organised as follows. Section 3.2 gives a brief overview of the major components and associated electrical loads/features of modern vehicle's power supply system. It provides the necessary background to appreciate the technologies and systems investigated on the LEV. The LEV system components and experimental work conducted are described in Section 3.3. The LEV combines high efficiency alternators, ultracapacitors enhancing vehicle's energy and power storage capability and finally alternative power sources such as photovoltaic panels. Having presented the LEV, the experimental approach, developed to evaluate the impact on fuel consumption and emissions of electrical energy associated with vehicle subsystems, is then described. The next subsection presents the data collected with the proposed experimental approach to evaluate energy efficiency, energy harvesting by auxiliary systems and to reduce the use of parasitic electrical loading on a typical vehicle's daily usage.

The experimental approach and its findings were then verified using a typical real world driving cycle (i.e. typical commuting route) combining urban, interurban and motorway driving as described in Chapter 4.

3.2 Major components of an automotive electrical power supply system

An automobile's electrical system can be divided into three parts; a) a starter motor to crank an ICE, b) an energy storage device(s) storing energy necessary for vehicle's propulsion, recuperation and standby safety systems, c) a main electrical generator which provides power either by using vehicle's engine or using power electronic devices (i.e. DcDc convertors) and finally d) the rest of the electrical architecture including electronic control units (ECUs), sensors, actuators, cabin comfort electrical features. A typical Jaguar Land Rover vehicle power supply system is shown in Figure 3.1, where the electrical system can be divided into four main parts, a) the main and secondary battery (i.e. start/stop battery), b) an alternator and c) the rest of the electrical supplies including vehicle electrical loads and cabin features that are particularly managed during start/stop operation.

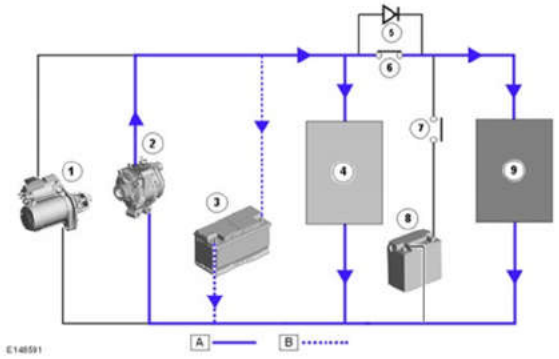

A = Primary battery supply; B = Battery charging/discharging

1) Tandem Solenoid Starter (TSS) motor
2) Generator
3) Primary battery
4) Power and engine management system loads
5) Field Effect Transistor (FET)
6) Contactor 1 closed
7) Contactor 2 open
8) Secondary or auxiliary battery
9) Sensitive loads

Figure 3.1. Schematic of a typical Jaguar Land Rover ICE electrical power supply system that supports start/stop functionality

The starter component has not been considered in this study as the major objective was to develop a power supply system that efficiently manages the operation of the vehicle focused on optimising fuel consumption and applicable to all future vehicle powertrain configurations. The initial start-up phase (i.e. cranking phase) on future vehicle applications including hybrid configuration is subject of future research.

3.2.1 Electrical storage energy devices

The emerging continuous requirements of high function reliability increase, averaged and stand-by power demand, long life-cyclability, high energy re-occupation and finally constant reduction on fuel consumption can only be met with combined energy storage devices and 'clever' energy management devices.

Recent developments in lead-acid batteries for high power applications have seen the introduction of new features such as active material layers, absorptive glass mat separators, wound electrodes etc. Assuming a sealed cell design, this gives a great advantage in overall performance over the use of lead-acid batteries. The most popular automotive types of 12-volt batteries used lately in automotive applications, including ICE, MHEV and other xEV configurations are:

- Valve-regulated lead-acid (VRLA) batteries so called 'maintenance-free' cells. VRLA batteries can withstand at least three times higher capacity turnover than conventional SLI batteries. AGM batteries, with their unique glass-fiber mat design can either be derived in prismatic or spiral-wound plate geometries and are superior for high-rate partial state of charge (HRPSOC) operation,
- Lithium-ion batteries use lithium-ion technology to provide high cyclability rates, lighter designs than SLI lead-acid batteries and high energy density levels ($Whkg^{-1}$). Lithium-ion batteries often have an integrated battery management system (BMS) to ensure efficient operation of the battery without exceeding its charge/discharge capability.

At Jaguar Cars Ltd, the batteries that are used in production line vehicles are AGM vented batteries. The capacities of the batteries are various however most commonly used are 95Ah/850CCA, 80Ah/800CCA. Figure 3.2 shows a typical 80Ah/800CCA VARTA AGM lead-acid battery:

Figure 3.2. Typical 12V 80Ah/800CCA VARTA battery AGM technology

Further details on VRLA batteries and other alternative future types of energy storage may be found in Pavlov (2017). On the other hand, the use of alternative devices such as Electrolytic double-layer capacitors used in parallel with lead-acid batteries has also been limited used to complement overall performance as needed for the continuous high peak power demand and low temperature capability. Their high power and energy density superiority comparing to batteries and their extremely long

shallow-cycle life are considered a complementary device to the primary battery used in vehicular applications.

Electrochemical capacitors (EC) also called 'supercapacitors' or 'ultracapacitors' or 'power capacitors' have been known for many years, however, only in the nineties they became famous in the context of hybrid electric vehicles (Conway 1999; Grbovic 2013; Burke et al. 2013). The reasons why electrochemical capacitors are able to raise considerable attention are visualized in Figure 3.3 in a "Ragone plot" where a plot of specific energy vs specific power is illustrated (Grbovic 2013):

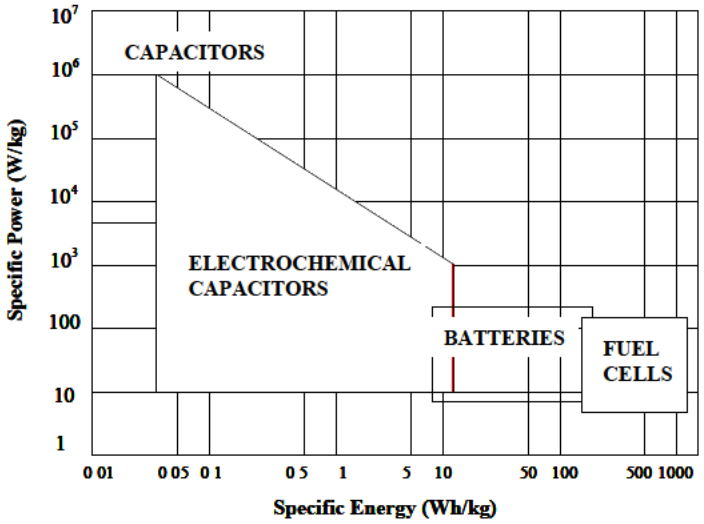

Figure 3.3. Ragone plot for various energy storage and conversion devices

Electrochemical capacitors fill in the gap between batteries and conventional capacitors such as electrolytic capacitors or metallized film capacitors. Batteries and low temperature fuel cells are typical low power devices whereas conventional capacitors may have a power density of $>10^6$ watts per dm^3 at very low energy density (Grbovic 2013; Burke et al. 2013). Electrochemical capacitors may improve battery performance in terms of power density or may improve capacitor performance in terms of energy density when combined with the respective device. In addition, electrochemical capacitors are expected to have a much longer cycle life than batteries because no or negligibly small chemical charge transfer reactions are involved.

In contrast with batteries, ultracapacitors offer several benefits that appear well suited to hybrid and EV applications such as higher power density, lower internal impedance and longer life cycle time.

It seems sensible to couple ultracapacitors and batteries to improve the power source of a vehicle. The higher power density of the ultracapacitor can reduce the size and weight of the power source, as determined by the vehicle performance (peak power) requirements. Also, the lower impedance

ultracapacitor can supply peak powers more efficiently than the battery, leading to increased overall system efficiency. More details of the characteristics of ultracapacitors can be found in Appendix C, section C.2.

3.2.2 Power generation devices

Today's ICE vehicles using an alternator to power the vehicle's electrical system and to recharge the energy storage devices integrated into the vehicle's architecture. The energy storage devices (i.e. batteries) need to be fully charged or charged at acceptable levels to provide electrical power when a) vehicle is in standby mode and all safety systems withdrawn power for operation, b) vehicle's power requirements cannot be met due to alternator's output capability (i.e. low vehicle engine speed).

The alternator is usually an engine-driven, synchronous, 3-phase alternating current (AC) generator. A synchronous generator is used because it allows the output voltage of the machine to be controlled easily by varying its field (Hughes 2008). In general, alternators are composed of a field winding, stator windings, a rectifier, and a voltage regulator.

Rectifiers are used to convert AC current generated by the stator windings into a direct current (DC) for supplying it to the vehicle's electrical system.

Voltage regulators sense alternator output voltage and control the field coil current to maintain a voltage set point according to the regulator's internal voltage reference while electrical loading is varying during vehicle operation. This is achieved by making current flow through the field winding whenever output voltage drops below reference and stopping the flow of current through the field winding when the output voltage rises above the reference voltage. The appropriate regulator reference voltage is determined according to the vehicle's voltage control strategy within the battery's charging envelope usually depending on temperature.

In Jaguar Land Rover, the most common alternator type currently used in production vehicles is the SC series with current outputs of 150A, 180, 200 and 220A. Since the SC alternator has been used in most of the production vehicles, this research has been focused on the physical and electrical properties of this type of alternator to develop an adequate Simulink model based on its performance. The SC type of alternator is a belt-driven 3-phase synchronous generator converting rotational mechanical input from the front-end ancillary drive (FEAD) into a regulated voltage via a regulator to the battery terminals. The rotor winding is excited by current from the ignition switch through the slip ring via the brushes. The magnetic field is created with the rotor claws becoming opposite poles. When this rotates due to the belt on the alternator pulley, a 3-phase AC voltage is generated in the stator winding and the rectifier

converts this into DC voltage. Figure 3.4 shows the characteristic of a voltage regulator mounted on an SC alternator:

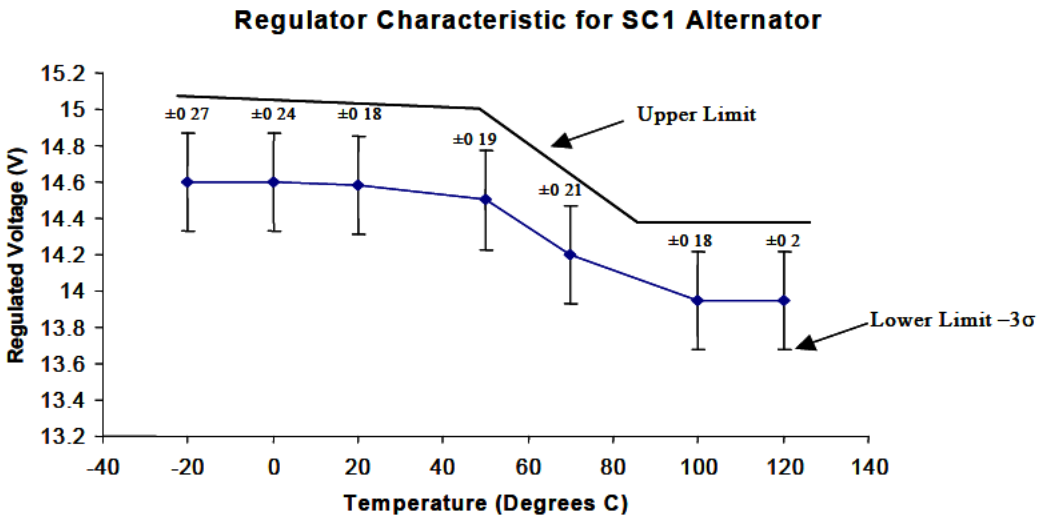

Figure 3.4. Nominal characteristic of a regulator for SC series alternator with upper and lower limits

The alternator must be capable of generating an output current throughout the operational range of the engine, which may be from 500rpm to 6-8000rpm dependent upon the type of the engine. With appropriate gearing through the use of pulleys, it is possible to operate within a speed range of 1500rpm to 18000-24000rpm (Hughes 2008). The maximum current output of the alternator depends on engine speed, temperature and operating voltage. An example of this dependency is shown in Figure 3.5:

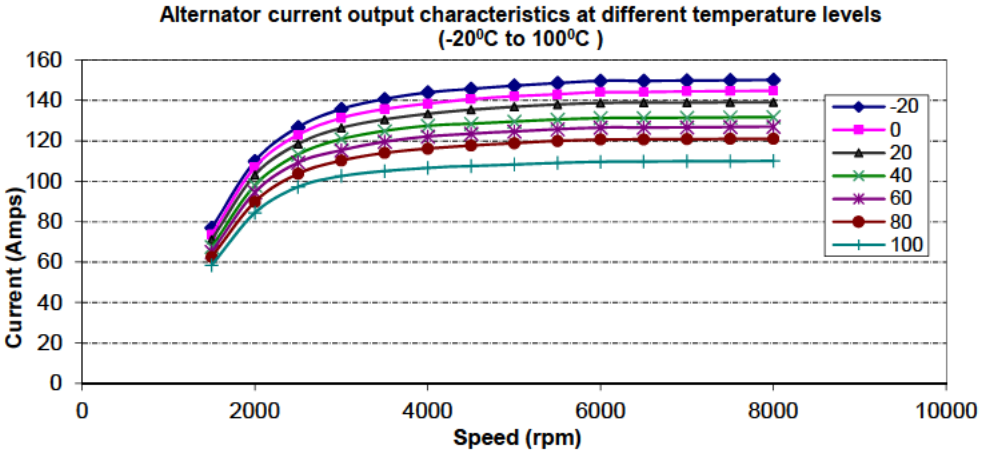

Figure 3. 5. Current output characteristics of a typical automotive alternator (DENSO SC1 130A), measurements taken at 13.5V

Since 2016, alternator rectification methods have been moved using high efficiency diodes (HED) or synchronous active rectification (SAR). SAR methods replacing diodes with high-performance

transistors, offering 2gr.km^{-1} savings while EU has confirmed by recognising them as eco-innovations. More details of such alternators can be found in Hughes (2008).

3.2.3 Automotive electrical PowerNets

The electrification of traditional systems poses a new challenge to the industry which is the appropriate use of electrical energy to support new electrical systems/features with no adverse effects on the total fuel consumption (for ICE vehicles) or estimated EV range (i.e. for battery electric vehicles). Vehicle's total electrical consumption is depending on the continuous expansion of its electrical architecture as a result of the introduction of new safety features and powertrain configurations as well as the desire to meet customer's expectations in comfort, infotainment and driver information levels.

Embedded networked systems of modern high luxury vehicles can consist of up to 100 independent ECUs in order to deliver vehicle's operations and customer's features. These systems are characterised by a high degree of interaction and consist of different various communication protocols such as Controller Area Network (CAN), Local Interconnect Network (LIN) and most recently FlexRay. Future vehicles will incorporate autonomous driving and provide additional safety and comfort electrical systems, demanding higher levels of power on a continuous basis.

On the other hand, electrical systems and comfort cabin features have been increased rapidly as a consequence of a continuous feature and attribute improvement that all automotive manufacturers would like to offer to new customers. In parallel, fuel economy targets on a yearly basis introduce the necessary replacement of mechanical engine auxiliary systems (i.e. pumps, fans) into electromechanical or electrical ones. The electrical load requirements for typical automotive electrical features have been described previously in Chapter 2, table 2.2. However, in order to estimate or even better calculate total electrical loading levels during normal vehicle operation conditions, it is necessary to know the operation of the individual electrical loads and their various modes. For automotive vehicles and their electrical loads operation, the following assumptions can be made:

- Certain vehicle electrical systems will operate on a continuous basis depending on engine running. This category includes control modules of safety systems, digital instrumentation clusters, actuators such as fuel pumps, fuel injectors, spark plugs, etc.
- Certain vehicle electrical loads that operate infrequently, for a short period of time when the vehicle operates but have no major impact on its electrical power supply system such as chassis loads (i.e. air suspension, electric anti-roll control), electrical braking, cabin seats (i.e. electrical position adjustments), indicators, electric windows, electric sunroof operation, etc.

- Certain vehicle electrical loads that operate infrequently for a short period of time when the vehicle operates, have a significant impact on electrical power supply system such as engine cooling fans.
- Cabin Comfort features which are enabled by the customer or due to its automatic operation such as heated glazing, climatic seating, cabin blowers, heated mirrors, heated steering wheel and infotainment.

The opportunity that rises with the above electrical loads and its operation, in terms of electrical energy management, is to exploit the ability to adjust the overall electrical load depending on the activation/partial activation or not of some of the features. The ability to reduce these loads provides the opportunity to reduce the alternator/generator activity and thereby achieve fuel economy benefits at a relatively low cost.

3.3 Low Emissions Vehicle (LEV) project

Up to date, governments around the world keep releasing and agreeing on strict regulations to limit emissions of carbon dioxide. The latest CO_2 targets for new passenger car fleet averages are:

- China: 120 gr CO_2/km in 2020
- Europe: 95 gr CO_2/km in 2021
- USA: 89 gr CO_2/km in 2025
- India: based on weight: 113 gr CO_2/km in 2021-22 for 1150klg average weight and petrol fuelled fleet

If the average CO_2 emissions of a manufacturer's fleet exceed its limit value in any year from 2012, the manufacturer has to pay an excess emissions premium for each car registered which is up to:

- €5 for the first g/km of exceedance
- €15 for the second g/km
- €25 for the third g/km
- €95 for each subsequent g/km.

From 2019, the cost will be €95 from the first gram of exceedance onwards. These are heavy penalties for manufacturers in case of exceedance and thus, measures and heavy investment on projects to reduce CO_2 emissions are increasing dramatically (Climate Action - European Commission 2020)

One of the key technology research projects the author initiated to investigate the development of high efficiency power generation concepts for Jaguar Land Rover was the LEV project. The complete LEV project was based on three main key characteristics that a highly efficient vehicle should include:

- High efficiency in power generation by using advanced electrical generators with an optimised overall operation strategy,
- Energy harvesting from new energy sources (i.e. solar panels)
- Greater efficiency in energy use by minimising average electrical loading during vehicle operation introducing optimised operation strategies (i.e. electrical energy management control strategies)

Main objective of this project was to investigate alternative storage and power generation technologies while demonstrating fuel economy and reduction of vehicle emissions under real world conditions. In addition, an understanding of the effect of electrical energy on the overall fuel consumption on Jaguar Land Rover vehicles was a predecessor in order to realise the benefits of new technologies on today's vehicles.

In today's luxury-class vehicles, the electrical and electronic components can draw up to 3.5kW-4.0kW, a table of typical electrical features and their consumption is shown in Chapter 4, section 4.3. Some electrical energy is consumed in every vehicle mode operation even when it is on standby and not moving (i.e. idle state). Heinrich et al. (2015) and Monetti et al. (2011) state that the effect of 100Watt has on fuel consumption is 0.1l per 100km, leading to an increase in CO_2 emissions of 2.5gr.km^{-1}. Therefore, translating this further to electrical current consumption (A), 100W of electrical power based on a voltage set point of 14V represents an electrical load of 7.1A, or approximately 0.35gr.km^{-1}.A^{-1}. For this reason, an experimental investigation of electrical energy based on the alternator's current output and the impact of it on the overall vehicle fuel consumption has been included as part of the overall LEV research. Measurements of vehicle's electrical current consumption (A) and fuel consumption in miles per gallon (mpg) measured by the vehicle were needed to estimate the relation of CO_2 emissions and vehicle's electrical current consumption in terms of g.km^{-1}.A^{-1} based on Jaguar Land Rover vehicle testing measurements. Therefore, the following LEV's project system level requirements have been selected:

Vehicle architecture functional requirements

The high-level requirements identified for this vehicle project were focused on introducing new architecture for conventional vehicles with better energy efficiency both at generation and consumption stages. The functional requirements for this improved electric architecture within a conventional ICE vehicle were summarised on the following:

- **Bi-directional energy flow** for engine cranking/operation and support of vehicle's electrical loading.

- **Voltage bus stability** under every possible vehicle condition, protect against load dump and undesired high frequency load operation.
- **Improve electrical efficiency** of energy and power generation.
- **Add energy recuperation** through the generator to reduce the generator mechanical power request to the engine.
- **Include** energy recuperation from other sources.
- **Improve electrical energy storage capability** both in size and peak demand.
- **Reduce fuel consumption** and emissions under real world conditions.

Storage device requirements

High-level requirements identified for this project was set based on maximum capability of the combined energy storage devices that will be used on the vehicle to achieve the following:

- **Charging power:** Besides high power charging the storage device must also be able to be charged with low power during parking with good efficiency (e.g. charging from the solar cells).
- **Voltage level:** The voltage level in the "power" bus and therefore also for the storage device must be within "safe" limits of a 14V Powernet operating range, this is specified $6V < x < 16V$ DC.
- **Power net integration:** The storage device will be directly coupled to the generator and must be able to be charged with the generator.
- **Energy capability:** The storage device must have a sufficient energy capacity to allow the supply of electrical loading and any auxiliaries during Eco Stop phase.
- **Lifetime:** The combined storage device must offer a high cycling and high lifetime. The new storage device must have a lifetime that is comparable to the typical calendar lifetime of a state-of-the-art lead-acid battery (AGM currently used). The higher the storage costs the higher must be the lifetime to amortise the higher costs with the fuel saving benefits.
- **Operation:** The storage device must have the flexibility to be used in a wide SoC range without a dramatic decrease of lifetime or functionality. Furthermore, it must have the flexibility to be used whenever the system is able to deliver electrical energy with high efficiency.
- **Technology:** The storage must be based on the market available and safe storage technology.
- **Discharging:** Besides high-power discharging for the electrified auxiliaries the storage must also be able to be discharged with low power during parking with good efficiency.

Power generation requirements

The requirements for power generation needed to meet all the above in terms of energy storage and functional operation limits that have been set for this project, therefore we have the following:

- **Power generation:** Capable of power generation when vehicle on move and when vehicle on park with engine Off.
- **High braking energy recuperation** with a maximum limit of 4kW when vehicle in operation.
- **Variable voltage regulation:** Include smart interface to send/receive control signals to and from the generator to be able to alter its operation based on vehicle & battery conditions.
- **Voltage limit operation:** generation within appropriate voltage limits, i.e. $6V < x < 16V$.

3.3.1 LEV architecture topology

In order to meet the above functional, power generation, and energy storage requirements while increasing efficiency and energy recuperation of the testing vehicle, the conventional power supply system has been embedded with the following technologies:

- **Ultracapacitors,** used in parallel with a primary battery to boost recharge operation and minimise the primary battery's high-power cycling demand.
- **High Efficiency alternator,** using high efficiency diodes (HED) at rectification stage, maximising efficiency at 77%.
- **Efficient climate performance,** using predictive strategies to maintain optimum cabin temperature performance with minimum impact on fuel consumption.
- **Solar panels**, additional power generation devices coupled to the main power supply system converting solar energy into electrical contributing to the overall system power availability.
- **Reduction of parasitic loading** using a state-of-the-art energy management supervisory controller to maximise recuperation while achieving low fuel consumption.

Figure 3.6 illustrates the key technologies used on LEV's vehicle prototype:

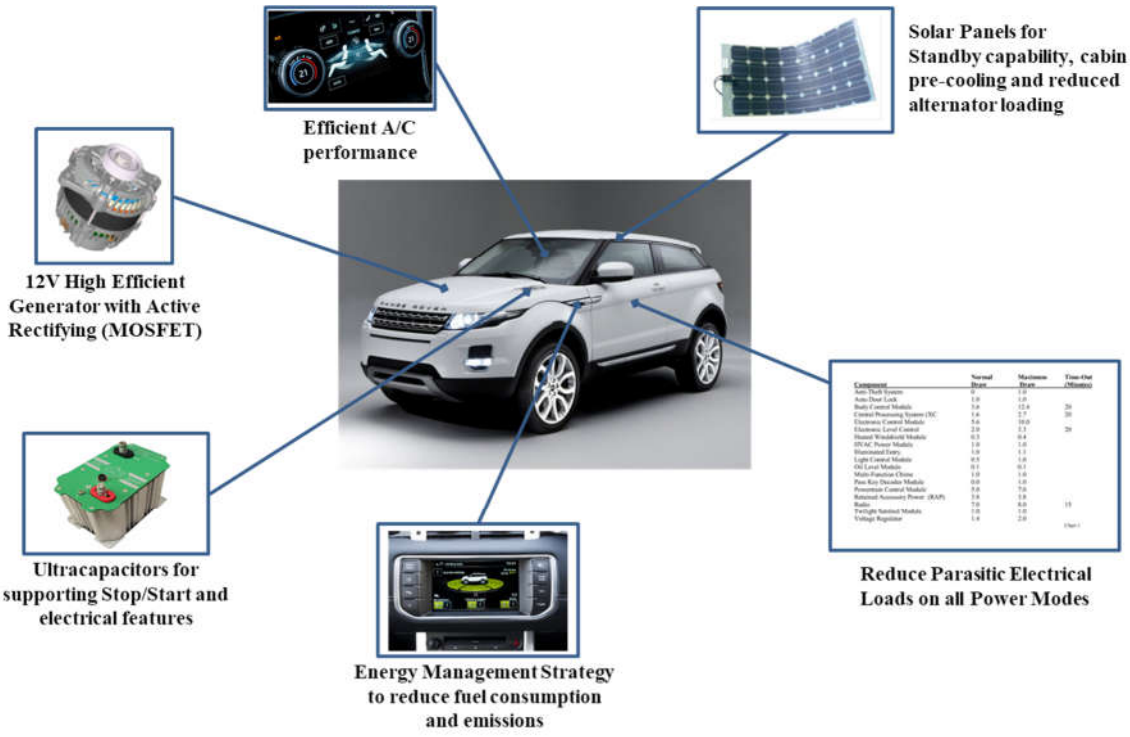

Figure 3.6. Low emissions vehicle technologies

3.3.1.1 LEV ultracapacitors module

Ultracapacitors can allow reducing the size of the primary power source (such as batteries, fuel cells, etc.). A combination of a battery and an ultracapacitor can provide a more powerful and reliable system for engine starting traction and pulse discharge/load levelling while in parallel offer less space and weight, very good cold weather starting, increased battery life and maintenance free operation. Also, it can deliver high current for fast preheating of catalysts, support a full electrical power steering or and provide local power for any type of actuator. A system consisting of a reduced size battery and an ultracapacitor will be commercially highly competitive with the battery-only system (Grbovic 2013).

Ultracapacitors can be also used for regenerative braking on vehicles because of their ability in rapid charge. In all cases, they are devices that can be used as a short-time energy storage device with high power capability and allow to store the energy obtained from regenerative braking. This energy will be used for the next phase of acceleration and boost the acceleration. Figure 3.7 shows two different ways of connecting an ultracapacitor to support an individual load or boost the system voltage of the conventional electrical system:

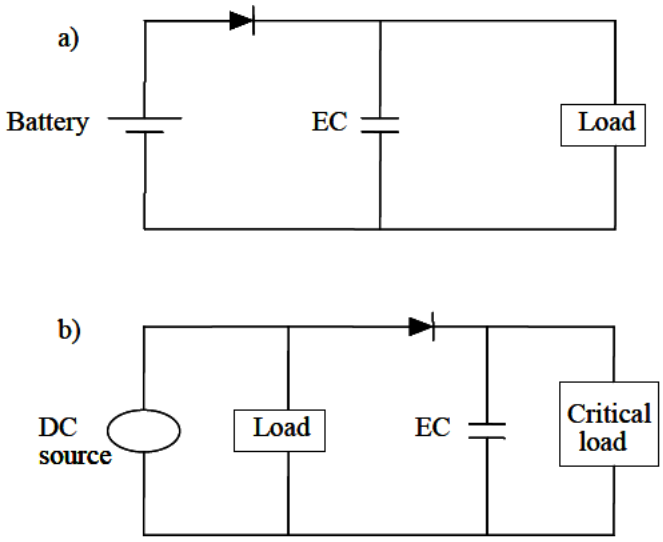

Figure 3.7. a) Ultracapacitor connected in parallel to the battery to provide a current boost on high load demands b) DC powered device involving heavy switching currents. Ultracapacitor protects the critical load from large voltage drops

For the LEV project, configuration A has been integrated into the vehicle's existing power supply system. Two 16V ultracapacitor modules from IOXUS were designed and packaged within the vehicle's engine bay. The modules consisted of 6 cells of 2.7 Volts nominal voltage, each of capacity of 333F and 500F respectively. For the demonstrator vehicle, we used the smaller capacity module of 333F coupled in parallel with the 12V Absorptive Glass Matt (AGM) type lead-acid battery. Below Figure 3.8 shows the 16V 333F ultracapacitor module as used in the demonstrator vehicle:

Figure 3.8. IOXUS Single cells of 2.7V and 2700/3000F (left) as included in the 333F module (right)

With the addition of the ultracapacitor module, the secondary battery used in the original power supply architecture to support stop/start electrical features was made redundant. The complete integrated battery/ultracapacitor system has been evaluated in the real world and an analysis of its impact in high transient load demand conditions has been made. The system supported the main

functions of the vehicle such as cold cranking, steady-state and high transient loads based on driving conditions as well as frequent stop/start operations. In addition, the combined ultracapacitor/lead-acid battery system provided extended electrical support when the vehicle was in discharge mode/alternator switched off. Figure 3.9 shows LEV's power supply system topology including the integration of the ultracapacitor module:

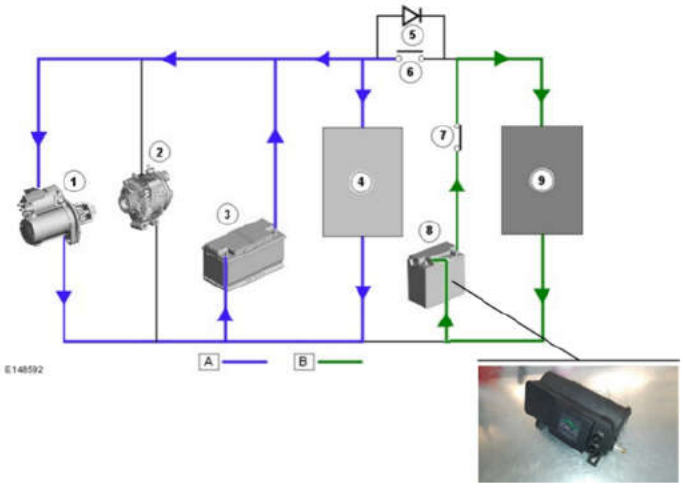

A = Primary battery supply; B = Secondary supply charging/discharging

1) Tandem Solenoid Starter (TSS) motor
2) Generator
3) Primary battery
4) Power and engine management system loads
5) Field Effect Transistor (FET)
6) Contactor 1 closed always
7) Contactor 2 closed
8) Auxiliary battery replaced with Ultracapacitors
9) Sensitive loads

Figure 3.9. LEV's power supply system topology including ultracapacitors module

Figures 3.10 and 3.11 illustrate the operation of the ultracapacitor/battery system on a typical stop/start driving cycle as a customer's vehicle will experience on a daily basis:

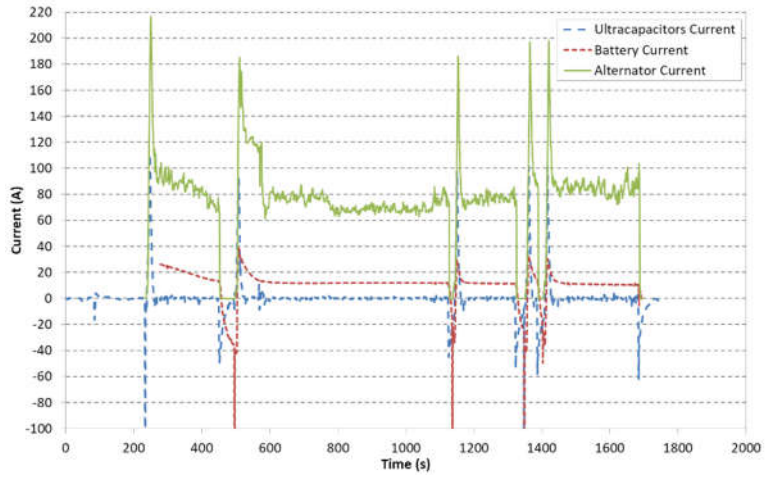

Figure 3.10. Operation of Ultracapacitors module /battery during real world driving including Stop/Start phases

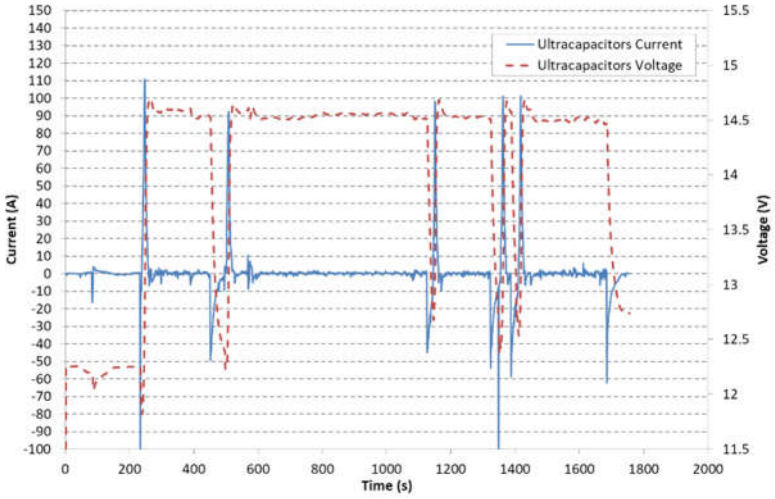

Figure 3.11. Ultracapacitor's voltage and current responses during Stop/Start phases

Figure 3.10 shows the operation of the ultracapacitor/lead-acid battery system as integrated into the demo vehicle and tested on real world driving conditions including various engine running and stop/start phases. The ultracapacitor voltage and current responses follow the vehicle's system behaviour. The ultracapacitor guarantees that peak power during stop/start events is shared without exceeding its limits. This reduces the power required to be exchanged with the battery, which reduces the number of cycling, potentially leading to an improved lifecycle.

Having the combined module connected to a power supply system offers superior voltage stability during heavy electric load cycling conditions while the ultracapacitor's lower resistance offers the perfect device to support high power demand peaks or deficits (i.w. when the battery is in low SOC) when needed. Energy stability and efficiency are also increased due to less severe development of aging

effects within the battery cell due to reduced battery contribution to support such high electrical load cycling.

In addition, the combined module offered faster warm cranking responses as expected as well as superior cold cranking performance. The vehicle has been tested in extreme cold conditions using environmental static chambers, down to -30°C. Figure 3.12 shows the comparison of cold cranking testing performance between battery only, and battery/ultracapacitor combined in parallel:

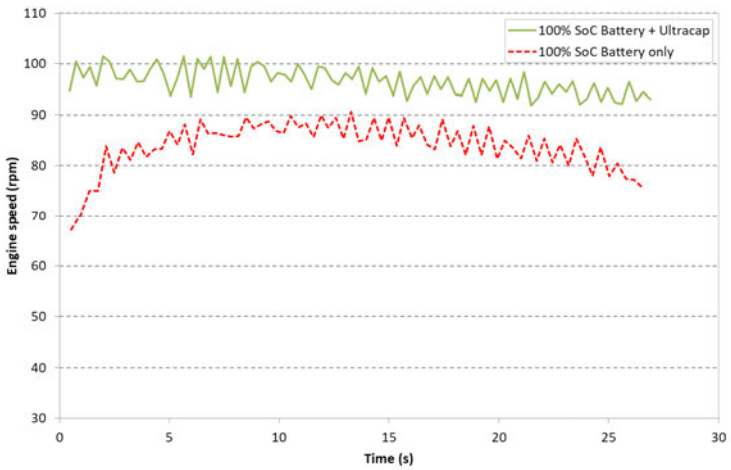

Figure 3.12. Ultracapacitors cranking performance combined with vehicle's primary battery

On the other hand, ultracapacitors have some limitations/disadvantages when used on real automotive applications. Unfortunately, ultracapacitors tend to have significantly higher self-discharge rates than batteries. Self-discharge or discharge under load is one major disadvantage and always take it into consideration when used in real world applications. Most automotive manufacturers fulfill specific requirements with regards long term storage and vehicle safety (i.e. vehicle's energy storage device must provide sufficient energy to crank a vehicle parked for as long as 31 days (Pickering 2001). A test method was applied to measure the effect of self-discharge over time on the selected module. The test measures the decrease in voltage over time after all power sources are disconnected from the capacitors. This is important when you consider that the time the cranking current can be maintained and the initial power available are both functions of the capacitor voltage. The self-discharge rate needs to be low and ideally zero. Self-discharge rate shows a temperature dependency with discharge rate increasing with increasing temperature. It can be seen that the self-discharge rates significantly depend on temperature. Therefore, it was important to assess them at the extremes of our temperature range (-40^{0}C to +50^{0}C). The test procedure to measure self-discharge was the following:

- Condition the capacitors to the desired temperature (i.e. 4 hours minimum).
- Charge the capacitors to the desired voltage. When fully charged hold the voltage on the capacitors for 30 minutes.
- Disconnect the power supply and leave to self-discharge whilst monitoring and recording the voltage every 25 second intervals.
- Repeat for other temperature values in the range (-40^0C to + 50^0C)

Figure 3.13 shows self-discharge rates of the module under different temperature conditions:

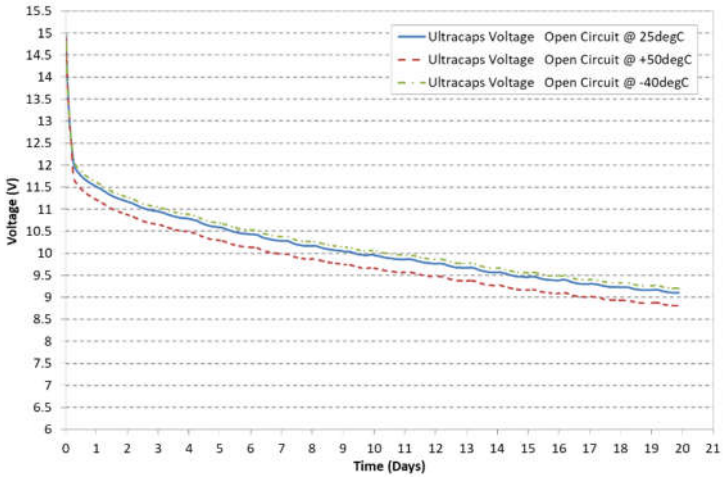

Figure 3.13. Self-discharge performance of the 333F module under various temperature conditions

Figure 3.14 shows that approximately after 3 days, the module has reached 11V which is acceptable, however, this is defined as a low voltage level for real automotive applications. In general, the automotive system voltage range should not exceed 11.5V, as most automotive manufacturers start switching off several subsystems to protect against total battery failure and vehicle breakdown. Therefore, isolating or active monitoring devices are needed to protect ultracapacitors and/or batteries to reach very low voltage levels leading to a total vehicle breakdown.

3.3.1.2 High efficiency alternator

High efficiency alternators carry improvements in their core design with regards to rectification process, filling factor in the stator slots and improved overall efficiency which reaches approximately 77% depending on the rectification method.

The high efficiency alternator used for this project included high efficiency diodes (HED) in its rectification process. Current rectification process on conventional alternators to convert alternating

into direct current (DC) is operated with diodes located on the rectifier bridge. Standard diodes induce a voltage drop on the diode junction, leading to 10% efficiency losses. The new diode technology of HED has a reduced voltage drop in forward direction with the effect of reducing the power losses during the rectification process.

Additional improvements to increase efficiency were done by improving the filling factor in stator slots which resulted in lower copper losses. HED alternators due to their improved efficiency during real world conditions are part of the EU's Eco-Innovation accreditation scheme (Climate Action - European Commission 2020). Figure 3.14 shows a typical Lundell type alternator with its high efficiency diodes topology:

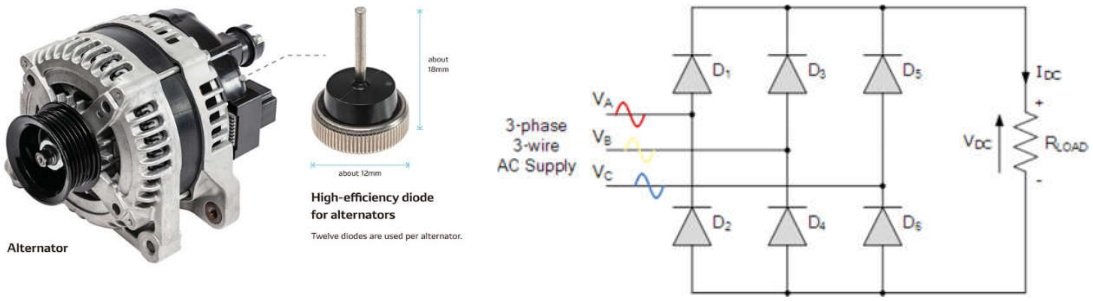

Figure 3.14. HED Lundell type alternator and its HED rectification full-wave 3-phase rectification topology

3.3.1.3 LEV Photovoltaic (PV) panels

Innovative technologies can help to reduce emissions as European Commission encourages eco-innovation on all levels. Under eco-innovation, all manufacturers can be granted emission credits equivalent to a maximum emission saving of 7g.km^{-1} of CO_2 per year for their total fleet of vehicles if they develop and implement their vehicles with innovative technologies, based on independently audited verified data (Climate Action - European Commission 2020).

Photovoltaics are commonly used in many applications however are still not commonly used in the automotive industry yet. There are some advantages when it comes to integration on automobiles in which automotive companies are still considering limiting factors such as weight, loss of panoramic roofs, vehicle take rate and the integration effort needed to include this extra device in the control strategy of vehicle's power supply for relatively low efficiency turnover system. However, as stated in Chapter 2, several automotive OEMs have researched or plan to integrate a PV panel in their model range including Hyundai as the most recent confirmed OEM that reported to use the technology to charge some of the battery cells on a hybrid model.

When solar radiation incidents a surface, it is either reflected or absorbed by the material of the surface. The absorption of light means its conversion to another form of energy which is usually heat. Materials with the ability to convert this energy of absorbed photons into electrical energy are semiconductors such as silicon, gallium arsenide, cadmium telluride or copper indium diselenide. When sunlight hits the solar cell, the surface (i.e. n-type semiconductor) of it absorbs electrons. As a result, free electrons and broken bonds called holes (i.e represented as h^+) are produced within the material. The electrons migrate to the front surface of the solar cell, which is manufactured to be more receptive to the free electrons (negative charge). The resulting imbalance of free electrons and holes (positive charge) creating a potential difference in the two sides of the solar cell. The rest of the holes recombine and disappear. In addition, a certain percentage of solar irradiation is being reflected and another passes through the cell without being absorbed until meets the electrode on the back side (+ve electrode). Depending on the material of the semiconductors layers and the intensity of the solar irradiance that can be absorbed, a solar cell can provide 0.5V-1V and a current density of 20-40mA/cm^2 (Quaschning 2019).

The crystalline silicon solar cells are the most commonly used forming 95% of the total global production (Quaschning 2019). Depending on the structure of the material they are constructed, there are several types such as monocrystalline cells (c-Si), polycrystalline cells (m-Si), amorphous (a-Si) and thin film cells.

For this project, a solar panel would offer several benefits to the overall vehicle electrical energy management strategy:

- It could provide continuous charging to the vehicle's main battery as well as to the ultracapacitor when vehicle is standstill/switched off.
- Eliminate quiescent current drain (typical 15-20mA for Jaguar Land Rover vehicles) as well as minimise ultracapacitor self-discharge maintaining its SoC level at an acceptable level.
- Upon certain vehicle conditions, it could support auxiliary systems related to customer comfort such as park climate functionality which offers cabin preheat, cabin venting and engine preheat based on temperature conditions.
- When vehicle operates (engine on), the solar panel could supply electrical current to support vehicle engine base load thus reduce alternator loading with immediate effect on fuel consumption and CO_2 emissions

Upon investigation of several PV technologies, several 2nd and 3rd generation technologies currently tend to be too expensive with not high efficient or automotive robust compliant. However, the potential to improve does exist. Some developing technologies (i.e. Gallium Arsenide) currently achieve far greater efficiency than conventional silicon PV cells (Gallium Arsenide efficiency is up to 40%) but are prohibitively expensive. Others (i.e. various thin film technologies) have various attractive properties

(i.e. flexibility, potential for semitransparency, lightweight) and are not necessarily prohibitively expensive, but require improvements in robustness, automotive-type production (in particular use in curved glass) and conversion efficiency in order to become feasible.

For this experiment, two monocrystalline solar panels were selected with the potential to be fitted on the panoramic roof of the candidate vehicle manufactured in Germany and China respectively. ENECOM panels were suitable due to their lightweight design, thin profile and the available customisation that could offer to fulfill the project requirements. Data parameters for the one of the PV panels used are shown in Figure 3.16 below:

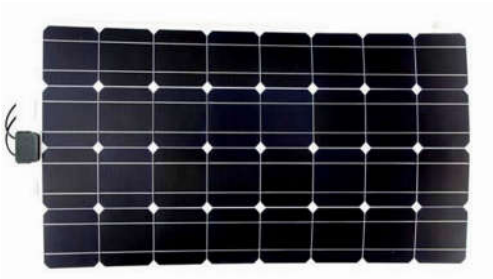

Part Number:	**Enecom HF150-6-18**
Maximum Power1 (Pmax)	150W
Voltage at Pmax, Vmp	17.05V
Current at Pmax, Imp	8.8A
Short-circuit current, ISC	9.5A
Open-circuit voltage, VOC	20.64V

Table 3.1. Enecom PV panel and its critical parameters

An ENECOM monocrystalline solar panel (i.e. HF150-6-18), manufactured in Germany, was finally selected prior to fit on the panoramic roof of the test vehicle. The solar panels have been tested under various solar load (W/m^2) conditions (i.e. 600W, 800W, 1000W and 1100W) using Jaguar Land Rover static environmental chambers with special solar load devices. Multiple tests run over 10 hours period, collecting all possible data with regards to solar panel current output performance, electrical efficiency achieved on different solar activity levels, temperatures and maximum load output achieved. Data collected can be found in Appendix C, section C.3. Figures 3.15 and 3.16 show the performance with regards current output of both solar panels under continuous steady-state solar activity:

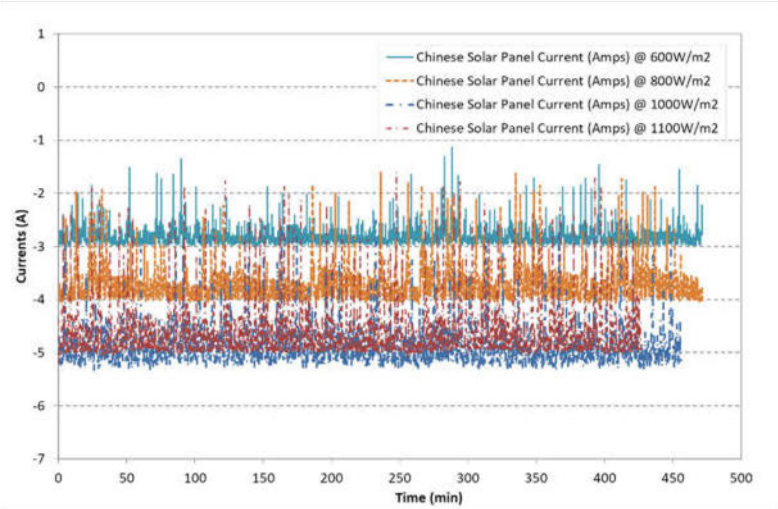

Figure 3.15. Current output achieved under various solar loading levels ($W.m^{-2}$)

Below Figure 3.16 shows an electrical power comparison between both solar panels under different solar activity levels:

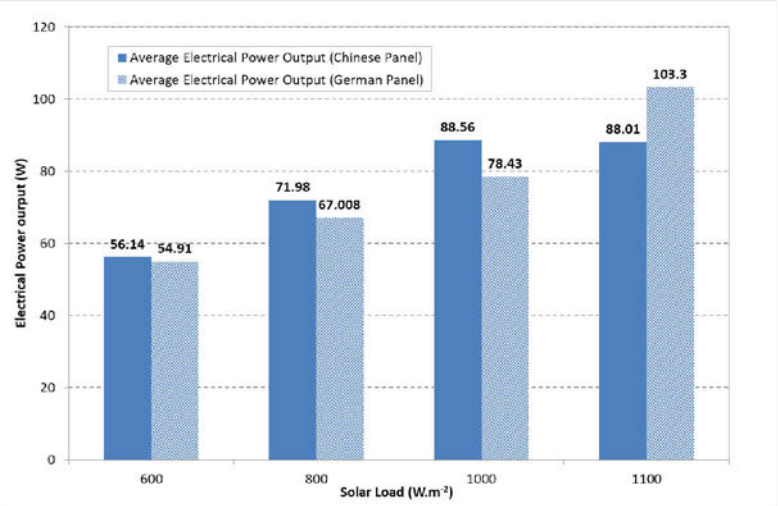

Figure 3.16. Solar panel comparison with respect to Electrical Power Output achieved during testing

It is worth noting that both solar panels achieved electrical power output close to 100W despite the manufacturer's nominal output claimed to be at 150W and 200W respectively. The selected solar panel has been connected to the vehicle's electrical system via an MPPT (Max Power Point Tracking device). The MPPT charge controller adjusts its input voltage to harvest the maximum power from the solar array and then transforms this power to supply the varying voltage requirement of the main battery plus any extra loads connected to it.

Figure 3.17 shows the Enecom solar panel as integrated on the roof of the LEV demonstrator without modifying the aerodynamics of the vehicle.

Figure 3.17. ENECOM's Solar Panel as integrated on the LEV's roof

With the solar panel integrated into vehicle's electrical system, we have incorporated all new technologies described above including vehicle's main AGM lead-acid battery, ultracapacitors module and a monocrystalline PV panel on the roof. Figure 3.18 shows the topology of the complete LEV electrical power system:

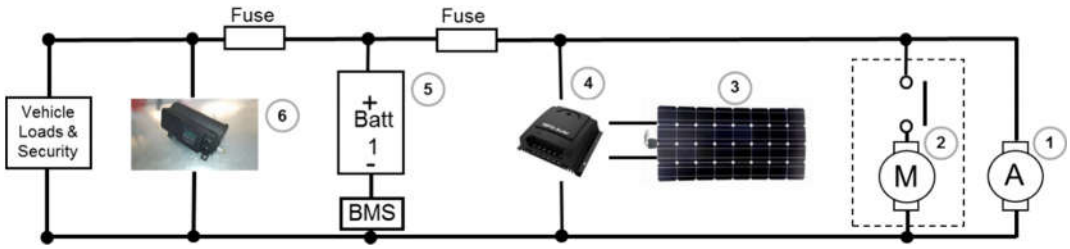

1. High Efficiency Alternator
2. Tandem Solenoid Starter (TSS) motor
3. Enecom PV panel
4. MPPT controller
5. AGM lead-acid battery
6. IOXUS Ultracapacitors

Figure 3.18. Topology of the LEV demonstrator's electrical power system

An initial use case control strategy was also developed, detailing the expected logic steps that would be run by the solar controller and identifying where the energy from the solar panel would be used in each scenario. This can be seen in Figure 3.19:

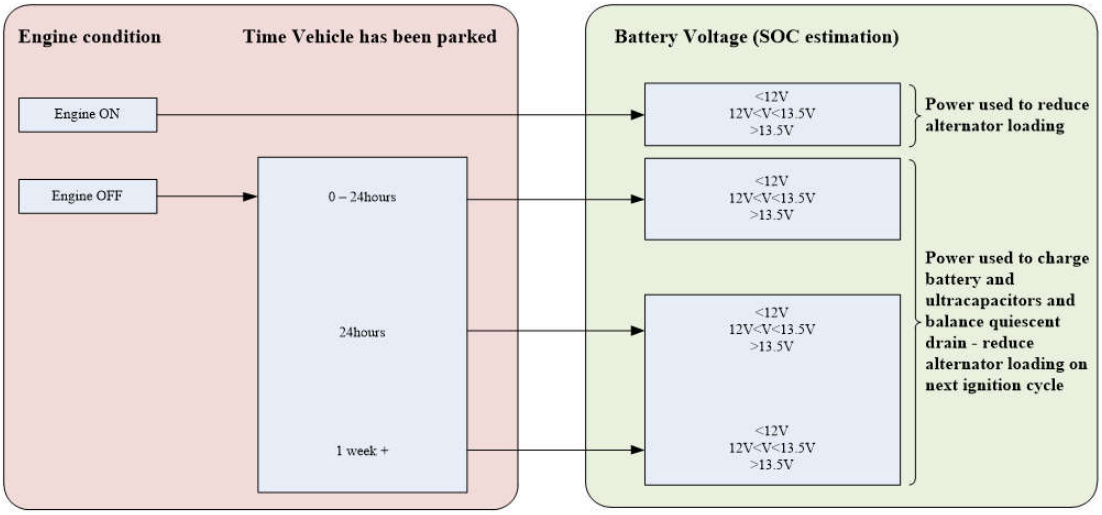

Figure 3.19. Initial use case control strategy integrating PV panel in LEV's power supply system.

The logic of the control strategy firstly looks at whether the engine is running or not. If the engine is running, energy from the solar panel is always to be provided to the main battery and ultracapacitor module thus reducing total alternator loading. If the engine is not running, the solar panel provides energy to cover the quiescent current drain and charge the battery to 100% SoC thus on the next ignition cycle, alternator loading will be at a minimum level as part of the power management strategy contributing to fuel economy. By having the complete system fully in operation with all new technologies included, various instrumentation channels were added to the vehicle in order to monitor and record all necessary information needed for the project.

LEV demonstrator vehicle was driven under various driving and environmental conditions while instrumentation captured valuable system data during summer and fall months. This was necessary to understand how the overall new technology will operate and support main vehicle operations while the vehicle was in driving mode or standstill (during parking). An example of the LEV's solar panel operation is shown in Figure 3.20 which shows the output achieved from a 2 day data collection snapshot under variable solar activity (i.e. overcast with sunny spells) and vehicle used under normal customer scenarios including driving and stand alone parking periods:

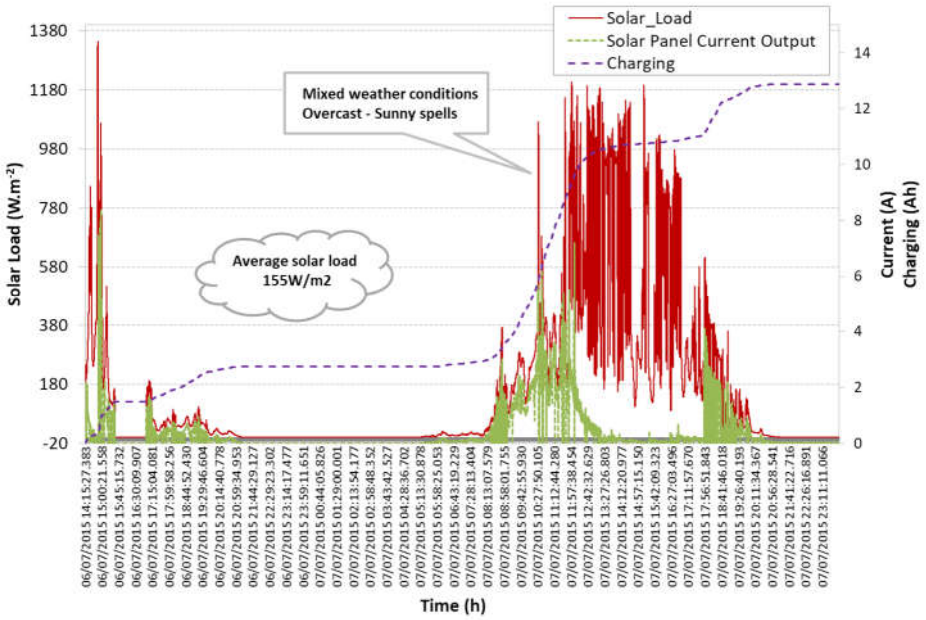

Figure 3.20. Solar panel contribution to LEV's overall charging strategy

As shown in Figure 3.20, the solar panel's output during the day reached approximately 8.5A. The average solar load activity achieved was 155W/m^2 while the estimated contributing charge levels to the battery over a 33hour period reached 13Ah. On the contrary, but as expected, the solar panel switched off completely during the evening/night time, resulting in the battery discharging due to the vehicle's quiescent current drain (i.e. 20-25mA drain). Furthermore, the solar panel's charging output was reduced to a minimum at midday (07/07/15), due to the very low charge required by the battery that had a high SoC level (i.e. approx. 100%). Finally, the graphs show the variability of solar activity recorded, which is dependant on weather and environmental conditions, resulting in reduced solar panel current output.

3.4 Summary

The aim of this chapter was to introduce the power supply system components used in the low emissions vehicle project describing the key design requirements needed to be met for the vehicle architecture, energy storage and power generation devices. The selection and use of ultracapacitors have been described including the advantages and disadvantages of its use with the proposed power supply topology. The selection of solar panels was described and it was shown that solar panels can be used as an integral part of energy harvesting, contributing to increased electrical efficiency of the LEV vehicle.

The control problem is identified towards the reduction of fuel consumption and the development of the appropriate electrical energy management control strategy to address this problem. An experimental methodology proposed in Chapter 4 will establish the relationship between fuel consumption and electrical energy in $g.km^{-1}A^{-1}$ as key criteria exploited in the design of the proposed energy management strategy described in Chapter 6.

Chapter 4

Problem formulation & experimental approach

4.1 Introduction

Chapter 2 reviewed criteria to design and evaluate the performance of electrical management systems and identified the need to quantify the impact of electrical loads on fuel consumption. This chapter proposes an experimental testing methodology to establish a relationship between fuel emissions and electrical energy in $g.km^{-1}A^{-1}$. The experimental approaches developed for both environmental-vehicle-testing-chamber and real world driving together with the resulting simple relationship between fuel emissions and electrical energy are key contributions to this work.

This chapter is composed as follows. Section 4.2 identifies targets and strategies to reduce vehicles' CO2 emissions to justify the impact of the alternator on an ICE vehicle's emissions. It then identifies the need to derive a suitably simple relationship to assess the fuel consumption resulting from the alternator usage to meet the load demands. Section 4.3 describes the range of electrical loads on a vehicle and identifies the need to quantify the contribution of each load to the overall fuel consumption. Section 4.4 describes the experimental approach adopted to measure the fuel and emissions for a realistic range of programmable sets of loads and operating conditions. It includes a novel specifically designed test driving cycle for use in an environmental vehicle testing chamber.

Section 4.5 describes the analysis of the experimental data recorded from vehicle testing. A statistical analysis is conducted to model dependencies and degree of correlation between fuel consumption in ml, fuel flow rate in $ml.s^{-1}$ and CO_2 emissions under various electrical loading conditions.

Section 4.6 focuses on validating the obtained relationship using a typical real world driving cycle (i.e. typical commuting route) combining urban, interurban and motorway. The applicability and

reproducibility of the results are established by measuring electrical loading to fuel consumption and emission during 115 commuting trips, between Coventry and Gaydon in the UK.

The criteria obtained in this chapter is incorporated as part of the proposed electrical energy management control strategy, presented in Chapter 6, to monitor and minimise the impact of electrical loading on vehicle's overall fuel emissions

4.2 Reducing automotive CO_2 emissions

Air pollution has a significant detrimental effect on the environment and the health of the population. Air pollutants include particulate matter (PM), ozone (O3), Nitric Oxide (NO), nitrogen dioxide (NO2) and sulphur dioxide (SO2) (EU regulation 2009). Transport accounts for approximately 26% of total emissions in the EU (EU, policy update 2014). Road traffic, with a total share of approximately 12%, is responsible for almost half of these emissions. The number of grams of carbon dioxide per km (g CO_2 km^{-1}) is used as a convenient surrogate to evaluate the emissions from vehicles.

Europe's target of 95 g $CO_2.km^{-1}$ means a fuel consumption of approximately 4.1l/100 km for petrol and 3.6l/100km for diesel (EU regulation 2009; EU policy update 2014) If the average CO_2 emissions of a manufacturer's fleet exceed this limit, the manufacturer has to pay an excess emissions premium for each car registered of €95 from the first gram of exceedance onwards. In parallel with legislation to reduce emissions, safety consideration has resulted in an increase in the weight of the vehicles. The latter makes meeting future emission targets even more challenging. It is realised that the automotive industry can no longer meet the challenge presented by the stringent CO_2 targets purely by improving standard internal combustion engine (ICE) technology. Additional measures, on a vehicle level, are necessary to reach such stringent targets. Examples of improvements include improved vehicle aerodynamics, lightweight design, low rolling resistance tyres, LED lighting, more efficient transmissions (automatic dual-clutch transmissions) and the electrification of auxiliary components (i.e. electric water pumps, electric engine cooling fans) and propulsion increasing vehicle electrical efficiency (Chiara et al. 2011; Eymman et al. 2011). In the past, 42V systems (comprising a 36-volt battery and a 42-volt alternator) with lead-acid battery highlighted the advantages of higher operating voltages in terms of efficiency (Stoppok 2015). Since 2011, manufacturers are focusing on Mild Hybrid (MHEV) 12V/48V dual voltage power supply system configurations due to their higher efficiency, smaller cross-sectional area of cables and low risk mitigation against contact protection and arcing. MHEV systems combined with optimal power management strategies have been shown to offer potential fuel savings (EE-VERT 2011; Zifan et al. 2016; Vallur et al. 2015; Rick et al. 2015).

The conversion of most traditional auxiliary systems to electrical, by promising energy and efficiency improvements, requires a coordinated approach to electrical power generation, storage, distribution and use of electrical energy from a fuel economy perspective. With a continuous increase in vehicle functions for functional safety, comfort and fuel economy, future automobiles will consume more electrical power.

The development of control strategies optimizing power and energy usage requires the means to quantify the impact of vehicle's electrical features and its parasitic losses on fuel consumption and emission. Parasitic losses are associated with the auxiliary loads of the engine, such as the air conditioning (AC) compressor, the engine cooling system including cooling fans, any other components directly driven by the engine. Since those systems are generally driven directly by the engine via a belt-drive, constant losses occur during operation. The latter is exacerbated when then the engine operates in non-efficient zones.

The energy consumption of 12V electric loads has previously been analysed using simulation studies (Boulos et al. 2003; Gerke et al. 2007). A broad analysis of the contributions to the fuel consumption of both light and heavy duty vehicles caused by the electrical loads has been proposed in (Fenske et al. 2006; Rumbolz et al. 2011; Pettersson et al. 2006). Experimental studies on vehicle fleet report that approximately 8% of the fuel energy is used to operate electrical auxiliary loads (Fenske et al. 2006). Air conditioning (A/C) and engine cooling system were shown in (Lyu et al. 2007; Pirotais et al. 2002) to contribute up to 30% of the overall power consumption for the US EPA Urban Driving Cycle conditions, making it the main power consumer. The power consumption related to the engine cooling system is also significant as engine cooling fans can draw up to 1.2 to 1.5kW at the engine crankshaft with the alternator loading contributing significantly to the overall fuel consumption (Pang et al. 2004; Myung et al. 2007). However, there is a need to perform a sufficiently broad analysis of the impact of 12-volt electrical loading to the overall fuel emissions and consumption of a vehicle under real world driving conditions. This 12-volt electrical loading analysis is applicable to hybrid and non-hybrid powertrain configurations since 12-volt electrical systems are an integral part of modern vehicle architecture.

By reviewing the above literature, it is clear to quantify the effect of electrical loading operations of a vehicle, including auxiliary and parasitic losses, and how its operation impacts the alternator loading and consequently the fuel consumption and CO_2 emissions. A method to derive the impact of alternator loading and its application to a range of luxury vehicles with different vehicle powertrain configurations is proposed by the author. It presents a large data set, obtained under both controlled conditions in an environmental dynamometric chamber and under real world driving on a typical commuting route. These data will be useful to the research community to derive electrical energy management strategies.

4.3 Electrification of vehicle systems

The electrification of traditional systems poses a new challenge which is the appropriate use of electrical energy to support new electrical systems/features with no adverse effects on the total fuel consumption (for ICE vehicles) or estimated EV range (i.e. for battery electric vehicles). The electrical load requirements for typical automotive electrical features are described in Table 4.1.

Description of electrical features/loads	Range of current consumption [A]
Engine running	15-25
Heated glazing	20-50
Heated steering wheel	5-6
Climatic seats	5-11
Massage seats	2-3
Infotainment (In-Car apps, CD, DVD, Navigation)	2-20
Telematics	2-5
Pre-heating/Pre-cooling	5-10
Adaptive Lighting	0-20
Electrical Suspension	0-20
Cooling Box	2-3
Electric A/C compressor	5
ICE Cooling fans	5-120
Electrical Power Steering	5-6
Electrical Air Heaters (PTC)	0-50

Table 4.1. List of today's most typical automotive electrical features[3].

Table 4.2 presents a list of fuel saving systems based on 48-volt technologies. Mechanical components can be replaced with electrical components, resulting in reduced mechanical drag torque and friction losses in the engine. These features will however increase the electrical accessory energy pulled from the alternator, therefore increasing fuel consumption (Myung et al. 2007; Campbell 2012). The combination of all ancillary loads represents a considerable source of energy consumption.

[3] Note the wide variability [73A- 354A] on the overall electrical load depending on the activation/partial activation or not of those features

Description of 48V electrical features/loads	Range of current consumption [A]
Belt driven Integrated Starter Generator (BISG)	0-85
eARC (electric Anti-Roll Control)	0-50
eSC (electric Super Charger)	0-80

Table 4.2. List of 48-volt technologies that most likely will be introduced to automotive industry.

One of the challenges associated with managing current and future electrical loads is the wide variability in terms of overall load for 12V systems or 48V technology [0-215A]. The opportunity, in terms of load management, is to exploit the ability to adjust the overall electrical load depending on the activation/partial activation or not of some of the features. The alternator/generator is typically controlled to fulfill the demand of the vehicle's electrical loads, as well as to recharge the main/secondary energy storage (i.e. battery) when required. The ability to reduce these loads provides the opportunity to reduce the alternator/generator activity and thereby achieve fuel economy benefits at a relatively low cost.

Vehicle's fuel consumption levels depend on several factors including powertrains architecture, vehicle weight, transmission type, braking system, aerodynamics, tyres and electrical energy demand due to the electrical features supported by an alternator. Parasitic electrical loading, as defined previously, has a significant impact on fuel consumption for traditional ICE vehicles. It is therefore a prerequisite for the automotive industry to reduce the impact of parasitic loading whilst at the same time leads towards efficient electrical systems implementation. Research to date has mostly focused on the impact of some of the electrical features related to the vehicle's operation and their impact on the vehicle's overall power dissipation and fuel economy under specific emissions cycles. Few studies have been able to provide a sufficiently broad analysis of the impact of electrical loading on the overall fuel emissions under real world driving conditions.

The following sections describe the material and methods developed to analyse the impact of electrical energy on fuel consumption.

4.4 Experimental methodology

The vehicles tested under controlled experimental conditions included luxury SUV and saloon types with engines of 2.2l 4-cylinder diesel, 2.0l 4-cylinder petrol, 5.0l V8 petrol and 4.4l V8 diesel. All vehicles were based on Jaguar Land Rover conventional 12-volt vehicles, equipped with 12V high efficiency alternators as the primary generating power source. The variety of engine sizes and vehicle types investigated provides a means to generalise the results to different powertrain and to evaluate the impact of parasitic loads for different engines, powertrains and vehicle setup. The SUV 2.2l Diesel was then selected to collect real world fuel consumption estimations.

The power supply system was modified to control the 12-volt electric loading levels applied to the alternator by using an external electronic programmable load bank (i.e. 12V/150A). This electronic load can vary the electrical load from 0A to 150A in steps of 1A. An external mechanical switch was necessary to isolate the actual electrical load of the vehicle during testing. When the switch was in an open position, the alternator could only respond to the electrical loading applied through the external electronic load bank whilst the rest of the vehicle was powered through the main 12-volt lead-acid battery. A smaller secondary battery (12-volt, 14Ah) was added to the system and connected to the alternator line. The role of the secondary battery was to provide excitation voltage whilst the alternator was disconnected from the main power supply system of the vehicle. It allowed the alternator to operate and produce electrical power. Figure 4.1 illustrates the external load bank connectivity as integrated within the power supply system of the vehicle.

The current of the alternator was measured via a current clamp on the lead connecting the alternator to the electronic load. This was connected to instrumentation equipment as well as to the high speed controlled area network (HS CAN) bus. The HS CAN bus lead was connected to the diagnostics port and to a laptop running diagnostic software. This setup measured relevant vehicle and power supply system parameters such as alternator torque, vehicle speed, engine speed, ambient temperature, engine coolant temperature and other data available on the vehicle CAN bus. The tool used to extract the information from the HS CAN bus was CANape, a software parameterisation tool by Vector Informatik. The sampling time of 0.15s was selected as most of the electrical loads considered are driven by the vehicle's comfort/cabin systems therefore their low frequency switching operation can be recorded using slow sampling time. In addition, such sample time benefits the overall memory size required to record the data output. Data evaluation and analysis were conducted using data processing tool vSignalyzer from CANape.

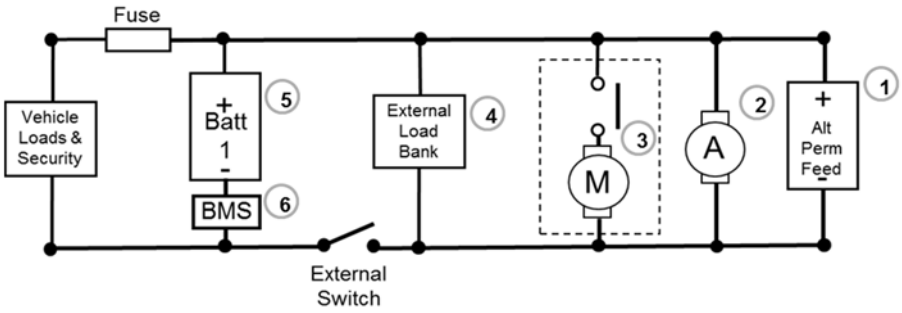

1. 12-volt secondary battery (permanent feed)
2. 12-volt alternator
3. 12-volt starter motor
4. Electronic load bank (0A-150A)
5. 12-volt primary battery
6. Battery monitoring sensor

Figure 4.1. Power supply configuration of the test vehicles with an external electrical load bank use to simulate the parasitic loads.

4.4.1 Experimental variability

While previous studies provide profound insights on optimisation techniques and methods to increase fuel efficiency and economy, most of them are evaluated on certification cycles which lack the representativeness of the real world driving conditions. One of the issues with most of the testing under controlled conditions is the lack of real world representativeness with NEDC and real-world emission differing by almost 50g.km^{-1} in 2016 (Archer 2017). Therefore, it is important for our experimental approach to be tested using two different approaches, driving using environmental dynamometer chambers as well as carrying out real world testing.

Vehicle testing carried out in environmental dynamometer chamber minimises variability due to the environment and ensures reproducible test conditions in terms of vehicle, engine operating temperatures and electrical load demands. Electrical loading demand is controlled manually using an electronic load bank connected to the vehicle system. Therefore high frequency step changes do not occur. The use of a particular drive cycle on a dynamometer should also reduce the throttle input variability compared to a real world environment. Engine speed and vehicle speed variability are however expected due to the human driver following the set drive cycle.

Vehicle testing carried out in real world conditions is less repeatable than chamber testing. Vehicle and engine speed variabilities are expected to increase significantly under real world driving conditions due to the diversity of operating conditions and external factors that may affect drivers' inputs. In addition, environmental factors together with the engine operating conditions are significantly more

variable. For example, at the start of the journey, the vehicle would be cold and not operating under the most optimal conditions. Electrical load demand is also dynamic and depending on engine operations and vehicle's electrical system demand. However, if real world tests are carried out under controlled conditions, it has been found that they could be reproducible to within 5% (Eberth et al. 2004). Therefore to mitigate the variability, it is necessary to carry out a statistically representative number of test repetitions and to drive to be within specific dynamic and electrical loading boundary conditions. The vehicle was driven as per normal customer scenarios with electrical features switched off/on based on environmental conditions (i.e. ambient & cabin temperature conditions). The cabin's electrical feature usage was as realistic as possible replicating customer's input. This return journey has been repeated 115 times to provide a sufficient number of samples of data to generate related correlations.

4.4.2 Experimental driving cycle definition

As described in the previous section, the alternator will only respond to the changes in the electronic load during the whole experiment. Any other electrical energy source variation is supported by the main battery and does not contribute to the total ancillary load applied to the alternator. The fuel consumption can be affected by the engine energy dissipation levels. They depend strongly on engine thermodynamics, engine friction, thermal management and drivetrain architecture. Energy losses occur in the transmission system due to friction of moving parts and auxiliary loads such as pumps, actuators and cooling systems (Myung et al. 2007; Campbell et al. 2012).

An experimental driving cycle was developed to analyse the effect of electrical energy on fuel flow, fuel consumption and alternator efficiency. It takes into consideration the test vehicle variety (i.e. different engine sizes, vehicle types) and includes low and high speed driving. For each test, the vehicle was held at 0 $km.h^{-1}$ for two minutes, and then accelerated to varying speed levels and held for two minutes, before decelerating according to the same profile in terms of decreasing speed. The electronic load bank was used to vary the electrical load, with the same load applied to the whole driving cycle. Multiple driving cycles were performed for each five different loads namely: 0A, 25A, 50A, 75A and 100A (±0.05A). Figure 4.2 illustrates the experimental test cycle as applied to all test vehicles.

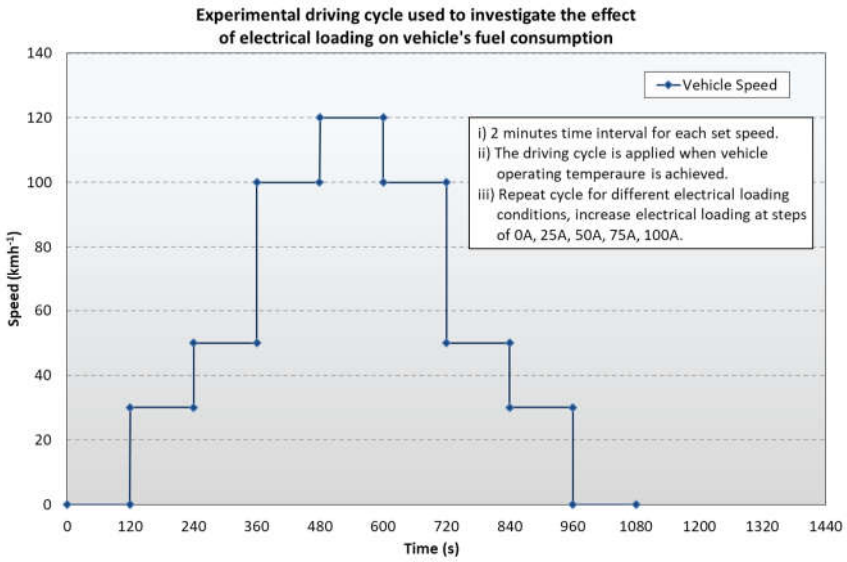

Figure 4.2. Experimental driving cycle used to investigate the effect of alternator loading on fuel consumption

The proposed current load intervals of 25A are believed to represent a realistic step change likely to occur frequently during the operation of the vehicle. Lower electrical loading levels impose no significant changes on the voltage or alternator torque levels and do not, therefore, have a significant impact on fuel consumption. Alternator loading over 100A is considered to be a high electrical loading which can only occur for extreme environmental conditions (i.e. very low or hot temperatures) where the customer could engage most of the comfort features available (i.e. heated/cooled seats, heated steering wheel, max A/C, high cabin blower speeds) to adjust the cabin environment. However, when the cabin set temperature is achieved or the customer pre-set conditions are met, the operation of those features is minimised or switched off as they do not need to operate further, subject to customer preference.

4.4.3 Experimental testing method

Several parameters were measured and logged to support the statistical analysis:

- Fuel consumption in (ml),
- Fuel flow rate in ($ml.s^{-1}$),
- Vehicle and Engine speed in ($km.h^{-1}$) and (rpm) respectively,
- Engine coolant and ambient temperatures in degree Celsius,
- Alternator current output (A) and torque (Nm),

- Battery current (A) and voltage (V),
- Switching status of the electrical features of the vehicle.

Throughout the tests, fuel flow and total fuel consumption were compared with the vehicle speed and alternator current loading to determine the effect of the electrical energy on the fuel consumption as translated in CO_2 emissions in terms of $g.km^{-1}$ and ml in total fuel consumption. The tests were completed using environmental dynamometer chambers at an ambient temperature of 20^0C to minimise the impact of temperature.

Prior to the tests, all vehicles were 'normalised', driven until the normal operating temperature was reached for each type of engine. As many factors can affect the overall fuel consumption of a vehicle, as described in previous sections, prior to each test, all test vehicles had to:

- Soak in ambient temperature of 20^0C overnight ensuring normalised temperature across all mechanical and electrical parts of the vehicle.
- Prefill all testing vehicles to maximum fuel tank level prior to each test phase
- Test vehicles operated at a speed of 60mph for a minimum of 15 minutes prior to each session. This ensured that the engine operating temperature was achieved (i.e. engine coolant and transmission oil temperature elevated to normal operating levels) with the engine efficiency reaching thermodynamically normal operating levels with all components reaching stabilized operating conditions.

The test vehicles were controlled by a driver and a co-driver in the passenger seat monitoring logged data through CANape. For each different electrical loading level, four test repetitions were conducted on each vehicle and results were compared and analysed. Microsoft® Office Excel and MATLAB® were used for the data analysis. Equation (1) details the calculation of fuel flow rate values, denoted FF, where the flow rate is expressed in $ml.s^{-1}$ with the fuel consumption, denoted FC, in ml and the time, denoted t, in second.

$$FF=FC\times t \tag{4.1}$$

A flowchart of the test method conducted at this experiment including initial vehicle pre-run is shown in Figure 4.3. The data analysis method is presented in the next section followed by the experimental results.

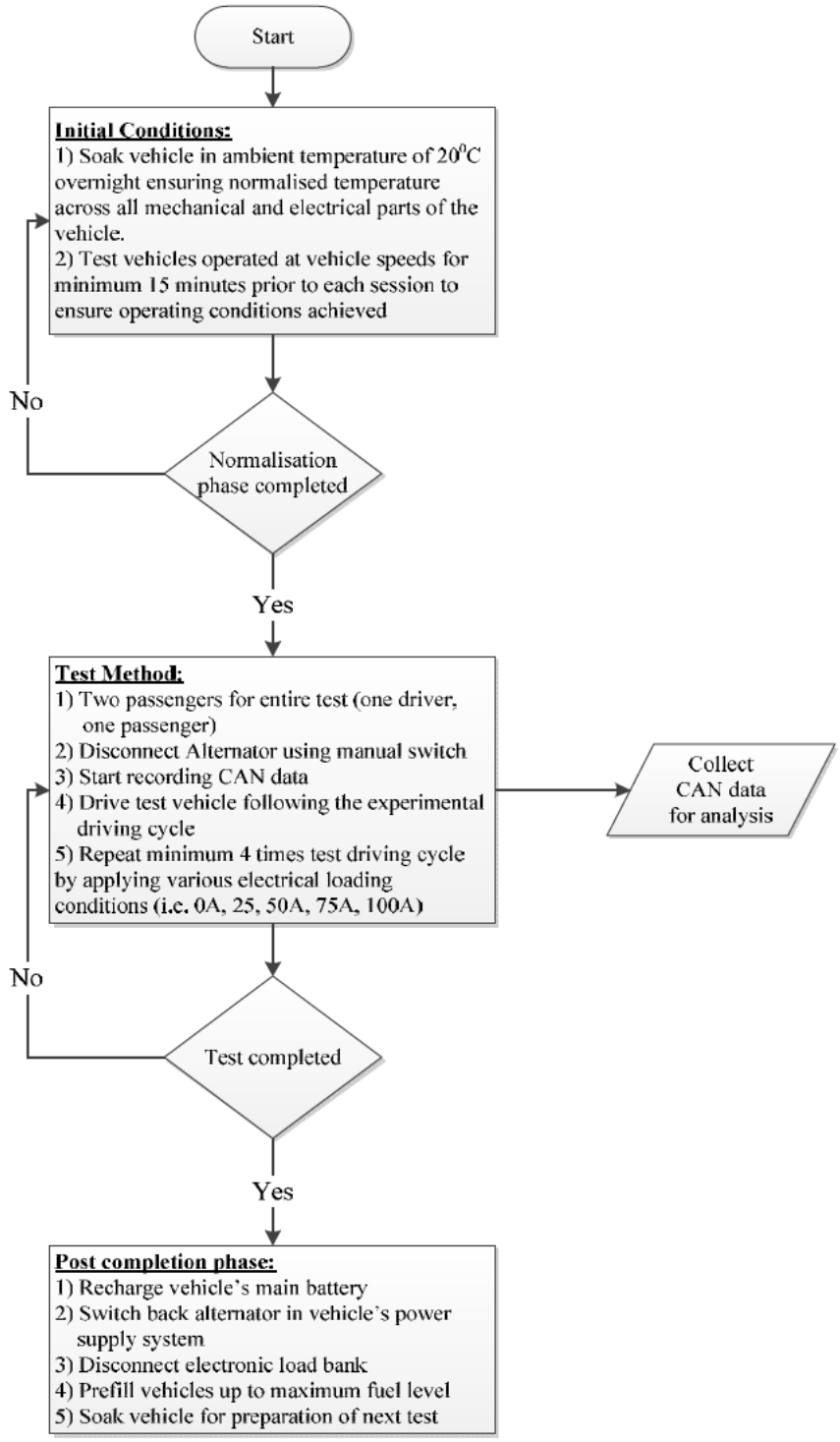

Figure 4.3. Flowchart showing the methodology outlining all major steps from start to end of the testing procedure.

4.4.5 Statistical analysis

To minimise the impact of the engine and vehicle speed variability to reach the desired steady-state speed, the effect of the electrical energy on fuel emissions was only being investigated during the steady-state speed phases and not during acceleration or deceleration between phases. All available test data obtained from all test vehicles in the dynamometer chamber test sessions were compared. The test data collected are independent samples collected multiple times from different types of vehicles (i.e. SUV, large saloons), and different types of engines (i.e. series, V-type) including petrol and diesel fuelled over the proposed experimental driving cycle described in Figure 4.2. The analysis used in this experimental work is based on descriptive and inferential statistics. The analysis of data broadly consists of two phases: (1) an exploratory phase, in which measures of central tendency using box plots, histograms, Confidence Interval (CI) for the mean and standard deviation are calculated and graphed and (2) an inferential phase, in which based on the population sample the most significant characteristics were identified and hypotheses about the relationship between them presented. It is believed that this test procedure and its resulting analysis will serve as a guideline for future tests of this nature, highlighting the important findings to consider in subsequent experiments.

4.5 Analysis of experimental results

4.5.1 Electrical loading test under controlled conditions

Figures 4.4 and 4.5 illustrates typical engine and vehicle speed variations over the experimental driving cycle as taken from one of the test vehicles (i.e. SUV V8 diesel). It can be seen, that both engine and vehicle speeds vary over the drive cycle and within each two minutes period where the vehicle and engine speed should be constant.

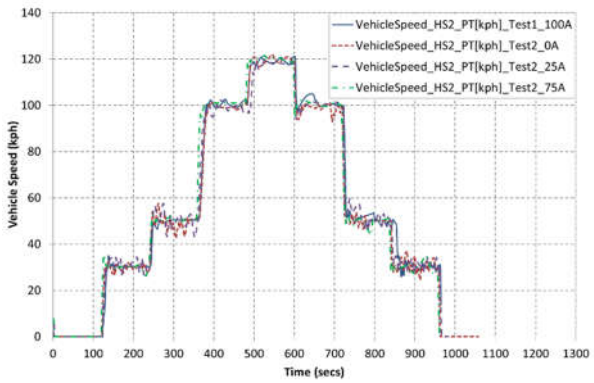

Figure 4.4. Vehicle speed profile variation during experimental driving cycle

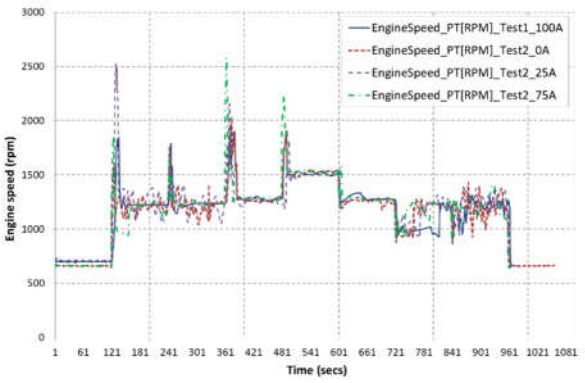

Figure 4.5. Engine speed profile variation during experimental driving cycle

The effects of engine speed variations on the overall fuel consumption can be analysed by investigating the mean values and their errors achieved for different electrical loading levels. Figure 4.6 illustrates interval plots of the engine speed and its means achieved for all test vehicles. By observing the engine speed variation for all types of vehicles, it can be concluded that engine speed varied in the range of 0-45rpm (i.e. min, max) for series type engine vehicles while 0-75rpm for V type engine vehicles. The variation seen cannot be a variable factor to the overall fuel consumption levels achieved for each vehicle.

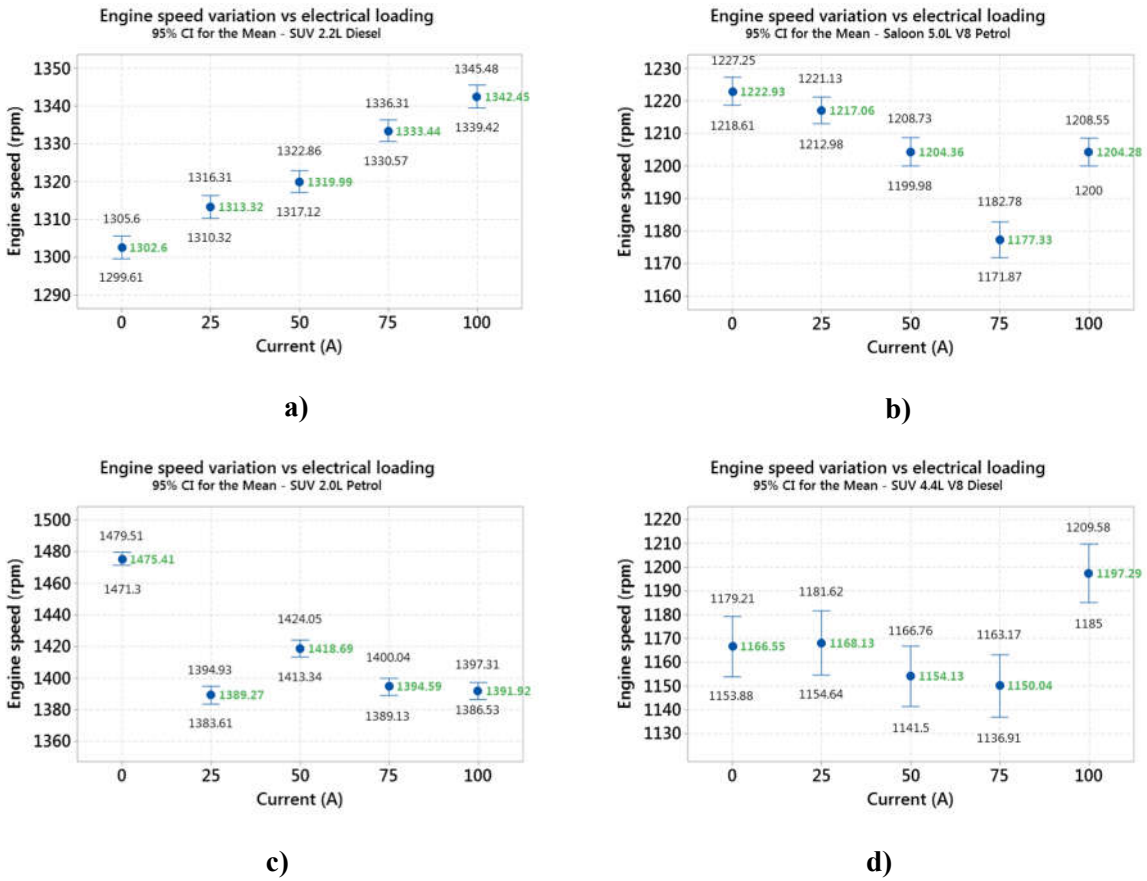

Figure 4.6. Mean and 95% confidence interval for engine speed across electrical loading range for a) SUV 2.2L Diesel, b) SUV 2.0L Petrol, c) SUV 4.4L V8 Diesel, d) Saloon 5.0L V8 Diesel

4.5.2 Fuel consumption and electrical loading

The relationship between electrical loading and fuel consumption was studied by considering both the overall fuel consumption and the fuel flow rate for each drive cycle and for each type of vehicle. Figure 4.7 illustrates the mean and media variation for each type of vehicle across the range of 0A to 100A. Highlighted in red the median values and in black the mean values for each test and vehicle type. It can be seen, that the overall data measured from the V-type engines show smaller levels of variation

in comparison to the smaller in-series engines. Particularly for SUV 2.2L diesel, the data across the range indicate larger variation with median values closer to the upper most positive quartile. Data distribution for the SUV 2.0L petrol is different from all the other types, particularly in the area of 50A electrical loading, which seems to have the largest impact on the total fuel consumption.

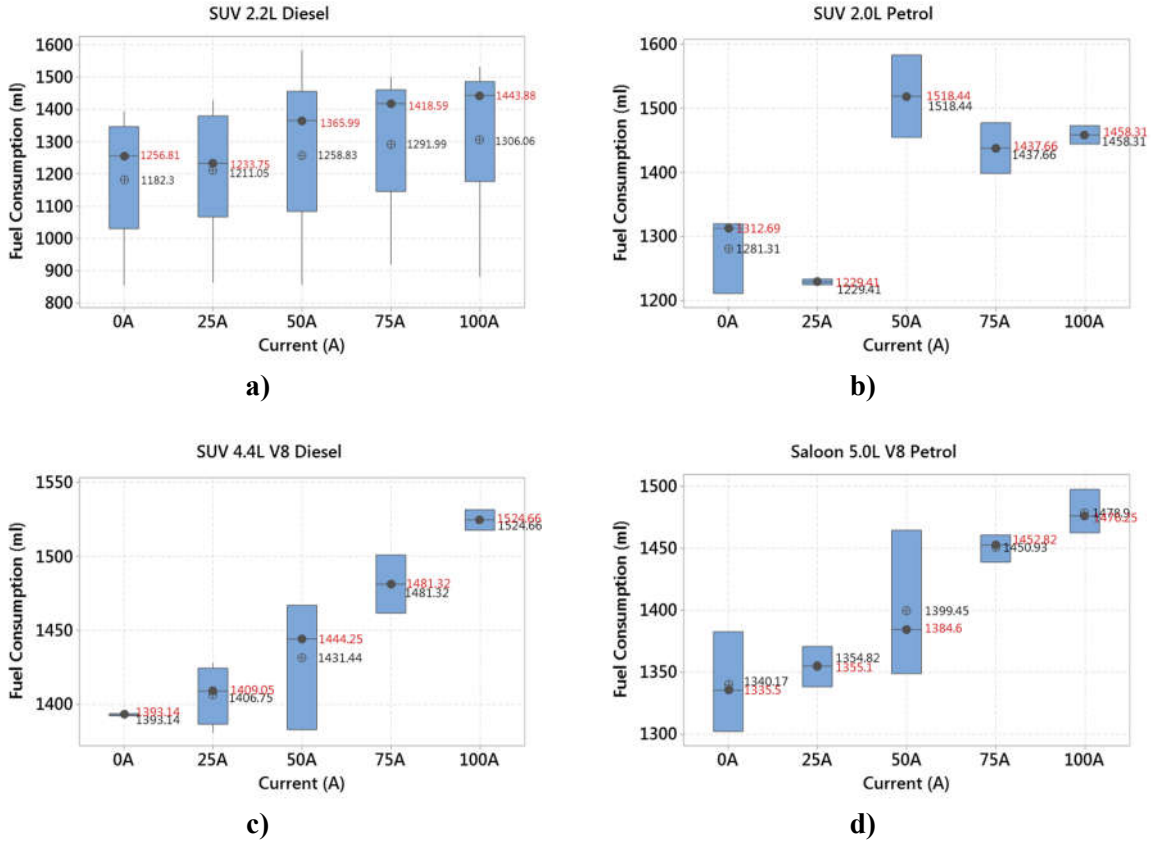

Figure 4.7. Fuel Consumption, given in terms of mean '⊕', median '•' and standard deviation for each vehicle at five different electrical loading conditions for a) SUV 2.2L Diesel, b) SUV 2.0L Petrol, c) SUV 4.4L V8 Diesel, d) Saloon 5.0L V8 Petrol

The effects of electrical loading on the overall fuel emissions can be analysed by investigating the impact on fuel flow rates for different electrical loading levels and compare those with the overall fuel consumption achieved for those levels.

Figure 4.8 illustrates interval plots of the fuel flow rates and its means achieved for SUV 4.4L V8 Diesel and the Saloon V8 respectively on different electrical loading levels (i.e. 0A to 100A). Our interval plots show 95% confidence interval for the mean of fuel flow rates and its spreads. The results of the SUV 2.0L petrol vehicle immediately deviate from the rest three vehicles. The effect of 50A electrical loading comparing to 0A is significantly high and reaches approximately 11% higher than the figure with no electrical loading applied to the engine. This result is subject to further investigation in order to understand the impact of the alternator loading on this particular engine and vehicle type. For the rest of the test vehicles, fuel flow rates are distributed across the full range of electrical loading in a

similar pattern with small deviations. Fuel flow rates are significantly higher, in the range of 10% (Saloon 5.0L V8 petrol) to 16% (SUV V8 Diesel), when 100A applied to the engine comparing to that of 0A. It can be that on both Saloon 5.0L V8 petrol and SUV 2.2L Diesel vehicles when high electrical loading (i.e. higher than 50A) is applied, fuel flow rates intervals achieved do not overlap with them below 50A as per SUV 4.4L V8D, an indication that high electrical loading on those engines has a much greater effect than the rest of the vehicles.

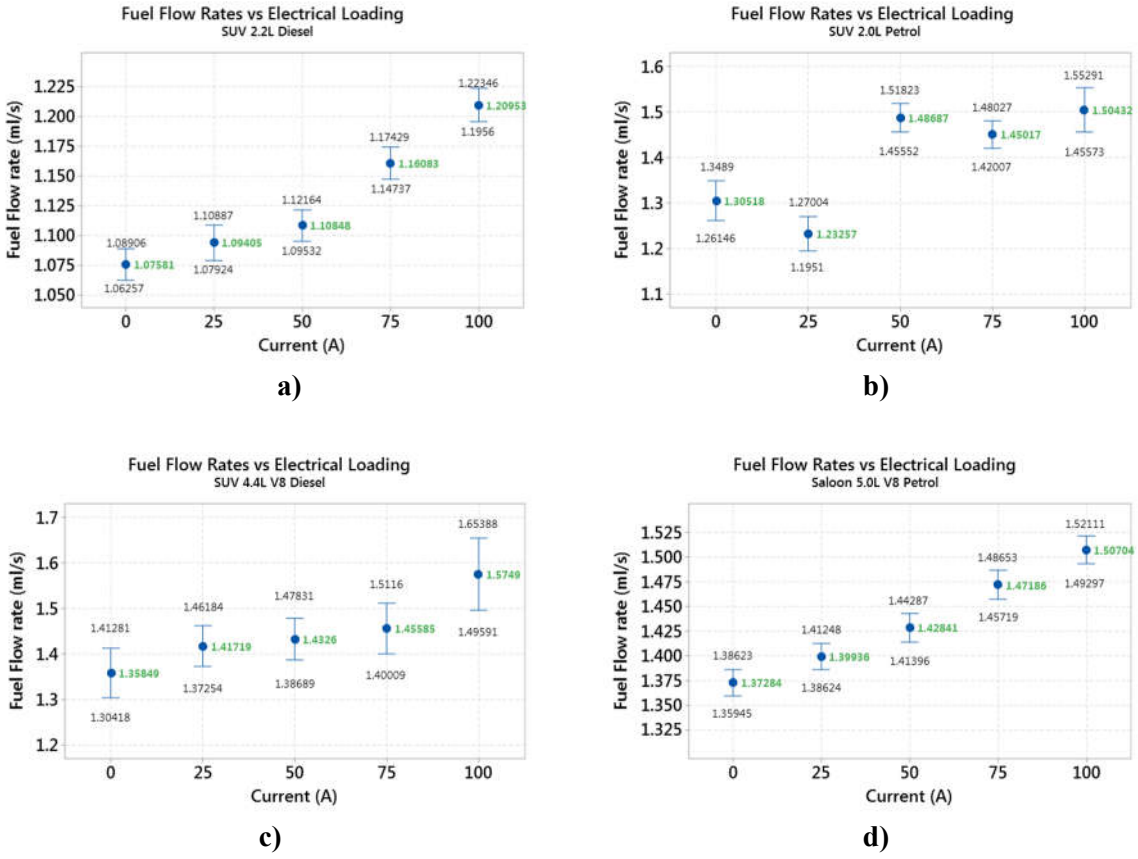

Figure 4.8. Mean and 95% confidence interval for the fuel flow rates across electrical loading range for a) SUV 2.2L Diesel, b) SUV 2.0L Petrol, c) SUV 4.4L V8 Diesel, d) Saloon 5.0L V8 Diesel

Increasing the electrical load applied throughout the experimental driving cycle from 0A to 100A increased fuel consumption by 12.1%, 13.81%, 10.35% and 9.44% for a SUV 2.2L Diesel, a SUV 2.0L petrol, a Saloon 5.0L V8 petrol and a SUV 4.4L V8D, respectively, as shown in Figure 4.9.

The impact of electrical loading to large capacity engines in V arrangement was found to be smaller than that for smaller capacity engines in series. By contrast, the difference between 0A and 25A for each vehicle was only 0.97% for the SUV 4.4L V8D but reached 1.93% for the SUV 2.2L D. The SUV 2.0L Petrol exhibited higher than expected fuel consumption increase when 50A was applied, it is subject for further investigation.

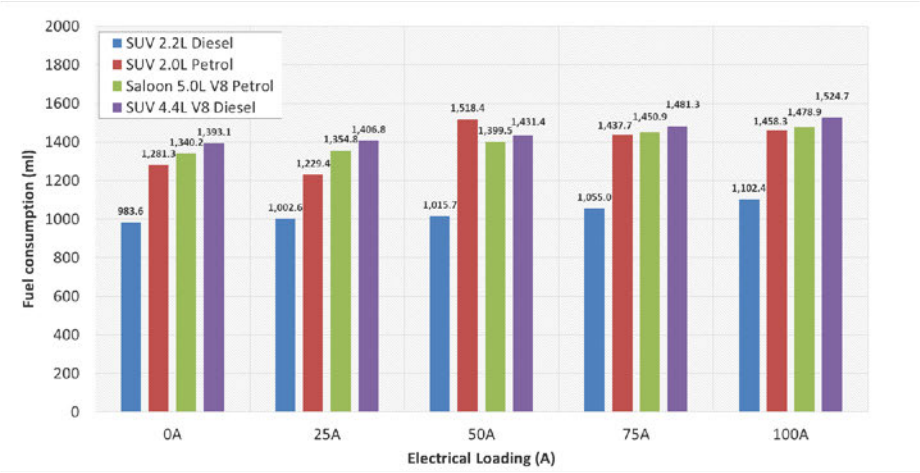

Figure 4.9. Average fuel consumption comparison in ml of fuel for each vehicle at different electrical loading conditions

Figure 4.10 depicts the fuel consumption distribution displayed graphically in a histogram. The data range is approximately 700ml with no indicated outliers. The distribution is represented by two groups, one group including 0A and 25A variables which have similar concentration areas as confirmed by their mean values with a 2.45% difference between them. The load levels 50A, 75A and 100A form a second modal on the distribution around the 1500ml point. This indicates that electrical loading conditions above 25A have a significant impact on fuel consumption from 6.5% to 11% higher compared to the 0A electrical conditions.

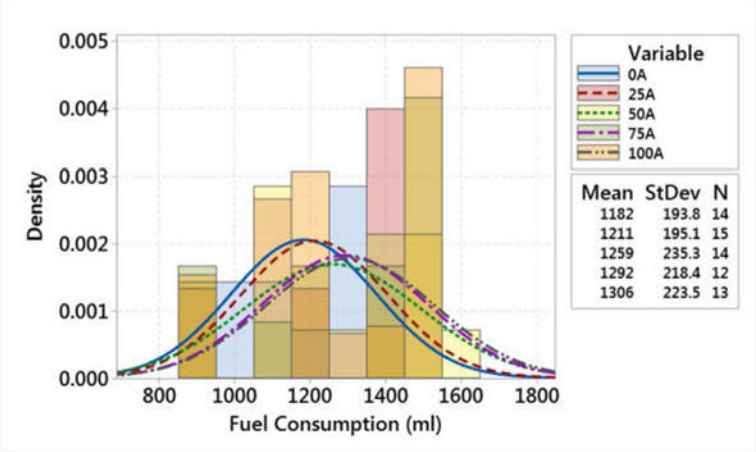

Figure 4.10. Histogram distribution comparison for each vehicle at different electrical loading condition

4.5.3 Alternator torque as a function of electrical loading

Alternator torque variation plays a significant role in each vehicle tested and its fuel consumption levels. Table 4.3 illustrates alternator torque values achieved for each type of test vehicles used in this experiment.

It is clear that torque distribution for our test vehicles presents a similar pattern with an increasing non-linear behaviour across the electrical loading range. On both SUV V8 Diesel and Saloon V8 Petrol vehicles, torque distributions followed a similar non-linear pattern with the latter reporting higher torque values comparing to the rest of the test vehicles. Similarly, both SUVs with 2.2L and 2.0L engines respectively achieved similar torque levels across the electrical range with the latter achieving a higher than expected final value while 100A electrical load applied to the system.

Vehicle Type	0A	25A	50A	75A	100A
SUV 2.2L Diesel	1.314±0.010	4.655±0.010	6.535±0.018	9.654±0.021	9.815±0.034
SUV 2.0L Petrol	3.195±0.012	5.006±0.034	6.824±0.043	10.583±0.068	14.096±0.094
SUV 4.4L Diesel	1.643±0.072	2.115±0.098	6.030±0.136	9.478±0.240	12.178±0.298
Saloon 5.0L Petrol	1.748±0.009	4.342±0.023	8.146±0.032	12.817±0.054	17.468±0.043

Table 4.3. Torque mean values (in Nm) with 95% confidence interval across the electrical loading range

4.5.4 Fuel flow rates as a function of electrical loading during idle conditions

A comparative analysis of fuel consumption translated as fuel flow rate when the vehicle enters engine idle operation, therefore vehicle standstill, is presented in this section. During this period, vehicle engine's fuel consumption is only used to support engine operation and any other associated electrical and mechanical features however the vehicle consumes fuel without any distance being driven. Any increase in the percentage of the idling period is in the direction of a higher fuel consumption rate that impacts the overall economy of any automobile. Today's vehicles have incorporated associated systems (i.e. stop/start) to help overall fuel economy and minimise the impact of fuel consumption when the vehicle is on prolonged standstill periods. During our experiment, stop/start functionality was deselected allowing the vehicle's engine to operate when the vehicle was brought to idle.

Figure 4.11 presents a summary of the fuel flow rate as a function of alternator loading for all vehicle types used in our investigation. Comparing the results between the SUV 2.2L Diesel and the SUV 2.0L Petrol shows that both vehicles experience similar increases in fuel consumption due to increased

loading at idle. The mean difference of fuel flow rate for the SUV diesel from 0A to 100A was 35% while for the petrol was approximately 41.3%. However, fuel flow rate percentage differences for the Saloon V8 petrol was 23% and a remarkable 70% increase on the SUV V8 diesel. Finally, comparing all four types of vehicles, the V8 Petrol saloon had the highest fuel flow rate across the whole electrical loading range as well as some specific variation on 100A range. The variation of the effect of electrical loading on the engine depends on the type of engine due to its inertia, load balance under transient condition and susceptibility to alternator torque applied to meet the electrical loading. In Figure 4.11d for example, increasing the electrical load from 75A to 100A had less impact on the fuel flow rate than the 75A limit. This behaviour can be explained by taking into account the torque output provided by the alternator and how it varied with the electrical load. In addition, the engine calibration process was incomplete on this particular prototype vehicle which played a significant role in the overall operation of the engine and its fuel consumption to parasitic loads. The relationship of alternator torque output and the effect of this on different types of engines are subject of further investigation.

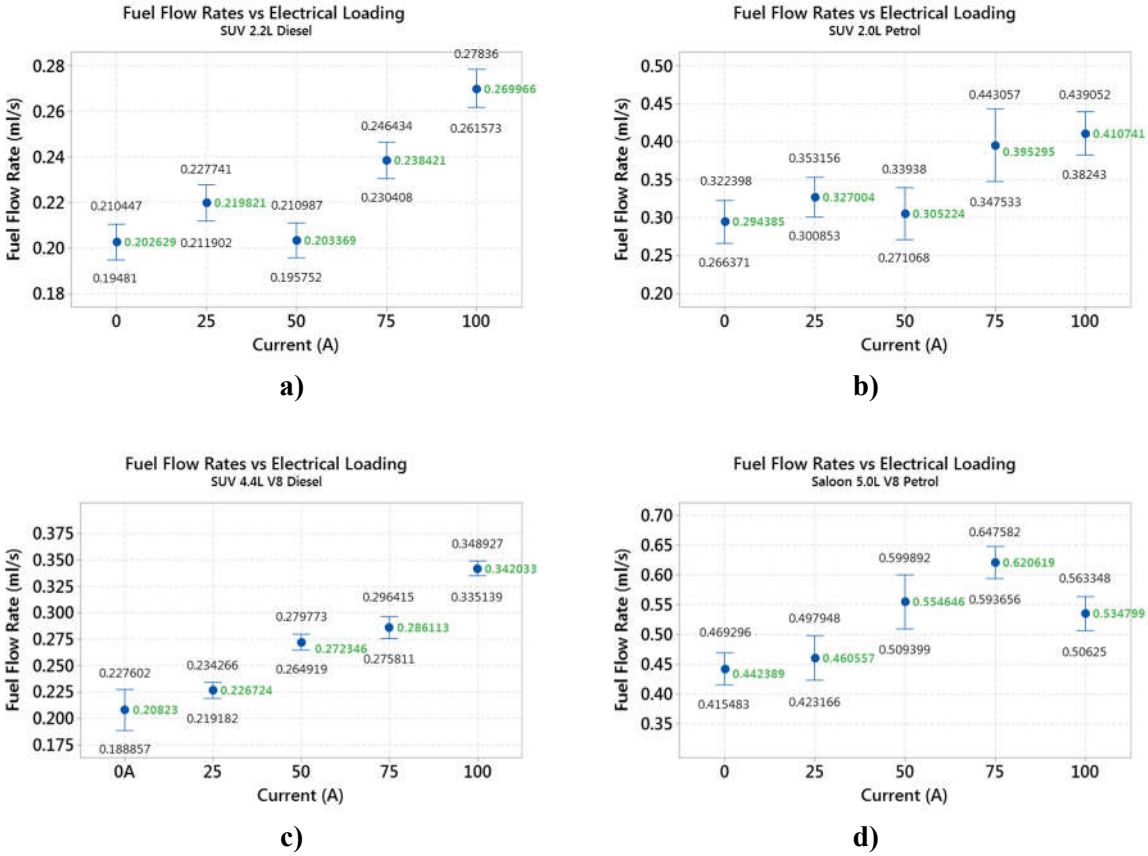

Figure 4.11. Mean and 95% confidence interval for the fuel flow rates during idle for a) SUV 2.2L Diesel, b) SUV 2.0L Petrol, c) SUV 4.4L V8 Diesel, d) Saloon 5.0L V8 Diesel

4.5.5 Fuel emissions CO_2 as a function of electrical loading

This section analyses the measured impact electrical loading result on vehicle's fuel emissions across the full range as defined by our experiment. Our experimental results showing that as fuel consumption is strongly associated with fuel emissions, electrical loading impacts as a result overall fuel emission figures.

Figure 4.12 presents a summary of the overall fuel emissions achieved as a function of electrical loading for all vehicle types used in our investigation. Comparing the results between the SUV 2.2L Diesel and the SUV 2.0L Petrol shows that both vehicles experience similar increases in fuel consumption however the results achieved on the SUV 2.0L Petrol are more variable between 25A and 75A range. For the SUV 2.2L Diesel, the impact of 100A on the overall emissions was 13.54% and that of the SUV 2.0L Petrol 26.3%.

Furthermore, comparing the V-type engine vehicles, the impact of the alternator loading on the overall fuel emissions achieved was lower than that of the series type engines with 9.77% for the SUV 4.4L V8 and 11.2% for the Saloon 5.0L Petrol V8.

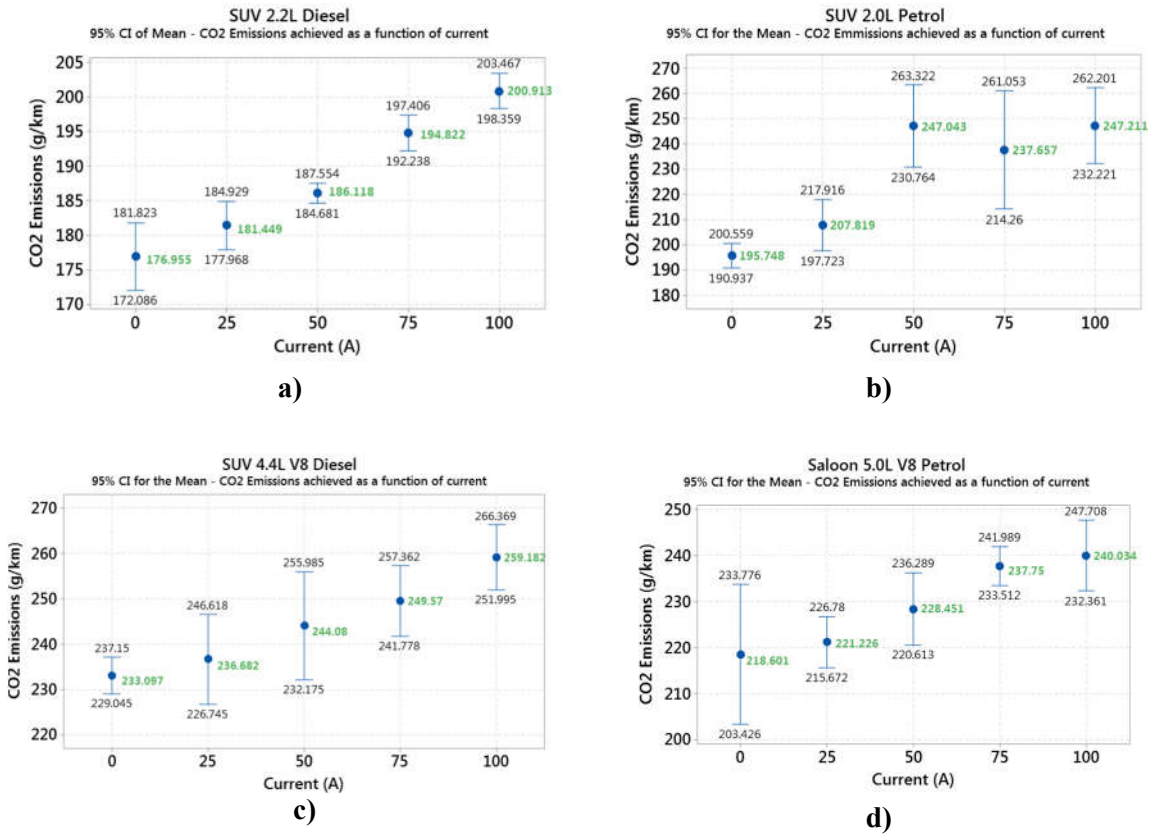

Figure 4.12. Mean and 95% confidence interval for the CO2 emissions over the drive cycle a) SUV 2.2L Diesel, b) SUV 2.0L Petrol, c) SUV 4.4L V8 Diesel, d) Saloon 5.0L V8 Diesel

Figure 4.13 provides a comparison of fuel consumption in gr.km^{-1} as a function of electrical loading for each electrical load step taken during the overall experiment. The points on graphs represent the difference in fuel emissions when comparing different electrical loading levels (i.e. 0A-25A, 25A-50A). Comparing the results between the SUV 2.2L Diesel and the SUV 2.0L Petrol, the impact of electrical energy on the petrol vehicle is more variable compared to that of the diesel vehicle. In addition, between the two fuel type variants, petrol and diesel, the effect of electrical energy on petrol vehicles was higher than that of the diesel variants.

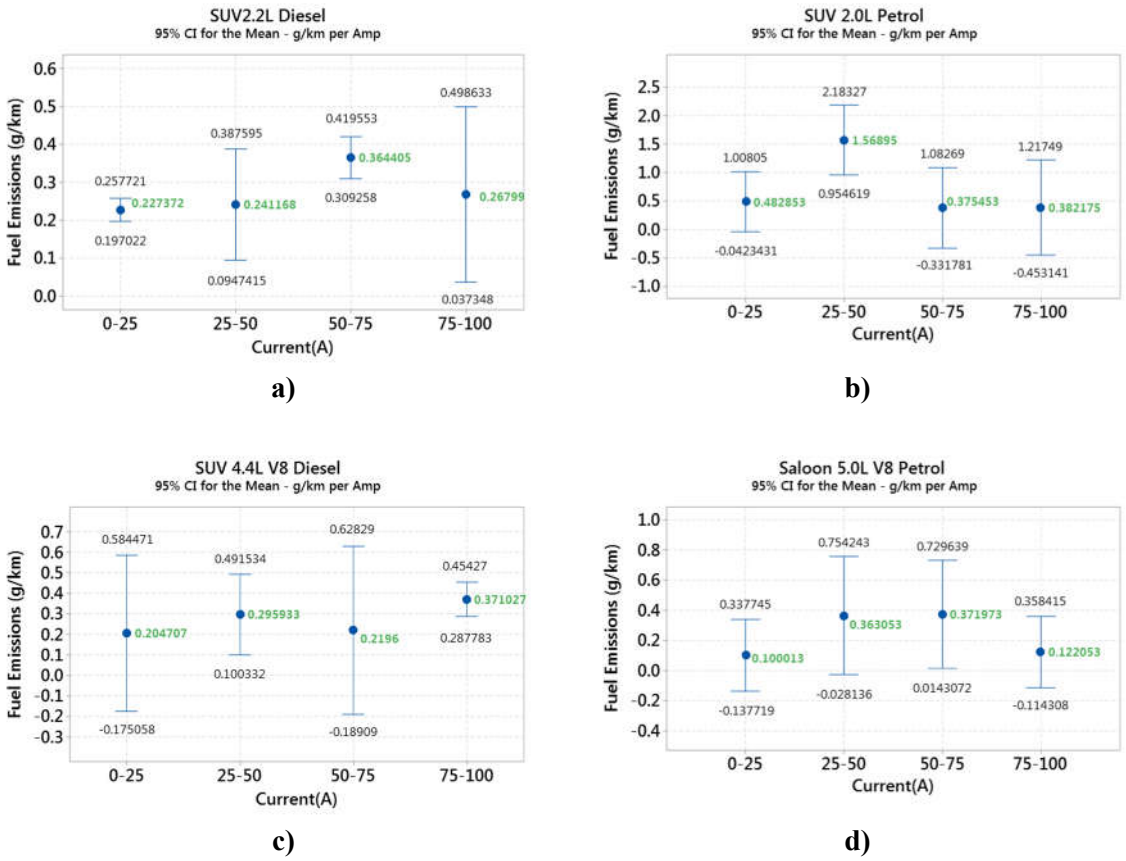

Figure 4.13. Mean and 95% confidence interval for g.km^{-1}.A^{-1} emissions over the drive cycle for a) SUV 2.2L Diesel, b) SUV 2.0L Petrol, c) SUV 4.4L V8 Diesel and d) Saloon 5.0L V8 Diesel.

Figure 4.13a shows the variation of the electrical energy effect on the achieved g.km^{-1} of CO_2 during testing. The effect of the first 25A on CO_2 is smaller than the next steps on 50A and 75A while again decreased from 75A to a maximum value of 100A. Similarly, Figure 4.13b shows a similar variation of the electrical energy effect on the achieved g.km^{-1}of CO_2 during testing. The effect of the first 25A on CO_2 is lower than that on vehicle used in Figure 4.13a while for the next steps of 25A applied of electrical loading (50A, 75A, 100A), the effect is higher than the vehicle shown in Figure 4.13a. For electrical loading levels between 75A and 100A, the impact of electrical energy on the overall emissions is significant comparing to the vehicle shown in Figure 4.13a with final values for 75A of 0.3719 g.km^{-1}.A^{-1} comparing to 0.2196 g.km^{-1}.A^{-1} for SUV V8 Diesel. However, the contribution of 100A electrical

loading to the Saloon's V8 Petrol emissions was lower than SUV's 4.4L V8 Diesel, estimated at 0.1220 $g.km^{-1}.A^{-1}$.

Figures 4.13c and 4.13d show again the effect of electrical energy on the achieved $g.km^{-1}$ of CO_2 during testing with a vehicle with a V-type engine. Comparing the results between the SUV 4.4L V8 Diesel and the Saloon 5.0L V8 Petrol, the impact of electrical energy on the petrol vehicle is more variable compared to that of the diesel vehicle. The effect of the first 25A applied on CO_2 for the petrol vehicle used as shown in Figure 4.13d is higher than that on the diesel V8 as shown in Figure 4.13c. Similarly, for the next steps of 25A applied of electrical loading (50A, 75A, 100A), the Saloon 5.0L V8 petrol achieved more variable results than that of the diesel as shown in Figure 4.13a. In particular, the effect of electrical loading to the $g.km^{-1}.A^{-1}$ achieved between 25A and 75A was estimated at 0.36 - 0.37 $g.km^{-1}.A^{-1}$ while between 75A and 100A, the effect was lower reaching 0.09 $g.km^{-1}.A^{-1}$.

Vehicle Type	0-25A	25-50A	50-75A	75-100A
SUV 2.2L Diesel	0.227±0.030	0.241±0.146	0.364±0.055	0.268±0.231
SUV 2.0L Petrol	0.483±0.525	1.569±0.614	0.375±0.707	0.382±0.835
SUV 4.4L Diesel	0.143±0.585	0.296±0.196	0.219±0.408	0.371±0.083
Saloon 5.0L Petrol	0.100±0.237	0.363±0.391	0.372±0.358	0.091±0.341

Table 4.4. Impact of electrical loading on fuel consumption in per $g.km^{-1}.A^{-1}$ - mean values with 95% confidence interval across the electrical loading range

Table 4.4 presents all results for all test conditions. Finally, by analysing all experimental measurements, in a histogram form, Figure 4.14 illustrates the overall distribution of $g.km^{-1}.A^{-1}$ for each vehicle and a comparison between diesel and petrol engines respectively.

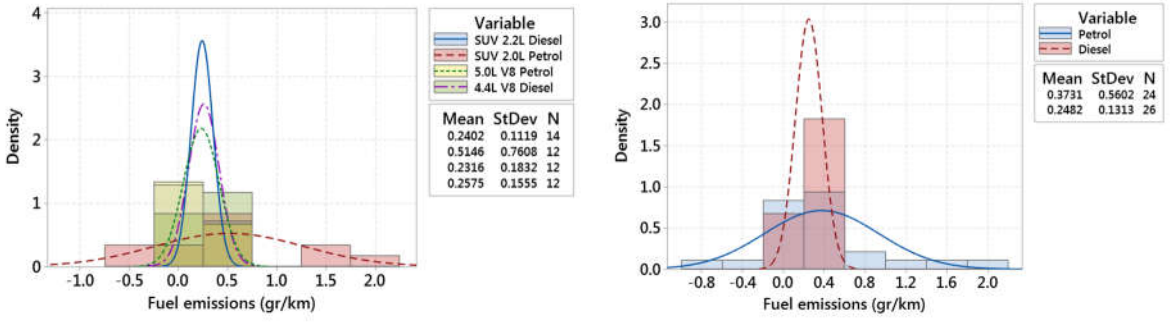

a) **b)**

Figure 4.14. Overall distribution of $g.km^{-1}.A^{-1}$ emissions achieved for a) all vehicle variants, b) between petrol and diesel variants

The calculated mean value achieved on diesel engine variants as shown is 0.2482 $g.km^{-1}.A^{-1}$ and that of the petrol engines is 0.3731 $g.km^{-1}.A^{-1}$ assuming that alternator loading is applied linearly in the range of 0A to 100A.

For our simulation studies, the mean value of 0.2482 $g.km^{-1}.A^{-1}$ will be used to derive the fuel consumption index (FCI), an input to the Electrical Energy Management System (EEMS). EEMS will be fully described and assessed in Chapter 6.

Additionally, by analysing the interval plots of the mean values of fuel flow rates, as statistically calculated for SUV 4.4L V8 Diesel (Figure 4.8), a polynomial fit has been derived to provide the contribution of electrical energy to fuel consumption in ml. The equation is as follows:

$$F = 0.00001I^2 + 0.0002I + 0.0012 \quad (4.2)$$

where F is fuel consumption in *ml* and I is electrical current in Amps.

Equation 4.1 will be used as part of the EEMS assessment in Chapter 6, demonstrating the benefits of the developed energy management system on vehicle's fuel savings.

4.6 Real world driving cycle analysis

A series of real world recordings have been conducted using one of the testing vehicles in order to understand the impact of electrical energy on vehicle's CO2 emissions under real world driving scenarios. For the purpose of this investigation, a typical commuting route, as shown on Figure 4.15, was chosen while different customer usage scenarios were also included as part of the customer naturalisation factor that adds variation to the overall results. Different electrical loading scenarios included:

- Comfort features/electrical loads switched On/Off based on personal preferences.
- The AC compressor was switched on/off, where possible, in order to include a variation factor of AC on fuel consumption impact.
- Several journeys were conducted with the alternator completely off (i.e. switched Off using software manipulation) in order to measure total vehicle fuel consumption performance excluding the effect of ancillary electrical loading.

One of the major objectives in conducting real world driving cycle analysis is to assess vehicle performance in terms of fuel consumption based on electrical loading variation caused by customer input. The purpose of this investigation was to correlate the experimental results measured by using environmental chambers and manually controlling total electrical loading applied to the alternator, and

that of real world performance with alternator loading variations based on customer input patterns as per normal vehicle operation. Conclusions drawn by this comparative analysis will be used as part of the development of vehicle's supervisory electrical energy management system.

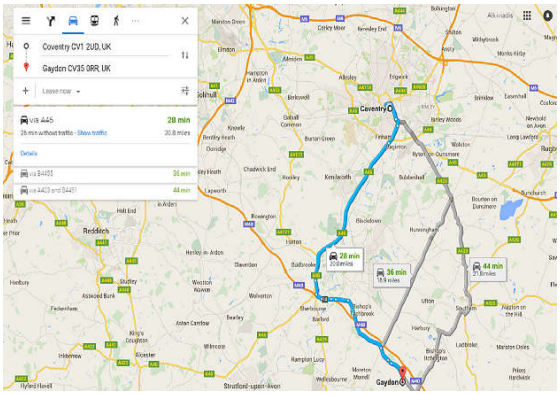

Figure 4.15. A typical return journey from Coventry to Gaydon, typically 21miles each way.

4.6.1 Analysis of real world experimental results

The vehicle used during real world driving conditions was SUV 2.2L Diesel. The impact of electrical loading on fuel consumption and emission levels have been estimated using vehicle collected from a total of 115 journeys. Figure 4.16a illustrates vehicle emissions data which have been clustered into three categories: one with the lowest CO_2 emissions achieved when the alternator was switched Off diagnostically, a second one with data with higher CO_2 emissions achieved as a function of higher electrical loading supported by the alternator and finally a third category with the highest CO_2 emissions achieved due to high electrical loading between 75A to 115A. For the first cluster, the alternator was switched off via software. In this mode, vehicle's electrical power supply system was supported by the battery and ultracapacitor. Figure 4.16b illustrates the variation of the achieved CO_2 emissions as a function of alternator's electrical loading output including a regression linear fit to the overall data.

A further analysis has been conducted on the sample of data (i.e. 115 return journeys) as illustrated in Appendix G. Figure 4.17 represents an interval plot with the mean value achieved based on the overall data recorded. The mean value of 0.2918 $g.km^{-1}.A^{-1}$

The impact of alternator electrical loading on the overall CO_2 emissions is summarised in Figures 4.17 and 4.18. The mean value achieved is 0.298 $g.km^{-1}.A^{-1}$, as shown in Figure 4.17. This value is close enough to the mean value achieved from vehicle testing using the dynamometer chambers. However, real world driving conditions introduce variability (i.e. aerodynamics, road friction, engine speed/vehicle speed) which contributes to the overall result. Figure 4.18 presents the result with more details on the spread. Analysing the distribution in detail, we can observe two outliers with a set of data

far away from the rest of the sample. The data represent a driving commuting route different from the one above due to unforeseen circumstances (i.e. road diversions due to roadworks) however all data have been included to the overall completeness of this study.

a)

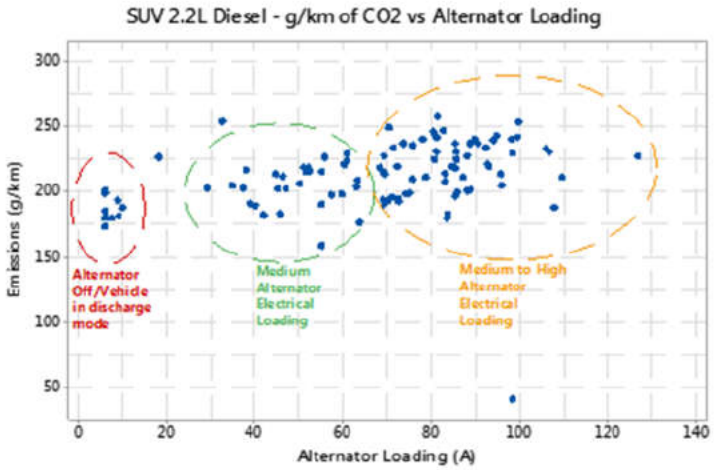

b)

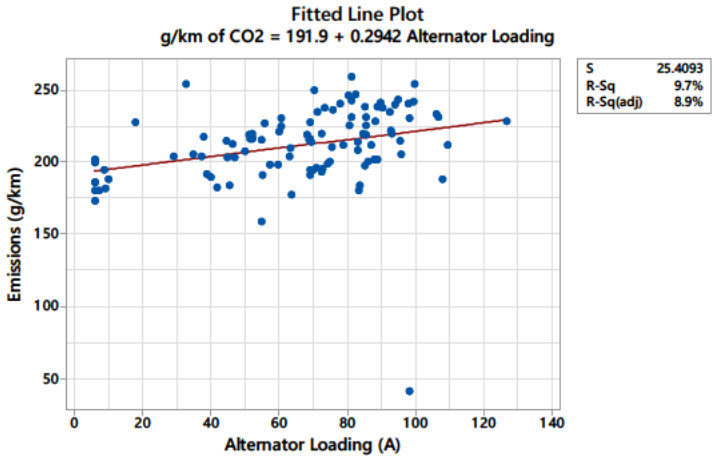

Figure 4.16. a) Vehicle emissions g.km^{-1} clustered in 3 groups based on alternator electrical loading levels. b) Fitted line (linear) based on overall data

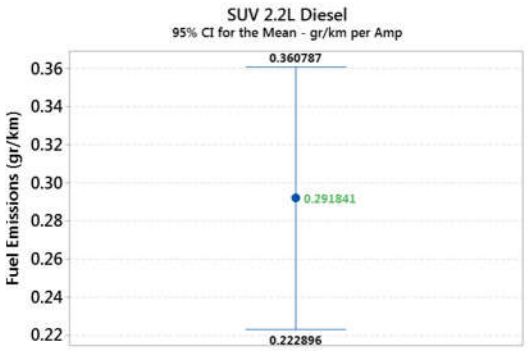

Figure 4.17. Mean of vehicle emissions g.km^{-1} achieved as a function of electrical loading

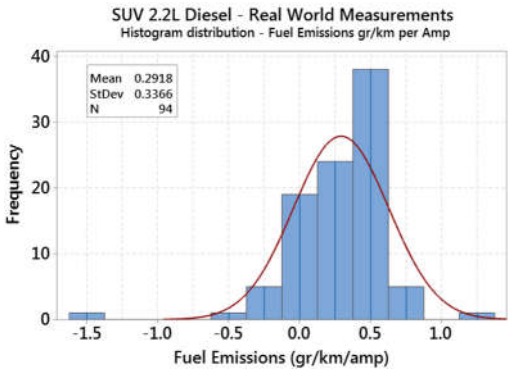

Figure 4.18. Histogram distribution of fuel emissions achieved as a function of electrical loading

4.7 Summary

This Chapter has proposed a unique experimental methodology to analyse and model the impact of the operation of electrical features/loads onto both petrol and diesel vehicles' fuel consumption levels and translated into g.km^{-1}.A^{-1}. Experimental data were obtained from both a new proposed driving cycle applied to test vehicles using dynamometer chambers and driving under real world driving conditions using a typical commuting route between Coventry, UK and Gaydon, UK.

Vehicles' fuel consumption, fuel flow rates and fuel emissions were analysed using descriptive and inferential statistics under different electrical loading conditions applied to the test vehicles by an external electronic programmable load bank.

It was found that duty cycle variations in electrical energy usage, due to customer's input or vehicle's systems operation, could significantly affect the vehicle's overall performance in terms of fuel consumption.

By analysing overall results on fuel flow rates achieved, indicated that the rate distribution across the full range of electrical loading is projected in a similar pattern with small deviations for all test vehicles except for the SUV 2.0L petrol. By applying an electrical load of 100A to both V-type engine vehicles, fuel flow rates increased as much as 10% and 16% respectively for petrol and diesel. In vehicles with engines in series, applying a 100A load results in 15% and 12% for petrol and diesel, respectively. The vehicle with the greatest effect on fuel flow rate due to high electrical loading conditions was the SUV 4.4L V8 diesel.

It was observed that, when the engine is at idle, the fuel flow rate increased almost linearly with an increase in current loading. In addition, applying a high load current of 100A when vehicle is idling, results in a very significant fuel flow rate increase (e.g. 70% higher for the SUV V8 diesel). The V8

Petrol saloon type was also found to have the highest fuel flow rate across the whole electrical loading range.

By contrast, engines in series arrangement resulted in a lower fuel flow rate increase at 35% for both petrol and diesel.

Using the described experimental approach, the calculated mean value achieved on diesel engine variants was 0.2553 $g.km^{-1}.A^{-1}$ and that of the petrol engines was 0.4701 $g.km^{-1}.A^{-1}$ assuming that the alternator loading was applied linearly in the range of 0A to 100A. Furthermore, analysing all experimental data gathered from the real world driving, using one of the test vehicles (i.e. SUV 2.2L diesel), the mean value achieved was 0.2918 $g.km^{-1}.A^{-1}$. This value is similar compared to the results demonstrated from the vehicles tested using dynamometer chambers. Future analysis will include testing the rest of the test vehicles using a dynamic electrical loading profile applied to the vehicle's power supply system and compare its emissions under real world conditions.

Quantifying the effect of electrical energy on the vehicle's fuel emissions allow the formulation of an electrical energy management strategy, presented in chapter 6, that will minimise the vehicle's alternator/generator output and control the operation of electrical loads/features in order to minimise its impact on fuel emissions and consumption.

Chapter 5

Vehicle power supply and electrical loading modelling

5.1 Introduction

This chapter describes the original simulation model developed to investigate the impact of new and innovative technologies used in a modern vehicle platform. A model is a simplified (often mathematical) description of a system (Hawkins and Allen, 1991), developed for a specific purpose. The challenge, when modelling a system for off-line modelling with a view to ultimately convert it into real time code for an online application, is to find a compromise, such that the model is sufficiently simple to be manageable, easy to integrate within vehicle's software system and complex enough to represent the required system states.

The proposed model is one of the contributions of this thesis due to its accuracy that has resulted from the exploitation of good quality data used to calibrate it. This model was also essential in developing the fuzzy management strategy proposed in Chapter 6.

The remainder of this Chapter is composed as follows. Section 5.2 presents the original MATLAB®/Simulink™ model, designed and implemented to simulate the vehicle's power supply system. The simulation model includes the battery model, an existing model developed using an impedance spectroscopy method (Karden et al. 2000), the alternator model, the associated 12V electrical loads/features which play a significant role in this work, the solar panel model and its operational strategy as it was integrated into the LEV project and finally the ultracapacitors model. The alternator, which plays a key role in this work, is modelled in Section 5.4. The vehicle's IOXUS ultracapacitors module was modelled based on the capacitance and resistance measurements carried out during the IOXUS cells performance characterisation, see section 5.5. Section 5.6 models the solar

panels as evaluated using the LEV. Section 5.7 describes the electrical loads that are required to be considered by the energy management system. Section 5.8 describes the verification and validation of the developed models as the complete software strategy is intended to be compiled into an application software downloadable to the vehicle's main power supply ECU.

5.2 Automotive vehicle battery modelling

This section starts with the definition of key parameters and states to be considered in the model including the state of charge (SoC), nominal capacity C_N, and effective capacity C. Battery state parameters most often used are the capacity and the SoC. SoC: is the charge level of the battery. For the definition of the SoC two descriptions exist, which define either the fully charged or the fully discharged state as a reference point. The latter definition is common, since the SoC is directly linked to the amount of charge that can be discharged from the battery at its current state without prior charging. From an electrochemical point of view, this definition is however not precise, since the discharged state of the battery cannot easily be defined. As an example, if the cut off voltage is reached during discharge, the voltage will re-raise after the current is switched Off. The influence of temperature and current on the discharge characteristic and thus on the SoC is the same as for the determination of the capacity (Bohlen 2008). For a valid SoC definition, both the discharge, denoted Q_{dch} and the capacity, denoted C, have to be specified:

- State of Charge $SoC\ (I,\ T)$: refers to the amount of charge $Q_{dch}\ (I,\ T)$ discharged at a given temperature T, current I and the actual capacity $C\ (I,\ T)$, where T and I are kept constant during the discharge. The units of SoC are percentage points (100% = full, 0% empty).
- Nominal capacity C_N: is the amount of charge that can be discharged from a fully charged battery until a certain cut-off voltage is reached. It is determined by the mass of active material contained in the battery and is dependent on the discharge rate, temperature and the state of health (SoH) of the cell (Bohlen 2008). Usually, nominal capacity is the capacity that a new battery should have after a full charge and discharged at nominal temperature and with the nominal current. Information about the capacity as a function of the discharge rate and temperature can often be found in battery data sheets. An empirical formula that describes the dependency of battery capacity on the discharge rate was proposed by Peukert as the well-known Peukert law (Linden 2001). The units of capacity are Ampere-Hour (Ah). The exact actual battery capacity can only be determined by a complete discharge of the battery. Naturally, this is an unsuitable procedure for battery monitoring in most applications.
- Effective capacity $C\ (I,\ T)$: is the level of actual available capacity the battery has after a full charge when it is discharged at a given current I and temperature T.

The above definitions hold for electrochemical double layer capacitors, however, they are rarely used. Instead, the capacitance in Farad is frequently used to characterise these devices.

5.2.1 Battery model equivalent circuit

As batteries are non-linear and highly dependent on parameters such as temperature, SoC and short term charging/discharging history, the implementation of a battery model with high precision on all environmental conditions is consequently impossible. Two key elements are required for real automotive applications, fast computing and small parameterization effort. This can be achieved by employing equivalent electrical-circuit models and representing physico-chemical processes by electrical components such as inductors, capacitors and resistors.

This physical-based model selected for this project was developed in the Institute of Current Rectification and Electrical Drives (ISEA) in collaboration with Ford in Aachen, Germany. The non-linear impedance of the battery was measured using an impedance spectroscopy method (Karden et al. 2000).

Impedance spectroscopy is a measurement method to determine the transfer function of a system in the frequency domain (Karden 2001). It is often convenient to describe the system behaviour in the frequency domain, since differential equations that describe the system in the time domain pass into simple linear equations in the frequency domain. The Fourier transform links the two domains and allows calculating the time response of a system from its frequency response and vice versa (Karden et al., 2001).

For electrical and electrochemical systems, the impedance $\underline{Z}(\omega)$ is equivalent to the transfer function with the current $\underline{I}(\omega)$ as the input and the voltage $\underline{U}(\omega)$ as the output signal. By imposing a sinusoidal current or voltage signal on the system and measuring the amplitude and phase shift of the output signal, the complex impedance for this frequency can be determined. The procedure is repeated for many frequencies in the range of interest in order to derive a continuous spectrum. One benefit of impedance spectroscopy is the fact that spectra measured on electrochemical systems can often be interpreted as the impedance spectra of lumped element models composed of the standard devices resistor, inductor and capacitor.

The appropriate equivalent-circuit model used for the battery model includes an internal resistance R_i, an inductance L, constant phase elements (CPE) consisting of a double layer capacitance, the charge transfer resistances R_{ct1} and R_{ct2}, the resistance R_{gas} of the gassing reactions, the equilibrium potential of the gassing reactions $U_{0,gassing}$, and the dc voltage of the battery cell $U_{0,cell}$. Finally, diffusion is

represented by the Warburg impedance Z_W as described by Karden et al. (2000); Karden (2001) and Bohlen (2008).

A parallel connection of a CPE element and a resistor is referred to as a ZARC element (see section 5.2.4). R_i, the internal resistance of the cell, is mainly determined by the conductivity of the electrolyte and the electrical pathway including poles, grid and active masses (Karden 2001; Karden et al. 2002). R_{ct} and CPE describe the transient behaviour, which is caused by the charge transfer reaction in combination with the double-layer capacitance at the surface of the electrodes. In addition, only one diffusion element is employed for the whole battery cell and finally, a parallel current path for the side reactions (i.e. gassing) which occur mainly during charging has been included. Figure 5.1 shows the equivalent circuit used for the interpretation of the measured impedance data:

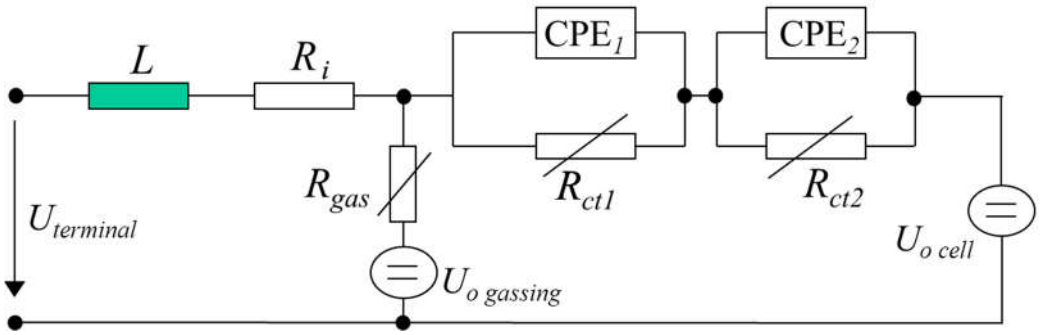

Figure 5.1. Equivalent circuit representation of the battery model

The initial battery model has been parameterised for a 36-volt absorptive glass matt (AGM) battery and nominal capacity of 27Ah (ISEA battery model manual 2002). The author has subsequently modified parameters to match the characteristics of a 12-volt AGM battery with a nominal capacity of 90Ah. This model has been used to simulate voltage responses during highly dynamic current profiles and during certain driving cycles and scenarios, such as combined suburban and city traffic cycles (CSCT), drive-idle- drive (DID) cycles and real world commuting drives (Pickering 2001).

5.2.2 Inductance and internal ohmic resistance

The inductance L of the battery was determined by a least-square fitting procedure from its high frequency impedance values (Karden 2001). The inductance is mainly caused by the geometry of the cell and, therefore, the inductance is regarded as independent from internal or external factors such as temperature and state of charge.

On all electrochemical storage devices, the resistance R_m of the metallic connectors and the metallic grid cause an ohmic voltage drop. R_m is generally linear and relatively insensitive to temperature and state of charge. Metallic conductors show a small positive temperature coefficient of resistance (Karden et al. 2002). Active masses and the electrolyte contribute to the overall resistance of the cell. While active masses contribute little to the cell resistance due to their high conductivity, the electrolyte contributes significantly to the resistance of the cell. The electrolyte resistance R_{el} is highly sensitive to temperature and electrolyte concentration and consequently to the state of charge (Karden 2001; Karden et al. 2002). For very low concentrations the electrolyte passes into pure water and the conductivity approaches very low values. For high concentrations the conductivity decreases again; the nominal electrolyte concentration of lead-acid batteries is close to the maximum of the conductivity. The dependencies of the internal ohmic resistance were determined from the impedance spectra at the corresponding conditions (Karden 2001; Karden et al. 2002).

From measurements on the complete cell, the contributions of conductors, active mass and electrolyte can hardly be distinguished and are therefore mostly subsumed to an internal series resistance $R_i = R_m + R_{am} + R_{el}$. The over potential due to R_i is:

$$\Delta U_i = R_i \cdot I \tag{5.1}$$

5.2.3 Charge transfer calculation

Charge transfer is characterised by a highly non-linear relationship which is given by the Butler-Volmer equation between the current density and the corresponding over potential. ΔU_{ct}:

$$j = j_0 \left[e^{\frac{\alpha n N_A e}{R_m T} \Delta U_{ct}} - e^{\frac{(1-\alpha) n N_A e}{R_m T} \Delta U_{ct}} \right] \tag{5.2}$$

A positive current density corresponds to charging, a negative to discharging. The factor j_0 is the exchange current density, n is the number of electrons involved in the chemical reaction, N_A is the Avogadro number, e is the elementary charge, R_m is the universal gas constant, T is the absolute temperature and α is a factor that defines the asymmetry with respect to charging and discharging (Karden, 2001; Bohlen, 2008).

5.2.4 ZARC elements

ZARC elements consist of RC circuits. Each RC circuit combines a resistance and a CPE element connected in parallel. ZARC elements are used to model a depression of capacitive semi-circles in the complex impedance domain (Karden 2001; Karden et al. 2002). Depression will always occur if the

relaxation time (or limiting frequency) is not single valued but distributed around a mean. Such distribution arises, among others, from the spatial extension of the electrode/electrolyte interface in rough or porous electrodes. Together with the non-linearity of the resistance of the main reaction (charge transfer) R_{ct} and the capacitance C_{dl}, this leads to a distribution of relaxation times:

$$\tau_0 = {\omega_0}^{-1} = R_{ct} C_{dl} \tag{5.3}$$

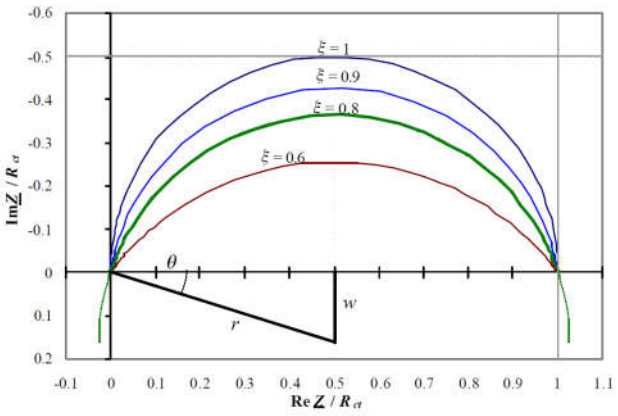

Figure 5.2. Complex-plane impedance diagram of the impedance of ZARC elements with different CPE exponents ξ.

Figure 5.2 shows depressed semicircles arising from ZARC elements with different CPE exponents (Karden 2001). All impedances are normalised to R_{ctm} . For ξ=0.8, the impedance arc can be regarded as part of a circle with radius $r > {R_{ctm}}/{2}$ and its center 'below' the real axis (positive imaginary coordinate). For a CPE exponent ξ=1 the CPE transforms into a normal capacitor:

$$\frac{1}{Z_{ZARC}} = \frac{1}{R_{ctm}} + A \cdot (i\omega)^{\xi} \text{ with } 0 < \xi < 1 \tag{5.4}$$

The three parameters which characterise the ZARC element (RA , and ξ) are determined from the measured impedance spectra. The non-linearity of both ZARC elements with current, as expressed by the non-linearity of the resistances R_1 and R_2 as well as the capacitive elements A_1 and A_2 have to be taken into account. The value of R_1 resistance has been determined by a least-square fitting algorithm from the measured impedance spectra and an approximation of a 'fit' equation of the current dependency given by:

$$R_1(I_{R1}) = \alpha + b \cdot \tanh(c \cdot (I_{R1} + d)) \tag{5.5}$$

The four new model parameters ($\alpha b c$ and d) are also determined by another least-square fitting procedure and represented in the model by a look-up table. The non-linearity of the R_2 resistance is also determined by another least-square fitting algorithm from the impedance measurements of the whole battery and shows typical Butler-Volmer behaviour as described at 5.3.2.

The non-linearity of the capacitive elements A_1 and A_2 is described by (ISEA battery manual, 2002) and equals to:

$$A_1 = e \cdot R_1^{(\xi-1)} \text{ and } A_2 = e \cdot R_2^{(\xi-1)} \tag{5.6}$$

where e is defined in a look-up table as per the other four parameters α, b, c and d. More details of the electrical representation of the ZARC elements may be found in (ISEA battery manual 2002).

5.2.5 Heat effects in lead-acid batteries

An important factor that affects the performance of a lead-acid battery is the internal heating that occurs during charging/discharging cycles. It is generally known that all batteries warm up on both charge and discharge. A lead-acid battery is a complex electrochemical system and is based on primary and secondary reactions which cause heat effects. An excellent introduction to the lead-acid battery principles and descriptions of charge transfer reactions may be found in Gibbard (1978); Zemasky et al. (1982) and Redey (1998). In order to predict the thermal effects in the battery, the approach proposed in Gibbard (1978) and Berndt (2001) has been adopted. According to Gibbard (1978) there are two sources of heat effects in lead-acid batteries, the reversible heat effect and the Joule heating. The reversible heat effect is given by:

$$T\Delta S = Q_{reversible} \tag{5.7}$$

where T is the temperature and ΔS the change of entropy.

The reversible heat is determined by thermodynamic data of the cell reactions, typically 3.5% of the drawn energy. Joule heating is caused by kinetic parameters and by the ohmic resistance of the conducting elements including the electrolyte and is given by:

$$Q = (E - E_0)i \tag{5.8}$$

where E is the actual voltage of the battery, E_0 is the open-circuit voltage of the battery and i is the current.

The total heat which is generated is the total sum of the Joule effect and the reversible heat effect. Heat generation is more significant in charging cycles since the charge-transfer reactions that take place in the battery are increased during charging (Berndt 2001). In general, there are two factors that determine the heat of a battery: heat generation within the battery and heat dissipation from the battery in various ways such as heat radiation, heat flow through the components of the battery and heat transport by a medium. More details of the heat effects in a battery may be found in Berndt (2001); Gibbard (1978); Zemasky et al. (1982) and Redey (1998).

In order to develop the thermal model, theory based on thermodynamic equations has been used Berndt (2001); Gibbard (1978). Temperature variations of a battery during charging or discharging are described by:

$$\frac{dT}{dt} = \frac{1}{C_{bat}}\left[\frac{dQ_{gen}}{dt} - \frac{dQ_{diss}}{dt}\right] \text{ (Js}^{-1}\text{ or W)} \tag{5.9}$$

where $^{dQ_{gen}}/_{dt}$ is the generated heat per unit of time and $^{dQ_{diss}}/_{dt}$ is the dissipated heat per unit time. The heat capacity C_{batt} is given by:

$$C_{batt} = \frac{\sum m(i)C_p(i)}{\sum m(i)} \quad \text{(kJ kg}^{-1}\text{K}^{-1}\text{)} \tag{5.10}$$

where $m(i)$ is the mass of the battery in kgr and $C_p(i)$ is the specific heat of the battery expressed in $Jkg^{-1}K^{-1}$. The specific heat C_p of vented lead-acid batteries is approximately (Berndt, 2001; Gibbard 1978):

$$C_p = 1 kJkg^{-1} K^{-1} \tag{5.11}$$

Heat dissipation is distributed by heat radiation, heat flow by conductivity and heat flow by a medium Berndt (2001) and Gibbard (1978). Heat radiation is given by the law of Stefan-Bolztmann:

$$\frac{dT}{dt} = \varepsilon\sigma {T_1}^4 - {T_2}^4 \quad \text{(Wm}^{-2}\text{)} \tag{5.12}$$

where ε is the Stefan- Boltzmann constant which equals to $5.67 \cdot 10^{-8}$ ($Wm^{-2}K^{-4}$), σ is the emission ratio of the material which equals to 0.95 for plastic materials used in batteries and T_1 is the battery temperature and T_2 the ambient temperature. Heat flow by conductivity is given by:

$$\frac{dQ}{dt} = \text{f}\lambda\frac{\Delta T}{d} \quad \text{(W)} \tag{5.13}$$

where f is the surface area in m^2, λ the specific heat conductance for plastic equals to $0.2 Wm^{-1}K^{-1}$, ΔT is the temperature difference between the inside and outside wall of the battery case and d is the thickness of the medium (i.e. container wall). Finally, heat transport by a medium such as air is usually applied on stationary batteries and depends on the height of the sides of the battery. For vented lead-acid batteries this is estimated to be (Gibbard 1978; Zemasky et al. 1982; and Redey 1998):

$$\frac{dQ}{dt} \approx [2,4] \quad \text{(W m}^{-2}\text{K}^{-1}\text{)} \tag{5.14}$$

Based on the theory described above for heat effects on VRLA batteries, a MATLAB®/Simulink™ thermal model has been developed. The thermal model has been incorporated within the scaled version of the 12V AGM battery model. Details on the layout of the MATLAB®/Simulink™ model may be found in Boulos et al. (2003).

5.2.6 Gassing reactions model equivalent circuit

Gassing reactions for battery simulation is a topic of ongoing research including multiple type of batteries (i.e. VRLA, lithium-Ion). As described in ISEA battery manual (2002) assumptions adopted for this model is that the 'gassing' reaction in a VRLA type battery only consists of oxygen evolution at the positive electrode and oxygen recombination at the negative electrode with no corrosion of positive grid material and no hydrogen evolution at the negative electrode. Furthermore, it is considered that oxygen recombination at the negative electrode takes place without polarizing this electrode. Therefore, the equilibrium potential of the oxygen circulation reaction $U_{ogassing}$ can be set to 1.68V (Berndt 2001). As shown in Figure 5.1, a simplified gassing reactions model followed in this approach is:

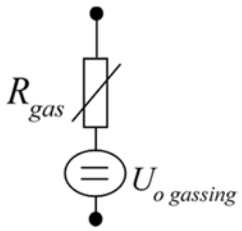

Figure 5.3. Simple model of the side reactions for a VRLA battery cell (i.e oxygen circulation)

During charging, a current path is in parallel to the charging reaction current passing through R_{ct1} and R_{ct2} (since gasses are minimum during discharging). During this operation, at least one of the charge transfer resistances approaches the infinity (battery near to fully charged). That means that no current passes through the parallel parts but only from the gassing reactions branch. The gassing reaction current is given by the Tafel approximation of the Butler-Volmer equation:

$$I_{gas} = I_o e^{k_1 \eta} e^{k_2(\vartheta - \vartheta_o)} \tag{5.15}$$

where I_o, k_1, k_2 are constants, $\eta = (U - U_{ogassing})$ and U is voltage cell, ϑ is 25°C and ϑ_o is cell temperature. The parameter k_2 has been taken from the literature:

$$k_2 = \frac{1}{10K} \ln 2 \tag{5.16}$$

Parameters I_o and k_1 have been determined from a float charging experiment as described in ISEA battery manual, (2002) at a temperature of 25°C and are:

$$k_1 = \frac{1}{207mV} \ln 10 \tag{5.17}$$

and

$$I_o = 5.85 \cdot 10^{-6} A \tag{5.18}$$

The parameter k_1 demonstrates that for every 207mV increase in over potential, the float charge current will rise for one decade (ISEA battery manual 2002).

5.2.7 State of Charge (SoC) and open-circuit voltage calculation

To model SOC estimation, assumptions based on approximations have been made and followed by the author. Firstly, for an approximation of the SoC, a current integration with appropriate limits (0%...100%) is employed. In addition, the effective capacity has been used as part of the overall estimation. Introducing effective capacity in the model is a possible way to take into consideration the discharge periods with average currents higher than the battery's nominal current I_{20}. According to Peukert's law, the effective capacity depending on several factors such as temperature, aging effects and degradation will be less than the nominal capacity. The limits of the integration of the current depend on the effective capacity of the battery.

The open-circuit voltage represents the DC voltage of the battery model and is calculated from the molality ($^{mol}/_{kg}$) of the sulfuric acid inside the battery. The average molality of the sulphuric acid is expressed as a function of the discharged charge as per below equation:

$$m(Q) = m_{Battvoll} - \frac{Q}{F\, M_{el}} \text{ and } Q = \int I_{gas} dt \tag{5.19}$$

where F is the Faraday constant and equals to 96485 C/mol, $m_{Battvoll} = 7.65\ ^{mol}/_{kg}$ and $M_{el} = 0.117kg$. AGM batteries are completely sealed therefore the value of the parameter $m_{Battvoll}$ is determined by the OCV of a fully charged battery and the parameter M_{el} is defined by a constant current discharge experiment described in Mauracher (1996) and Eckard (2001).

5.4 MATLAB®/Simulink™ alternator model representation

In order to study the transient and steady-state characteristics of the alternator system, analytical models need to be developed. However, analytical models are not quite suitable for long-term analysis due to their complexity, which causes a large computation time reducing their usability for real world applications. Therefore, a suitably accurate hybrid alternator model has been developed by the author, based on both physical laws and measured data.

To derive a hybrid model for an alternator, a number of assumptions are needed to simplify its structure as a synchronous machine. The most significant of these assumptions is to neglect the presence of third and higher harmonics and the presence of booster diodes in the analysis according to Haus der Technik (1994) and Hughes (1969). This assumption substantially simplifies the analysis but does introduce errors of $\pm$ 5A over the speed range from 1800rpm-18000rpm. However, the alternator speed is normally between 1800rpm (idle) and 6000rpm (vehicle cruising speed) and the estimated maximum error in the current over this range is about $\pm$ 3A (Hughes 1969). The model used for simulations is based on measured data provided from tests conducted using several 14V automotive alternators (DENSO SC1, 130A). These alternators are capable of delivering 60A at 1500rpm and up to 150A at 6000rpm depending on ambient temperature, engine speed and voltage system level.

The DC output voltage of an alternator is controlled by regulating the current flowing through the field winding. The regulation of the output voltage is accomplished by switching a power transistor and comparing the error signal with zero. The power transistor frequency of operation varies depending on the manufacturer.

The derived model is based on the switching field current regulator. For the purposes of the simulation, it is sufficient to model the power transistor as a voltage-controlled switch. To derive the value of the field current, an amplified error signal is generated by subtracting the alternator output voltage V_0 from the reference voltage V_{ref} (V_{ref} is a nominal value, which varies as a function of the alternator's heatsink temperature, typically between 13.9V and 15.1V) and multiplying it by a proportional gain K_p (K_p is empirically chosen depending on the dynamics of the system). The error signal is modelled as a dependent current source K_p (V_{ref}-V_0). Note that in normal conditions $V_{ref} > V_0$ so I_0 is always positive. Figure 5.4 shows the resulting simplified circuit of the developed field current regulation system with a voltage regulation compensator:

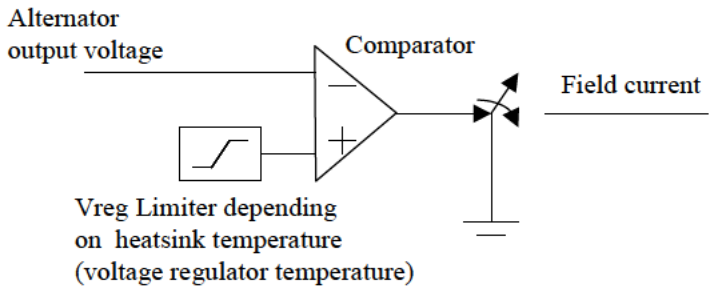

Figure 5.4. A simplified representation of a field current regulation system with a voltage compensator

5.4.1 Alternator model based on empirical data

The battery model voltage is an input to the alternator model. Outputs of the model are maximum current output and maximum torque output. The alternator model consists of three parts:

1) The voltage regulation block regulates the system voltage according to the heatsink temperature input. The heatsink temperature is the ambient temperature around the area where the voltage regulator is mounted on the alternator.

2) The current output look-up table. The maximum output current is one of the outputs of the alternator and is dependent on temperature, engine speed and system voltage. A look-up table has been created from experimental measurements which have been conducted on various SC1 130A alternators. From the experimental measurements, it has been found that the current output of the developed alternator model is also dependent on the system voltage. The system voltage affects the maximum current output of an alternator and therefore impacts the fuel economy of the vehicle (McAuliffe et al. 1999). An extra look-up table has been added to include this dependency. This is used to allow for the change in maximum alternator current output with changing voltage. The correction is necessary because as a common practise, manufacturer's data are measured values that have been taken at a fixed voltage of 13.5V. The element of temperature and voltage has not been included therefore measurements at the alternator current output have been made and a table with the corrected maximum current output of the alternator as a function of voltage has been produced and can be found at Appendix D, section D2).

3) Maximum alternator torque look-up table. This block provides the maximum alternator torque output. These torque data have been obtained from DENSO for the SC1 130A alternator. The data have been measured at a fixed voltage of 14.25V at an ambient temperature of 25 ^{0}C (Appendix D, section D2).

Finally, a function has been incorporated into the model, which attempts to replicate the 'boost phenomenon' of the alternator. It increases the maximum current output for a certain period of time to match the behaviour observed in practice. During its warm-up period, the alternator generates a maximum current 10%-15% higher than its actual current characteristic output. This non-linear effect lasts approximately 10 minutes (Pickering 2001). Figure 5.5 shows the non-linearity of the 'boost phenomenon' average for a range of different ambient temperature levels (-20^{0}C to +100^{0}C) from the combined results from 3 different samples of SC1:

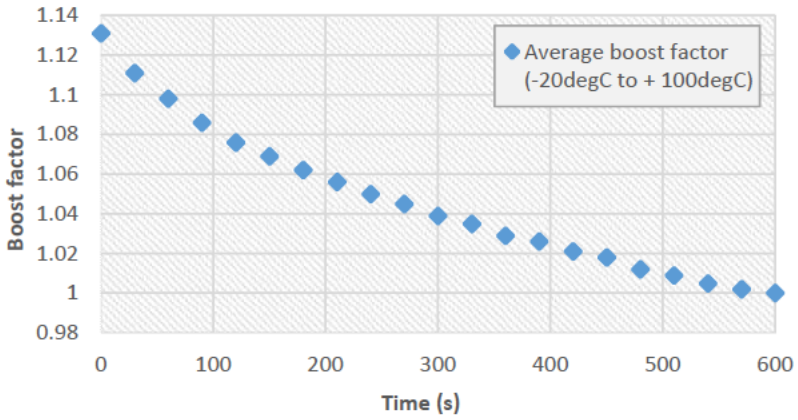

Figure 5.5. The average boost factor in temperature range of –20^{0}C to +60^{0}C

The final MATLAB®/Simulink™ layout of the developed alternator model including the voltage regulation block, the current output estimation block and the alternator torque estimation block can be found at Appendix D, section D2.

5.5 MATLAB®/Simulink™ ultracapacitors model representation

5.5.1 Ultracapacitors equivalent circuit

A model has been developed from first principles to simulate the behaviour of the ultracapacitors. Using an equivalent electrical circuit shown in Figure 5.6 the model consists of a series connection of an inductance L, an internal resistance or equivalent series resistance Ri, and the capacitance C of the cell:

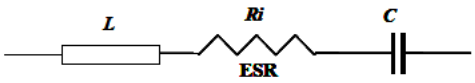

Figure 5.6. Equivalent electrical circuit for an ultracapacitor

The total voltage across the ultracapacitor is:

$$V_{total} = L\frac{di}{dt} + IR_i + \frac{1}{C_{cell}}\int idt \qquad (5.20)$$

where L is the inductance, R_i is the internal resistance, I is the current in Amperes, C is the capacitance in Farad and finally, di is the change in current.

The actual charge and discharge current limits are dependent on the size of the ultracapacitor cell and internal I^2R loss giving rise to increasing internal cell temperature. To characterize the performance of the ultracapacitor, especially in dynamic operation, the values specified in the data sheets are often not sufficient. Hence, additional tests to obtain parameters such as capacitance and internal resistance as a function of frequency, temperature and cell voltage had to be performed. A modelling approach has been adopted with data information obtained from Ford technical research centre in Aachen regarding the variation of the capacitance and the internal resistance as a function of voltage and temperature on ultracapacitors. The information was based on impedance spectroscopy measurements that have been conducted on different types of ultracapacitor cells (i.e. Maxwell Technologies 2.5V/2600F and NESS 2.7V/5000F cells) and scaled to IOXUS ultracapacitor cell characteristics. Three parameters (capacitance C, inductance L and internal resistance R_i) were measured as a function of cell voltage and cell temperature.

The performance of the selected IOXUS cells was analyzed using a Digatron test bench. It is a programmable current source that can control the charge and discharge rate of energy storage devices. Two different tests were performed: a capacity test and a test to determine the internal resistance of the analyzed cells. In addition, the self-discharge rate of the cells was measured.

The DC-capacitance of the ultracapacitor cells at room temperature was measured. The IOXUS cells were charged up to the nominal cell voltage of 2.7 V for several hours. Afterward, the cells were discharged using a constant current of 10 A until ΔU was approximately 0.2 V. This allows us to determine the capacity of the cells for specific operating points as a function of the cell voltage. The duration of the discharge time Δt was measured. The equivalent amount of charge, which was extracted from the cells was determined using the following equation:

$$\Delta Q = I \cdot \Delta t \tag{5.21}$$

At the beginning, a nearly linear voltage drop occurred. After discharge, a relaxation was found and the voltage increased to a constant value. Based on the measured voltages, the differential voltage ΔU was determined. The capacitance of the cell at this operating point can be calculated as follows:

$$\boldsymbol{C} = \frac{\boldsymbol{\Delta Q}}{\boldsymbol{\Delta U}} \tag{5.22}$$

The test was repeated for all cells measuring the capacitance as a function of voltage in the range of 1.7V to 2.7V. Figure 5.7 shows a mean capacitance of C = 3026F and standard deviation $\sigma = 87.2F$. The capacitance test was performed with all 6 cells. Figure 5.8 shows the distribution of the measured values at nominal voltage and nominal temperature of 25^0C. The classes in the histogram are set to 20F. The mean capacitance value is C = 3068F and the standard deviation $\sigma = 22.9F$.

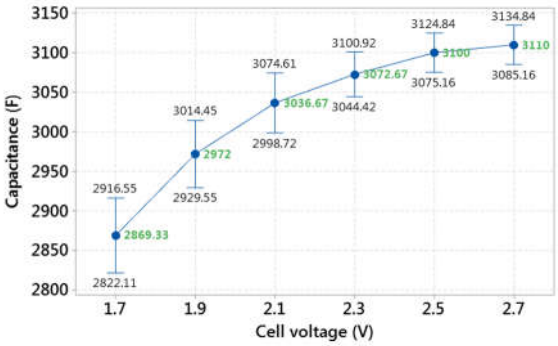

Figure 5.7. Capacitance measured as function of cell voltage at 25^{0}C

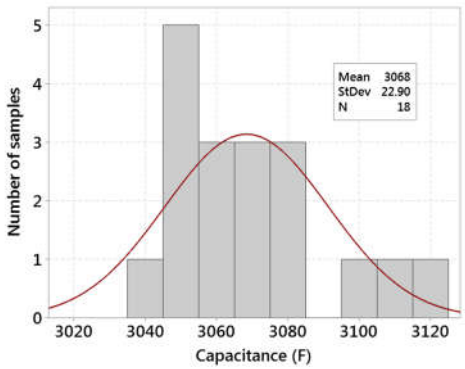

Figure 5.8. Distribution of the capacitance at nominal voltage and 25^{0}C

Using the same Digatron test bench, the internal resistance of the cells was also measured. The IOXUS cells were charged or discharged with a high constant current ($I_{\text{charge/discharge}} = \pm 100$ A). At a certain point of time the charging or discharging current was switched off. The voltage responses of the cells were analyzed and the internal resistance at room temperature was calculated using Ohm's law:

$$R_{\text{i}} = \frac{\Delta U}{I} \tag{5.23}$$

The results are listed in Appendix E, section E.3. Figures 5.9 show the corresponding distribution of the measured ESR with mean value of 0.2147mΩ and standard deviation $\sigma = 0.004$mΩ. The classes in the histogram are set to 0.125 mΩ.

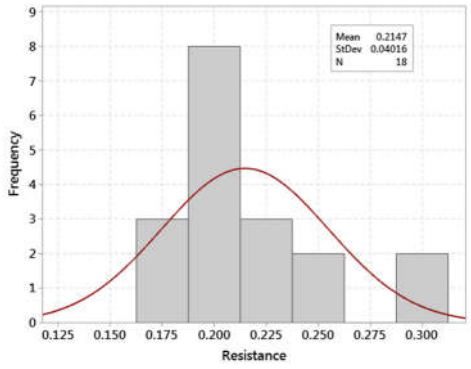

Figure 5.9. Distribution of the internal resistance measured at 25^{0}C

The dependency between internal resistance and frequency could not be measured with the Digatron test bench due to its lack of precision is not precise to model the dynamic behavior of the boostcaps. Impedance spectroscopy (see Chapter 3) was adopted to characterize the performance in dynamic

operation and measure the dependency of the internal resistance from temperature, cell voltage and frequency.

To model the entire impedance of the supercapacitors, an inductor representing the inductive behavior of the cells and a resistor representing the internal resistance at crossover frequency had to be added in series to the complex pore impedance. Equation 5.24 gives the mathematical expression for the complex pore impedance:

$$\mathbf{Z_p(j\omega)} = \frac{\mathbf{R_p \coth\sqrt{j\omega R_p C_p}}}{\sqrt{\mathbf{j\omega R_p C_p}}} \tag{5.24}$$

To obtain a suitable model for a simulation tool such as MATLAB®/Simulink™, the model in the frequency domain has to be transformed into the time domain. Mauracher (1996) found a suitable solution for the transformation of the complex pore impedance. Using the equivalent electrical circuit shown in equation 5.5, the impedance of the complex pore impedance can be modeled according to Buller et al. (2001) and Mauracher (1996). It consists of a series connection of RC circuits. The more RC circuits are utilized (Figure 5.10), the better the impedance of the porous structure of the electrodes will be approximated. The values of the elements of the equivalent electrical circuit are determined by equations (5.24) and (5.25).

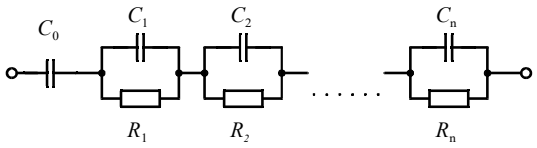

Figure 5.10. Equivalent electrical circuit to model the dynamic behavior of supercapacitors

$$\mathbf{C = C_0 and C_n = \frac{C}{2}} \tag{5.25}$$

$$\mathbf{R_n = \frac{2\,R_p}{n^2\pi^2}} \tag{5.26}$$

Figures 5.11 and 5.12 show graphically the variation of cell capacitance and internal resistance as a function of voltage and temperature:

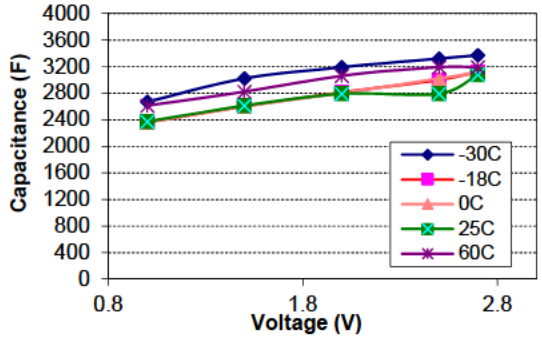

Figure 5.11. Cell capacitance as a function of temperature and voltage

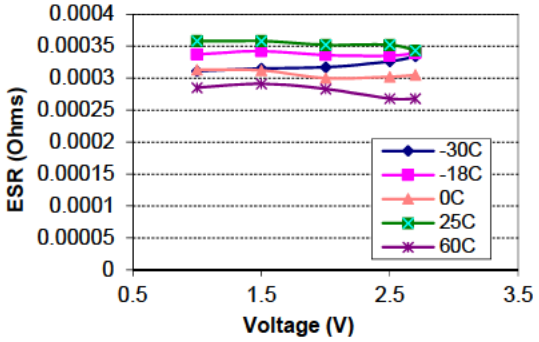

Figure 5.12. Cell internal resistance as a function of temperature and voltage

The Simulink model layout representing the IOXUS module is shown in Appendix. The developed MATLAB®/Simulink™ model has been correlated against experimental electrical current data such as an Integrated-Starter-Generator (ISG) profile including deep discharge and charge cycles, engine cranking profiles and real world driving electrical loading profiles. The validation included different initial cell voltages (2.5V and 2.7V) and different temperatures from -30ºC up to +50ºC. Simulation results can be found in Appendix E, section E3. Figure 5.13 shows the performance of the developed Simulink model against experimental results as taken as measured in the test vehicle:

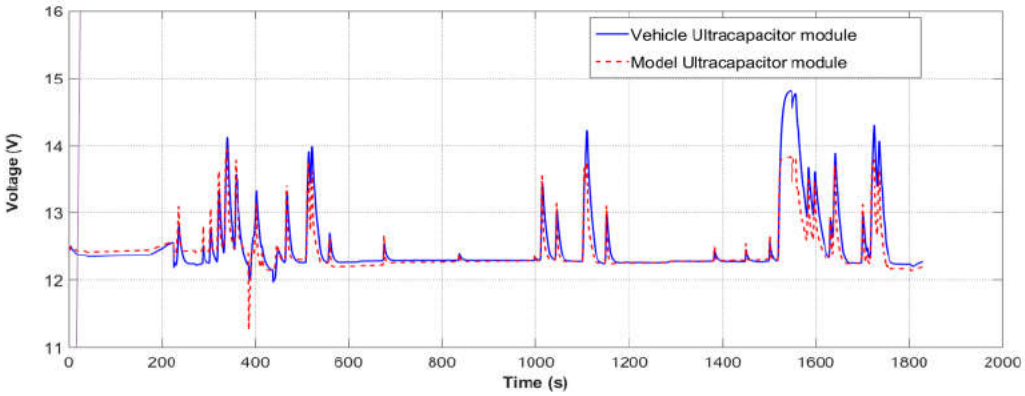

Figure 5.13. Model voltage profile performance against experimental data

It can be seen there is a good correlation of the simulation model with the actual module exhibited by a relatively consistent small error during a long-term simulation (i.e. 30 minutes). The voltage output of the model was based on a typical real world high frequency electrical loading profile as applied during real world conditions.

5.6 MATLAB®/Simulink™ solar panel model representation

5.6.1 Equivalent electrical circuit of a photovoltaic cell

The electrical equivalent circuit used in this research is the double diode solar cell (Cibira et al. 2014; Bellia et al. 2014; Sharma et al. 2013). The circuit consists of a source of constant current connected in parallel with a rectifying diode, due to the recombination of the charges and additionally by another diode. It also contains a resistance R_{sh} which simulates the leaking current losses (due to variation in the manufacturing process and defects) and a resistance R_s which simulates any other electrical load losses. Figure 5.14 shows the equivalent circuit of the double diode the model implemented in this thesis:

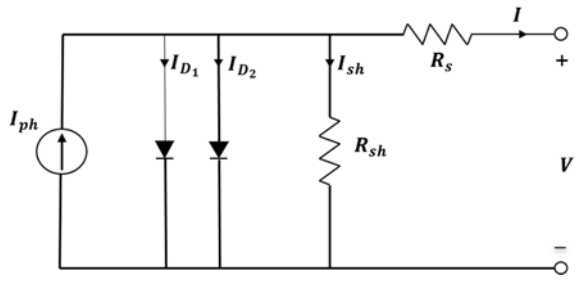

Figure 5.14. Equivalent circuit of a double diode solar cell including parasitic resistances R_s and R_{sh}.

The effects of the second diode to the equivalent circuit of a solar cell are higher when low voltage levels are applied to the circuit. At high voltages the ideality factor of the device, which measures the quality of the material, is close to 1. However, when low voltage is applied, the ideality factor gets closer to 2 so the need for an additional diode in parallel is necessary to model the junction recombination.

The cell's terminal current is calculated using Kirchhoff's Current Law (KCL):

$$I = I_{ph} - I_{D1} - I_{D2} - I_{sh} \tag{5.27}$$

where I_{ph} is the photogenerated current, I_{D1} is the current of the first diode, I_{D2} is the current of the second diode, and I_{sh} is the current passing through the shunt resistance. The equation for calculating the current in the cell's terminals is as follows:

$$I = I_{ph} - I_{O1}\left(e^{\frac{V+IR_s}{n_1 V_{T_1}}} - 1\right) - I_{O2}\left(e^{\frac{V+IR_s}{n_2 V_{T_2}}}\right) - \left(\frac{V+IR_s}{R_{sh}}\right) \quad (5.28)$$

where the new parameters are V which is the voltage at the terminals of the cell, I is the current at the terminals of the cell and R_s the total series resistance of the junction as the current passes through it, which is the total contact resistance of the silicon and the metal contacts. As R_s increases, the terminal voltage becomes progressively lower. High values of series resistance besides the reduction of the short-circuit current, can also impact the fill factor and reduce it (PVeducation 2020).

R_{sh} is the shunt resistance which simulates the leaking current with the p-n junction. When the value of the R_{sh} resistance is low it can cause power losses by providing to the generated current an alternate path to flow which reduces the amount of current flowing through the solar cell junction and the voltage itself. At low solar irradiance, the shunt resistance has a higher impact on the efficiency of the solar cell.

V_{T12} is the thermal voltage in volts and given by:

$$V_T = \frac{n_j K T_C}{q},\ j = 1, 2,\ (V_T \text{ is 25.85mV for a single cell at room temperature}) \quad (5.29)$$

where K is Boltzmann's constant and equals to $1.381\times 10^{-23} J/K^{\ o}$, T_C is the temperature of the cell in Kelvin ($0^o = 273^o$K), q is the elementary charge and equals to $1.602 \times 10^{-10} Coulomb$, N is the ideality factor of the diodes due to the recombination phenomenon (n usually = 2) and the non ideal diffusion (n = 1) which happens in the p-n junction area. By knowing the ideality factor of the diode allows measuring the quality of the material. Lower values reflect better material, smaller dark saturation current and higher power output.

The remaining parameters of equation 3.27 are $n_1 n_{\ 2}$ which are the diffusion and the recombination diode ideality factors respectively and finally I_{O1}, I_{O2} which are the saturation currents of the first and the second diode respectively.

Within the electrical characteristics of the solar panel, temperature affects significantly the performance of the solar panel as the photo-generated current and the open-circuit voltage (maximum voltage output with no load connected) are directly affected by it according to diffusion theory of Shockley (Technical report, Kassel University 2003).

In addition, shading has also a significant effect on the performance of the cell. Shading can be caused when there is an interference between the sun and a solar panel, this interference is caused by clouds, snow, leaves falling on the panel, dust and dirt (Kassel University report 2003; Patel et al. 2008; Chang et al. 2010). For simplicity, shading has not been modelled or characterised for this thesis

however real world irradiation data has been used incorporating various solar conditions while the vehicle is moving.

The approach followed by the author was to develop a MATLAB®/Simulink™ solar cell block using Simscape/SimElectronics. The model combines several double diode electrical circuits including temperature as a variable input. These circuits were parameterised based on the datasheet information from the ENECOM solar panel. The resulting solar panel Simulink model developed is shown at Appendix D, section D4.The developed Simulink model has been validated using experimental data collected from the LEV project (as described in Chapter 3) under real world driving conditions. Figures 5.15 and 5.16 show the performance achieved by comparing the current output of the simulation with that obtained experimentally with the LEV for various solar activity levels. It is shown that the model achieves a very good correlation compare to the actual measured solar panel including conditions with steady-state or high frequency changes of irradiance levels as measured from the solar sensor. The simulation output signals are compared against the corresponding measured signals from various vehicles. The Root-Mean-Square of the Error (RMSE) performance index is used to assess the mismatch between the model and the actual measured data. RMSE performance index is defined by:

$$RMSE = \sqrt{\frac{1}{N}\sum_{i=1}^{N}\left(y_{expi} - y_{measi}\right)^2} \tag{5.30}$$

where N is the number of samples, y_{expi} is the expected or modelled value and y_{measi} is the measured value of observation. The RMSE value achieved was 0.049 in a range of 0-8A. The high frequency step changes can be explained due to the position of the vehicle against the solar direction and certain natural effects such as shading from the surroundings and overcast periods during driving resulting in low solar activity. Further simulation results and detailed model performance analysis can be found in Appendix E, section E4.

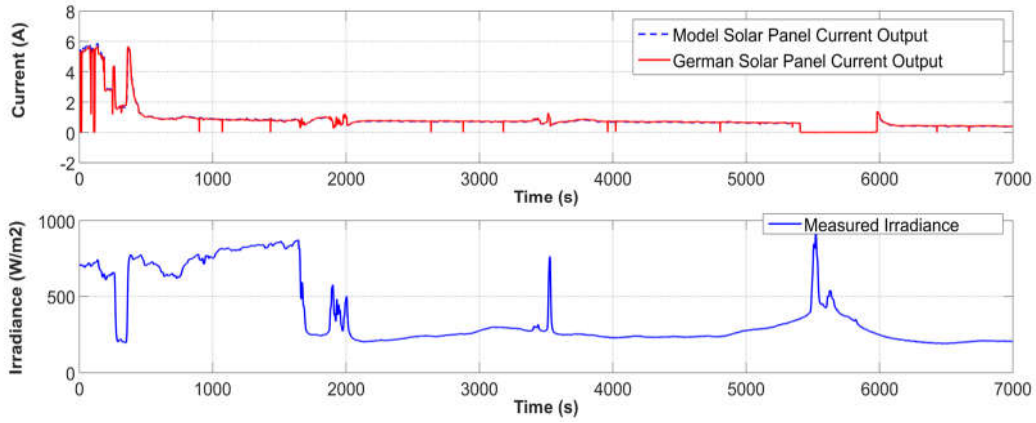

Figure 5.15. MATLAB®/Simulink™ model performance under real world irradiance exposure

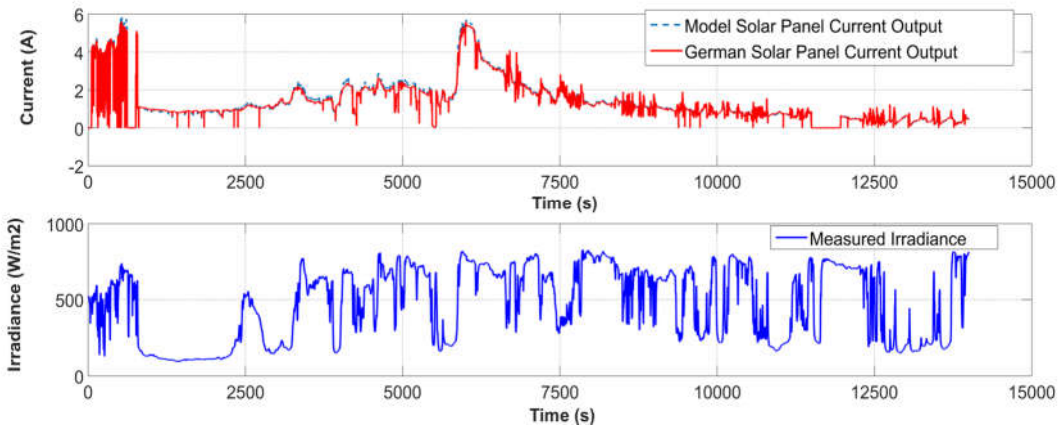

Figure 5.16. MATLAB®/Simulink™ model performance under real world irradiance exposure

5.7 MATLAB®/Simulink™ electrical loads model representation

5.7.1 Vehicle Electrical features/loads

A high-end luxury vehicle has many features and systems that can draw power and therefore electrical load current. Initially, in order to calculate the total electrical load and be able to control the operation of the electrical features, it was necessary to understand the operation of those features/systems when the vehicle operates or is parked with its engine Off. There were two simplifications that the whole modelling and approach on vehicle's electrical loads were based:

i. Certain systems will always be operational whenever the engine is running. Examples of such systems are air conditioning compressor, In-Car entertainment including navigation, telematics, the control modules of safety related systems, actuators such as pumps, injectors, spark plugs and powertrain systems related to the operation of the engine. Consequently, it is possible to encompass the operation of those systems within a steady-state load current that is assumed to be drawn whenever the engine is running, called engine running load.

ii. Certain electrical loads will only operate intermittently and then only for a short period of time. Such loads are anti-lock braking system (ABS), electric seat adjustments, electric windows, electric sunroof, light indicators and any other electrical system that operates in a similar manner. For the purpose of this research, such intermittent operation of electrical loads is not included as part of the developed control strategy since the effect on the vehicle's electrical consumption levels will be minimum on long-term driving conditions.

By taking into consideration the above assumptions, the operation of electrical features and systems which will not operate constantly but will operate automatically or by customer's input and for a long

period of time may significantly affect the fuel consumption of the vehicle. However, electrical features and systems have various modes of operation. For example, heated screens operate on an On/Off strategy while cabin blowers or engine cooling fans operate based on a predetermined control strategy which allows running at different speeds or on pulse width modulation PWM mode depending on the vehicles driving conditions.

Table 5.1 summarises the electrical features included in this thesis while categorising them into two main categories, those which operate on an On/Off strategy and others with variable operation upon driving conditions:

Electrical Load Description	System Providing Information	Current consumption/ Operation	Modelling capability
Cabin Features/Electrical Loads			
Heated Front Screen	Climate Control System	Fixed consumption ON-OFF / Depending on external conditions	Yes
Heated Rear Screen	Climate Control System	Fixed consumption ON-OFF / Depending on external conditions	Yes
Heated Mirrors	Climate Control System	Fixed consumption ON-OFF / Depending on external conditions	Yes
Heated Steering Wheel	Climate Control System	Fixed consumption ON-OFF / Depending on external conditions	Yes
Heated Wiper Park	Climate Control System	Fixed consumption ON-OFF / Depending on external conditions	Yes
Heated Seats-Front/Rear	Electrical Body System	Fixed consumption ON-OFF /depending on cabin conditions	Yes
Heated Steering Wheel	Electrical Body System	Fixed consumption ON-OFF /depending on cabin conditions	Yes
Cabin Ventilation Fans	Climate Control System	Fixed consumption ON-OFF / Depending on external conditions	Yes
Exterior/Interior Lighting			
Side lights	Electrical Body System	Fixed consumption ON-OFF	Yes
Dip Beam	Electrical Body System	Fixed consumption ON-OFF	Yes
Main Beam	Electrical Body System	Fixed consumption ON-OFF	Yes
Front Fog Lights	Electrical Body System	Fixed consumption ON-OFF	Yes
Rear Fog Lights	Electrical Body System	Fixed consumption ON-OFF	Yes
Brake Lights	Electrical Body System	Fixed consumption ON-OFF	Yes
Powertrain loads			
Engine Cooling Fan	Engine Management System	Variable consumption through variable speed / depending on passenger's cabin conditions	Yes
Air Conditioning Compressor	Climate Control System	Variable consumption through variable displacement / depending on passenger's cabin conditions	Yes
Adaptive Damping in suspension	Suspension system	Two fixed values of current / Hard or Soft / depending on driver or road conditions	Yes
Infotainment			
In Car Entertainment (Radio, CD, DVD)	Infotainment System	Variable consumption / depending on switch modes, brightness, volume etc.	Yes

Telematics System	Electrical system	Variable consumption/ Depending on external conditions	Yes
Navigation System	Infotainment System	Fixed consumption ON-OFF	Yes

Table 5.1. Electrical loads/features categorised based on their operation mode

Most of the electrical loads/features described in Table 5.1 are resistive loads. For example, if a certain electrical load draws 20A with the voltage at 13.5V, would draw only 18.5A when the supply voltage reduces to 12.5V. However, other electrical features and their consumptions are based on the engine operating conditions. For example, the engine management system is used to control the speed of the engine cooling fan. It sets a specific PWM duty based on engine and air conditioning requirements, and the fan(s) are driven based on the fan duty demand.

Based on cooling fan measurements on various vehicles, the relationship between fan PWM duty and current drawn is non-linear, as shown in Figure 5.17:

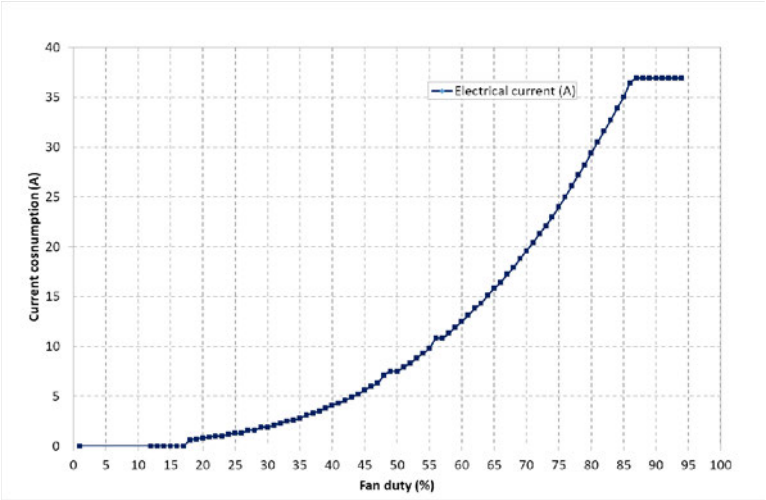

Figure 5.17. Typical engine cooling fan load current vs PWM set duty

Electrical load consumption is expected to be variable across vehicle model types. If the estimation of the electrical system load current was unreliable, the effectiveness of the electrical energy management system and its impact on fuel economy would be inconsistent. Therefore, measured data of load currents for those individual loads were obtained from 5 different vehicles of the same vehicle model as per LEV's test vehicle. Mean values with standard deviation were then calculated as per Table 5.2:

Electrical Load Description	μ value (A)	σ (A)	2σ (A)	3σ (A)
Cabin Features/Electrical Loads				
Heated Front Screen	40.38	0.96	1.92	2.88
Heated Rear Screen	10.5	0.27	0.54	0.81
Heated Mirrors	2.3	0.17	0.35	0.89
Heated Steering Wheel	4.2	0.11	0.54	0.91
Heated Wiper Park	7.55	0.05	0.1	0.15
Heated Seats-Front/Rear	7.66	0.09	0.19	0.35
Heated Steering Wheel	5.45	0.05	0.15	0.19
Cabin Ventilation Fans (max speed)	21.40	1.27	2.54	3.81
Exterior/Interior Lighting				
Side lights	7.16	0.28	0.56	0.84
Dip Beam	7.70	0.1	0 2	0.3
Main Beam	7.70	0.11	0.22	0.33
Front Fog Lights	2.7	0.16	0.32	0.48
Rear Fog Lights	3.7	0.07	0.14	0.21
Brake Lights	0.95	0.09	0.18	0.27
Powertrain loads				
Engine Cooling Fan (low speed)	1.05	0.23	0.46	0.69
Engine Cooling Fan (high speed)	36.9	0.5	1	1.52
Air Conditioning Compressor	3.65	0.27	0.54	0.81
Engine running at idle	14.2	0.44	0.88	1.32
Engine running at 1500rpm	14.5	0.11	0.22	0.54
Engine running at 3000rpm	15.1	0.14	0.29	0.79
Infotainment				
In Car Entertainment (Radio, CD, DVD)	2	0.47	0.94	1.21
Telematics System	0.5	0.1	0 2	0.25
Navigation System	0.2	0.1	0.15	0.17

Table 5.2. Mean values of electrical loads with up to 6 sigma variation measured on 13.5V

The results given by Table 5.2 show that the maximum variation of specific electrical features such as In-Car entertainment and engine cooling fans can reach up to 1.21A and 1.52A respectively. The measurements used to compile Table 5.2 were based on a fixed voltage set point of 13.5V. Since the

voltage of the vehicle changes based on the vehicle's charging conditions, the current consumption is also variable by Ohm's law. However, this level of variation is not significant and therefore not accounted within the overall modelling approach. The developed MATLAB®/Simulink™ model including the above electrical features is described in Appendix D, section D5. An extensive validation using experimental data from different vehicle models and under various environmental conditions is also included in Appendix E, section E2. Figures 5.18 and 5.19 are examples of the performance of the model simulating vehicle's electrical loading during CSCT and DID cycles:

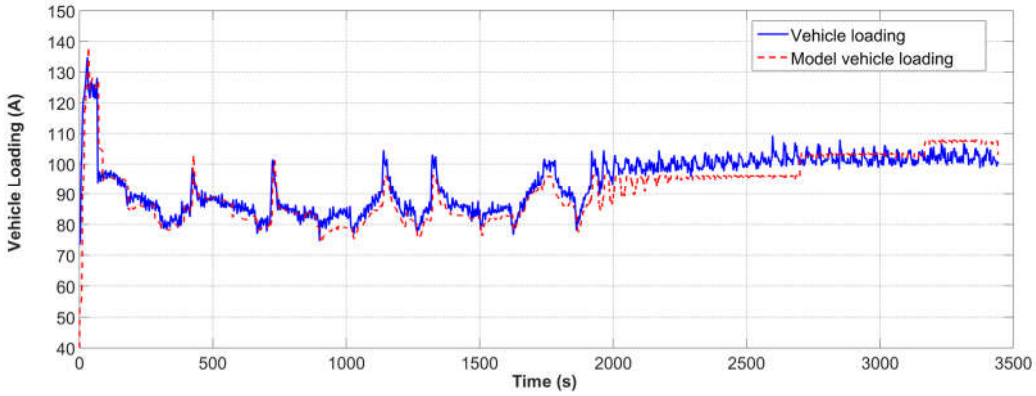

Figure 5.18 MATLAB®/Simulink™ electrical loading model performance under CSCT cycle

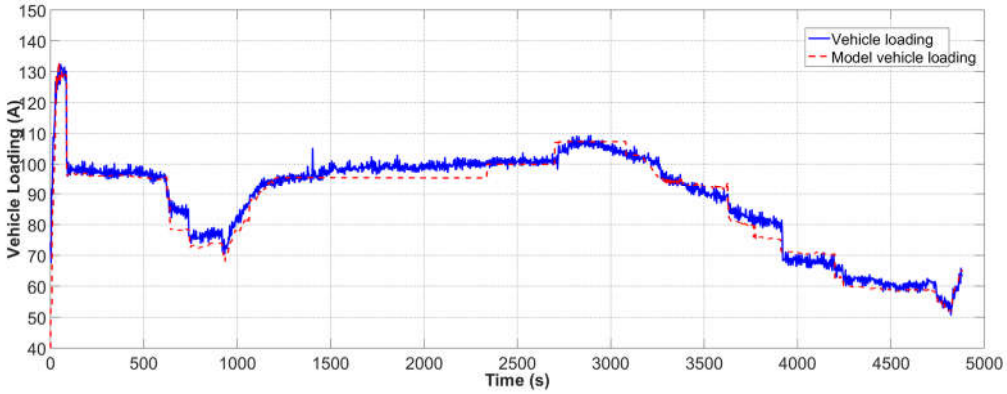

Figure 5.19. MATLAB®/Simulink™ electrical loading model performance under DID cycle

It is clearly shown that the performance of the simulation model is within the design criteria across the whole test duration and on different driving cycles. Details on the design criteria set for the complete MATLAB®/Simulink™ model can be found in section 5.8.2. The performance of the model is also by the RMSE performance

5.8 MATLAB®/Simulink™ mode validation with experimental data

5.8.1 Simulation method

In this study, an approach has been developed to simulate the models described in this Chapter including the battery model, the alternator model and the electrical loads. This makes use of measured data from actual experiments on test vehicles. Details of the test procedure which applies to all Jaguar Land Rover vehicles that include 14V traditional charging system as part of their powertrain may be found in Pickering et al., (2001). The procedure provides a consistent method of testing a vehicle charging system that provides repeatable results and sufficient information regarding the effectiveness and acceptability of the performance of the charging system according to approved acceptance criteria. The 'acceptance criteria' are based on the capability to support the vehicle's electrical loads and preserve the state of charge (SoC) of the battery as high as possible. The 'acceptance criteria' for the vehicle power supply tests are fully described in Pickering et al., (2001).

A list of different instrumentation channels providing the necessary information to analyse the performance of the charging system of the vehicle can also be found in Pickering et al., (2001). The channels that have been selected from the list and used to validate the developed simulation system are:

i. *The load current demand* variation during the time of the test, different as expected for each type of test and climate conditions (cold or hot scenarios). The total current demand has been provided as $I_{LOAD} = I_{ALTERNATOR} - I_{BATTERY}$
ii. *The ambient temperature around the compartment of the battery* (air above battery) into the engine bay or into the boot as most of JLR vehicles have been fitted with the battery into the boot.
iii. *Vehicle engine speed* (rpm) provides the alternator speed through the pulley ratio.
iv. *The ambient temperature around the compartment of the alternator* into the engine bay (Alternator Front Air Inlet).
v. *The heatsink temperature* is the reference alternator temperature for the voltage regulation of the alternator (Alternator Regulator Heatsink Surface).
vi. *The electrolyte battery temperature* within the battery pack (Battery Cell 3 Electrolyte).

During the validation of the developed MATLAB®/Simulink™ system, the following have been compared:

i. Vehicle alternator current output vs maximum model alternator current output
ii. Vehicle battery current output vs maximum model battery current output
iii. Vehicle battery voltage output vs maximum model battery voltage output

iv. The state of charge (SoC) rate of the vehicle battery vs the SoC rate of the model battery. (Note that the Ah rate is a result of the integration of the battery current and is an indication of the SoC of the battery).

v. The electrolyte temperature rate of the vehicle battery vs estimated model electrolyte temperature.

Figure 5.20 shows the overall MATLAB®/Simulink™ model layout of the developed power supply system including all sub-components as described above:

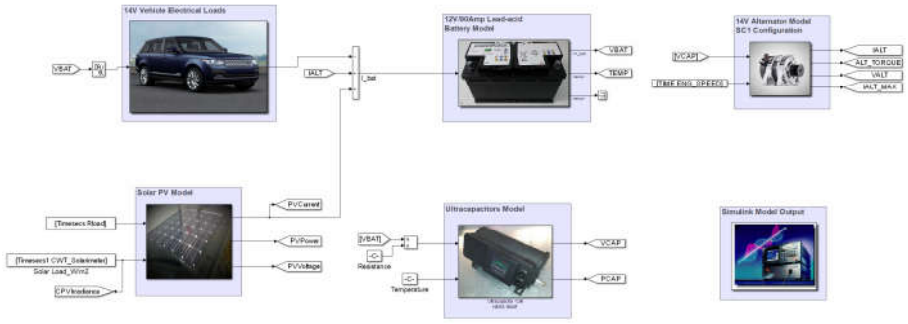

Figure 5.20. Simulink layout of the developed electrical power system

5.8.2 MATLAB®/Simulink™ model performance

Experimental data have been collected from various vehicle charge balance tests. Data of 3 different types of vehicles (x103, x202 and x350) and different temperature levels (-10^{0}C, 0^{0}C, +40^{0}C) and for two different types of driving cycles (combined driving cycle (CC) and the drive-idle-drive (DID) cycle) have been loaded into the Simulink models. Details on the specifications of the driving cycles and the description of the tests may be found in Appendix E, section E.1. The simulation results have been compared with the actual vehicle test results against certain design criteria. The design criteria defined within Jaguar specification (Pickering et al., 2001) are as follows:

i. Accuracy: Battery and Alternator voltages within 0.5V of experimental data
Battery and Alternator currents within 5A of experimental data

ii. Fast Simulation time: To enable to run any type of charge-balance test with no significant delays

iii. User friendly: To allow any electrical engineer to be able to use the developed simulation system without requiring any particular skills of using the software.

iv. Repeatability: To provide accurate simulation results for any condition

v. Adaptability: To incorporate any new system (electrical or mechanical) or be integrated into any software architecture within the company specifications.

A full analysis of the system and the correlation results of the system with experimental results may also be found in (Boulos 2003). An example of the performance of the developed power supply system against the experimental data is shown in Figures 5.21 and 5.22. Simulation results are also included in Appendix E, section E.2. Table 5.3 presents the RMSE performance indices for several signals of interest:

Driving cycle	Temp [ºC]	Vbat [V] [8….15.5]	Valt [V] [12….15.5]	Ibat [A] [-50….100]	Ialt [A] [0….200]
CSCT	-10	0.4922	0.4858	4.8242	4.4766
	0	0.3319	0.3230	4.2342	3.9674
	40	0.4012	0.3946	3.9112	3.8122
DID	-10	0.5022	0.4200	4.9689	4.677
	0	0.4859	0.2937	4.5688	4.3411
	40	0.4662	0.2894	4.1219	3.5664

Table 5.3. RMSE performance indexes calculated for various power supply system signals at different temperatures

The simulation results correspond to alternator currents and load demand (subplot 1); battery currents (subplot 2); battery voltage (subplot 3); and state of charge (SoC %) (subplot 4). In trace 1, the solid line is the load demand, the dashed line is the model alternator current and the dotted line is the actual alternator current. In traces 2-4, the solid line represents the actual variable and the dashed line represents that from the model.

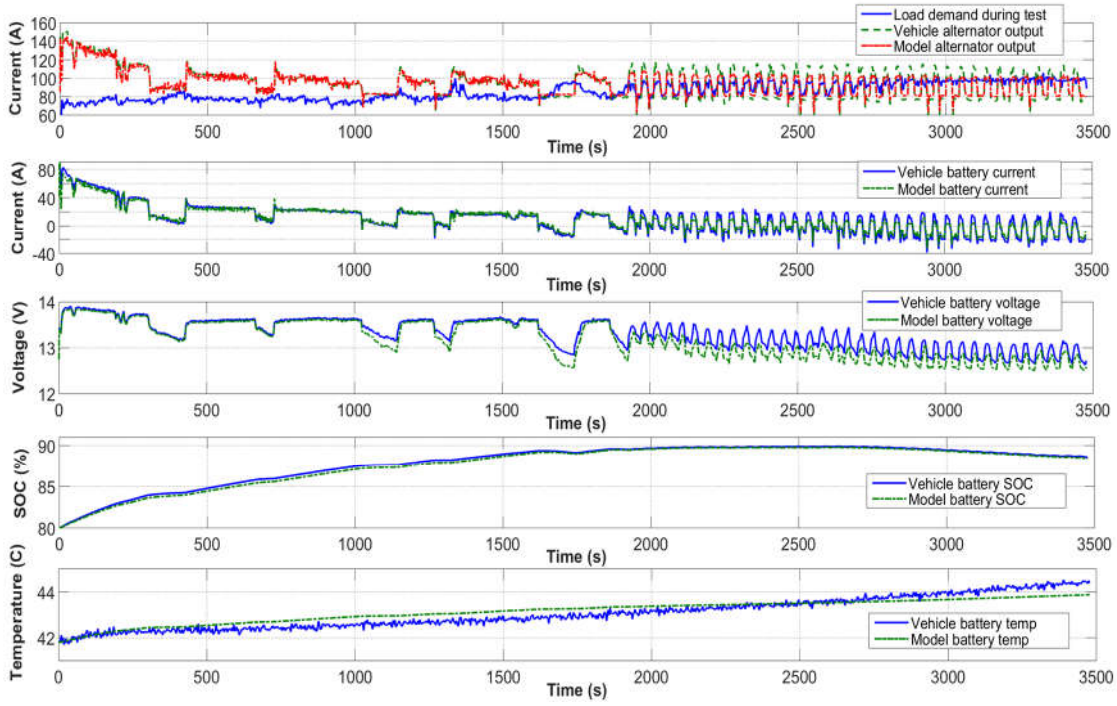

Figure 5.21. Simulation results at ambient of +40^{0}C, CSCT test

Figure 5.21 shows that the developed system meets the desired design criteria throughout the test. In particular:

Subplot 1. Alternator output vs load demand. The absolute error (in suburban period) of the model alternator current output is 5-6A and is underestimated compared to that of the vehicle's alternator current output.

Subplot 2. Battery current. The absolute error on the battery model current level is 5-6A and does meet the specific design criteria.

Subplot 3. Battery voltage. The absolute error of the battery voltage is within the range of $\pm$ 0.5V throughout the test. It is worth noting that the maximum voltage difference occurs in the 'city traffic' cycle.

Subplot 4. SoC. The battery model SoC indicates a similar trend to the measured data with almost identical final state of charge.

Subplot 5. Internal temperature. The model internal temperature was a similar trend with the actual cell 3 temperature and the final result is underestimated by +0.3 ^{0}C of the battery's cell 3 (battery middle cell) temperature.

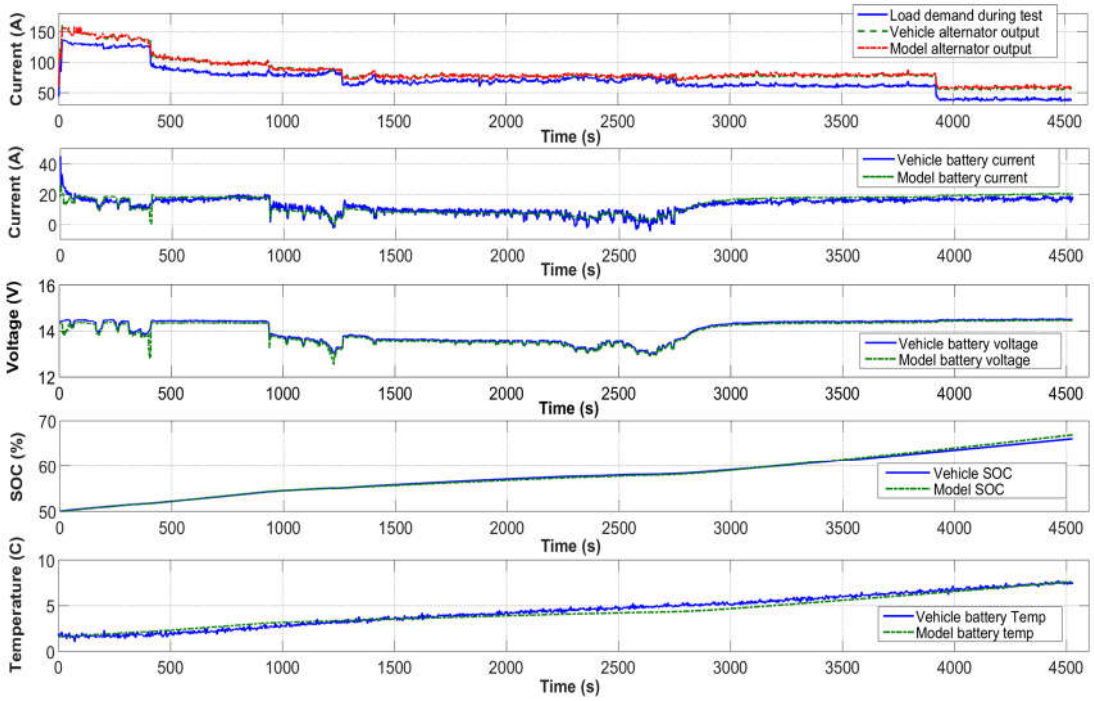

Figure 5.22. Simulation results at ambient of +0^{0}C, DID test

Figure 5.22 shows that the developed system meets the design criteria throughout the test. In particular:

Subplot 1. Alternator output vs load demand. The absolute error of the model alternator current output is 5A underestimated comparing that of the vehicle's alternator current output throughout the test (idle-drive-idle period).

Subplot 2. Battery current. The absolute error on the battery model current level is less than 5A throughout the test.

Subplot 3. Battery voltage. The error of the battery voltage is within the range of $\pm$ 0.5V. It is worth noting that 'simulation spikes' occur throughout the test.

Subplot 4. SoC. The battery model SoC indicates a similar trend to the measured data with almost identical final state of charge.

Subplot 5. Internal temperature. The model internal temperature estimation is within the range of $\pm$ 0.2^0C relatively good with that of the actual cell 3 (battery middle cell) temperature and the final result is almost identical.

5.9 Summary

This Chapter has described the theory, the original implementation and critical analysis of the model of the power supply system. The model includes the main battery, the alternator, the ultracapacitor module, the solar panel and finally the individual electrical loads.

The battery model representation throughout the tests showed a relatively good accuracy within the range of the design criteria (Appendix E). Inaccuracies in the Simulink model are due to the difference in internal resistance between the model and the actual VARTA lead-acid batteries. The internal resistance of a lead-acid battery model depends on the state of charge, ambient temperature, electrolyte chemical reactions and the current that is drawn during a particular load demand. These parameters have been taken into account to develop a three-dimensional (3-D) look-up table in order to 'correct' the internal calculations of the battery model and improve its performance against experimental data. The 3-D 'look-up' table has been developed using experimental data that have been collected from particular battery bench tests. In addition, a thermal MATLAB®/Simulink™ model has been developed to simulate heat effects that occur inside lead-acid batteries during charging/discharging current cycles. The developed model has been validated and its functionality has enhanced the overall performance of the battery model.

The alternator model with its current and voltage output representation has shown good agreement throughout the tests and in most of the cases meets the design criteria. The voltage regulation

implementation helps to identify the performance of the battery. It is suggested that the proportional gain of the voltage regulator should be kept at high levels to have a fast response to the current demand in order to achieve the desired system voltage level. It has also been shown that the model can be easily implemented to simulate future types of alternators (SC2, SC3 etc.) to cover the complete range available.

The ultracapacitor model has been developed and validated by using technical data available and correlated with experimental profiles. Using impedance spectroscopy modelling approach as used by Karden (2001); Karden, et al. (2001) and Bohlen (2008) the developed models have been modified and parameterised to improve performance and correlation against experimental data. Simulation results showed a good correlation of the models with experimental results provided from the test vehicle's ultracapacitor module.

Finally, the developed solar panel model has been validated under various solar load (W/m^2) conditions using experimental data collected during the summer and winter months capturing all possible environmental conditions under variable solar irradiance. The model has shown a good correlation and performance against experimental data collected from the test vehicle.

The original model created by the author and presented in this chapter will be used in the following chapters to design a global energy management system with the use of Fuzzy Logic Control (FLC). The critical evaluation of the overall model and its control strategy will exploit the simulation scenarios discussed and presented in Chapter 4 and a full analysis will be provided in Chapter 6.

Chapter 6

Electrical energy management strategy using type-1 fuzzy logic control

6.1 Introduction

This chapter presents the development of the Energy Management Estimator strategy using Fuzzy Logic Control (FLC). It exploits the vehicle power supply system formulated in Chapter 5. The simulation studies are performed in the SIMULINK environment where the proposed Energy Management strategy, as well as the following vehicle plant model, are implemented. The complete simulation environment structure is presented in Appendix D.

The FLC energy management strategy is the main contribution of this thesis in terms of control. The proposed controller exploits the measured electrical power demand, the calculated fuel consumption index (FCI), the customer's 'feel factor', the usage of cabin's features under various driving conditions, the battery's state of charge and the vehicle's system electrical stability.

It then minimises the impact of electrical power consumption to the vehicle's total fuel consumption by reducing when appropriate the operation of the electrical features to minimise power usage therefore fuel consumption. With the proposed energy management strategy, any future vehicle powertrain configuration, from micro/mild hybrid to full electric, will have the potential to reach higher fuel efficiency and reduced gas emissions for conventional vehicles or contribute to better EV range for hybrid or fully electric vehicles.

This Chapter is organised as follows. Section 6.2 describes the fuzzy logic concepts exploited in the controller design. Section 6.3 presents the algorithm for the fuzzy logic electrical load management system. Section 6.4 presents the scenario designed to evaluate the proposed strategy under operating

realistic conditions. Section 6.5 analyse the simulation results and demonstrate the benefits of the proposed approach.

6.2 Basic concept of fuzzy logic

Traditional mathematical modelling as commonly used in the sciences engineering and economics, refers to traditional classical mathematics. This mathematical modelling is usually connected with some 'rationalizations' necessary to transform problems from their intuitive basis into a mathematical form. Such rationalizations are the transformation of the notions which are vaguely fixed into a clear crisply determined ones (Gottwald et al. 1995). Another aspect of such rationalizations is the assumption that for all test conditions under which a particular system is operating, precise data with error bounds are available. There are many diverse applications for which it is impossible to get specific or relevant data required due to homogeneity of a process or impossibility to obtain such specific parameters (Gottwald et al. 1995). A difference between fuzzy logic and Boolean logic is that boolean logic uses a two-state representation while fuzzy logic uses membership degrees which range between 0 to 1(Kassem 2012).

Fuzzy logic is a logical approach to vehicle's power supply system as a non-linear and time-varying plant. The decision making of the fuzzy logic uses deterministic rules that are suitable to model uncertainties and robust against measurement noise and disturbances. A fuzzy logic system performs better than traditional control methodologies in the tasks where the data are too complex to be processed by traditional analysis methods or when there are high levels of uncertainties in the input sources of data causing huge inexact blurred ambiguity. Existing literature demonstrates diverse application areas in the context of fuzzy logic control as described in Kheir et al. (2004); Lu et al. (2012); Zhou et al. (2011); Tareq et al. (2015) and Qiao et al. (2016). The knowledge of an expert can be coded into rule-based approach and used in decision making. The main field of application is in the area of automatic control: in closed loop as well as in open loop control situations. The methodology of fuzzy control as a way to process fuzzy information, the result of which is called a fuzzy controller, is characterised by the following two basic ideas; i) a fuzzy controller has to be able to act on crisp input data to create crisp output data, and ii) the design of a fuzzy controller is in general rule based, allowing the treatment of only qualitatively given process information (Gottwald et al. 1995).

Both of these ideas force a fuzzy controller to be able to cope with qualitative information. To design a fuzzy controller means to design a rule base that connects (linguistic) values of the fuzzy input and output variables and afterward to transform this rule base into a fuzzy relation. The transformation of a rule base into a fuzzy relation can be solved either explicitly in determining some fuzzy relation or

implicitly in developing a method to ‘‘join’’ the partial information about the overall fuzzy relationship between input and output variables contained in each single rule.

In all such situations, exact notions or precise data need suitable sets of objects (i.e. temperatures, frequencies, states of processes) which are named *crisp sets* and deviate from *fuzzy sets*. Intuitively, in real applications or systems, there isn't a method or scale which divides membership from non-membership for some suitable set or marks the transition from one property to its opposite one. The gradual transition from membership to non-membership can be realised with fuzzy sets.

6.2.1 Type-1 fuzzy logic systems

A type-1 fuzzy logic system maps crisps inputs into crisp outputs. Fuzzy inference process consists of four major stages; fuzzifier, rule base, interference engine and defuzzifier as shown in Figure 6.4:

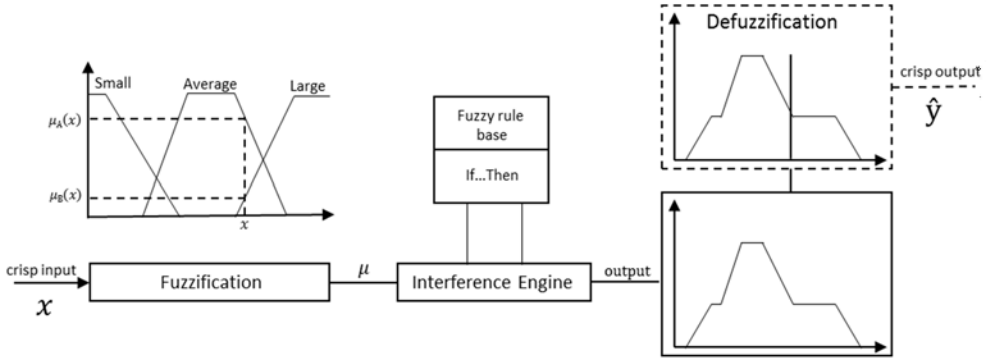

Figure 6.1. Type-1 fuzzy logic system including all stage of inference process

Additionally to Type-1 fuzzy logic systems, (Zadeh 1975) proposed Type-2 fuzzy logic systems. Type-2 fuzzy sets and systems are slightly different from those used in classical fuzzy logic as they deal with the uncertainty of measurement and any rule uncertainty (Mendel 2001). This is the reason why Zadeh proposed to represent this uncertainty by using type-2 fuzzy sets (Zadeh 1975). The differences between Type-1 fuzzy systems can be summarised to the below key points:

- Deal with uncertainty which is present in fuzzy logic (i.e. consequence of a fuzzy rule in a system)
- Type-2 membership functions are three dimensional, considering an uncertainty U of the membership functions

Further details of type-2 fuzzy systems can be found in (Mendel et al. 1999; John et al. 2007).

6.2.1.1 Fuzzification

The fuzzification stage maps input crisp values into fuzzy sets. The procedure includes mapping each input to its corresponding set and accordingly finding the membership value by which this input belongs to the sets (Lee 1990). There is more than one method of fuzzification. In our research we mainly focus on singleton fuzzifier as it converts a crisp value into a fuzzy singleton within a certain universe of discourse and a fuzzy singleton is a precise value; hence no fuzziness is introduced by the fuzzification process at this stage (Kassem 2012). Singleton fuzzification is expressed in equation (6.13) (Mendel 1995).

6.2.1.2 Rule base & inference engine

To design a fuzzy controller, amongst other significant design parts, means to design a rule base that connects linguistic values of the fuzzy input and output variables, which sums up the relevant qualitative information, and transformed a fuzzy relation. Rules can be developed by experts or can be extracted by numeric data, or pseudo-exactly determined data (i.e. numeric data with error bounds).

The rule base is composed of the rules representing the routine and paradigm that the system behaves. In each rule, there are antecedents and consequents in an *if-then* statement. Antecedents are represented by the fuzzy sets of input linguistic variables of the fuzzy logic system while consequents are represented by the fuzzy sets of output linguistic variables. As an output, the system maps the input crisp value into fuzzy sets. Therefore, it is necessary, logic rules to be activated related to those linguistic variables (Mendel 1995). There are different approaches to this development process, the MAMDANI approach and the Takagi, Sugeno and Kang (TSK) approach.

Mamdani/Assilian (1975) proposed to build up a fuzzy relation *R* out of inputs and output variables u, υ, of control rules as described in equation (6.14), for an engine-boiler combination and is often referred to as MAMDANI approach or a MAMDANI controller.

$$\text{IF } u = A_i \; THEN \; \upsilon = B_{\overline{\upsilon}} \; 1,..n \tag{6.1}$$

The second approach, a more direct ‘combination’ of all the control rules which are supposed to ‘act’ in parallel was used by Holmblad/Østergaard (1982) and later on in a modified form by Sugeno/Nishida (1985). Sugeno-type fuzzy systems proposed by Takagi, Sugeno and Kang (TSK) as an attempt to create a systematic approach to generating fuzzy rules from a given set of input and output data. In this approach, the control rules as described in equation (6.14) are slightly modified in such a way that their outputs are crisp values and the inputs remain fuzzy values. Remembering that the input

variable u may be a *k-dimensional one,* $u = (u_{1,} \dots \mu_{k})$.The fuzzy rules in a Sugeno-type mode take the form:

$$\text{IF } u = A_i \textit{ THEN } v = f_i(u_{1,} \dots \mu_{k} i) = 1,..n \tag{6.2}$$

where A is fuzzy set and $f_i(u_{1,} \dots \mu_{k})$ is a real function (Takagi 1985).

Fuzzy Inference engine is another important part of the reasoning system. It can be defined as a computing framework based on the concepts of fuzzy set theory, fuzzy *if-then* rules and fuzzy reasoning. A fuzzy inference mechanism models the process of reasoning, through interpolation between fuzzy rules. Fuzzy inference methods are classified in direct and indirect methods. Sugeno-type FIS uses weighted average to compute the crisp output while Mamdani-type FIS uses the technique of defuzzification of a fuzzy output.

A direct well-known method is Mamdani where the set of fuzzy rules applied is supplied by experienced human operators. Commonly used Mamdani inference finds the centroid of an output continuous fuzzy set. For example, let us use the fuzzy sets with multiple linguistic variables as below:

$$R^l: IFu_{1} \text{is } F_1^l \text{ and } u_2 \text{is } F_2^l \dots\dots \text{and } u_p F_p^l \textit{ THEN } v \textit{ is } G^l \tag{6.3}$$

where $l = 12,\dots MM$ is the number of rules in the rules base, p is the number of inputs. $F_1^l F_{2}^{l},.. F_{p}^{l}$ are fuzzy sets in $U_1 U_{2},.. U_{p}$ and G^l is fuzzy set in V. The inference engine uses these *if-then* rules to map the input sets in $U = U_1 \times U_2 \times \dots \times U_p$ to output set in V. Each rule can be interpreted as a fuzzy implication. The *'THEN'* operator is modelled using the fuzzy implication, so assuming $F_1^l \times F_2^l \times \dots \times F_p^l$ be$A$ and $G^l = B$, rule shown in (6.16), is interpreted by the inference engine as $A \to B$. The mapping results from $\mu_A(u)$ to $\mu_B(v)$ where $u \in U$ and $v \in V$, u and v are linguistic variables and input numerical values are x and y where $x \in U$, $y \in V$. Taking in consideration the interpretation performed by the inference engine, equation (6.4) is expressed as:

$$\mu_{R^l}(xy) = \mu_{A \to B}(xy) \tag{6.4}$$

To compute the firing strength $f^l(x)$ of the l^{th} rule R^l, the calculation shown in equation (6.1) is conducted, where $*$ is the chosen product *t-norm:*

$$f^l(x) = \mu_{F_1}(x_1) * \mu_{F_2}(x_2) * \dots * \mu_{F_p}(x_p) \tag{6.5}$$

After the calculation of the firing strength $f^l(x)$ for each rule R^l we can determine the final output fuzzy set B^l. The final output fuzzy set B is determined by combining the output fuzzy set for each rule using a *t-conorm* operator.

In order to perform certain operations on fuzzy sets such as union or intersection, a *t-norm* (for intersection) and a *t-conorm* (for union) on the fuzzy sets' membership functions have been widely used. The most commonly used *t-norms* and *t-conorms* in fuzzy logic engineering applications are the product (*) or minimum (min) *t-norm* and the maximum (max) *t-conorm* (Mendel 1995, 2000).

6.2.1.3 Defuzzification

The defuzzification process maps fuzzy output sets into crisp values with respect to a fuzzy set (Zadeh 1975; Mendel 1995). The defuzzified value in Fuzzy Logic Controller (FLC) represents the action to be taken in controlling the process.

The Sugeno-type fuzzy systems do not include defuzzification process as the crisp result is obtained using weighted average of the rule's consequent call. Weighted average method is also alternatively called 'Sugeno defuzzification' method and is valid for fuzzy sets with symmetrical output membership functions and produces results very close to the Center of Area (CoA) method. Each membership function is weighted by its maximum membership value. The crisp value according to this method is:

$$\bar{y} = \frac{[\sum_{i=1}^{n} \mu_{B_i}(y_i) y_i]}{[\sum_{l=1}^{n} \mu_{B_i}(y_i)]} \tag{6.6}$$

where $\sum$ denotes the algebraic sum and where $B_1, B_2, \ldots B_n,$ are the output fuzzy sets and y_i is the value where the middle of the fuzzy set B_i is observed.

A Mamdani-type fuzzy system differs from other fuzzy systems, the output variable are fuzzy sets therefore defuzzification is needed. There are different methods for defuzzification of the aggregated output fuzzy variables, amongst others the most commonly used are:

- Center of Sums method (COS): In this method, the overlapping area is counted twice. The defuzzified value $\bar{y}$ is defined as:

$$\bar{y} = \frac{[\sum_{i=1}^{M} y_i \cdot \sum_{i=1}^{l} \mu_{B_i}(y_i)]}{[\sum_{i=1}^{M} \cdot \sum_{i=1}^{l} \mu_{B_i}(y_i)]} \tag{6.7}$$

  where l is the number of fuzzy sets, M the number of fuzzy variables and $\mu_{B_i}(y_i)$ the membership function for the *i*-th fuzzy set.
- Center of Gravity (COG)/Centroid of Area (COA) method. This method determines the centre of gravity (centroid) $\bar{y}$, of the output fuzzy set B. The total area of the membership function distribution used to represent the combined control action is divided into a number of sub-areas. The area and the center of gravity or centroid of each sub-area is calculated and then the summation of all these

sub-areas is taken to find the defuzzified value for a fuzzy set B. The defuzzified value denoted as $\bar{y}$ using COG is defined as:

$$\bar{y} = \frac{[\sum_{i=1}^{I} y_i \mu_B(y_i)]}{[\sum_{i=1}^{I} \mu_B(y_i)]} \tag{6.8}$$

where y_i indicates the sample element, $\mu_B(y_i)$ is the membership function, and I represents the number of elements in the sample. The summation from $i = 1$ till I denotes the support of the fuzzy set B.

Other commonly used defuzzification methods are the maxima methods including First of Maxima method (FOM), Last of Maxima (LOM) method and finally the Mean of Maxima (MOM) method. These methods consider values with maximum membership. More details on those defuzzification methods can be found on (Mendel 1995).

6.3 FL Electrical energy management strategy

6.3.1 Global energy management strategy objectives

Jaguar Land Rover vehicle applications and its new powertrain configurations are composed of electrical subsystems as described in Chapters 2 and 3. The purpose of the proposed Electrical Energy Management System (EEMS) is to harmoniously coordinate the collective action of those individual electrical systems, when selected by the customer or by automatic operation, in order to achieve a set of objectives as listed below:

- Maintain battery SoC within operating range while vehicle's fuel consumption kept low
- Minimise the operation of the alternator/generator therefore reduce its impact to vehicle's fuel consumption. This objective introduces an On/Off state of the alternator based on battery's SoC.
- Minimise usage of electrical power consumption by reducing the operation of electrical loads to minimum therefore maintain low energy usage footprint.
- Maximise solar panel's output when vehicle is parked and engine not running. Battery SoC levels will be maintained high (i.e. upon adequate solar irradiance levels) resulting to reduced alternator operation on next vehicle usage.

Furthermore, realising LEV's experimental results as described on Chapters 3 and 4, a novel approach has been taken to enhance the performance of the proposed EEMS by introducing two critical characteristics, as described below:

- **Fuel consumption index (FCI):** is based on 'economic trading' concept. In case of high fuel consumption, due to high electrical energy usage, the 'price' becomes high therefore the need to limit or decrease it is necessary. EEMS limits overall electrical power allowance to benefit fuel economy. On contrary, on low fuel economy consumption scenarios, the use of electrical loads is promoted therefore the permitted overall electrical current allowance is higher. FCI is the result of the relationship of electrical energy (i.e. alternator loading) expressed in fuel emissions ($g.km^{-1}$), as described in Chapter 4.
- **Customer satisfaction index (CSI):** A novel approach to this control strategy is the inclusion of the 'feel factor' or CSI, a conceptual approach to retain customer's satisfaction and convenience related to cabin's temperature and associated heated/cooled features which includes front and rear heated/cooled seats, heated steering wheel and cabin blowers part of the climate control system. This approach introduces a Human Machine Interface (HMI) logic into our strategy, allowing customer's intervention to balance trade-off levels of convenience to benefit fuel consumption. CSI includes three predefined levels of comfort and convenience as described below:
  - **Low level:** When this predefined level is selected, the operation of the EEMS benefits fuel economy and minimises at maximum electrical load operation.
  - **Normal level:** When this level is selected, EEMS operates in a certain mode to achieve a balanced attribute performance while limiting fuel consumption. However, the trade-off levels of fuel economy vs attribute performance are lower than those when customer selected 'low level'.
  - **High level:** This predefined level offers higher attribute performance close to an open-loop system with very limited consideration of fuel consumption as a limiting factor. Electrical power consumption, as expected, is higher than the other two

Figure 6.5 depicts graphically the economic trading concept as applied to the EEMS, including its key characteristics of FCI and CSI:

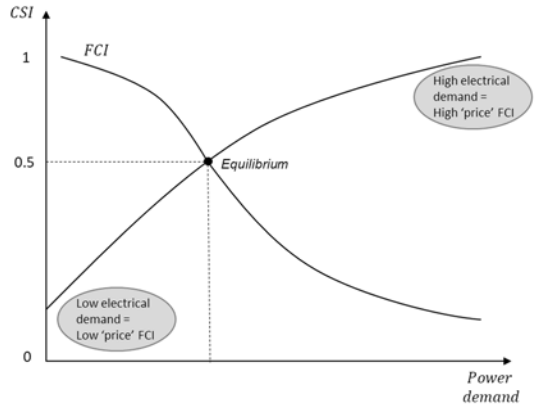

Figure 6.2. EEMS critical characteristics based on economic trade concept

In order to meet the above well-defined critical objectives and characteristics, the overall FLC EEMS is realised into two main individual control schemes:

- A *local FLC based alternator power strategy* which mainly regulates alternator's output based on battery's SoC levels and
- A *global FLC based electrical load shedding strategy* realised into two individual FL controllers:
  - *An FL based controller (*FLC*_glazing)* is regulating the operation and the output of individual electrical features based on FCI levels. The selected electrical features are related to customer's visibility and convenience including heated front screen (HFS), heated rear window (HRS), heated wiper park (HWP) and heated mirrors (HMR).
  - *An additional FL based controller (*FLC*_cabin)* is regulating the operation of cabin electrical features related to customer's convenience and comfort based on FCI and CSI levels. The electrical features included at this part are heated steering wheel (HSW), both front and rear heated/cooled seating (FS/RS) zones and finally cabin blower (BLW) as the key element to maintain and reach cabin temperature set points.

The design of all three fuzzy logic controllers is done by using heuristic engineering knowledge allowing a trial-error-trial technique, a technique that allows to extract information from existing vehicle powertrain platforms and improve the subjected areas of vehicle operation. Figure 6.7 depicts the overall FLC as incorporated within the simulation power supply system plant:

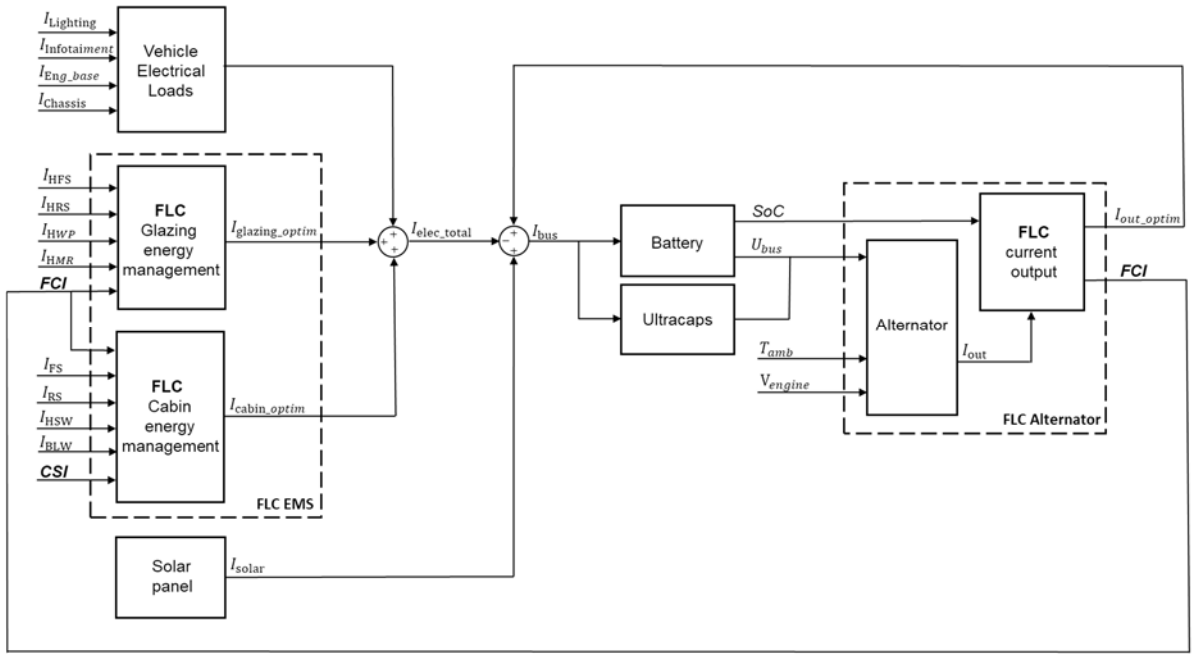

Figure 6.3. FLC Energy Management System including FLC based alternator strategy

6.3.2 Local FLC alternator strategy

The alternator smart strategy is realised without priori knowledge of any future battery state of charge or future electrical load demand but it uses real-time information to output alternator's duty cycle as a function of battery's SoC (see Chapter 5, section 5.2.7) and total electrical power demand (see Chapter 5, section 5.7). The inputs are battery SoC and alternator current output I_{out} and outputs are the optimum alternator current output I_{out_optim}, FCI and torque T_{orque_out}[4]. Figure 6.7 depicts FL alternator control strategy as incorporated within alternator plant:

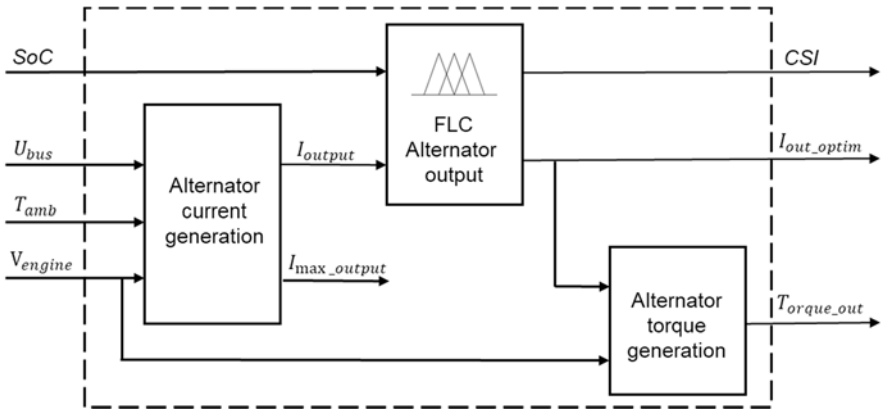

Figure 6.4. Alternator Fuzzy logic control strategy

6.3.2.1 Implementation of membership functions

A significant part of the design process of a fuzzy logic control is to use strong fuzzy rules and accurate membership functions (MFs), this allows the fuzzy logic approach to enhance the operation of the subject plant. The proposed MFs are developed based on the pre-calculated limits of battery's SoC and alternator's current output. For this controller, after a trial and error method, we used triangular and trapezoidal MFs. During the tuning process, we used trapezoidal MFs close to the limits of the battery SoC to eliminate oscillations on the output response. Both types of MFs are good choice for fast computation as needed on a real application.

Battery SoC range is divided into seven overlapped levels {VL (very low); L (low); LM (low medium); M (medium); MH (medium high); H (high); VH (very high)} representing the state of charge range from 0% to fully charge 100%, dividing the permitted operating range into five concourses starting from the lower value of 50% to the higher value of 80% with the target value of 60% as depicted in Figure 6.8a.

[4] Torque output is not considered in the simulation studies for this thesis

Electrical loading is divided into seven overlapped levels {VVL (very very low); (VL (very low); L (low); M (medium); H (high); VH (very high); VVH (very very high)} from 0A to full electrical loading of 200A as shown in Figure 6.8b. Finally, optimum alternator output is divided similarly into 5 overlapped levels {VL (very low); L (low); M (medium); H (high); VH (very high)} from 0A to the maximum optimal current of 200A to fully support max electrical loading demand, as shown in Figure 6.8c. The overlapping between the concourses guarantees a smooth transition within the optimum operational region. Figure 6.9 shows the input and output variables describing their boundaries and depicts the shape and ranges of the concourses:

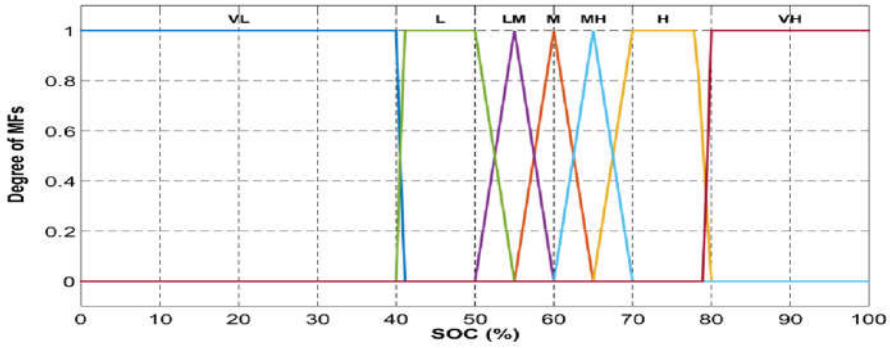

(a) State of charge (%)

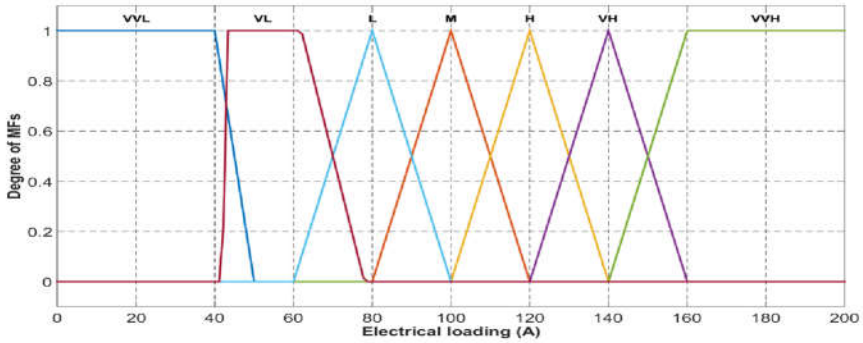

(b) Electrical loading (A)

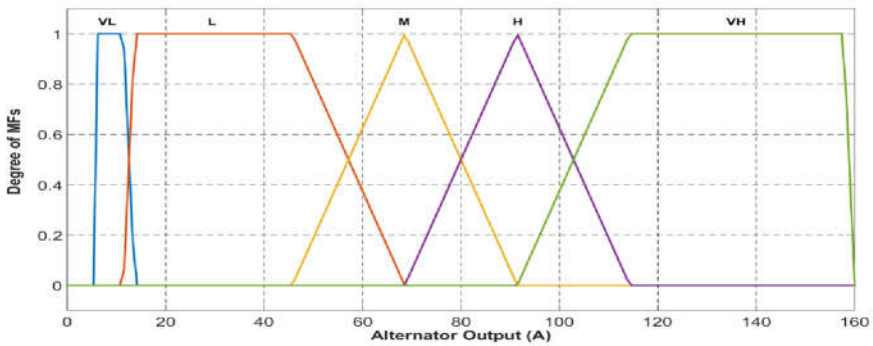

(c) Alternator Output (A)

Figure 6.5. Membership functions of the alternator fuzzy logic strategy: (a) battery SOC; (b) electrical loading; (c) alternator output

6.3.2.2 Implementation of fuzzy logic rules

The proposed fuzzy rule base was developed from two inputs: alternator loading and battery SoC. These inputs are fuzzified and then fed into the fuzzy controller. The optimal rule base was found using a trial-error-trial method but also taking into consideration the expertise knowledge gained from LEV experimental data. The performance of the FLC depends heavily on its fuzzy rules. The rule base for the 49 rules is built to relate the two inputs with the alternator current output. In summary:

- If SoC is very high (VH), i.e. $SOC \geq SOC_{high}$, the alternator is switched Off (i.e. torque applied to the engine is insignificant) therefore the impact of electrical energy on vehicle's overall emissions is kept at a minimum.
- If SoC is very low (VL), i.e. $SOC \leq SOC_{low}$, the alternator is fully used and kept at maximum to support both overall electrical demand as split between the energy devices and the electrical loads of the vehicle. However, the alternator's duty cycle has been tuned to gradually increase to keep the balance of supporting the electrical demand while maintaining the battery's SoC operating range.
- At all other SoC levels, depending on electrical demand and battery's SoC levels, the alternator's output is kept at an optimum level maintaining a balance of power supply stability and impact on fuel emissions and consumption.

The fuzzy logic rule base are presented in Table 6.1 and the surface plot for the FLC variables is shown in Figure 6.9:

	SOC (State of Charge)						
Alternator loading	VL [0-40]	L [40-55]	LM [50-60]	M [55-65]	MH [60-70]	H [65-80]	VH [80-100]
VVL [0-50]	M	M	M	M	L	L	VL
VL [40-80]	H	H	M	M	M	H	VL
L [60-100]	H	H	H	H	H	H	VL
M [80-120]	H	H	H	VH	VH	VH	VL
H [100-140]	VH	VH	VH	H	VH	VH	VL
VH [120-160]	VH	VH	VH	VH	VH	VH	VL
VVH [140-200]	VH	VH	VH	VH	VH	VH	VL

Table 6.1. Rule table for fuzzy logic alternator controller.

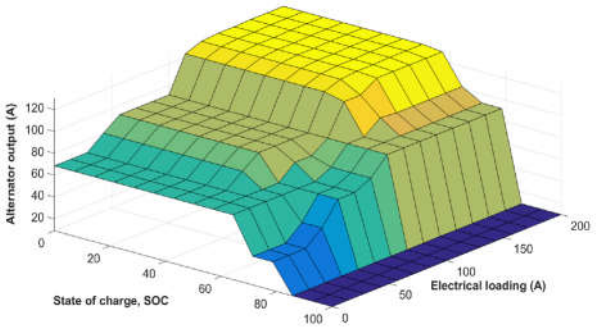

Figure 6.6. Surface plot of the alternator FLC

6.3.3 FLC Electrical energy management strategy

The FL electrical energy management system is also realised without knowledge of future driving conditions or future vehicle's total electrical demand. It only uses real-time information to compute fuel consumption index and vehicle's electrical feature usage. The FLC based Energy Management system includes two subsequent control strategies, the FLC_*glazing* and the FLC_*cabin, both* controlling total electrical load allowance for all customer comfort and convenience electrical features within the vehicle's cabin. The inputs of FLC_*glazing* strategy are:

- **Electrical load demand:** the value of the output current of all manageable electrical features I_{Load_demand} (see Chapter 5, section 5.7). The selected electrical features are related to customer's visibility and convenience including heated front screen (HFS), heated rear window (HRS), heated wiper park (HWP) and heated mirrors (HMR).
- **Fuel Consumption Index (FCI):** an indication of the impact of electrical current consumption (A) on vehicle's fuel emissions (g.km^{-1}) (see Chapter 4, see section 4.5.2)

The output variables of FLC_*glazing* strategy is the optimal vehicle's total glazing electrical feature optimum demand $I_{\_glazing\_optim}$.

The inputs of FLC_*cabin* strategy are:

- **Electrical load demand:** the value of the output current of electrical features (see Chapter 5, section 5.7) regulating the operation of cabin electrical features related to customer's convenience and comfort. Such cabin electrical features including both front (FS) and rear heated/cooled seating (RS) zones, cabin blower (BLW) and heated steering wheel (HSW).
- **Fuel Consumption Index (FCI):** the impact of electrical current consumption (A) on vehicle's fuel emissions in g.km^{-1} (see Chapter 4, see section 4.5.2)
- **Customer Satisfaction Index (CSI):** pre-selected levels of customer convenience and satisfaction as described in section 6.3.1.

The output variable of the FLC_*cabin strategy is* vehicle's total cabin electrical optimum allowance $I_{\_cabin\_optim}$. Figure 6.11 depicts the proposed FLC based Electrical Energy Management system:

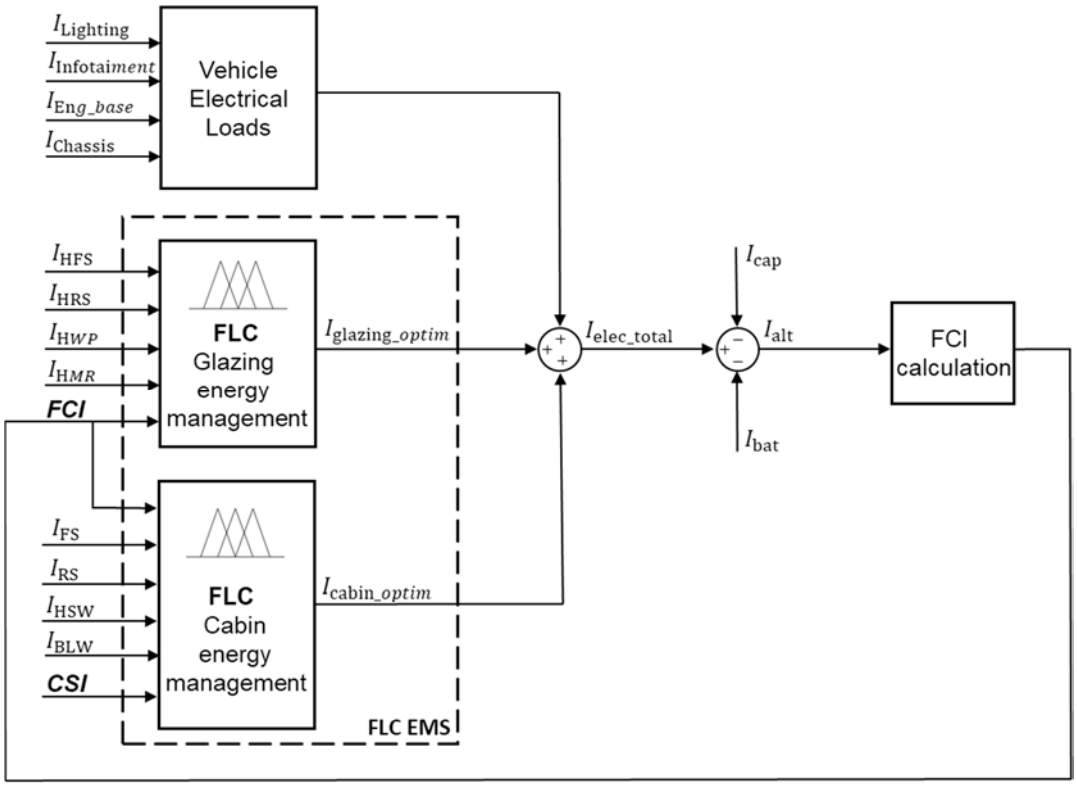

Figure 6.7. Global FLC Electrical Energy Management System

6.3.3.1 Implementation of membership functions

The proposed (MFs) are developed based on the operational limits of each individual electrical feature. Electrical features divided into similar overlapped levels are as follows:

- Heated front screen is divided into two levels, {LP (low power); HP (high power)} from 0A to 50A
- Heated rear screen is divided into two levels, {LP (low power); HP (high power)} from 0A to 25A
- Heated mirrors is divided into two levels, {LP (low power); HP (high power)} from 0A to 4A
- Heated wiper park is divided into two levels, {LP (low power); HP (high power)} from 0A to 10A
- Heated steering wheel is divided into two levels, {LP (low power); HP (high power)} from 0A to 6A
- Heated front seats (pair) are divided into two levels, {LP (low power); HP (high power)} from 0A to 18A
- Heated rear seats (pair) are divided into two levels, {LP (low power); HP (high power)} from 0A to 18A

- Cabin blower is divided into three levels {LP (low power); MP (medium power); HP (high power)} and its range is from 0A to 35A. Cabin blower speed is variable and dependent on the automatic operation of the climate control system or it can also be selected manually by the customer. Figure 6.11 shows the membership functions (fuzzification) of the electrical features as inputs to both controllers in the integrated ELMS:

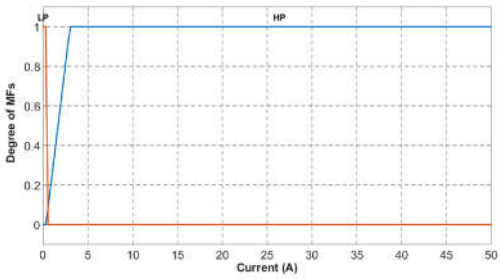

(a) Heated front screen

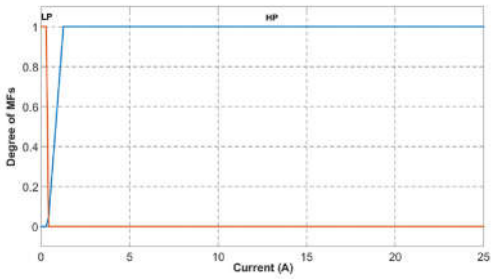

(b) Heated rear screen

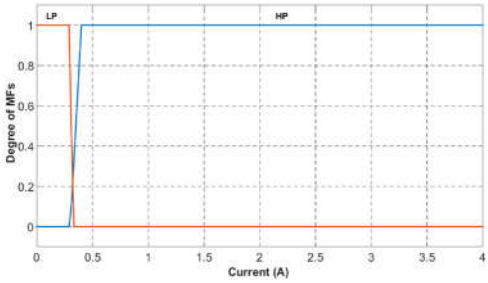

(c) Heated mirrors

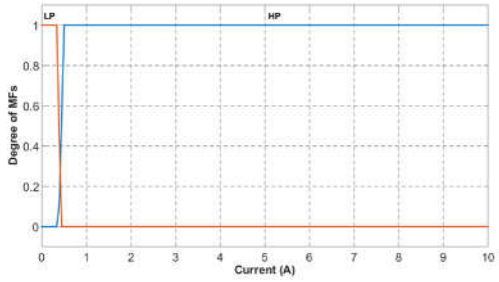

(d) Heated wiper park

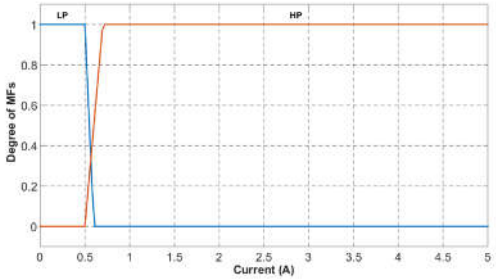

(e) Heated steering wheel

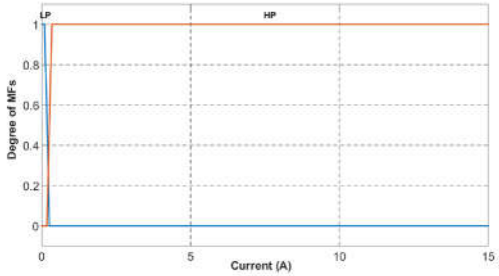

(f) Front heated/cooled seats

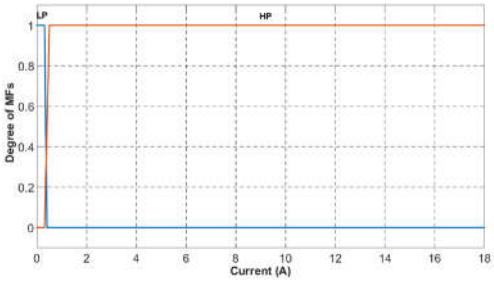

(g) Rear heated/cooled seats

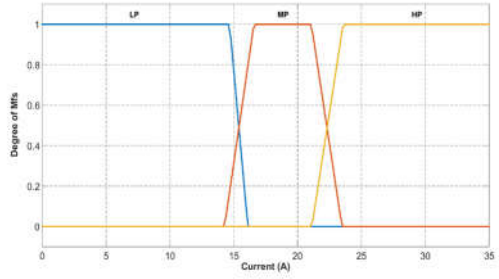

(h) Cabin blower

Figure 6.8. Membership functions of the electrical features/loads

FCI is very important input to the overall control strategy. It is divided into seven overlapped MF levels {VL (very low); L (low); LM (low medium); M (medium); MH (medium high); H (high); VH (very high)} representing $g.km^{-1}$ of CO2. These concourses represent the contributing fuel emissions due to electrical energy usage to vehicle's total fuel emissions starting from 0 $g.km^{-1}$ to 45$g.km^{-1}$. The overlapping between the concourses guarantees a smooth transition within the operation region. The weight factor of this input is higher than the rest, this reflects the priority of the controller to decide amongst the inputs and prioritise the actions in order to minimise the impact of electrical energy on vehicle's emissions.

CSI input, as a novel approach to the proposed EEMS, is divided into three levels {L (low); M (medium); H (high)} and its normalised range is from 0 to 1. Figure 6.12 shows the membership functions of the FCI and CSI inputs as used from both controllers:

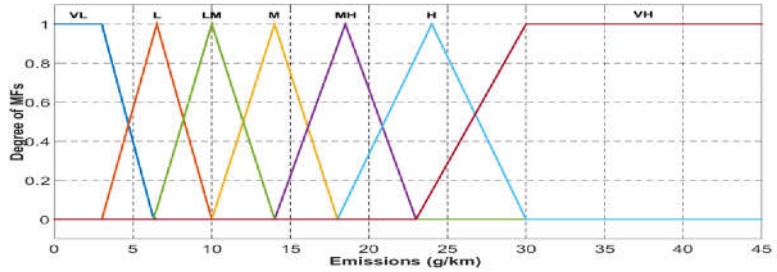

(a) Fuel Consumption Index

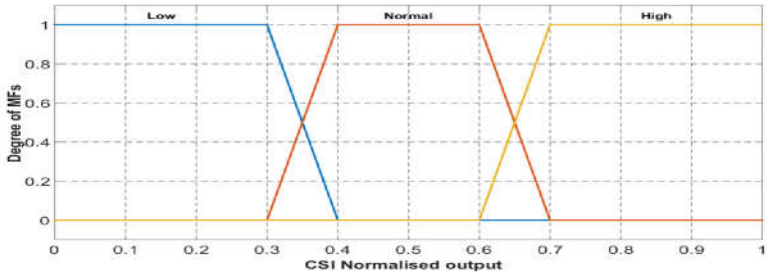

(b) Customer Satisfaction Index

Figure 6.9. Membership functions of FCI and CSI as used by FLC_*glazing* and FLC_*cabin*

The output of both controllers (defuzzification) is the electrical energy allowance to meet the overall electrical demand requested. Both electrical load allowance outputs have been divided into 6 overlapped MF levels {VVL (very very low); VL (very low); L (low); M (medium); MH (medium high); H (high)} with a range from 0A to 70A. The membership functions have been chosen based on experimentation and actual vehicle testing including individual attribute test performance feature. Figure 6.13 show the membership functions of the outputs:

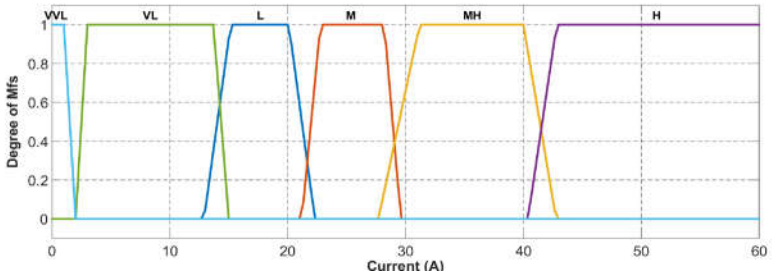

(c) Optimal total electrical load allowance

Figure 6.10. Membership functions of the output electrical load allowance realised as $I_{\_glazing\_optim}$ and $I_{\_cabin\_optim}$

6.3.3.2 Implementation of fuzzy rules

The performance of both FL controllers within Electrical Energy Management System, FLC_*glazing* and FLC_*cabin*, depend heavily on the fuzzy rules developed. A fuzzy rule base (inference stage) was developed for each of the controllers described in section 6.3.3.1.

For FLC_*glazing*, the optimal rule base was found from vehicle testing and experimentation. A rule base of 112 rules (i.e. 2^4 x7) is built to relate the 5 inputs with the output electrical loading, four inputs with 2 overlapped levels and one input (i.e. FCI) with 7 overlapped levels.

Table 6.2 describe the rule base of the FLC_*glazing* within the ELMS. The top row of the table describes the sets of the FCI while the left column includes all combinatory rules between all 5 inputs including HFS, HRS, HMR, HWP and FCI. The output of the rule base is a combination of all possible states of the electrical features and their output based on FCI. The combined rules are explained as follows:

- If no electrical loads/features are selected by the customer or low power features (i.e. HMR, HWP) are enabled then the electrical load allowance is very low based on FCI.
- If high power loads are selected (i.e. HFS, HRS) by the customer and fuel consumption index is high (i.e. high fuel consumption) then the current allowance of those electrical features is reduced (therefore their power allowance) until fuel consumption index reach lower levels
- If all electrical features have been selected by the customer, or automatically due to the environmental conditions (i.e. very cold temperatures), then the FLC has been tuned to minimise the operation of those loads at an initial stage, due to the impact of high fuel consumption rate. Power consumption allowance is restored when FCI reaches lower levels.

Electrical features		FCI (Fuel Consumption Index)						
		VL [0-40]	L [40-55]	LM [50-60]	M [55-65]	MH [60-70]	H [65-80]	VH [80-100]
When HFS=LP AND HRS=LP AND HMR=LP/HP AND HWP=LP/HP	$I_{\_glazing\_optim}$	VL	VL	VL	VL	VL	VL	VL
When HFS=HP AND HRS=HP/LP AND HMR=HP/LP AND HWP=HP/LP		MH	MH	MH	M	M	L	L
When HFS=HP AND HRS=HP AND HMR=LP AND HWP=LP		M	M	M	L	L	L	L
When HFS=HP AND HRS=HP AND HMR=HP AND HWP=LP		MH	MH	M	M	M	L	L
When HFS=LP AND HRS=HP AND HMR=LP AND HWP=LP		L	L	VL	VL	VL	VL	VL
When HFS=LP AND HRS=HP AND HMR=HP/LP AND HWP=LP/HP		L	L	L	L	VL	VL	VL
When HFS=LP AND HRS=HP AND HMR=HP AND HWP=HP		M	M	L	L	L	L	L
When HFS=HP AND HRS=HP AND HMR=LP AND HWP=HP		H	H	MH	MH	M	M	L
When HFS=HP AND HRS=LP AND HMR=HP/LP AND HWP=HP/LP		MH	MH	M	M	L	L	VL
When HFS=LP AND HRS=LP AND HMR=HP AND HWP=HP		L	L	L	VL	VL	VL	VL

Table 6.2. Rule base of FLC_*glazing* fuzzy logic controller

The relation between the input and the output variables can be clearly related in the surface plot as shown in Figure 6.14. Some key characteristics of this relation based on the rule are:

- HFS power allowance is prioritised differently compared to the rest of the heated loads, the controller allows longer operation of the load even though FCI reports medium high to high levels. This is explained due to the legal requirements on the operation of this heated element, prioritised against other loads and scheduled to operate longer. However, if FCI is reporting high levels, the power allowance of this feature remains low.
- HRS power allowance is more restricted than HFS due to the lack of legal requirements on its operation. The rule base has been developed to restrict performance of this feature as a trade-off to fuel economy.
- HMR and HPW are less power consuming electrical features. Since HMRs are related to driver's visibility, power consumption allowance is higher than HWP due to its low power consumption

levels. On contrary, HWP is limited when FCI reports high levels, as at this stage no electrical features should operate.

The surface plot of the FLC variables is shown in Figure 6.14:

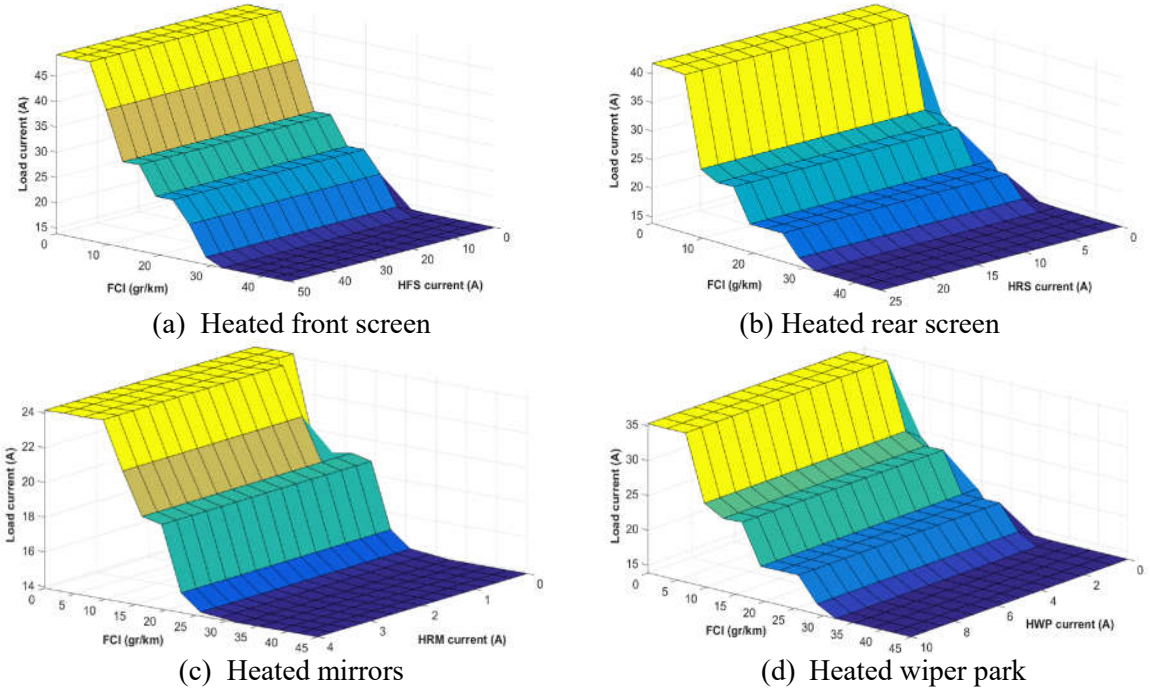

Figure 6.11. Surface plot for the FLC operation of the electrical features based on FCI

For FLC_*cabin*, the second FL controller within the proposed EEMS strategy, the optimal rule base was developed similarly from vehicle testing and attribute feature experimentation. A rule base of 504 rules (i.e. 2^3 x3x7x3) is built to relate the 6 inputs with the output electrical current allowance, three inputs (i.e. HSW, heated/cooled front/rear seats) with 2 overlapped levels, one input with 3 overlapped levels (i.e. cabin blower), one input (i.e. FCI) with 7 overlapped levels and finally another input with 3 overlapped levels representing CSI. The output of the electrical features based on FCI and CSI can be clearly related in the surface plots as shown in Figures 6.15 and Figure 6.16. Key characteristics of this relation are described below:

- HSW power allowance is at lower priority comparing to others loads. Power allowance gradually reduces since FCI reports low to low medium levels. However, when CSI is selected from normal to high levels, power allowance levels are increased.
- Heated/cooled seats power allowance mapping is similar as these loads have similar electrical load operation and share similar priority index. As heated or cooled seats retain the feeling of warmth or coldness due to the thermal conductivity of the particular fabric/leather of the seats, those electrical loads can be limited even when FCI report medium levels of fuel consumption. Seat operation gradually reduces when FCI increasing and can reach 100% power allowance limitation when FCI

approaching high levels. On the other hand, heated/cooled electrical function of the seats ramps up when CSI levels increased from low to normal levels.

- Cabin blower operation is different from the rest of the electrical features as it is a variable load based on blower speed settings. Its rule set weight has been set high, equal to one, against CSI as this will determine the efficiency of climate control and the temperature within the cabin. Cabin blower power consumption is reduced gradually based on FCI levels but it will remain at its low power consumption levels even though FCI index is critically high. Based on CSI, its power allowance gradually increases with full allowance at high levels of CSI.

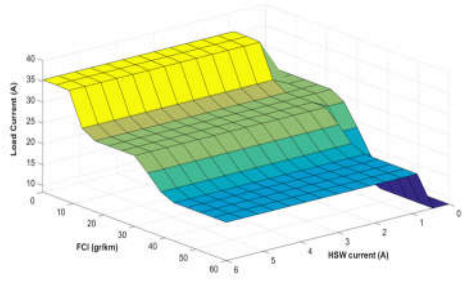

(a) Heated steering wheel

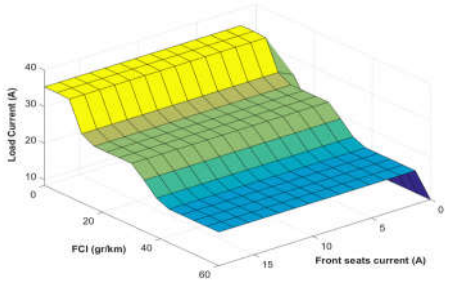

(b) Heated/cooled front seats

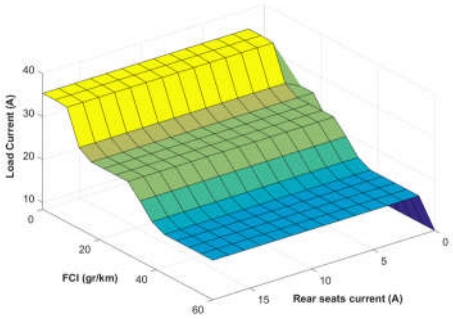

(c) Heated/cooled rear seats

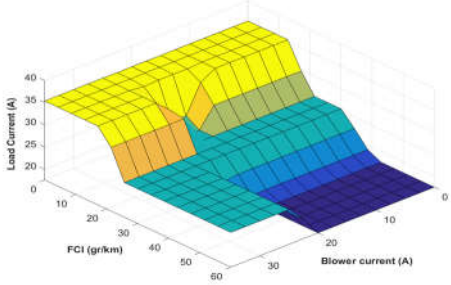

(d) Cabin blower

Figure 6.12. Surface plot for the FLC operation of the electrical features based on FCI

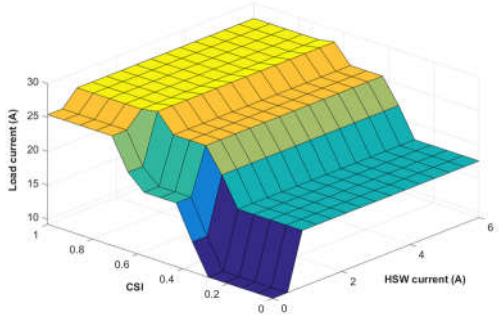

(a) Heated steering wheel

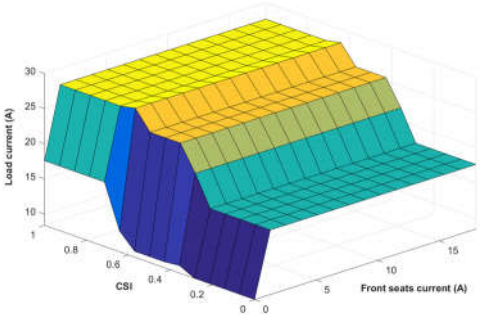

(b) Heated front seats

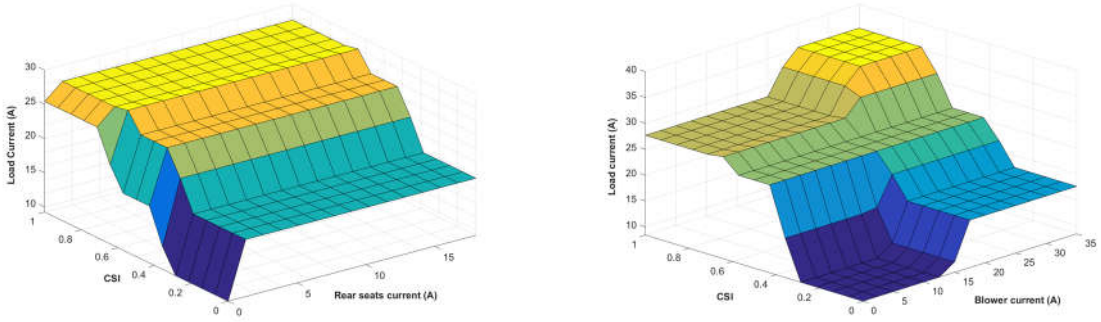

(c) Heated rear seats (d) Cabin blower

Figure 6.13. Surface plot for the FLC operation of the electrical features based on CSI

6.4 Simulation scenarios

This section presents the simulation studies to investigate the effectiveness of the proposed FLC based EEMS applied to perform energy-efficient electrical feature usage and minimise the impact of electrical energy usage on vehicle's overall fuel consumption. It exploits the control algorithm formulated in section 6.3 and the power supply system model developed in Chapter 5. The development of EEMS and its simulation studies are performed in MATLAB®/Simulink™ environment. The complete simulation environment structure is presented in Appedix D.

To assess the performance of the strategy, multiple simulation scenarios denoted as Test-case 1 to Test-case 3 are proposed. Each test case concerns different driving conditions including various electrical loading usage scenarios as well as variations of the comfort levels of the customer. The rationale to introduce a variation on the above test cases is summarised as below:

- *Ambient temperatures:* The ambient temperatures for tests have been chosen to provide stress to the vehicle and power supply but also to ensure the certain electrical features that need to be included in the evaluation of the EEMS will operate. They have also been selected based upon the availability of data regarding the power supply performance at that temperature.
    - The *lowest temperature* selected for our simulations was -5.5^{0}C. At this low temperature, charge acceptance of the battery effectively reaches its lowest level at this point and remains unchanged below this temperature. In addition, electrical heating features within the cabin are expected to operate longer while customer satisfaction index CSI is expected to be high most for the duration of the testing.
    - The *highest temperature* selected for our simulations was at +40^{0}C. This has been selected based upon environmental data collected around the world. The environmental data shows significant variation in ambient temperature during the day for hot climate

conditions with variations of between 15^0C to 25^0C being considered normal. In this case, $+40^0$C, with maximum solar load is a good compromise for the most likely day to day stress that a vehicle and its power supply system may experience. At extreme high temperatures, high engine cooling loads are engaged therefore higher contribution from battery sources is expected to meet cooling demand within the cabin, therefore high CSI for cooling.

- *Medium temperatures* selected for our simulations were at $+25^0$C and $+10^0$C. The temperatures used in this range are chosen to give the best chance of capturing the operation of all possible electrical features including some engine base (i.e. related to emissions) loads that may occur at only these temperatures. At such typical moderate climate conditions of $\approx 25^0$C, no significant electrical power demand is considered due to vehicle's climate control while on lower or higher temperatures there is a significant electrical power drain due to customer's increased usage of comfort features or cabin temperature heat demand. In addition battery charge acceptance is at its optimum temperature level, therefore battery contribution is the key factor at this range to achieve a balance between FCI and CSI.

- *Solar loading levels:* Various solar radiation levels have been used for the purposes of the simulation studies. Typically, the annual average horizontal solar radiation for Europe on the earth's surface is 120 W/m^2. This minimum value covers more than 80% of the population of the Eu-27 countries as stated by Climate Action, EU (2020). Real world solar irradiance profiles as recorded from LEV's solar load sensor have been used to analyse the performance of the solar panel under realistic conditions.
- *Battery charge levels:* Differing battery charge requirements are applied for different tests such as 90%, 80%, 70% and 50%, mainly due to the variation in charge acceptance capability of the battery with temperature and battery SoC. They have been also selected to demonstrate the ability of the FL controllers to maintain battery SoC levels within the acceptance optimum range as defined between 50% and 80%.
- *Road speed profiles:* The road speed profiles have been chosen with reference to available data from testing and reports from various testing facilities used by JLR. Two specific driving cycles are used which have been briefly described in Chapter 5, these are the Drive-Idle-Drive (DID) cycle and the Combined Suburban and City Traffic Cycle (CSCT). Both driving cycles have been selected to provide a variety of conditions that illustrate how well the FLC based EEMS can cope with various engine speeds and electrical load levels. The road speeds have also an impact on the power supply's electrical functions as well as the power generation capability. Additionally, a typical commuting driving cycle has also been added as part of the data recorded from LEV. Using a typical real world driving scenario

adds realism to the overall simulation assessment and produce the evidence needed to implement such FLC strategy on real vehicle applications.

- *Electrical features:* The electrical features used during the tests have been selected based on the likelihood of them being frequently operated. As such, the vehicles are not tested with every possible electrical load switched On because this condition is expected to be an extremely rare condition.
- *Engine Off Power Management:* Engine Off load management is a key characteristic to the proposed FLC based power management strategy. During long duration parking (i.e. vehicle parked at work environment), solar energy harvesting will contribute significantly to i) eliminate the level of battery discharge allowed for a single operational period therefore reduce the risk of damage due to battery discharge and ii) vehicle operation will resume with battery charge levels very high, close to 100%, therefore greater battery usage allowance during engine running conditions. This will reduce alternator's duty cycle while offering great benefits to vehicle's overall fuel consumption.

6.4.1 Test-case 1 Drive-Idle-drive (DID) cycle scenario

The speed profile used in this scenario is the DID cycle as described in Chapter 5 and details of the cycle are included in Appendix E. This cycle demonstrates the capability of the power supply system to maintain optimum fuel consumption levels during high engine speed and idle periods. For this particular driving scenario, we have introduced several noise factors, part of the real world variation that every vehicle and its power supply system is exposed to. The variations include:

- Initial battery SoC set at various levels.
- Initial ambient temperatures set at different levels.
- Introduce CSI variation to demonstrate the performance of the control strategy based on different customer selected levels.

6.4.2 Test-case 2 Combined Suburban & City Traffic (CSCT) cycle scenario

The speed profile used in this scenario is the Combined Suburban & City Traffic cycle as described in Chapter 5 and details of the cycle are included in Appendix E. This cycle demonstrates the capability of the power supply system and its FLC based power management system to maintain optimum fuel consumption level during low engine speed levels and stop-start cycles. For this particular driving

scenario, we have introduced several noise factors, part of the real-world variation that every vehicle and its power supply system is exposed to. The variations include:

- Initial battery SoC set at various levels.
- Initial ambient temperatures set at different levels.
- Introduce CSI variation as per Test-case 2.

6.4.3 Test-case 3 Real world driving cycle based on LEV experiment

The speed profile used in this scenario is a typical commuting driving cycle as described in Chapter 4 and is part of the real world driving conditions recorded using the Low Emissions Vehicle (LEV). Figure 6.17 shows an engine and vehicle speed profile as recorded using the LEV vehicle:

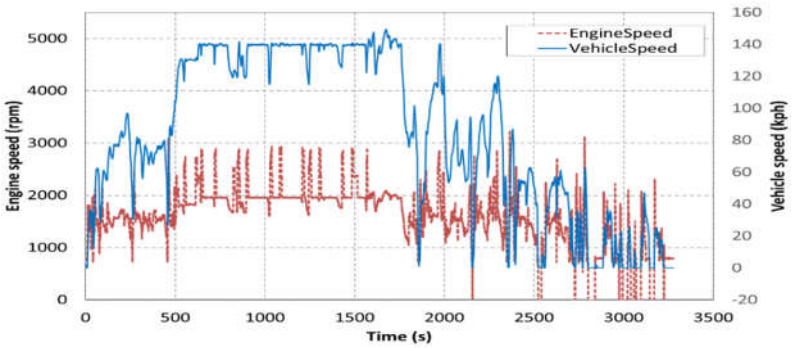

Figure 6.14. Real World driving cycle

This cycle demonstrates a typical commuting route including low city traffic speeds, stop-start and high speed phases. Using real world measured data, we will demonstrate the capability of the FLC based power supply management strategy to achieve high levels of CSI while maintaining optimum fuel consumption levels at various conditions. For this driving scenario, we have also included variability similar to the above two driving scenarios including:

- Initial battery SoC set at various levels.
- Initial ambient temperatures set at different levels
- Introduce an ENR phase, including engine Off quiescent current drain applied to vehicle's power supply system.
- Introduce supplementary battery charging during ENR phase due to solar harvesting.
- Introduce CSI variation as per Test-case 1 and Test-case 2.

6.4.4 Solar load irradiance levels

Solar irradiance levels have been measured while conducting LEV experiment and the data have been used for our simulation purposes. Figure 6.18 shows two solar irradiance profiles as having been measured by LEV's solar sensor. Plot (a) depicts a typical solar load variation during the real world driving cycle which averages at 445.5 Wm^{-2} while plot (b) depicts a 10-hour recorded data of solar irradiance while the vehicle was on ENR phase. The average solar power of this recording was measured at 716.4 Wm^{-2} on a sunny day with minimum overcast spells. The data collected was from 8.30am to 6.15pm. For our simulation scenarios, we purposely vary solar irradiance levels in order to analyse the effect of such variation on the overall charging performance and fuel economy.

(a)

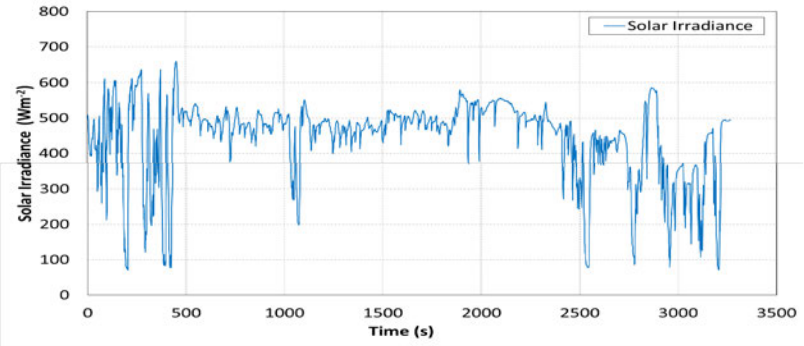

(b)

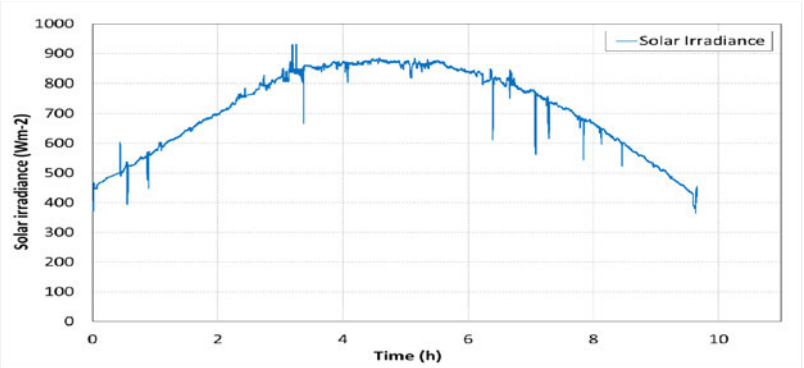

Figure 6.15. a) Real world measured solar irradiance during engine running conditions, b) Real world measured solar irradiance during ENR phase

The simulation setups for the test scenarios Test-case 1 to Test-case 3 including the variation of certain inputs of the overall strategy are summarised in Table 6.3:

Test Case	Driving profile	Ambient Temperature	Initial Battery SoC	Solar Irradiance levels
Test-case 1 • Typical DID scenario • Two levels of initial SoC • Performance assessed by energy balance and fuel consumption	DID	i. $+40^0$C ii. $+25^0$C iii. -5.5^0C	i. 50%, ii. 60%	Solar panel Not used
Test-case 2 • Typical CSCT scenario • Two levels of initial SoC • Performance assessed by energy balance and fuel consumption	CSCT	i. $+40^0$C ii. $+25^0$C iii. $+0^0$C	i. 70%, ii. 80%	Solar panel Not used
Test-case 3 • Real world driving cycle • One level of initial SoC • Performance assessed by energy balance and fuel consumption	Real world commuting cycle	i. $+25^0$C ii. $+0^0$C	i. 70%,	i. Real world solar profile ii. ENR solar profile

Table 6.3. Summary of three test-cases used in the simulation studies.

6.5 Simulation analysis

6.5.1 Local FLC alternator strategy performance

Prior to assessing the performance of the overall EEMS strategy, it is important to demonstrate the benefits of the proposed FLC alternator strategy. The simulation scenarios used for this assessment, used the driving profile from Test-case 2 with two different initial battery SoC levels set at 70%, and 90% demonstrating the operation of the alternator as developed and described at section 6.3.2. Figures 6.19-20 depict the performance of the FLC based alternator strategy compared to the conventional over CSCT driving cycle. The simulation results correspond to: vehicle's electrical load demand and alternator output (subplot 1); battery current (subplot 2); battery voltage (subplot 3) and state of charge (SoC %) (subplot 4). In trace 1, the solid line is the vehicle electrical load demand, the dashed line is the FLC based alternator current output and the dotted line is the conventional alternator current output. In traces 2-4, similarly, the dashed line represents the performance of other parts of the power supply system when FLC alternator strategy is applied while the dashed line represents system performance operating with conventional alternator.

Figure 6.19 depicts the performance of the developed FLC based alternator strategy comparing to the conventional system. The speed profile used in this test scenario is described in Appendix E, section

E.1. In subplot 1, the initial battery SoC condition is at 70% which is close to optimum level of 80%. The conventional alternator operates as an open-loop system, therefore, retain charging function until limited by the capacitance of the battery or the levels of electrical demand needed. On the other hand, FLC based alternator operation supports charging and electrical loading until battery SoC reaches 80%, at approximately 1000 secs, then switches to a minimum charging mode (i.e. trickle-charge operation) in order to maintain battery SoC levels while providing electrical support to vehicle's load demand. For the second half of the driving cycle, an oscillation on the battery's current and voltage output is exhibited due to the vehicle's acceleration and deceleration phase. This engine speed variability is reflected upon the alternator's operation resulting in such oscillation current mode. However, the developed FLC based alternator strategy outweighs the conventional alternator operation by reducing its current output to minimum needed to maintain battery's target SoC levels. This, in a long term, increases system stability and robustness.

Sublots 2 and 3 depict battery currents and voltages achieved during this test scenario. While on conventional system battery charges at maximum current rating, based on its SoC levels, FLC alternator limits charging rate to minimum levels as needed to maintain battery's charging levels at 80%. System voltage level also reflects this optimal operation with levels kept below 13V when 80% SoC has been achieved.

Sublpot 4 depicts battery's SoC during the driving cycle. While on the conventional alternator strategy the battery is still charged above 80%, FLC alternator reduces its output to a minimum to maintain that target. The priority is given to minimise the alternator's output to a minimum, therefore significantly reducing its impact to fuel consumption. The effect of FLC based alternator strategy on fuel consumption will be extensively discussed as part of the simulation analysis of the overall FLC based EEMS.

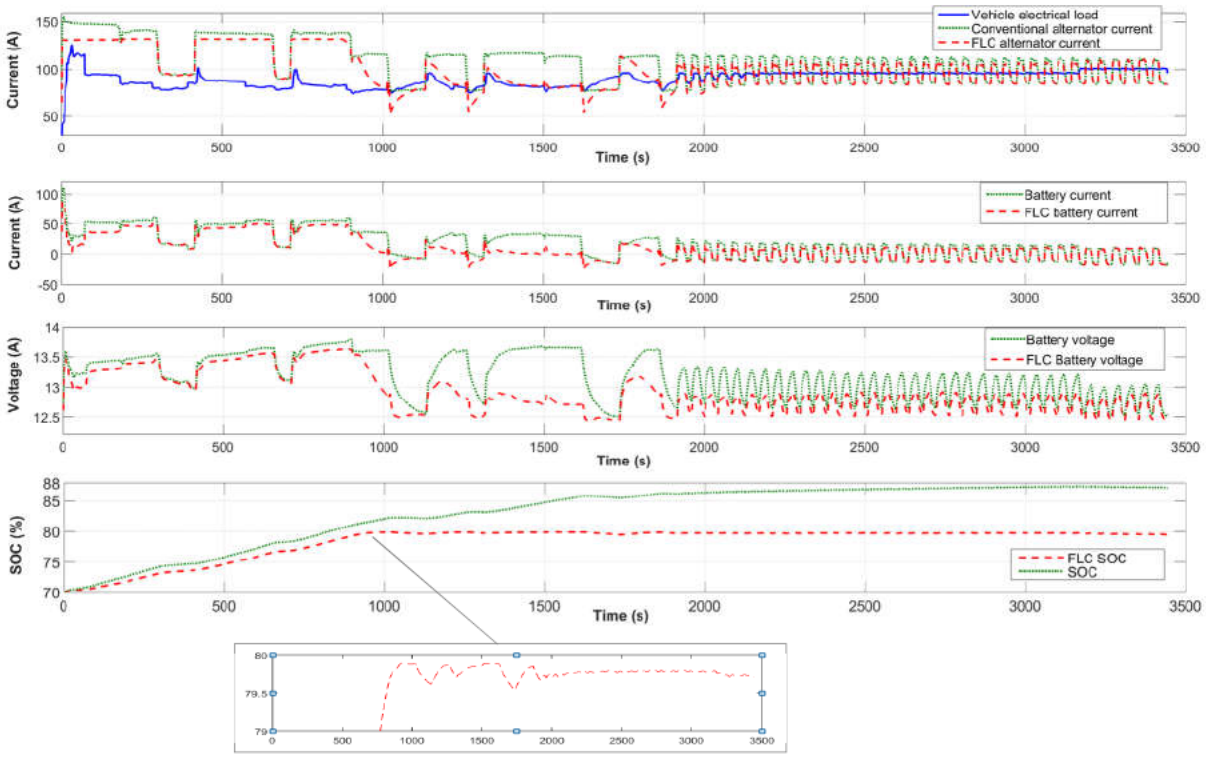

Figure 6.16. Simulation results at ambient of +40^{0}C, CSCT test output at 70% initial battery SoC

Figure 6.20 depicts the performance of the developed FLC based alternator strategy comparing to the conventional system however in this test scenario the initial battery SoC level is set to 90% which is higher than 80% the battery should be maintained. In subplot 1, the conventional alternator maintains charging function until battery's SoC reaches 100%. This is detrimental to the overall lifecycle of the battery as accelerates aging and increases efficiency losses on a system level. On the other hand, FLC based alternator operation is switched Off at high SoC levels. Battery supports the electrical load demand until its SoC levels reach 80%, at approximately 450 secs. The alternator operation resumes to a minimum charging mode (i.e. trickle-charge operation) in order to support electrical demand while maintaining battery SoC target level.

Subplots 2 and 3 depict battery currents and voltages achieved during this test scenario. On a conventional alternator system, battery charges at maximum current rating therefore its voltage levels reach as high as 14.5V. Battery operates at voltage levels higher than 12.9V throughout the driving cycle. On the other hand, with FLC alternator strategy, alternator operation is set to discharge mode (i.e. alternator switched Off). During discharging, battery voltage levels reach 12.2V for the first 500 secs. When alternator operation resumes, battery voltage recovers and regulates below 13V during trickle charging mode. Finally, subplot 4 depicts battery's SoC during this test scenario as maintained to a target level of 80%.

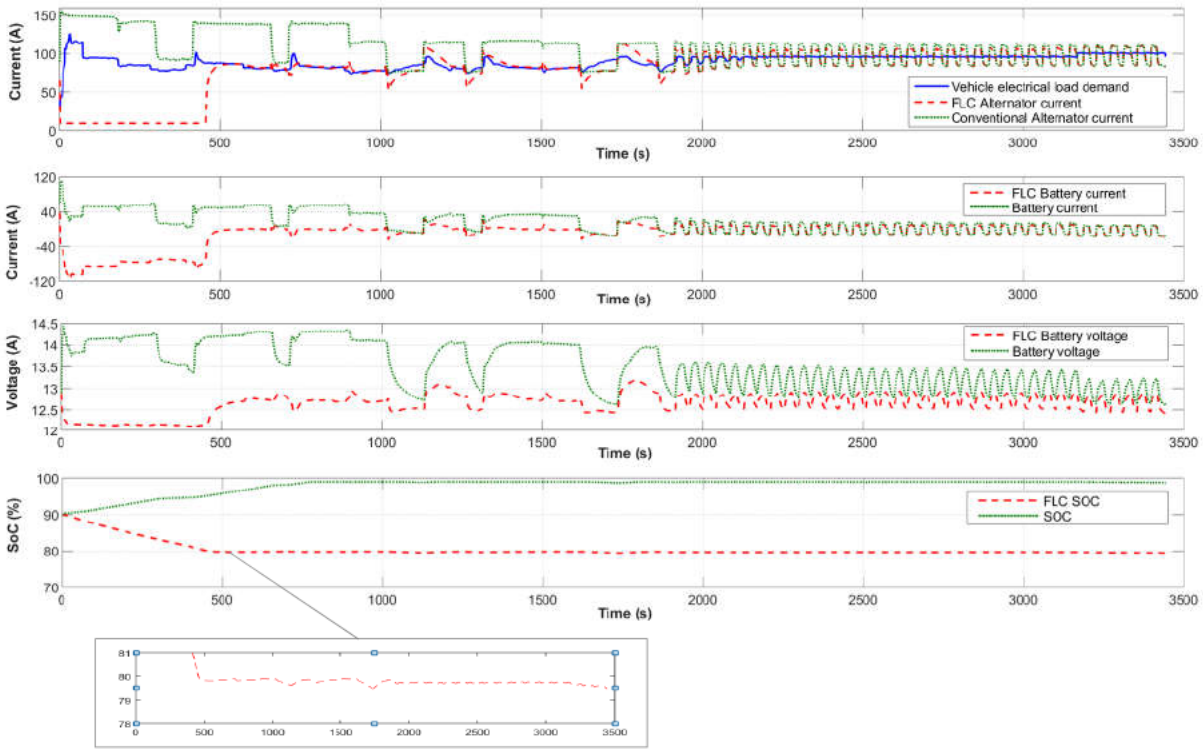

Figure 6.17. Simulation results at ambient of +40^{0}C, CSCT test output at 90% initial battery SoC

Test scenarios including high battery SoC levels is a particular area of discussion at this study due to the great fuel savings the proposed FLC based alternator strategy introduces together with the use of the photovoltaic panel as an extra means of energy source. A detailed analysis of the simulation results and the benefits of the proposed advanced power supply system and its FLC EEMS will be presented in the following section.

6.5.2 Global FLC EEMS simulation performance

At this section, we will demonstrate the performance of the proposed EEMS including various levels of CSI, different initial SoC levels, ambient temperatures and electrical loading conditions. The simulation scenarios used for this assessment are described on **Test-case 1, Test-case 2 and Test-case 3.** In addition, for **Test-case 3,** we also demonstrate solar panel's contribution to vehicle's fuel economy on a typical customer commuting trip. The simulation results correspond to: vehicle electrical load demand (subplot 1); alternator current output (subplot 2); battery current (subplot 3); battery voltage (subplot 4); battery SoC (subplot 5) and fuel consumption (subplot 6).

In trace 1, the solid line is vehicle's electrical load demand without EEMS (i.e. conventional power supply system), the dashed line is vehicle's electrical load demand as regulated by EEMS with CSI level set at 0 and denoted as FLC & FCI=0. The dotted line is vehicle's electrical load demand when EEMS is applied and CSI level is set at 0.5, denoted as FLC & CSI=0.5.

In traces 2-5, similarly, the solid line represents the performance of other parts of the power supply system during conventional operation while the dashed and the doted lines show the performance of the system when EEMS is applied and CSI is set either 0 or 0.5. Finally, in trace 6, the solid line is the contribution of electrical energy to total fuel consumption measured in ml over the duration of the test. The dashed and dotted lines represent the performance of the system when EEMS is applied and CSI levels are set to 0 and 0.5 respectively.

6.5.2.1 Test-Case 1 – DID driving cycle at ambient of +40^{0}C

At this test scenario, the only enabled electrical feature regulated by EEMS during the entire simulation was cabin blowers. Climatic seats as well as the rest of cabin electrical features have been switched-Off for the entire duration of the test. Initial battery SoC is set to 50%, which is considered to be worse case scenario. Such low SoC levels can only be achieved when vehicle is parked and not used for an extensive long period (i.e. 60days). DID cycle involves an initial driving period with constant vehicle and engine speed, followed by an idle period of 30mins and finally by another driving period of high vehicle and engine speed.

Figure 6.21 depicts the performance of the EEMS comparing to the conventional system. On the conventional power supply system, electrical load demand is not regulated by EEMS therefore it reaches a maximum value of 130A with a mean value recorded at 87.95A over the cycle. Cabin blowers (BLW) electrical consumption vary between maximum 33A and 17A during the test.

At the beginning of the test cycle, alternator output is set to the highest level to meet vehicle's electrical system demand including charging the battery (i.e. SoC increases). During idle phase, electrical load demand exceeds alternator's capacity (i.e. reduced engine speed) and therefore it results to battery discharge at a current level of -18A. This discharge is also reflected to battery voltage which reach as low as 12.02V comparing to 13.76V during constant speed driving phase. Fuel consumption is estimated at 708.2ml.

EEMS with CSI set at 0 (low level), is focused to minimise customer satisfaction to achieve maximum fuel economy benefits. Vehicle's electrical load demand is reduced to 111A with a mean value recorded at 79.24A over the cycle. The calculated control action from EEMS reduces the duty cycle of the cabin blowers from 33.6A (high speed) down to 15.11A (medium speed) for 670s. Cabin

speed drops further at 671s therefore EEMS reduces further its current consumption from 15.11A to 8.4A (low speed). The reduced electrical load demand is reflected in alternator's capacity during the idle period. The alternator provides electrical power on both battery and electrical features while the battery retains its charge levels (i.e. 60%). Exiting idle period, alternator's capacity meets total electrical demand resulting in battery charging at a current level of 65A towards the end of the test. Since battery's SoC level reaches 80% at 4500s, FLC based alternator strategy switches to trickle charging mode thus regulating battery charge at a level of 0-2A. Fuel consumption is estimated at 635.5ml, an improvement of 10.2% comparing to that of the conventional system.

When CSI is set at 0.5 (normal level), EEMS aims to improve fuel economy whilst simultaneously, allow higher electrical power allowance. During the initial phase, electrical load demand is limited to 118A maximum with a mean value recorded at 79.75A over the complete cycle. The calculated control action from EEMS reduces the duty cycle of the cabin blowers from 33.6A (conventional system) to 17.7A (medium speed) for 670s. Cabin blower speed drops further at 671s, resulting EEMS to further reduce its output to 9.42A (low speed). The performance of the power supply system follows similar performance as previously (i.e. CSI=0) however as expected, battery SoC reaches 80% at 4555s, 55s later than when CSI was set to 0. Fuel consumption is estimated at 639.8ml, an improvement of 9.7% comparing to that of the conventional system.

Comparing the performance of both strategies for two different CSI levels, the following observations are made. The contribution of electrical energy to fuel consumption reduces significantly over the conventional system even though the only electrical feature managed by the EEMS is cabin blowers. Improvements made in the range of 10.2% and 9.7% are significant for a specific driving cycle and ambient temperature. In addition, FLC based alternator strategy, contributes to better fuel economy, by reducing alternator's output to a minimum when the desired target SoC level (i.e. 80%) has been achieved.

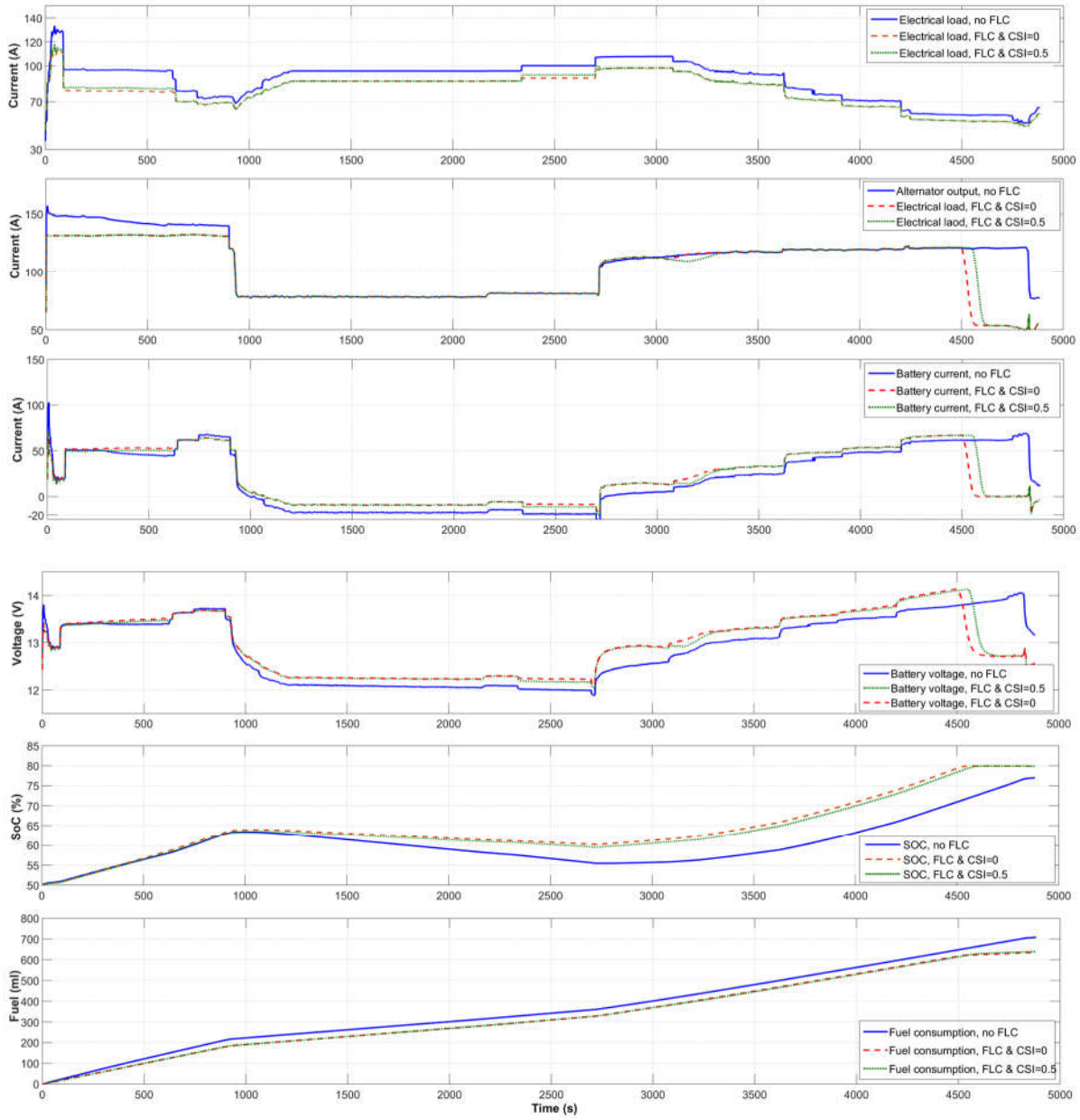

Figure 6.18. Simulation results at ambient of +40^{0}C, DID test output at 50% initial battery SoC

6.5.2.2 Test-Case 1 – DID driving cycle at ambient of -5.5^{0}C

In this scenario, electrical features enabled by the customer were heated front screen (HFS), heated rear screen (HRS), heated steering wheel (HSW), heated wiper park (HWP), heated mirrors (HMR), front and rear heated seats and finally cabin blowers (BLW). Initial battery SoC is set to 50%. The DID cycle is divided into three phases, initial drive period (0s - 900s), followed by an idle period (900s - 2700s) and finally by another drive period (2700s - 4515s).

Subplot 1. On the conventional strategy, at the initial phase of the test, total electrical load demand reaches a maximum value of 188.9A. The contribution of the cabin and glazing features to total electrical loading was set at 129.1A. HFS operated (40A) at the beginning of the test (40A) for 380s and switched Off until switched back On at 4267s. HRS operated (18A) for 1244s then switched Off, and On at 2742s until the end of the cycle. Front and rear heated seats operated for 1244s and 876s respectively with current consumption at 17A for front and 14A for rear seating. In addition, 3 electrical load peaks have been recorded at 866s, 2748s and 3643s due to the actuation of the electrical suspension (20A). The rest of the heated electrical loads (HSW, HWP and HMR) operated for the entire driving cycle. A mean value of 106.1A was recorded.

When EEMS is enabled, at the initial phase of the test, total electrical load demand is reduced as expected due to the calculated control of the strategy to minimise electrical loading whilst benefit fuel economy. When CSI is set at 0, maximum electrical load recorded at 112A. (39% reduction comparing to the conventional system). The contribution of the cabin and glazing features to the overall electrical loading has been limited to 47A, since FCI[5] is estimated very high (VH) at 32g.km^{-1}. EEMS continue to monitor and limit electrical loading for the rest of the cycle with a mean value recorded at 77.5A.

When CSI is set at 1, maximum electrical load recorded at 127.7A (32% reduction to the conventional system). The contribution of the cabin and glazing features to the overall electrical loading has been limited this time to approximately 60A. EEMS continue to monitor and limit electrical loading for the rest of the cycle with a mean value recorded at 82.74A.

Subplot 2. On the conventional system, for the first 900s, alternator output is measured at 159A, as responding to electrical load demand including battery charging (i.e. SoC increases). With EEMS enabled, alternator output follows similar trend as per conventional system however its output is reduced to 131.4A due to the decreased load demand.

During idle phase, alternator output is set to 83A since its output is limited due to engine speed. Similar performance is observed with EEMS enabled too.

Towards the end of the cycle, on conventional system, alternator output is set to maximum to meet load demand and recharge battery. With EEMS enabled, the alternator output is reduced to minimum at 3700s (CSI=0) and 4150s (CSI=1) respectively since battery's SoC increased at 80% (subplot 5). Finally, the alternator output responds to HFS (On at 4267s) and increases its output to meet the demand.

Subplot 3. At initial phase, electrical load demand exceeds alternator output therefore battery discharges at a level of -30A (conventional system) while recovering when electrical features are switched Off. During idle, battery discharges at -18A however due to HRS switches Off at 1244s, load

[5] FCI overlapped levels are defined on section 6.5.2, graph 6.12a

demand reduces thus allowing limited battery recharge at 2A. At the end of the cycle, the conventional system provides limited charging to the battery at 41A until HFS switches On at 4267s. This reduces alternator output to minimum, resulting to battery charging of only 16A.

With EEMS enabled, alternator output supports load demand and battery charging. During idle, regulated load demand benefits alternator capability to support limited battery charging at 2A. At the end of the cycle, battery current increased to 61A (CSI=0) however when SoC reach 80%, the current level is reduced to 0-2A as alternator output is limited (i.e. trickle charge mode).

Subplot 4. At the beginning of the cycle, battery voltage fluctuates from 12V to 13.43V (conventional system) as expected reflecting alternator's capacity to meet electrical demand. However, with EEMS enabled, battery voltage level achieved is higher at13.5-13.75V due to the limited regulated load demand.

During idle, battery voltage is set as low as 12.02Vmainly due to alternator's output is dependent on engine speed. This is reflected on all three different strategies. At the end of the cycle, voltage level achieved is 13.41V for the conventional system, and 14.43V and 13.9V for CSI=0 and CSI=1 respectively. EEMS reduces voltage level to 12.67V when battery charge reached 80% SoC.

Subplot 5 & 6. The operation of all three strategies (i.e. conventional, CSI=0 and CSI=1) is reflected to battery SoC levels and fuel consumption estimations. Battery SoC level, when conventional system is used, increased to only 69.43% compared to 80% when EEMS is enabled. Furthermore, the contribution of the electrical energy to fuel consumption, with conventional system was estimated at 768ml whilst EEMS is enabled, fuel consumption was estimated at 593ml (CSI=0) and 639.6ml (CSI=1), an improvement of 22.7% and 16.7% respectively. Figure 6.22 depicts the performance of the EEMS comparing to the conventional system.

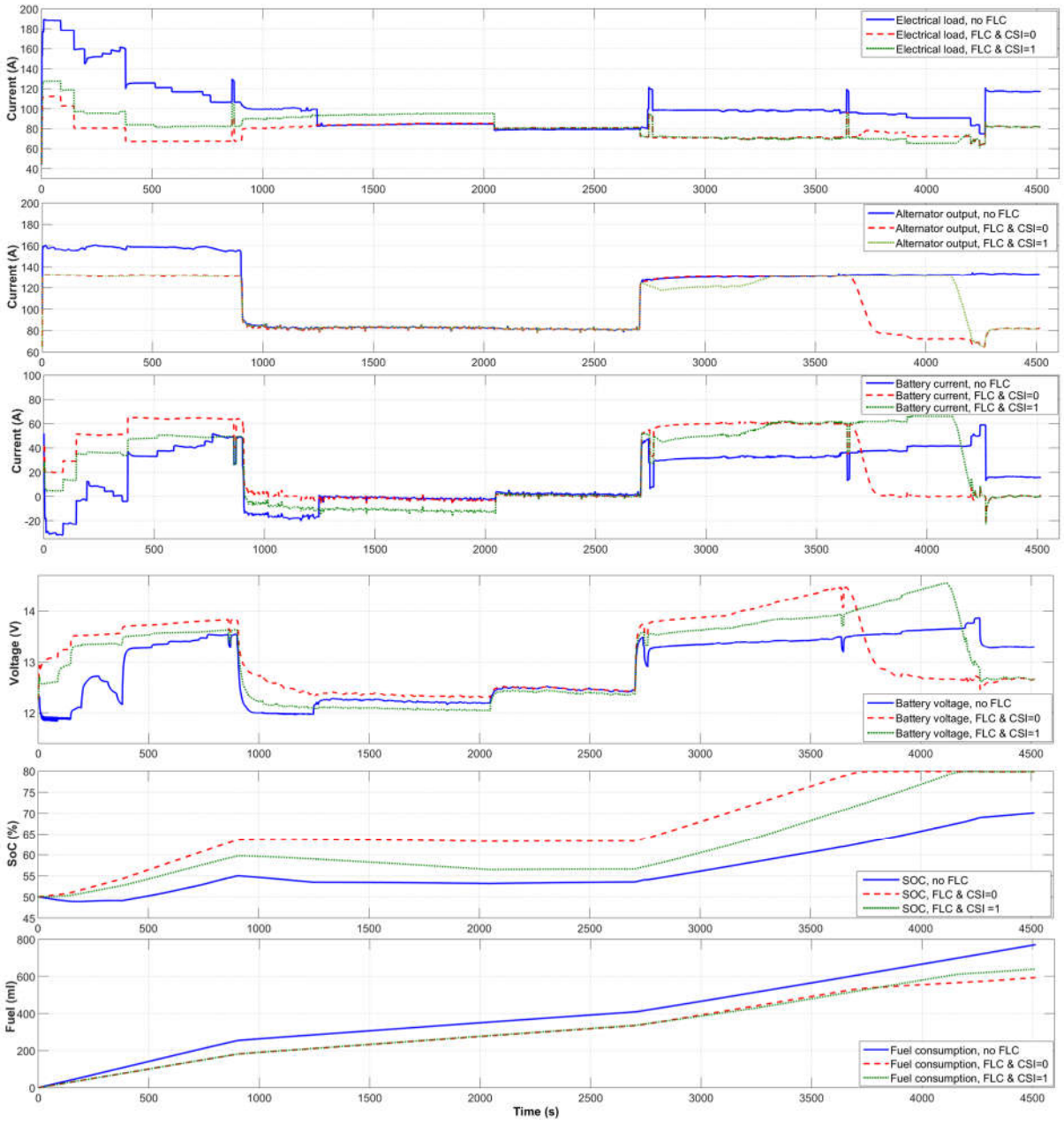

Figure 6.19. Simulation results at ambient of -5.5^{0}C, DID test output at 50% initial battery SoC

Table 6.4 includes a summary of test scenarios with CSI set to low, normal and high. From the results, it is clear that at 40^{0}C ambient, EEMS improves fuel consumption contribution by 10.3% (highest) and 6.3% (lowest) compared to the conventional operation. It is noteworthy, that Test-case 1 is a worst case scenario for any vehicle's power supply system. This is due to the fact that the system has to balance between battery recharge, due to low initial SoC levels and meet high electrical load demand. Therefore, 10% reduction achieved with EEMS is considered to be a good performance compared to conventional strategy.

Furthermore, at an ambient temperature of -5.5^{0}C, EEMS operation improved fuel consumption by 22.8% (CSI=0) and 16.7% (CSI=1). EEMS reduced electrical load allowance significantly, however, due to low battery SoC level, battery charge acceptance is high. A more detailed analysis is required to identify areas for improvement under these worst case conditions. This is included within the scope of further work.

DID cycle								
Electrical Loads	**Control Strategy**	**SoC (%)**	**Temp (^{0}C)**	**Alternator Output μ value (A)**	**Electrical Load Demand μ value (A)**	**FCI (g.km^{-1})**	**Fuel (ml)**	**Fuel Reduction (%)**
Cabin BLW	Conventional	50	40	107.9	87.95	26.77	708.2	-
	EEMS CSI = 0			101.3	79.24	25.14	635.5	10.3%
	EEMS CSI = 0.5			101.8	79.75	25.27	639.8	9.7%
	EEMS CSI = 1			104.6	84.62	25.96	663.4	6.3%
HFS, HRS, HSW,HWP, FS & RS, Cabin BLW	Conventional	50	-5.5	119.4	117	28.71	773.8	-
	EEMS CSI = 0			102.2	77.95	24.88	593	22.8%
	EEMS CSI = 0.5			103.1	79.6	25.17	609	20.7%
	EEMS CSI = 1			105.2	82.74	25.1	639.6	16.7%

Table 6.4. EEMS performance under different CSI levels at ambient temperature of 40^{0}C and -5.5^{0}C.

6.5.2.3 Test-Case 2 – CSCT driving cycle at ambient of 40^{0}C

In this scenario, electrical features enabled by the customer were front cooling seats and cabin blowers (BLW). Initial battery SoC is set to 80%. CSCT[6] cycle is divided into two phases, the suburban traffic phase (0s - 1920s), followed by the city traffic cycle phase (1920s - 3600s).

Subplot 1. On the conventional system, during the suburban phase, total electrical load demand reaches a maximum value of 143.8A. Cabin blowers vary between 33A for the first 183s, down to 27A for additional 100s, reduced to 22A for another 500s until operating at 17.5A for the rest of the driving cycle. Both front cooling seats operated at a total of 15.1A for the first 765s limited to 7.5A for the rest of the test cycle. A mean value of 96.55A for vehicle's total load demand has been calculated over the complete driving cycle.

When EEMS is enabled, at the initial phase of the test, total electrical load demand is reduced as expected due to the control action of the strategy. When CSI is set at 0, maximum electrical load recorded at 113.8A. (21% reduction comparing to the conventional system). The contribution of the cabin blowers and both front cooling seats to the total load demand is limited to 20A, since FCI is

[6] CSCT cycle is defined at Appendix E, section E.1

estimated high (H) at 22.4g.km^{-1}. EEMS continue to monitor and limit electrical loading for both cabin blowers and front seating. The calculated mean value of total electrical demand is 86.44A.

When CSI is set at 1, maximum electrical load recorded at 128.2 (11% reduction to the conventional system). The contribution of the blowers and front seating has been limited this time to 35A at the initial phase of the cycle whilst reduced to 17.5A at the second phase, allowing full duty cycle of the cabin blowers. The calculated mean value of total electrical demand is calculated at 94.24A.

Subplot 2. During the first phase of the cycle, on the conventional power supply system, alternator's output is measured at 149.8A, as responding to electrical load demand while its output fluctuates as limited due to low engine speed periods during the cycle. With EEMS enabled, alternator output follows similar trend as per conventional system however its output is reduced to 110A due to the decreased load demand. Since the initial battery SoC is 80%, the alternator output is kept to minimum –trickle charging mode.

Subplot 3. Battery charging is kept at good levels during the entire cycle with minimum periods of discharge due to alternator overloading (electrical load exceeds alternator capacity). Towards the ends of the cycle alternator output oscillates due to the acceleration/deceleration phase of the city traffic cycle.

With EEMS enabled, alternator output supports both load demand and battery charging. During idle, regulated load demand benefits alternator capability to support limited battery charging at 2A. Towards the end of the cycle, battery is recharged with currents as high as 61A (CSI=0) while reducing to 0-2A when reach 80% SoC and alternator switched to trickle charge mode.

Subplot 4. At the first phase of the cycle, under conventional operation, battery voltage fluctuates between 13.6V to 13.9V with five occurrences down to 12.7V due to low engine speed impact on alternator output (overloading). For the second phase of the cycle, battery voltage cycles between 13.4V and 12.75V, this cyclic behaviour is caused due to the dynamic operation of the alternator during acceleration/deceleration city traffic phase.

However, with EEMS enabled, battery voltage levels achieved are set to 12.7V -12.8V due to limited charging applied by the alternator (i.e. trickle charge operation at 80%). In addition, EEMS strategy reduces battery oscillations therefore improves battery voltage stability.

Subplot 5 & 6. The operation of all three strategies (i.e. conventional, CSI=0 and CSI=1) is reflected to battery SoC level and the contribution of electrical energy on vehicle's fuel consumption. Under conventional operation, battery charged up to 91.51% while under EEMS operation, battery's charge level regulated at 80% SoC.

The contribution of electrical energy to fuel consumption was estimated at 500.5ml (conventional system) whilst for EEMS estimated at 593m (CSI=0) and 639.6ml (CSI=1), an improvement of 22.7% and 16.7% respectively. Figure 6.23 depicts the performance of the EEMS comparing to that of the conventional system.

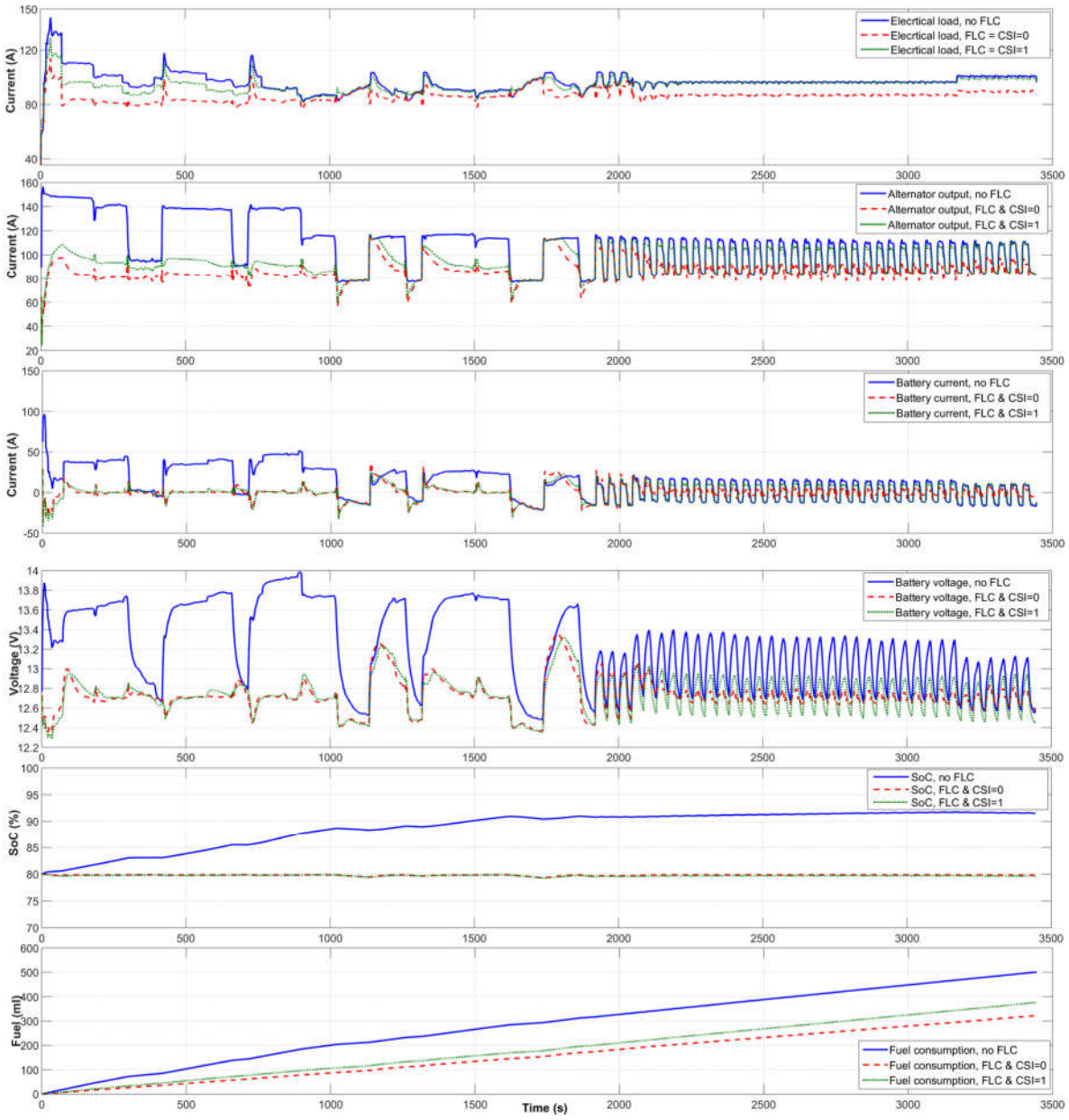

Figure 6.20. Simulation results at ambient of +40^{0}C, CSCT test output at 80% initial battery SoC

6.5.2.4 Test-Case 2 – CSCT driving cycle at ambient of +10^{0}C

In this scenario, electrical features enabled by the customer were heated steering wheel (HSW), front and rear heated seats and finally cabin blowers (BLW). Battery initial SoC is set to 80%.

Subplot 1. On the conventional system, during the suburban phase, electrical load demand reached a maximum value of 133.5A. Cabin blowers vary at 27A for the first 189s, reduced to 13.8A up to 1202s, until further reduced to 10.8A for the rest of the driving cycle. Front cooling seats operated at a total of 13.94A for the first 764s, reduced to 7A for the rest of the cycle. Rear seats, in a similar manner, operated at a current value of 17.45A for 477s, reduced to 8.7A for additional 400s until switched Off (877s). HSW operated at 5.1A constantly over the complete cycle. The variation of the above loads is reflected on the total electrical load which gradually reduced to 70A at the beginning of the city traffic cycle phase (2047s). Four high current peaks on 598s, 1384s, 2278s and 2314s are due to air suspension operation. A mean value of 112.5A has been calculated over the cycle.

When EEMS is enabled, at the initial phase of the test, total electrical load demand is reduced as expected due to the control action of the strategy on the heated loads. With CSI=0, maximum electrical load recorded at 90.1A. (32% reduction comparing to the conventional system). The contribution of the cabin blowers, both front and rear cooling seats and HSW to the total load demand is limited to 28A at the initial phase of the cycle since FCI is estimated high (H) at 21.8g.km^{-1}. EEMS continues to monitor and limit electrical loading (allowance reduced to 22.61A at 250s) however due to the rear seats being switched Off at 877s and FCI estimated at 17g.km^{-1} (medium level), EEMS continues to allow full operation of the rest of the electrical features (BLW, HSW and FS). The EEMS calculated mean current 76.31A.

When CSI is set at 1, maximum electrical load recorded at 128.2 (11% reduction to the conventional system). The contribution of the cabin blowers, both front and rear cooling seats and HSW to the total load demand is limited to 35.4A at the initial phase of the cycle since FCI is estimated high (H) at 24.35g.km^{-1}. EEMS continue to monitor electrical load consumption, while further reducing electrical load allowance down to 25.7A at 877s (rear seats switched Off) until the end of the cycle. The mean value of EEMS electrical load demand has been calculated at 96.48A.

Subplot 2. At the beginning of the cycle, on conventional system, alternator's output is measured at 159.8A, as responding to electrical load demand while its output fluctuates due to low engine speed periods during the cycle. With EEMS enabled, alternator output follows similar trend as per conventional system however its output is reduced to 89A (FCI=0) and 98.14A (FCI=1), responding to the reduced load demand. Since the battery initial SoC is 80%, the alternator output is kept to minimum

(i.e. trickle charging mode) output levels with mean value current calculated at 66.29A (CSI=0) and 70.17A (CSI=1) respectively.

Subplot 3. Battery current and its recharge performance reflects the alternator output (subplot 2) over the cycle. While on conventional system battery charging is high due to alternator's available capacity, under EEMS regulation, battery charging is kept at minimum (i.e. 0-2A) levels, maintaining SoC target at 80%. During the second phase of the cycle, battery current follows a cyclic waveform due to the start-stop driving phase of CSCT. Comparing to conventional system, EEMS battery current output performs a shorter cyclic amplitude which benefits system voltage stability.

Subplot 4. Battery voltage fluctuates between 13.6V to 14.9V during the suburban phase. This is caused due to alternator overloading under low engine speed periods included at this phase. For the second phase of the cycle, battery voltage oscillates similarly to alternator oscillating operation. However, when EEMS is enabled, battery voltage levels are kept between 12.5V - 12.9V (i.e. trickle charging operation) which improves system stability and robustness.

Subplot 5 & 6. The operation of all three strategies (i.e. conventional, CSI=0 and CSI=1) is reflected to battery SoC levels and fuel consumption estimations. Under conventional operation, battery SoC recharged up to 98% while under EEMS operation, battery's charge levels regulated at 80% SoC. The effect of the EEMS operation is demonstrated on fuel consumption. The contribution of electrical loading was estimated at 546.9ml for conventional system, 204ml when CSI=0 and 225.6ml when CSI=1. The improvement of the EEMS compared to the conventional system is at a level of 64% and 59% respectively which is significant savings to vehicle's total fuel consumption. Figure 6.24 depicts the performance of the EEMS comparing to that of the conventional system.

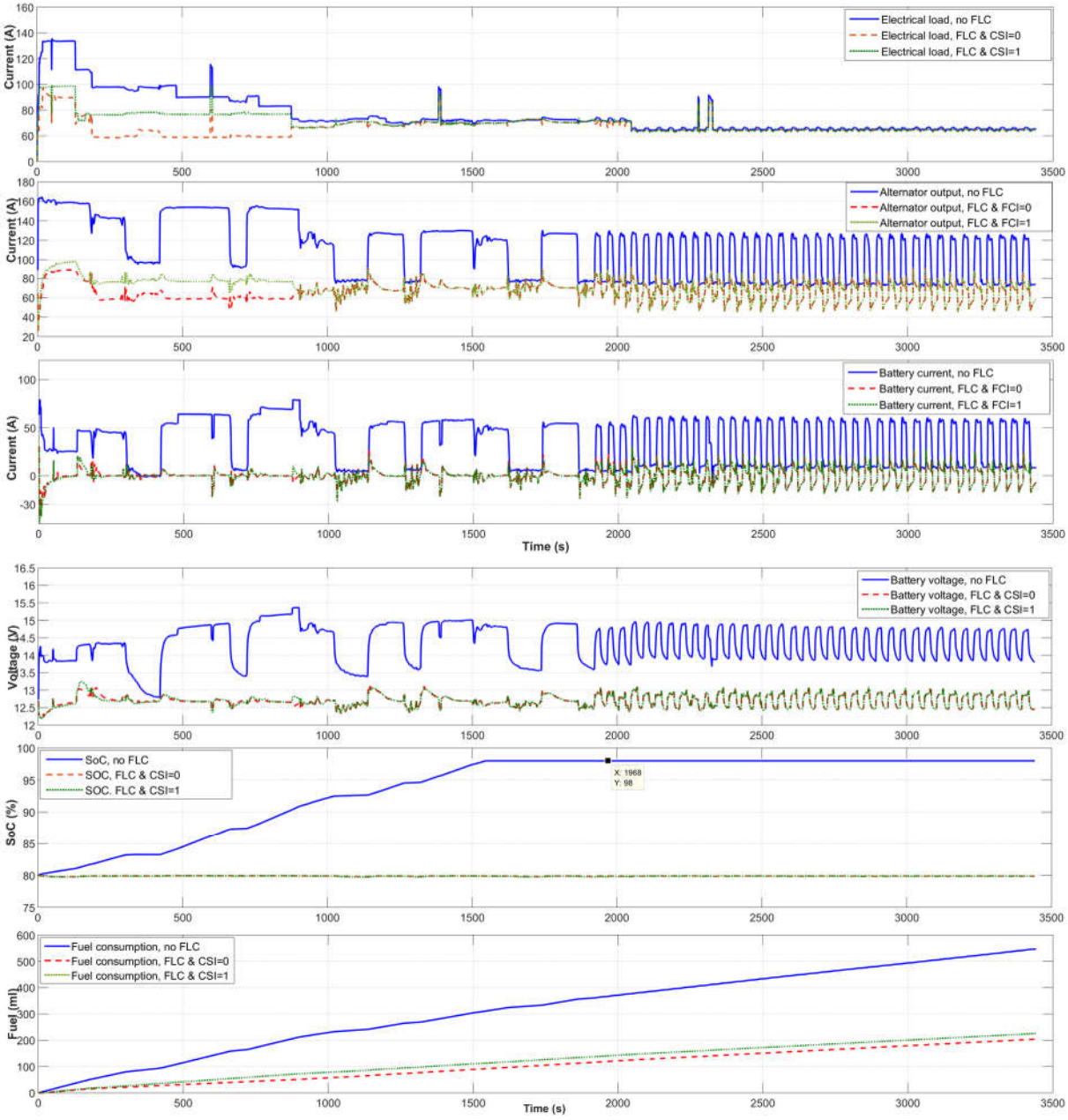

Figure 6.21. Simulation results at ambient of +10^{0}C, CSCT test output at 80% initial battery SoC

Table 6.5 includes a summary of test scenarios with CSI set to low, normal and high. From the results, it is clear that at 40^{0}C ambient, EEMS improves fuel consumption by 177.6ml equivalent to 35.5%, compared to the conventional operation. An observation can be made that the reported improvements, is a result of EEMS and the FLC alternator strategy working in parallel since alternator output is also reduced due to battery's SoC level at 80%.

Furthermore, at an ambient temperature of 10^{0}C, and with more electrical features enabled, the combined EEMS and FLC alternator strategy result to an improvement of 62.7%. However, it is also

evident from the results that with CSI set at 0 or 0.5, the improvement achieved was almost of the same level. This leads to the conclusion that the EEMS strategy, at this test scenario, didn't performed as expected when CSI was set to 0.5. A more detailed analysis is required to identify areas for improvement under real world driving conditions. This is included within the scope of further work.

CSCT cycle								
Electrical Loads	**Control Strategy**	**SoC (%)**	**Temp (^{0}C)**	**Alternator Output μ value (A)**	**Electrical Load μ value (A)**	**FCI (g.km^{-1})**	**Fuel (ml)**	**Fuel Reduction (%)**
Cabin BLW	Conventional	80	40	108.6	96.55	26.96	500.5	-
	EEMS CSI = 0			86.25	86.44	21.44	322.9	35.5%
	EEMS CSI = 0.5			86.63	86.86	21.5	324.9	35.1%
	EEMS CSI = 1			93.81	94.24	23.28	375.9	25%
Cabin BLW HSW FS&RS	Conventional	80	10	112.5	76.31	27.93	546.9	-
	EEMS CSI = 0			66.29	66.44	16.45	204.1	62.7%
	EEMS CSI = 0.5			68.6	68.75	17.03	216.3	60.5%
	EEMS CSI = 1			70.17	70.32	17.42	225.6	58.7%

Table 6.5. EEMS performance under different CSI levels at ambient temperature of 40^{0}C and 10^{0}C.

6.5.2.5 Test-Case 3 – Real world driving cycle at ambient of +10^{0}C

In this section, the result of simulating the proposed EEMS over a real world scenario will be presented. The scenario will include the use of a solar panel and its charging contribution to the vehicle's battery SoC and power supply system performance. In addition, an assessment of the EEMS over the complete test scenario will be made.

The test scenario is a typical work commute driving cycle as recorded from LEV's vehicle daily usage and shown in Figure 6.17. Solar irradiance profile used during the driving cycle and ENR phase has been shown in Figures 6.18a and 6.18b. The scenario includes the following three phases:

- Trip 1: work commute as specified in Test-case 3
- Day Park: 10-hour park (ENR) as specified in section 6.4.4
- Trip 2: return work commute to home

Figure 6.25 shows the vehicle speed and solar irradiance profiles over an approximately 12-hour time period. For simplicity, Trip 1 and Trip 2 are assumed to have identical drive cycles.

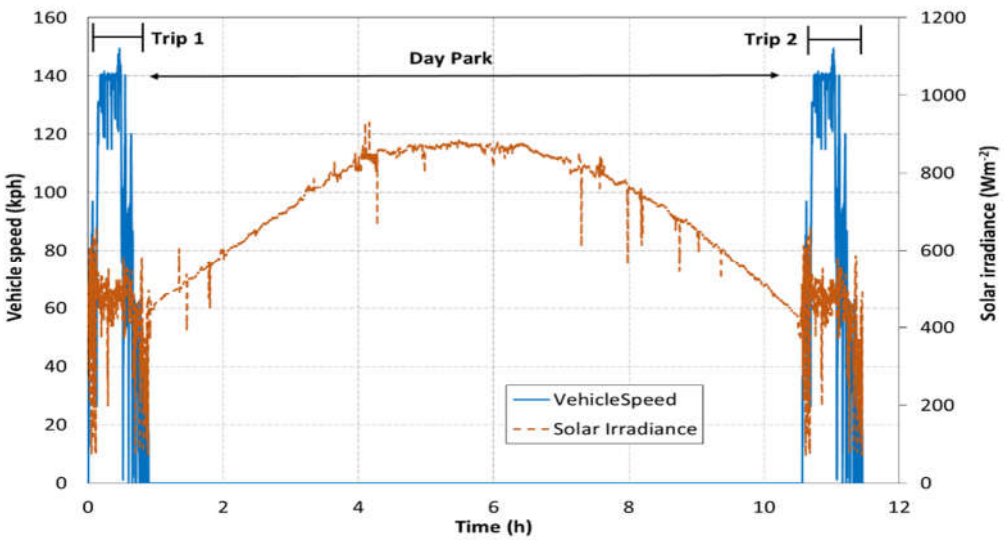

Figure 6.22. Vehicle speed and solar irradiance profiles over the complete real world test scenario

The simulation results correspond to: vehicle electrical load demand (subplot 1); alternator current output (subplot 2); battery current (subplot 3); battery voltage (subplot 4); battery SoC (subplot 5); fuel consumption (subplot 6); solar irradiance (subplot 7); solar panel current output (subplot 8) and battery charge in amp-hour (subplot 9).

In traces 1-6, the solid line represents power supply system's performance as similarly described on the previous scenarios (i.e. Test-case 1, Test-case 2) during conventional operation. The dashed line shows its performance as regulated by EEMS with CSI level set at 0.

Additionally, for this test case scenario we have included solar panel operation. In traces 7-8, the solid line represents solar irradiance and solar panel current output. Finally, in trace 9, the solid line shows battery charge performance in amp-hours.

Trip 1 (0s – 3271s): For this phase, the electrical features enabled by the customer were HRS, HSW, front and rear heated seats and BLW. Initial battery SoC is set to 70%.

Day park (3271s – 38071s): During this phase, vehicle is parked and ENR while all electrical systems are on sleep mode. Typical power consumption of Jaguar Land Rover vehicles, under sleep mode, is varying between 0.15mA to 0.25mA. For the purpose of our simulations, a quiescent current drain of 0.25mA has been applied to the simulation model equivalent to the test vehicle's power consumption.

Trip 2 (38071s – 41307s): For the commuting return phase, the same electrical features were enabled, however the operation of the loads was altered to add variability to the results.

Figure 6.26 depicts the performance of the power supply system. In detail, we have the following observations:

Trip 1(0s – 3271s):

Subplot 1. Under conventional operation, total electrical load demand reaches maximum value of 127A. Load demand varies based on the operation of the electrical loads with a mean value of 95.17A over this test phase. However, when EEMS is enabled, load demand has been regulated at a maximum value of 82A. A further reduction occurred when battery SoC reach at 80% (830s) and FLC alternator operates at lower levels while battery charging (i.e. trickle charging) is kept at minimum. A mean value of 71.1A has been achieved over the cycle.

Subplot 2. At the beginning of the cycle, during conventional operation, alternator's output is measured at 144A, while its output is reduced responding to the electrical load demand for the rest of the cycle. With EEMS enabled, alternator output follows similar trend as per conventional system however its output is reduced to 118A responding to the reduced load demand. When battery reach 80%, alternator output is regulated at 74A. From 2158s until the end of the cycle, due to vehicle's start/stop events, alternator output cycles to 0A (during engine stop phase). A mean current value of 79.5A is calculated over the test phase.

Subplot 3. During conventional operation, battery charge rates reflecting alternator's output variation. Under EEMS operation, battery charge current is higher at the beginning of the cycle comparing to conventional system due to the reduced electrical load allowance. At 830s, when battery SoC reach 80%, battery current is limited to minimum (0-2A) as expected. However, due to start/stop events, from 2158s until the end of the cycle, battery current cycles between 0A and -70A, as discharges during engine stop phases.

Subplot 4. Battery voltage levels increases from 13V to 14.1V under conventional operation. At the end of the cycle, due to vehicle's stop/start operation, the voltage cycles between 14V and 12.5V as expected due to the support of the electrical loading. Under EEMS operation, battery voltage initially rises to 14.5V, as a consequence of a limited electrical demand and high alternator current capacity. When battery SoC level reach 80%, voltage drops to minimum levels of 12.5V-12.7V. Similarly at the second half of the cycle, due to stop/start operation, battery voltage cycles between 12V to 13.8V.

Subplots 5 & 6. The performance of the two strategies (i.e. conventional, EEMS) is reflected on battery SoC and fuel consumption estimations. Under conventional operation, battery SoC recharged up to 89% with no limitations, while under EEMS operation, battery is recharged at 80% (830s) and regulated on this level for the rest of the cycle. The effect of the EEMS operation is also demonstrated on fuel consumption. The contribution of electrical loading to vehicle's fuel consumption was estimated

at 545ml (conventional system) whilst under EEMS operation was estimated at 318ml, a significant improvement of 41.7% over the cycle.

Subplot 7. On conventional system, battery is recharged with no limitations. Battery SoC reach 90% at the end of the cycle, equivalent to a recharge of 18Ah. In comparison, when EEMS is enabled, battery is recharged up to 80% (830s), equivalent to a recharge of 8.92Ah. Battery charge level remained at the target level of 80% until the end of the cycle.

Subplots 8 & 9. Solar panel current output is variable due to solar irradiance variability with a mean value of 4.23A achieved over this test phase. In addition, solar irradiance levels were measured at 673 Wm^{-2}.

Day park (3271s – 38071s):

Under conventional operation, battery discharges at a rate of 0.25mA over an approximately 10-hour period. As shown in subplot 7, battery voltage depletes slowly to 12.74V. From subplots 5 & 8, battery SoC reduced by 1.3% down to 88.7% equivalent reduction of 1.17Ah.

With solar panel integrated, part of the EEMS strategy, battery recharges maximum to 100% since solar panel current output exceeds vehicle's quiescent current drain. Mean current value over this period is calculated at 4.3A. Battery voltage (subplot 4) increased slowly and reached 13.56V at the end of this test phase.

Trip 2 (38071s – 41307s):

Subplot 1. In a similar manner as in trip 1 phase, when EEMS is enabled, total electrical demand is limited comparing to the conventional system. Peak current value reach 87A compared to 105.9A (conventional operation) however the reduction level is lower than that of trip 1 phase. A further reduction of total electrical load has taken place (39290s) due to both front and rear heated seats being switched Off. Mean current values achieved calculated at 60.15A and 95.03A for EEMS and conventional strategy respectively.

Subplot 2. On conventional operation, alternator's output is measured at 129.4A (maximum), while its output varies towards the end of the cycle due to vehicle's start/stop events. Mean current value calculated at 111.3A. With EEMS enabled though, the benefits of a fully charged battery are exploited by the strategy. Alternator operation is switched Off for 1000s, allowing the battery to discharge to a target level of 80%. When target level is met, its operation resumes providing limited charge (i.e. trickle charging mode). A mean current value of 37.06A is calculated over the cycle.

Subplots 3-4. During conventional operation, battery current and voltage levels vary according to the total electrical demand however at the end of the cycle, as the rest of the system, battery cycles between 54A and -61A while operating at voltage levels of 14.9V to 12.5V. Under EEMS operation at

the beginning of the cycle, battery SoC is at 100% level since the solar panel charged fully the battery during the day park phase. The alternator is switched Off and the battery discharges at a rate of 60A for a period of 1000s. When SoC reaches the target level, alternator operation resumes allowing limited battery charge current (0-4A) as expected. At the end of the cycle, due to vehicle's start/stop events, battery current cycles between 0A and -50A.

Subplots 5-7. The performance of the two strategies can be seen from the rest of the outputs including battery SoC, fuel consumption and battery charge in Ah. Under conventional operation, battery is fully charged to 98%, equivalent to an additional charge of 7.3Ah from the start of this test phase. The contribution of electrical energy to vehicle's fuel consumption estimated at 505.4ml. However, when EEMS is enabled, battery discharges until reach 80% target level. Due to low electrical load level and alternator operation switched Off for the first 1000s, fuel consumption contribution estimated at 88.1ml, a significant improvement of 82.5%.

Table 6.6 includes the performance of the conventional strategy compared to EEMS including all three CSI levels:

Real world cycle								
		Trip 1						
Electrical Loads	**Control Strategy**	**SoC (%)**	**Temp (^{0}C)**	**Alternator Output μ value (A)**	**Electrical Load μ value (A)**	**FCI μ value (g.km^{-1})**	**Fuel (ml)**	**Fuel Reduction (%)**
Cabin BLW HSW HRS FS&RS	Conventional	70	10	119.1	95.17	29.57	545.3	-
	EEMS CSI = 0			79.5	71.1	19.5	317.7	41.7
	EEMS CSI = 0.5			86.81	76.11	21.55	330.1	39.5
	EEMS CSI = 1			87.16	76.47	21.63	332.4	39
		Trip 2						
	Conventional	70	10	111.3	76.73	27.62	505.4	-
	EEMS CSI = 0			37.06	55.77	9.2	88.22	82.5
	EEMS CSI = 0.5			41.43	60.15	10.28	106.1	79.0
	EEMS CSI = 1			41.74	60.46	10.36	107.9	78.6

Table 6.6. EEMS performance under different CSI levels at ambient temperature of 10^{0}C

The benefits of integrating a solar panel within vehicle's power supply system are demonstrated on the test results from Trip 2. The contribution of electrical energy usage to vehicle's fuel consumption has been reduced by 82.5% (CSI=0), a significant reduction compared to the conventional operation. By combining all three phases for the entire driving cycle, EEMS achieved a reduction of 61% (CSI=0), 58.5% (CSI=0.5) and 58.1% for CSI=1. The benefits are even greater considering a vehicle usage over a duration of 5 days commuting, in that case, alternator's operation could be reduced to minimum due to high battery SoC levels achieved by the solar panel.

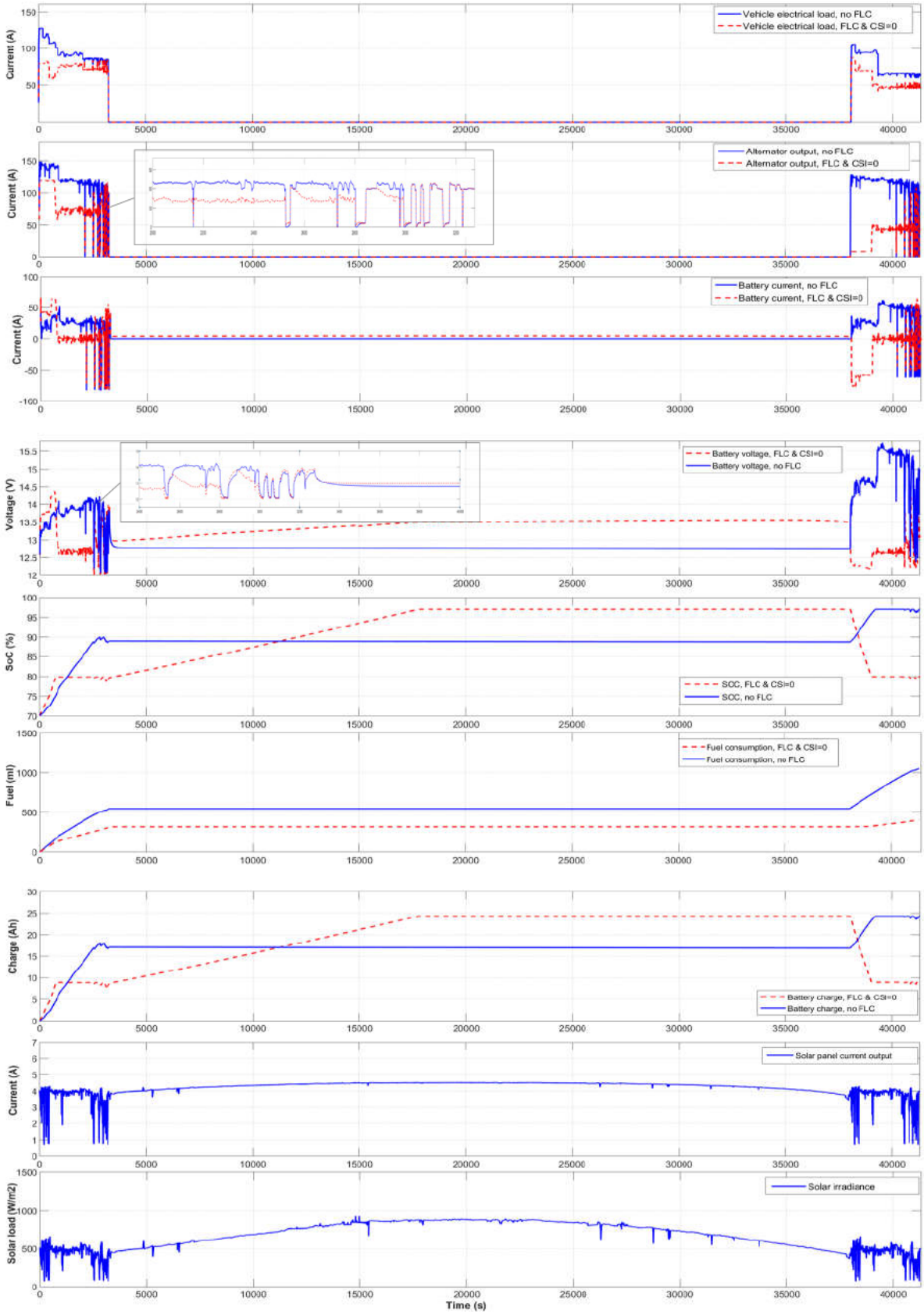

Figure 6.23. Simulation results at ambient of +10^{0}C, Real world cycle at 70% initial battery SoC

6.7 Summary

In this chapter, the development of EEMS using Fuzzy Logic control, has been described. The focus was to provide the development process of the proposed strategy including its key elements, FCI and CSI. EEMS incorporated two subsequent control strategies, FLC_*glazing* and FLC_*cabin,* both controlling total electrical load allowance for all customer comfort and convenience electrical features. The design process of the fuzzy logic controllers including fuzzy rules and membership functions, as part of the inference mechanism, were based on engineering judgement and experience.

In addition, an FLC based alternator strategy has also been developed as part of the EEMS strategy. The strategy minimised alternator operation at a certain battery SoC target level. This contributed to further savings on fuel consumption as described during the simulation results.

The chapter has also presented the simulation studies which are the culmination of the developments described in the previous chapters. The studies have exploited the statistical analysis in Chapter 4 together with the power supply system simulation model developed in Chapter 5. The test cases to evaluate the strategies were developed based on representative driving cycles as described in Chapter 5 and Appendix E.

In Test-case 1, when EEMS strategy is used, the electrical energy consumption levels have been decreased with a reduction of fuel contribution of 22.8% at an ambient of -5.5^{0}C and 10.3% at an ambient of 40^{0}C, compared to the conventional operation. EEMS strategy performed well on all 3 CSI levels. Although the electrical energy allowance is significantly reduced, power supply system prioritises battery recharging therefore any savings on fuel consumption are significantly reduced.

However, as the simulation study of Test-case 2 presents, when EEMS strategy is used, significant improvements of 62.7% and 35% have been achieved at an ambient temperature of 40^{0}C and 10^{0}C respectively. EEMS actions reduced electrical loading to similar levels as per Test-case 1, however as initial battery SoC is set at a target level of 80%, alternator operates at a trickle charge mode. Alternator output is significantly reduced contributing to high net fuel consumption savings.

In Test-case 3, EEMS strategy performed under real world test scenario. The strategy included solar energy harvesting throughout the test. By using the solar panel and its charging capability during day park phase, fuel contribution has been reduced overall to 61.4%, when CSI is set to 0 and 58% when CSI is set to 1. In particular, for the second phase of the test (trip 2), the benefit of the solar panel operation during day park phase contributes significantly to the power supply system operation and its performance. Alternator operated to minimum, resulting in the lowest fuel consumption levels recorded from all test case scenarios.

Chapter 7

Conclusions and Further Work

If you can dream it, you can do it.'
Enzo Ferrari

7.1 Introduction

This chapter presents the main contributions of this research, the overall conclusions and, finally, further improvements and areas of research that could be pursued. The issue discussed in this thesis has been formulated as an electrical energy efficiency control problem. It has been addressed by utilising the benefits of fuzzy logic control to form the proposed electrical energy management system (EEMS). The simulation work has been realised using MATLAB®/Simulink™ to facilitate its future integration with the company portfolio. The approach to develop such a complex system was based on the following framework:

- integrate new technologies on existing vehicle's power supply system and analyse potential benefits on fuel economy,
- carry out experimental measurement in environmental dynamometer chambers as well as on test vehicles operating on UK roads. Exploit these data to calibrate and validate the simulation models,
- develop a simulation model representing the vehicle's power supply system with a good correlation with experimental data and meeting the design criteria,
- develop an experimental methodology to obtain engineering data in order to formulate the relationship between electrical energy and fuel emissions,
- use the experimental data and its statistical analysis to provide an approximated relationship between the major objectives (i.e. fuel emission and electrical energy),
- use the developed relationship within the fuzzy logic control based EEMS to demonstrate the benefits of using such control techniques

In order for the power supply system to be represented as accurately as possible, several parts of an automobile's power supply system were modelled including battery, alternator, ultracapacitor, electrical loads, cabin electrical comfort features and finally a solar panel (Chapter 5). To ensure that the results obtained through simulations were realistic, a number of test drive scenarios were considered (Chapter 5 & 6). These test drive cycles, that included real world vehicle information, were used to first validate the models developed and provide the required confidence to exploit these models to evaluate overall system performance. These drive cycles were also utilised to develop test cases scenarios (Chapter 6) exploiting engine speed profiles and operation of electrical loads/ customer features to evaluate the performance of the electrical EEMS (Chapter 6). The proposed EEMS was realised using a combination of fuzzy logic controllers with extensive sets of rules designed based on the author's in depth knowledge of both system and problem domain. The effectiveness of the fuzzy EEMS was demonstrated under those test scenarios.

The major achievements and observations that can be drawn from this work are presented in Section 7.2 with potential future directions and improvements of the proposed energy management estimator in section 7.3.

7.2 Conclusions

In pursuing the research described in this thesis, a number of innovative proposals to the field of advanced electrical power supply systems and electrical energy management systems have been made. This section presents the conclusions derived from this work with focus on how it answered the research questions stated in Section 1.2 and reproduced here for convenience.

7.2.1 Will electrification have an impact on energy losses and electrical systems' efficiency?

The answer to this research question is yes. The last decade has witnessed a dramatic increase in electrical and electronic components on a typical 12-volt vehicle electrical system configuration. This increase has highlighted the need for appropriate electrical energy management schemes to reduce the electrical load impact on the vehicle's fuel economy. 12-volt electrical systems are still considered to be an integral part of any conventional or xEV powertrain configuration since major electrical systems and customer features are designed to operate on 12V. However, the increasing trend of comfort and

convenience customer features and the potential impact of them on energy conversion, efficiency and fuel economy dictate the use of electrical energy management intelligent strategies.

7.2.2 Can alternative cost effective technologies be used on conventional ICE vehicles to increase energy efficiency, recuperation and regeneration?

The answer to this research question is yes. Conventional ICE vehicles can use cost effective technologies including either hardware or software-based solutions to increase energy efficiency, regeneration and recuperation. The LEV project, described in Chapter 3, has provided Jaguar Land Rover with an ideal research platform to evaluate innovative technologies such as high efficient alternators, ultracapacitors and solar panels connected to an existing power supply system configuration. The outcome of the LEV project has been two fold. First, it has provided an excellent multipurpose vehicle platform incorporating key innovative and 'green' technologies that are available for integration and industrialisation. Integrating technologies such as solar panels and ultracapacitors and investigating its potentials under real world driving conditions, provided the company with 'know-how' and information that could be used for any future implementation. The 'saleable' feature offered by the solar panel is the capability to provide adequate charging to the main energy storage devices during quiescent current phases (i.e. sleep mode), where the vehicle's electrical safety systems consume electrical energy. In parallel, with the continuous development and implementation of telematics, whereby the customer can remotely instruct the vehicle to run certain operations when parked (i.e. remote cabin pre-conditioning), solar panels can provide additional electrical power to support such customer features. In addition, integrating ultracapacitors within the vehicle's architecture, enabled Jaguar Land Rover to explore any potential those devices may have in battery downsizing, support engine cranking during extreme cold conditions and boost the main electrical power supply system during high electrical load cycling.

Secondly, a software-based control strategy provided an integrated energy management solution that regulated the operation of customer's electrical features by minimising their impact on fuel consumption while maintaining customer satisfaction and convenience.

7.2.3 Does electrical energy consumption affect a vehicle's fuel consumption and emissions? Can this effect be experimentally derived and expressed as a mathematical relationship?

Yes, this thesis has demonstrated through experimental studies that electrical energy consumption via its electrical consumers plays a significant role in fuel consumption and vehicle's emissions. Using the LEV project, it provided a mechanism to assess the 'Energy Cost' associated with delivering customer level functions and features translated into a direct relationship to vehicle's fuel consumption and emissions. Extensive vehicle testing was conducted using environmental dynamometer chambers under various electrical loading conditions. This innovative approach led to an original formulation of the fuel consumption index to approximate the impact of electrical energy on fuel consumption (Chapter 4). Adopting this approach, introduced a real world derived relation, between fuel emissions and electrical energy that could be easily adopted for real-time vehicle applications without the need of complex model estimators that require computational power.

7.2.4 Can an integrated software-based solution reduce energy usage and result in fuel economy for conventional vehicles and increase the range for hybrid powertrain configurations?

It was identified in the literature review in Chapter 2, that various methodologies have been developed to contribute to several control strategies that benefit fuel economy by optimising ancillaries or alternatively proposed supervisory control strategies based on limited vehicle information. The evaluation of these methodologies included results obtained during a certain 'window' of operation (i.e. emission driving cycles) while the system operation varies within certain pre-defined limits with no adaptation to unexpected load changes. In this work, the effect of the variation of the electrical loading is included in the EEMS.

A significant achievement of the work presented is the development of EEMS, a fuzzy logic control based strategy that monitors the vehicle's electrical load demand and upon certain inputs regulate the operation of the electrical features. The aim of EEMS is to improve fuel consumption and emissions by managing cabin comfort and convenience electrical features based on the vehicle's fuel consumption levels, while maintaining customer satisfaction as formulated in Chapter 6.

The proposed strategy reduces electrical load operation based on fuel consumption index levels (FCI) while minimising the duty cycle of the alternator based on the battery's SoC. Fuel consumption index is a novel approximation derived from a statistical analysis conducted on a sample of data recorded from real world vehicle testing. This approximation formulates the relationship of electrical energy and vehicle's fuel emissions (Chapter 4). The introduction of a human interface machine element into the EEMS strategy enables the customer greater levels of interaction/control between the customer and vehicle's operation with direct impact on fuel economy. The customer is able to select the level of

performance expected (i.e. low, normal, high) from comfort electrical features within the cabin to benefit the vehicle's fuel economy. This novel concept has been formulated as a customer satisfaction index (CSI).

The FCI concept can be exploited to design solutions such as the proposed fuzzy logic based EEMS, using a heuristic approach of formulating an algorithm derived from experimental data analysis. The effectiveness of the derived concept will be dependent on the sample size of the data as well as the population (i.e. range of vehicle applications) that it has been extracted from.

Similarly, CSI and its human interface machine approach could be widely used on software-based electrical energy management systems applicable to conventional, hybrid and full electric powertrain configurations (i.e. PHEV, BEV) introducing a 'personalisation' feature to enhance customer experience.

Another significant part of the developed EEMS strategy was the integration of the two individual FLC controllers, FLC_*glazing* and FLC_*cabin*. FLC_*glazing* was designed to manage overall electrical load allowance from heated glazing elements around the vehicle such as heated front and rear screens, heated mirrors and heated wiper park. FLC_*cabin*, included customer comfort features such as heated/cooled front and rear seats, heated steering wheel and cabin blowers. Both controllers used FCI as an input, however on FLC_*cabin*, CSI was used as an additional input to the decision making mechanism. A rule base of 112 rules (i.e. 2^4 x7) was developed for FLC_*glazing* while 512 rules (i.e. 2^3x3x7x3) needed for FLC_*cabin*. A weighting factor for certain was used to prioritise the firing sequence of those rules as necessary for a smooth operation of such complex rule base mechanism.

Based on the simulation studies, it can be concluded that despite the complexity of integrating two individual FLC controllers within the EEMS strategy, the results as presented in Chapter 6, demonstrated that the EEMS control actions upon electrical load demand, saved energy and improved fuel consumption significantly under various driving conditions. However, for some specific scenarios (e.g. Test-case 1), under cold climate conditions, EEMS electrical load allowance is limited to a higher degree than other test case scenarios due to the high level of electrical loading involved. This confirms the need to explore an approach in which different global weighting factors could dynamically be changed to balance real world fuel savings with the expected attribute performance in such environmental conditions.

The realisation of the above components, such as the power supply model with its individual components including battery model, alternator model, ultracapacitor model electrical load models, and the FLC based EEMS has led to the design and implementation of a modular MATLAB®/Simulink™ software suite. The developed software suite has potential for use as a user friendly online tool and could be configured as a prototype system test purposes.

7.3 Further work

This section presents certain possible directions towards future investigation. This strategy was developed for powertrain configurations including 12-volt electrical systems and internal combustion engines. However, 12-volt system remains the main low voltage system for any hybrid type configuration (i.e. PHEV, HEV) as well as full battery electric vehicles (BEV). Therefore, the area of immediate further work is to quantify correlations between 12-volt electrical energy consumption and EV range prediction. The methodology for this work stream could include the combination of the developed power supply system that simulates electrical parameters based on dynamic environmental conditions and the use of real world measurements with different HEV battery packs and vehicle types. Using real world measurements has the advantage of predicting more realistic values but also relies on the available data and a statistical analysis derived from those experimental data. Any real world data should be extracted using various types of electrical vehicles and most importantly different sizes of high voltage battery packs. The wide aggregation level of the developed algorithm would allow a prediction mechanism applicable to different battery energy density sizes (i.e. Wh/l).

The modelling approach adopted in this study should be enhanced by: i) utilising a DcDc converter model which could replace the traditional alternator model, ii) introducing a 48-volt lithium – ion battery model by modifying the existing simulation model to match the critical characteristics of a lithium-ion battery and iii) introducing a 48-volt starter generator model by modifying the existing 12-volt alternator model to match the dynamic behaviour of the 48-volt machine under cranking and charging conditions. Adding the elements into the developed simulation environment would allow to consider more complex power supply system configurations whilst analysing the effect of electrical energy to vehicle's total fuel economy.

A further area of research should include additional heated/cooled features that future vehicle models will offer to the customer. Those features, called heated peripherals, include positive temperature coefficient (PTC) heaters, heated armrests, heated calfrests, heated cup holders and additional devices such as cabin interior fridges. Adding those electrical loads within the EEMS will enable the strategy to accommodate all possible electrical loads that influence the vehicle's power supply system and fuel consumption.

It is further considered that it may be worthwhile investigating a staged approach combining attribute performance within the decision mechanism of CSI. The novelty of the CSI concept and its effectiveness have been discussed in this thesis. However, including attribute performance for some key comfort and convenience features can provide further improvements from a customer satisfaction perspective. For example, for heated/cooled seats, the performance of the heating or cooling function could also be included as additional input to the CSI levels. This adds an additional customer

personalisation feature, which depending on ambient temperature conditions would allow to intervene and adjust the operation of those features emphasizing the performance against fuel consumption and vice versa.

Another significant area to explore further is the diagnostic capabilities of the developed system and the failsafe strategies that could be embedded as part of the proposed control strategy under real world conditions. In the automotive industry, the need for robustness and quality of the intended functionality within a product/automobile does not end when the product is sold to a customer. It is an important part of the service and maintenance during the complete lifecycle of the product. On-board diagnostics and fault monitoring is an essential part of every function signed-off prior to production. Diagnostic functions are built into the ECUs, making it possible to access diagnostic data necessary to self-diagnose and determine if the particular function/system/subsystem operates as intended.

For the proposed EEMS, an area for improvement is to implement a failsafe strategy and/or a system reaction that could be triggered when certain inputs of the functionality report invalid information (i.e. values outside the expected range of operation). The recovery mechanism should be based on diagnostic criteria that when met, will enable on-line solutions to be implemented. If this is not feasible, it should allow limited functionality of the EEMS under a predetermined operational framework (i.e. select a default or recovery mode with limited fuel economy benefits).

References

Archer, G., (2017). 'Designing representative vehicle tests, Lessons for EU regulations', *Briefing, Clean Vehicles & Energy Transport & Environment*.

Asada, T. and Maeda, S., (2008). 'A Stand-Alone Charging Management System to Improve Fuel Economy, Based on an Algorithm of Estimating Vehicle Motion'. SAE Technical Paper Series.

Asher, Z., Galang, A., Briggs, W., Johnston, B., Bradley, T. and Jathar, S., (2018). 'Economic and Efficient Hybrid Vehicle Fuel Economy and Emissions Modeling Using an Artificial Neural Network'. *SAE Technical Paper Series*, doi: 10.4271/2018-01-0315.

Averbukh, M., Rivin, B. and Vinogradov, J., (2007). 'On-Board Battery Condition Diagnostics Based on Mathematical Modelling of an Engine Starting System'. *SAE Technical Paper Series*.

Bao, R., Avila, V., and Baxter, J., (2017). 'Effect of 48 V Mild Hybrid System Layout on Powertrain System Efficiency and Its Potential of Fuel Economy Improvement'. SAE Technical Paper 2017-01-1175, 2017. doi: 10.4271/2017-01-1175.

Barr, A. and Veshagh, A., (2008). 'Fuel Economy and Performance Comparison of Alternative Mechanical Hybrid Powertrain Configurations'. *SAE Technical Paper Series*.

Beer, J. and Teulings, W., (2007). 'Optimized Start Strategy for Stop/Start Operation of a μ-Hybrid Vehicle'. *SAE Technical Paper Series*, doi: 10.4271/2007-01-0298.

Beher, U. and Werthschulte, K., (2009). 'Energy Management as Configurable System Software Function'. *SAE Technical Paper Series*.

Bennion, K. and Thornton, M., (2010). 'Integrated Vehicle Thermal Management for Advanced Vehicle Propulsion Technologies'. *SAE Technical Paper Series*.

Berndt, D., (2001). 'Valve-Regulated Lead-Acid Batteries', Journal of Power Sources, Vol. 100, pp: 29-46.

Blanke, H., Bohlen, O., Buller, S., De Doncker, R., Fricke, B., Hammouche, A., Linzen, D., Thele, M. and Sauer, D., (2005). 'Impedance measurements on lead–acid batteries for state-of-charge, state-of-health and cranking capability prognosis in electric and hybrid electric vehicles'. *Journal of Power Sources*, 144(2), pp.418-425.

Bohlen. O., (2008). 'Impedance-based battery monitoring' Dissertation thesis, RWTH Aachen, Germany.

Bosch GMbH (Ed.), R., (2014). 'Bosch Automotive Electrics And Automotive Electronics'. 5th ed. Wiesbaden: Springer Vieweg.

Boulos, A. M., Mahtani, J. L., Pacaud, C. and Burnham, K. J., (2003). 'Development of a Thermal Model to Accommodate Thermal Effects during Charging Cycles in Lead-Acid (SLI) Batteries'. *International Conference on Systems Engineering (ICSE)*, pp: 81-87.

Boulos, A., Pacaud, C., Burnham, K. and Mahtani, J., (2004). 'Validation of battery-alternator model against experimental data-a first step towards developing a future power supply system'. *Proceedings of the Institution of Mechanical Engineers, Part D: Journal of Automobile Engineering*, 218(1), pp.59-70.

Boulos, A., Pickering, S., Gerke, T. and Burnham, K., (2007). 'Development of a Power Net simulation tool using SABER®'. *Proceedings of the Institution of Mechanical Engineers, Part D: Journal of Automobile Engineering*, 221(12), pp.1535-1553.

Brabetz, L., Ayeb, M., and Tellmann, D., (2009). 'Efficient Vehicle Power Supply by Adaptive Energy, Charge and Heat Management of an Alternator - Super Capacitor System'. *SAE International Journal of Passenger Cars - Electronic and Electrical Systems*, 2(1), pp. 359-366.

Buller, S.; Karden, E.; Kok, D.; De Doncker, R.W. (2001). 'Modeling the Dynamic Behavior of Supercapacitors Using Impedance Spectroscopy', *Electric Vehicle Symposium EVS 18*, Berlin.

Burke, A., Miller, M., Zhao, H., Radenbaugh, M. and Liu, Z., (2013). 'Ultracapacitors in micro-and mild hybrids with lead-acid batteries: Simulations and laboratory and in-vehicle testing'. *2013 World Electric Vehicle Symposium and Exhibition (EVS27)*, doi: 10.1109/EVS.2013.6914961.

Campbell, J., Watts, W. and Kittelson, D., (2012). 'Reduction of Accessory Overdrive and Parasitic Loading on a Parallel Electric Hybrid City Bus'. *SAE Technical Paper Series*, doi: 10.4271/2012-01-1005.

Chang, H., Chen, C., Huang, L. and Lin, C., (2010). 'Implementation of a power supply with the characteristics of solar panels under partially shaded'. *IEEE Instrumentation & Measurement Technology Conference Proceedings*, pp14272-1476.

Chiara, F. and Canova, M., (2013). 'A review of energy consumption, management, and recovery in automotive systems, with considerations of future trends'. *Proceedings of the Institution of Mechanical Engineers, Part D: Journal of Automobile Engineering*, 227(6), pp.914-936.

Climate Action - European Commission. (2020). Road Transport: *Reducing CO2 Emissions From Vehicles-Climate Action - European Commission*. [online] Available at: <https://ec.europa.eu/clima/policies/transport/vehicles>.

Climate Action - European Commission. (2020).Climate Action: *Reducing CO2 Emissions From Cars Through Eco-Innovation - European Commission*. [online] Available at: <https://ec.europa.eu/clima/news/articles/news_2011072501_en>

Collaborative Project Seventh Framework Programme Theme 1.1 Greening, (2011). 'Energy Efficient Vehicles for Road Transport (EE-VERT)', In: EE-VERT Consortium, 2011.

Confer, K., Kirwan, J. and Engineer, N., (2013). 'Development and Vehicle Demonstration of a Systems-Level Approach to Fuel Economy Improvement Technologies'. *SAE Technical Paper Series*.

Couch, J., Fiorentini, L. and Canova, M., (2013). 'An ECMS-Based Approach for the Energy Management of a Vehicle Electrical System'. *IFAC Proceedings Volumes*, 46(21), pp.115-120.

Cross D., Hilton J., (2008). 'High Speed Flywheel Based Hybrid Systems for Low Carbon Vehicles'. In: *Hybrid and Eco-Friendly Vehicle Conference*. Coventry. IET HEVC, ISSN: 0537-9989.

Cross, D. and Brockbank, C., (2009). 'Mechanical Hybrid System Comprising a Flywheel and CVT for Motorsport and Mainstream Automotive Applications'. SAE Technical Paper 2009-01-1312.

Debert, M., Yhamaillard, G. and Ketfi-herifellicaud, G. (2010). 'Predictive energy management for hybrid electric vehicles - Prediction horizon and battery capacity sensitivity'. IFAC Proceedings Volumes, 43(7), pp.270-275.

Ehsani M, Gao Y and Emadi A., (2010). 'Modern electric, hybrid electric and fuel cell vehicles: fundamentals, theory, and design'. 2nd edition. Boca Raton, Florida: CRC Press.

Elahian, S., Abrushamifar, A., and Ale-Ahmad, A., (2012). *'*Optimal Fuzzy Logic Controller for Energy Management in Fuel Cell Hybrid Electric Vehicle*'*. IEEE Journal of Selected Areas in Renewable and Sustainable Energy (JRSE), pp. 1-5.

Eymann, T., Williams, K., Benninger, K., Vikas, A. and Lillie, C., (2011). 'Holistic Vehicle Energy Management - Moving Towards CAFE's Target'. *SAE Technical Paper Series*. doi: 10.4271/2011-01-1014 .

Fenske, G., Erck, R., Ajayi, L., et al, (2006). 'Parasitic energy loss mechanism impact on vehicle system efficiency'. Report, Argonne National Laboratory, Argonne, Illinois, USA.

Freyermuth, V., Fallas, E., and Rousseau, A., (2009). 'Comparison of Powertrain Configuration for Plug-in HEVs from a Fuel Economy Perspective'. *SAE International Journal of Engines,* 1(1), pp. 392-398. doi: 10.4271/2008-01-0461.

Gerke, T. and Boulos, A. (2008). 'Model Based Design of Robust Vehicle Power Networks'. SAE Technical Paper 2008-01-0898.

German J, (2015). 'Hybrid Vehicles – Technology Development and a Cost Reduction'. *International Council On Clean Transportation.* ICCT, US.

Gibbard H., F., (1978). 'Thermal Properties of Battery Systems'. Journal of the Electrochemical Society, Vol. 125, pp: 353 –358.

Gottwald, S. and Bandemer, H., (1995). 'Fuzzy Sets, Fuzzy Logic, Fuzzy Methods with Applications', John Wiley & Sons Pub. Co.

Grbovic, P. J., (2013). 'Ultra-Capacitors In Power Conversion Systems'. John Wiley & Sons, Ltd, pp.22-77.

Guerrero, M., Romero, E., Barrero, F., Milanes, M. and Gonzalez, E. (2009). 'Overview of medium scale energy storage systems'. In: Compatibility and Power Electronics. IEEE.

Gunti, S., Shaik, A., Rao, S. and Reddy, A., (2015). '*Development of Range Extended - Solar Power Assisted Electric Vehicle*'. SAE Technical Paper 2015-26-0111.

H. Patel and V. Agarwal, (2008). 'MATLAB-Based Modeling to Study the Effects of Partial Shading on PV Array Characteristics', *IEEE Trans. On Energy Conversion*, Vol. 23, No. 1.

Halvgaard, R., Poulsen, N., Madsen, H., Jorgensen, J., Marra, F. and Bondy, D., (2012). 'Electric vehicle charge planning using Economic Model Predictive Control'. In: *IEEE International Electric Vehicle Conference*. Held 3-5 April 2003 at Ankara University.

Harris, C., J., Moore, C., G. and Brown, M., (1993). 'Intelligent Control: Aspects of Fuzzy Logic and Neural Networks*'*, vol. 6, World Scientific Series in Robotics and Intelligent Systems.

Haus der Technik, (1994). 'Alternators In Automotive Applications – State of The Art and Development Trends', *Technical report*, Essen Germany.

Hienrich, P., Gossen, D., Oswald, E., and Knorr, R. (2015). 'Early Energy Estimation of Heterogeneous Embedded Networks within Adaptive Systems'. In: *Energy Efficient Vehicles - Dresden Instutute of Automobile Engineering – IAD*.

Hou, C., Ouyang, M., Xu, L. and Wang, H., (2014). 'Approximate Pontryagin's minimum principle applied to the energy management of plug-in hybrid electric vehicles'. Applied Energy, 115, pp.174-189.

Hughes, E., (1969). 'Electrical Technology', Longman Group Ltd, 4th edition.

Hughes, E., Smith, I., Hiley, J. and Brown, K., (2008). 'Hughes Electrical & Electronic Technology'. 10th ed. Harlow, England: Prentice Hall, pp.197-222.

Ivanov, V., (2015). 'A review of fuzzy methods in automotive engineering applications'. *European Transport Research Review*. 7:29. doi: 10.1007/s12544-015-0179-z.

Jang, J., Sun, C., Mizutani, E., (1997). 'Neuro-Fuzzy and Soft Computing: A computational Approach to Learning and Machine Intelligence'. Prentice Hall, Upper Saddle River, NJ.

John, R. and Coupland, S., (2007). 'Type-2 Fuzzy Logic: A Historical View'. *IEEE Computational Intelligence Magazine*, 2(1), pp.57-62.

Johri, R. and Filipi, Z., (2011). 'Self-Learning Neural Controller for Hybrid Power Management Using Neuro-Dynamic Programming'. *SAE Technical Paper Series*, doi: 10.4271/2011-24-0081 .

Karden E., (2002). ISEA Battery Model Manual, Ford of Europe, Aachen, Germany.

Karden E., Buller S. and De Doncker, R., W., (2000). 'A Method for Measurement and Interpretation of Impedance Spectra for Industrial Batteries'. *Journal of Power Sources*, (vol. 85), 72-78.

Karden E., Buller S. and De Doncker, R., W., (2001). 'A frequency-domain approach to dynamical modelling of electrochemical power sources'. 5th International Symposium on Electrochemical Impedance Spectroscopy, Marilleva (Trento, Italy).

Karden E., Thele M. and De Doncker, R., W., 'Impedance-Based Non-Linear Dynamic Battery Modelling for Automotive Applications'. *Journal of Power Sources*, (vol. 113), pp.422-430, Germany.

Karden, E., (2001). 'Using Low Frequency Impedance Spectroscopy for Characterisation, Monitoring and Modelling of Industrial Batteries', Dissertation thesis, RWTH Aachen, Germany.

Karden, E., Ploumen, S., Fricke, B., Miller, T. and Snyder, K., (2007). 'Energy storage devices for future hybrid electric vehicles'. *Journal of Power Sources*, 168(1), pp.2-11.

Karden, E., Shinn, P., Bostock, P., Cunningham, J., Schoultz, E. and Kok, D., (2005). 'Requirements for future automotive batteries – a snapshot'. *Journal of Power Sources*, 144(2), pp.505-512.

Karnik, N. and Mendel, J. (1999). 'Applications of type-2 fuzzy logic systems: handling the uncertainty associated with surveys'. In: *IEEE International Fuzzy Systems Conference Proceedings (Cat.No.99CH36315)*, (vol.3), pp. 1546-1551. doi: 10.1109/FUZZY.1999.790134.

Karnik, N., and Mendel, J. (1998). 'Introduction to type-2 fuzzy logic systems. In: *Fuzzy Systems Proceedings, IEEE World Congress on Computational Intelligence*, (vol.2), pp. 915 -920.

Kassem, S., (2012). 'A type-2 fuzzy logic system for workforce management in the telecommunications domain, Ph.D. dissertation, School of Computer Science and Electronic Engineering, University of Essex.

Keim, T., (2004). '42 Volts - The View from Today'. SAE Technical Paper 2004-21-0094.

Kelber, C., Quevedo, J. and Lessa, L., (2007). 'Compensation of Power Supply Fluctuations in Electric Power Steering (EPS) Systems'. SAE Technical Paper Series 2007-01-2647.

Kessels, J., Koot, M., Ellenbroek, R., Pesgens, M., Veldpaus, F., Bosch, P., Eifert, M. and Kok, D., (2004). 'Vehicle Modelling for Energy Management Strategies'. In: *Proceedings of the 7th international symposium on advanced vehicle control*, AVEC '04. Delft: Royal Dutch Association of Engineers (KIVI-NIRIA), pp.465-470.

Khajepour, A., (2014). 'Electric and Hybrid Vehicles: Technologies, Modelling, and Control: A Mechatronic Approach'. Chichester, England: Wiley.

Kheir, N., Salman, M., Schouten, N., (2004). 'Emissions and Fuel Economy Trade-off for Hybrid Vehicles using Fuzzy Logic'. Mathematics and Computers in Simulation 66, pp.155-172.

Koehler, S., Viehl, A., Bringmann, O. and Rosenstiel, W., (2012). 'Optimized recuperation strategy for (Hybrid) Electric Vehicles based on intelligent sensors'. In: *Control, Automation and Systems (ICCAS), 2012 12th International Conference on*, pp. 218-223.

Kokalj, G. and Ekachaiworasin, R., (2013). 'Challenges and Opportunities of Variant Calibration of Hybrid Vehicles'. SAE Technical Paper Series 2013-01-0128.

Kulkarni, S., Gandhi, N., Chaithanya, N. and Govindarajan, S., (2014). 'Ultra-Capacitor based Hybrid Energy Storage and Energy Management for Mild Hybrid Vehicles'. SAE Technical Paper Series 2014-01-1882.

Kuypers, M., (2014). 'Application of 48 Volt for Mild Hybrid Vehicles and High Power Loads'. *SAE Technical Paper Series*, doi: 10.4271/2014-01-1790.

Lakshminarasimhan, V. and Athani, G., (2013). 'An Intelligent Alternator Control Mechanism for Energy Recuperation and Fuel Efficiency Improvement'. *SAE International Journal Alternative Powertrains* 2(1):217-225. doi: 10.4271/2013-01-1750.

Lam, L., Louey, R., Haigh, N., Lim, O., Vella, D., Phyland, C., Vu, L., Furukawa, J., Takada, T., Monma, D. and Kano, T., (2007). 'VRLA Ultrabattery for high-rate partial-state-of-charge operation'. *Journal of Power Sources*, 174(1), pp.16-29.

Latimer, R., (2012). 'Solar Panel Integration – CR Gateway Report JLR1509'. *Jaguar Land Rover internal report*, UK.

Lee, J., Kwon, S., Lim, Y., Chon, M. and Kim, D., (2013). 'Effect of Air-Conditioning on Driving Range of Electric Vehicle for Various Driving Modes'. SAE Technical Paper 2013-01-0040.

Lee, W., Choi, D. and Sunwoo, M., (2002). 'Modelling and simulation of vehicle electric power system'. Journal of Power Sources, 109(1), pp.58-66. doi: 10.1016/S0378-7753(02)00033-2

Lee, W., Park, H., Sunwoo, M., Kim, B. and Kim, D., (2000). 'Development of a Vehicle Electric Power Simulator for Optimizing the Electric Charging System'. SAE Technical Paper Series. doi: 10.4271/2000-01-0451

Liaw, B. and Dubarry, M., (2007). 'From driving cycle analysis to understanding battery performance in real-life electric hybrid vehicle operation'. *Journal of Power Sources*, 174(1), pp.76-88.

Liu, Z., Ivanco, A. and Filipi, Z., (2016). 'Impacts of Real-World Driving and Driver Aggressiveness on Fuel Consumption of 48V Mild Hybrid Vehicle'. *SAE International Journal of Alternative Powertrains*, 5(2), pp.249-258.

Lu, D., Li, W., Xu, G., and Zhou, M., (2012). 'Fuzzy Logic Control Approach to the Energy Management of Parallel Hybrid Electric Vehicles'. In: *IEEE International Conference on Information and Automation.*

Lu, S., Weston, P., Hillmansen, S., Gooi, H. B. and Roberts, C., (2014). `Increasing the Regenerative Braking Energy for Railway Vehicles'. In: *IEEE Transactions on Intelligent Transportation Systems* 15.6, pp. 2506-2515. doi: 10.1109/TITS.2014.2319233.

Lukic, S. and Emadi, A., (2003). 'Effects of Electrical Loads on 42V Automotive Power Systems', SAE Technical Paper 2003-01-2257. doi: 10.4271/2003-01-2257.

Lyu, M., Doo, B. and Ku, Y., (2007). 'A Study of Vehicle Fuel Economy Improvement Potential by Optimization of the Cooling and Ancillary Systems of a Heavy Duty Engine'. *SAE Technical Paper Series*. doi: 10.4271/2007-01-1772.

Mackay, S., (2012). 'Reduction in parasitic losses by careful choice of alternator drive system'. SAE Technical paper 2012-01-0385.

Marie-Francoise, J.N, Gualous, H., Berthon, A., (2005). 'Artificial Neural Network Control and Energy Management in 42V DC Link'. In: *11th European Conference on Power Electronics and Applications*, pp. 1-8.

Masjosthusmann, C., Bueker, U., Köhler, U., and Decius, N., (2013). 'A Load Balancing Strategy for Increasing Battery Lifetime in Electric Vehicles'. SAE Technical Paper 2013-01-0499.

Matthews, T., Nishanth, D., (2013). 'Flywheel Based Kinetic Energy Recovery Systems (KERS) Integrated In Vehicles', *International Journal of Engineering Science and Technology* (IJEST), ISSN: 0975-5462, (vol 2), pp: 1694-1699.

Mauracher, P., (1996). 'Modeling and network optimisation for electric road vehicles', dissertation thesis, RWTH Aachen University of Technology.

May, G., Calasanzio, D. and Aliberti, R., (2005). 'VRLA automotive batteries for stop&go and dual battery systems'. *Journal of Power Sources*, 144(2), pp.411-417.

McAuliffe, S. and Pacaud, C., (1999). 'Vehicle Fuel Economy: The influence of Alternators', *Internal Technical report JA5H3/1/1,* Jaguar Land Rover.

Meissner, E. and Richter, G., (2005). 'The challenge to the automotive battery industry: the battery has to become an increasingly integrated component within the vehicle electric power system'. *Journal of Power Sources*, 144 (2), pp.438-460.

Mendel J., (1995). 'Fuzzy logic systems for engineering: a tutorial', In: Proceedings of the IEEE, (vol. 83 (3)), pp. 345-377.

Mendel J., (2000). 'Uncertainty, fuzzy logic, and signal processing'. *Signal Processing,* (vol. 80 (6)), pp.913-933.

Mendel, J., (2001). 'Uncertain Rule-Based Fuzzy Logic Systems: Introduction And New Directions'. Englewood Cliffs: Prentice-Hall.

Mikkelsen, K. and Lambert, S., (2011). 'Evaluation of a Hybrid Energy Storage System for EV's'. *SAE Technical Paper Series*, doi: 10.4271/2011-01-1376.

Mock, P., (2014). 'EU CO2 emission standards for passenger cars and light-commercial vehicles'. *ICCT* Berlin., [online] Available at: < http://theicct.org/eu-co2-standards-passenger-cars-and-lcvs>

Monetti, A., Otter., T., and Ulshofer, N., (2011).). 'System Base Chip For Partial Network Operation On The CAN Bus'. *Electronik Automotive*, no.11, pp. 24-27.

Montalto, I., Tavella lng, D., Casavola PhD, A. and De Cristofaro, F., (2012). 'Intelligent Alternator Employment To Reduce Co2Emission and to Improve Engine Performance'. *SAE International Journal of Alternative Powertrains*, 1(1), pp.1-11.

Montazeri-Gh, M. and Asadi, M. (2006). 'Influence of the Road Grade on the Optimization of Fuzzy-Based Hybrid Electric Vehicle Control Strategy'. SAE Technical Paper Series 2006-01-3293.

Moro, D., Cavina, N., Trivić, I., and Ravaglioli, V., (2010). 'Guidelines for Integration of Kinetic Energy Recovery System (KERS) based on Mechanical Flywheel in an Automotive Vehicle'. SAE Technical Paper 2010-01-1448. doi: 10.4271/2010-01-1448.

Müller-Lerwe, A., Busch, R., Rambow, T., Christen, U., Gussen, U. and Kees, M., (2008). 'Safety Aspects on a Micro-Hybrid Vehicle with Manual Gearbox'. *SAE International Journal of Passenger Cars - Electronic and Electrical Systems*, 1(1), pp.26-37.

Obayashi, K. and Tani, K., (2004). 'Concept of Vehicle Electric Power Flow Management System (VEF)'. SAE Technical Paper Series 2004-01-0361.

Page, R., Bedogne, R., Steinmetz, T., and Bryant, A., (2006). 'A "Mini-Hybrid" Transit Bus with Electrified Cooling System'. SAE Technical Paper 2006-01-3475. doi: 10.4271/2006-01-3475.

Paladini, V., Donateo, T., de Risi, A. and Laforgia, D., (2007). 'Super-capacitors fuel-cell hybrid electric vehicle optimization and control strategy development'. *Energy Conversion and Management*, 48(11), pp.3001-3008.

Panday, A. and Bansal, H., (2014). 'A Review of Optimal Energy Management Strategies for Hybrid Electric Vehicle'. *International Journal of Vehicular Technology*, vol. 2014, Article ID 160510, 19 pages. doi: 10.1155/2014/160510.

Pang, H. and Brace, C., (2004). 'Review of engine cooling technologies for modern engines'. *Proceedings of the Institution of Mechanical Engineers, Part D: Journal of Automobile Engineering*, 218(11), pp.1209-1215.

Passino, K. and Yurkovich, S., (1997). 'Fuzzy Control', *Addison-Wesley Pub. Co.*

Pavlov, D., (2017). 'Lead-Acid Batteries: Science And Technology'. 2nd ed. Sofia Bulgaria: Elsevier B.V.

Pettersson, N. and Johansson, K., (2006). 'Modelling and Control of auxiliary loads in heavy vehicles'. *International Journal of Control*, 79(5), pp.479-495.

Photovoltaic Systems Technology, (2003). Technical report, University of Kassel, Kassel, Germany.

Pickering, S. and Pacaud. C., (2001). 'X350 2003 MY Electrical Load Management Development System Functional Specification', FS-2W93-10300-AA, Jaguar Land Rover.

Pickering, S., and Pacaud, C., (2001). 'Vehicle Charging System Test Procedure – 14V Systems, JETP D07-01, Jaguar Land Rover Engineering Test Procedure, Jaguar Land Rover.

Pirotais, F., Bellettre, J., Lecorre, O., Tazerout, M., De Pelsemaeker, G. and Guyonvarch, G., (2002). 'A Model of Energetic Interactions Between a Car Engine, the Cabin Heating System and the Electrical System'. *SAE Technical Paper Series*. doi: 10.4271/2002-01-2224.

Plett, G., (2004). 'Extended Kalman filtering for battery management systems of LiPB-based HEV battery packs Part 1. Background'. *Journal of Power Sources* s0378-7753(04)00359-3.

Pollet, B., Staffell, I. and Shang, J., (2012). 'Current status of hybrid, battery and fuel cell electric vehicles: From electrochemistry to market prospects'. Electrochimica Acta, 84, pp.235-249.

Pveducation.org. (2020). Series Resistance | Pveducation. [online] Available at: <https://www.pveducation.org/pvcdrom/solar-cell-operation/series-resistance> [Accessed 13 March 2020].

Qiao, Z., Deng, W., Wu, J., Ju, F. and Li, J., (2016). 'Development of Battery/Supercapacitor Hybrid Energy Management System for Electric Vehicles Based on a Power Sharing Strategy Using Terrain Information'. SAE Technical Paper Series 2016-01-1242.

Qiao, Z., Deng, W., Wu, J., Ju, F. and Li, J., (2016). 'Fuzzy Supervisory Based Variable Frequency Control Strategy for Active Battery/Supercapacitor Combination in Electric Vehicles'. SAE Technical Paper Series 2016-01-1203.

Quaschning, V., (2019). 'Renewable Energy And Climate Change'. 2nd Edition. Wiley.

Rask, E., Santini, D., and Lohse-Busch, H.,(2013). 'Analysis of Input Power, Energy Availability, and Efficiency during Deceleration for X-EV Vehicles'. *SAE International Journal Alternative Powertrain,* 2(2), pp.350-361. doi: 10.4271/2013-01-1473.

Redey L, (1998). 'Heat Effects in Batteries and Measurements by Electrochemical Calorimetry'. The 13th Annual Battery Conference on Applications and Advances, CA, USA, 1998.

Rick, A. and Sisk, B., (2015). 'A Simulation Based Analysis of 12V and 48V Microhybrid Systems Across Vehicle Segments and Drive Cycles'. *SAE Technical Paper Series*. doi: 10.4271/2015-01-1151.

Rivera, M., (2011). 'Current and Next-Generation Energy Storage Devices for Micro Vehicle Applications'. *SAE International Journal of Materials and Manufacturing*, 5(1), pp.19-29.

Romanato, R., Acquaviva, F., Duma, F., Fuso, R. et al., (2018) '48 V Hybrid System Technologies to Develop the Most Efficient and Cleanest Diesel,' SAE Technical Paper 2018-37-0011, doi:10.4271/2018-37-0011.

Rumbolz, P., Baumann, G. and Reuss, H., (2011). 'Measurement of Internal Vehicle Power Flows in Real-world Operation'. *ATZ worldwide eMagazine*, 113(5), pp.52-57.

Sauer, D., Karden, E., Fricke, B., Blanke, H., Thele, M., Bohlen, O., Schiffer, J., Gerschler, J. and Kaiser, R., (2007). 'Charging performance of automotive batteries - An underestimated factor influencing lifetime and reliable battery operation'. *Journal of Power Sources*, 168(1), pp.22-30.

Sawai, K., Ohmae, T., Suwaki, H., Shiomi, M. and Osumi, S., (2007). 'Idling-stop vehicle road tests of advanced valve-regulated lead-acid (VRLA) battery'. *Journal of Power Sources*, 174(1), pp.54-60.

Schlabe, D. and Zimmer, D., (2012). 'Model-Based Energy Management Functions for Aircraft Electrical Systems'. SAE Technical Paper Series 2012-01-2175.

Sciarretta, A., Dabadie, J. and Albrecht, A., (2008). 'Control-Oriented Modeling of Power Split Devices in Combined Hybrid-Electric Vehicles'. SAE Technical Paper Series 2008-01-1313.

Sengupta, S., Gururaja, C., Hingane, S., K, P., Maniar, M., Mikuláš, O. and Pekar, J., (2017). 'Evaluation of Model Predictive and Conventional Method Based Hybrid Electric Vehicle Supervisory Controllers'. *SAE Technical Paper Series*, doi: 10.4271/2017-01-1253.

Sharer, P., Rousseau, A., Karbowski, D. and Pagerit, S., (2008). 'Plug-in Hybrid Electric Vehicle Control Strategy: Comparison between EV and Charge-Depleting Options'. SAE Technical Paper Series 2008-01-0460.

Shidore, N., Vyas, A. and Kwon, J., (2010). 'Impact of Energy Management on the NPV Gasoline Savings of PHEVs'. *SAE International Journal of Engines*, 3(1), pp.916-927.

Shin, W., Lee, J., Chung, S., Kim, S., Kwon, H., Lee, S. and Jackey, R., (2007). 'Two-Staged Modelling of Alternator'. SAE Technical Paper Series 2007-01-3471.

Sikchi, A., Khokar, R., Niranjan, U. and Raju, G., (2007). 'Charging System: Design Simulation & amp; Validation Methodology'. SAE Technical Paper Series 2007-01-0784.

Silva, C., Ross, M. and Farias, T., (2009). 'Analysis and simulation of "low-cost" strategies to reduce fuel consumption and emissions in conventional gasoline light-duty vehicles'. *Energy Conversion and Management*, 50(2), pp.215-222.

Soria, M., Trinidad, F., Lacadena, J., Sánchez, A. and Valenciano, J., (2007). 'Advanced valve-regulated lead-acid batteries for hybrid vehicle applications'. *Journal of Power Sources*, 168(1), pp.12-21.

Stence, R., (2004). 'Shifting to 42 Volt Hybrid Systems'. SAE Technical Paper 2004-01-3067. doi: 10.4271/2004-01-3067.

Stoppok, C., (2015). '48V Electrical Systems - A Key Technology Paving to the Road to Electric mobility', ZVEI (Die Elektroindustrie), German Electrical and Electronic Manufacturers' Association, Germany.

Surampudi, B., Redfield, J. and Ostrowski, G., (2008). 'Mild Regenerative Braking to Enhance Fuel Economy via Lowered Engine Load Due to Alternator'. SAE Technical Paper Series 2008-01-2560.

Takagi, T. and Sugeno, M., (1985). 'Fuzzy identification of systems and its applications to modeling and control'. IEEE Transactions on Systems, Man, and Cybernetics, SMC-15(1), pp.116-132. doi: 10.1109/TSMC.1985.6313399

Tanaka, E., Narita, T. and Maegawa, H., (2013). 'Fuel Economy Analysis of Alternator with Kinetic Energy Storage for a Conventional Vehicle'. *SAE International Journal of Passenger Cars - Mechanical Systems*, 6(2), pp.643-651.

Tareq, Z., Sulaiman, N., Hannan, M.A., Mohamed, A., Majlan, E.H., Daud, W.R.W, (2015). 'Fuzzy Logic Based Energy Management System for Hybrid Electric Vehicle'. *Review of Energy Technologies and Policy Research*, pp.29-36.

Tate, E., Harpster, M., and Savagian, P., (2009) "The Electrification of the Automobile: From Conventional Hybrid, to Plug-In Hybrids, to Extended-Range Electric Vehicles," *SAE Int J. Passeng. Cars - Electron. Electr. Syst.* 1(1):156-166, doi: 10.4271/2008-01-0458.

Thele, M., Karden, E., Surewaard, E. and Sauer, D., (2006). 'Impedance-based overcharging and gassing model for VRLA/AGM batteries'. *Journal of Power Sources*, 158(2), pp.953-963.

Thele, M., Schiffer, J., Karden, E., Surewaard, E. and Sauer, D., (2007). 'Modeling of the charge acceptance of lead–acid batteries'. *Journal of Power Sources*, 168(1), pp.31-39.

Tzeng, S., David Huang, K. and Chen, C., (2005). 'Optimization of the dual energy-integration mechanism in a parallel-type hybrid vehicle'. *Applied Energy*, 80(3), pp.225-245.

Ueno, M., Eguchi, H., Enomoto, T. and Ogawa, M., (2008). 'Study of Power Generation Loss Decrease in Small Gas Engine Cogeneration'. SAE Technical Paper Series 2008-32-0044.

Uzunoglu, M. and Alam, M., (2007). 'Dynamic modeling, design and simulation of a PEM fuel cell/ultra-capacitor hybrid system for vehicular applications'. *Energy Conversion and Management*, 48(5), pp.1544-1553.

Vallur, A., Khairate, Y. and Awate, C., (2015). 'Prescriptive Modeling, Simulation and Performance Analysis of Mild Hybrid Vehicle and Component Optimization'. *SAE Technical Paper Series*. doi: 10.4271/2015-26-0010 .

von Albrichsfeld, C. and Karner, J.,(2009). 'Brake System for Hybrid and Electric Vehicles', SAE Technical Paper 2009-01-1217. doi: 10.4271/2009-01-1217.

Waldman, C., Gurusubramanian, S., Fiorentini, L. and Canova, M., (2015). 'A model-based supervisory energy management strategy for a 12 V vehicle electrical system'. *Control Engineering Practice*, 44, pp.20-30.

Wallentowitz, H., Rappen, J., and Gossen, F., (1996). 'Fuel saving potential by weight reduction and optimizing by weight reduction and optimizing of ancillary components-simulation and bench test'. SAE technical paper 967164.

Zadeh, L., (1965). 'Fuzzy sets'. Information and Control, (vol.8 (3)), pp.338-353. doi: 10.1016/S0019-9958(65)90241-X.

Zadeh, L., (1975). 'The concept of a linguistic variable and its application to approximate reasoning'. In: *I. Information Sciences*, (vol.8 (3)), pp.199-249. doi: 10.1016/0020-0255(75)90036-5

Zemansky, M. W. and Dittman R. H., (1982). 'Heat and Thermodynamics', McGraw-Hill, New York.

Appendices

Appendix A Publications

- Boulos A. M., Mahtani J., L, Pacaud C., Burnham K. J., ***Development of a thermal model to accommodate thermal effects during charging cycles in lead-acid (SLI) batteries,*** Proc. Of 16th Conf. On Systems Engineering, ICSE 2003, Vol. I, Coventry, UK, Sep 2003, pp: 81-87.

- Boulos A. M., Pacaud C., Burnham K. J., Mahtani J. L., ***Validation of battery-alternator model against experimental data-A first step towards developing a future power supply system,*** Journal of Automobile Engineering, Proceedings of the Institution of Mechanical Engineers (IMechE), Part D, Vol. 218, Jan 2004, pp 59-70.

- Boulos A. M., Pickering S. R., Gerke T., ***Development of a Power Supply Simulation tool using SABER,*** 14th Annual Saber User Group (SNUG) 2005, May 2005.

- Boulos A. M., Pickering S. R., Gerke T., Burnham K. J., ***Development of a Power Net Simulation tool using SABER,*** Journal of Automobile Engineering, Proceedings of the Institution of Mechanical Engineers (IMechE), Part D, Vol. 221, Dec 2007, pp 1535 – 1553.

- Gerke T., Boulos A. M., ***Model-Based Design of Robust Vehicle Power Networks,*** SAE 2008-01-0898, SoCiety of Automotive Engineering, 2008 World Congress, Detroit, Michigan, USA, April 2008.

Appendix B Powertrain configurations

B.1 PHEV/BEV configurations

The plug-in hybrid electric drivetrain is designed to use the battery fully or partially to displace part of the primary energy source (Ehsani et al., 2010). The electrical energy used to power a PHEV comes from both the internal combustion engine and a battery pack. PHEVs have a larger battery pack than conventional HEVs do. In PHEVs, the battery can be fully charged with conventional home electric plugs before starting off. In this way, the vehicle can travel for a longer time in the pure electric mode, so that the engine is shut off for a longer time period. The drivetrain of a PHEV can be built in a series, parallel, or series-parallel configuration, with the possibility of charging the batteries on-board and also from an electrical outlet. Figure B.1 illustrates different PHEV powertrain topologies comparing to a typical BEV configuration including TTW efficiencies and energy losses based on power stage analysis:

a)

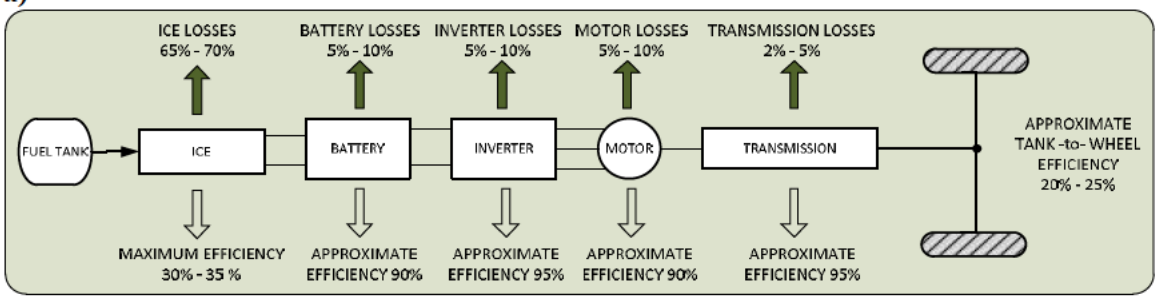

b)

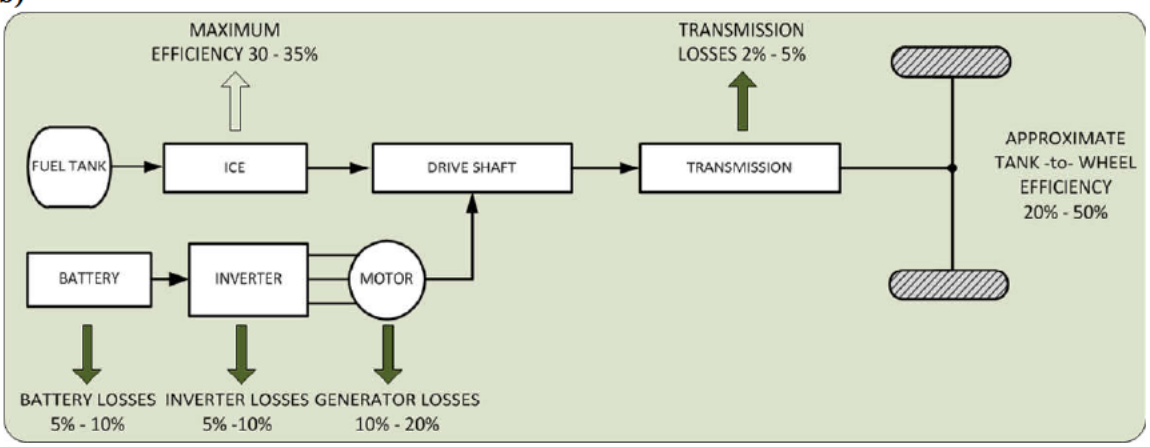

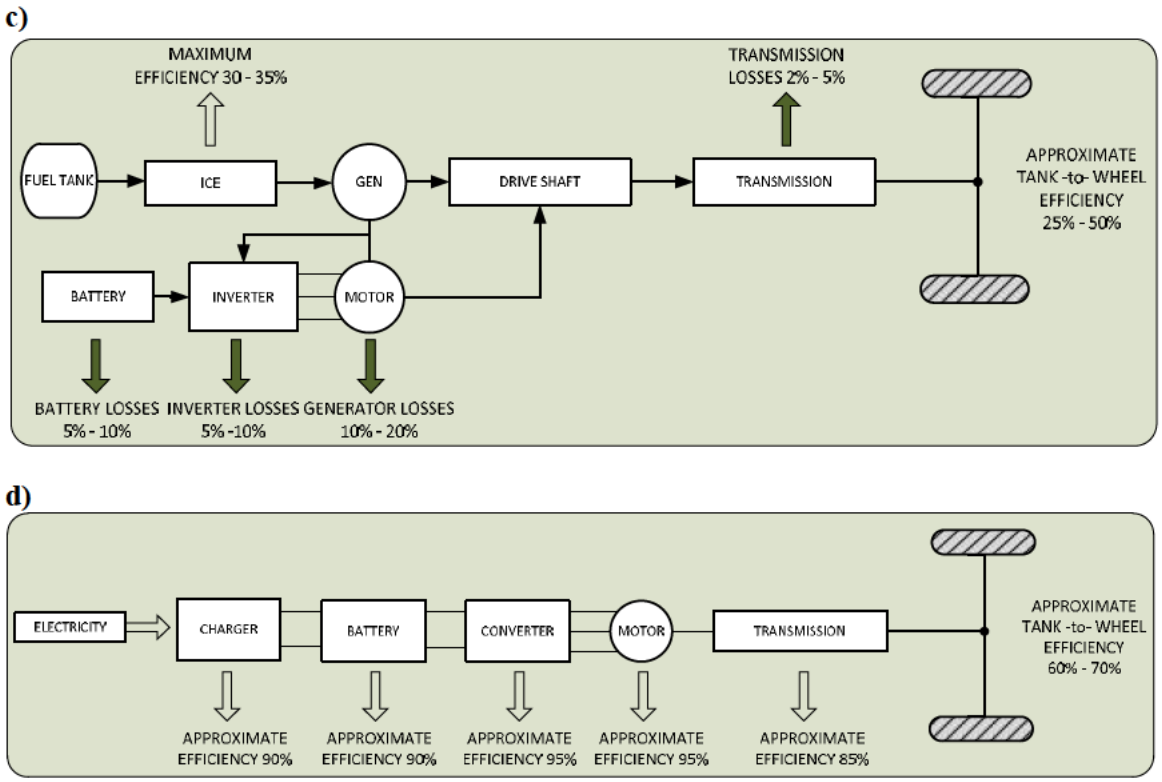

Figure B.1. TTW efficiency a) series PHEV b) parallel PHEV
c) series- parallel PHEV d) full BEV

The series PHEV configuration, as shown in Figure B.1a, is considered to be closer to an electric-intensive vehicle when compared to a parallel configuration. In this case, the vehicle's propulsion is purely from an electrical motor. ICE speed is completely decoupled from the wheel axles, and its operation is independent of vehicle operations. As a result, the engine can be operated consistently in a very high efficiency area. The Tank to Wheel (TTW) efficiency of a series PHEV is usually between 20% to 25% due to the low efficiency of the ICE and other technical constraints, such as battery capacity and drivetrain mass. (Freyermuth et al., (2008), Williamson, S., (2013).

In a parallel PHEV configuration, as shown in Figure B.1b, the vehicle has two traction sources, the electric machine and the ICE. The electric machine is often located in between the clutch and the transmission. By combining the two different traction sources, a smaller ICE and a smaller battery capacity pack can be used comparing to a series configuration, resulting to less drivetrain mass. Higher TTW efficiency ranges of 40% to 50% are easily achieved (Williamson, S., (2013), Khajepour, A., 2014).

Finally, the series-parallel system, as shown in Figure B.1c is the most commonly used system in currently available hybrid vehicles. The split system allows the engine speed to be decoupled (to some extent) from vehicle speed. On one hand, the power from the engine can flow mechanically to the wheel

axle via the ring of the planetary system. On the other hand, the engine power can also flow through the generator, producing electricity to drive the motor as main propulsion for the vehicle. PHEV vehicles are seen as one of the most promising means to improve sustainability of transportation by reducing reliance on fuel while retaining the driving range of conventional vehicles. (Williamson, S., (2013), Khajepour, A., 2014).

Battery electric vehicles (BEV) is a type of electric vehicle that uses chemical energy stored in battery cells, normally into a HV mega pack structure, to drive electric motors for propulsion. The main HV battery provides power to the motor and power DC/AC inverters during acceleration and normal operation, whereas, via regenerative braking during deceleration replenish available energy provided by the motors operating in generating mode. Electrical vehicles can deliver at least 70% energy efficiency, as shown in Figure B.1d, while ICE vehicles can be as low as 15% (Khajepour, A., 2014). The performance of BEVs is highly dependent on the cost, durability and performance of the energy sources used. Energy sources and charging station infrastructure are the main limitations preventing the mass production of BEVs. There is no currently a battery technology or a single energy source technology that can sufficiently meet all the performance requirements of BEVs (Khajepour, A., 2014).

B.2 MHEV 12-volt/48-volt configuration

A typical 12-volt/48-volt architecture includes: i) a 12-volt high power lead-acid battery, ii) a 48-volt battery (i.e. Li-Ion), iii) a 12-volt/48-volt DcDc Buck converter, iv) a 48-volt Belt-driven/crankshaft starter-generator (BISG/CISG), v) 12-volt electrical loads/features and finally iv) 48-volt electrical features, examples of 48-volt electrical loads is the electric Active Roll Control (eARC), this includes an actuator to reduce vehicle's body roll angle, and an electric Super Charger (eSC) that boosts engine horsepower output and efficiency when required, both such features have been recently introduced by various Automotive OEMs. Figure B.2 presents a typical 12-volt/48-volt configuration:

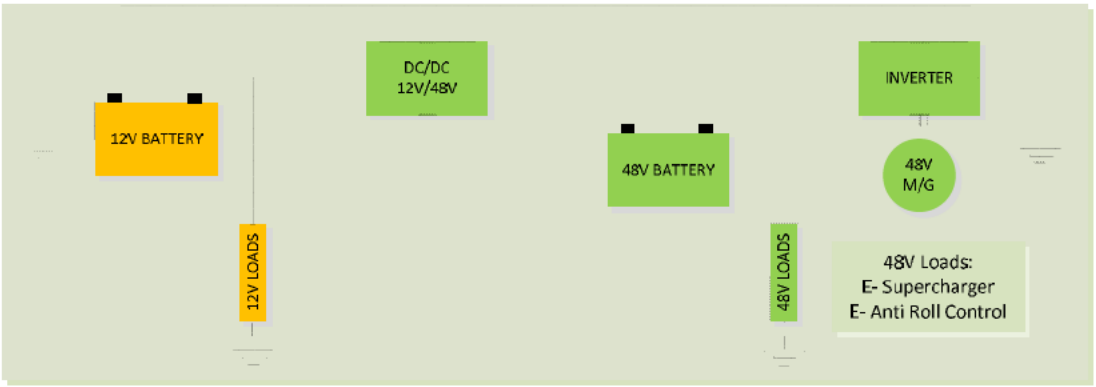

Figure B.2. Range Rover's 12-volt/48-volt system architecture

Appendix C Low Emission Vehicle components

C.1 Automotive lead-acid batteries

Within the last few decades, automotive industry has undergone a revolution in overall vehicle reliability. Battery reliability has been increased over its operational life in order to satisfy customer expectations.

Within the vehicle electrical system, the battery acts as the chemical energy storage device. It must be able to supply high currents for cold cranking briefly, and to supply some or all of the currents required by other systems for a limited period (when idle or the engine is not running).

Battery characteristics are influenced by the internal chemical reactions, and these reactions are affected by the ambient temperature, the SoC, the charging-discharging rate, and the charging-discharging history. Thus, it can be difficult to predict the charging-discharging current and the changes of the SoC. The current flowing into the battery is determined by the varying charging voltage and the internal impedance of the battery (ohmic resistance of the conducting materials and the internal resistance of the electrolyte Pavlov (2017).

The state of charge (SoC) of the battery is one of the most important factors during the operation of the vehicle. If the SoC of the battery is kept at high levels then the battery could provide sufficient energy during overloading situations and that will also affect its life cycle (Bosch .2014)

The battery acts as a reservoir which has to supply various electrical loads and must 'topped up' continuously by the alternator which acts as the energy supplier. If more energy has been taken out than is put in then the battery discharges and loses its capacity until becoming 'flat'. The ideal operation is a balanced 'exchange' of energy. Figure C.1 illustrates the current flow between the alternator the battery and the electrical equipment (Bosch 2014; Pavlov 2017):

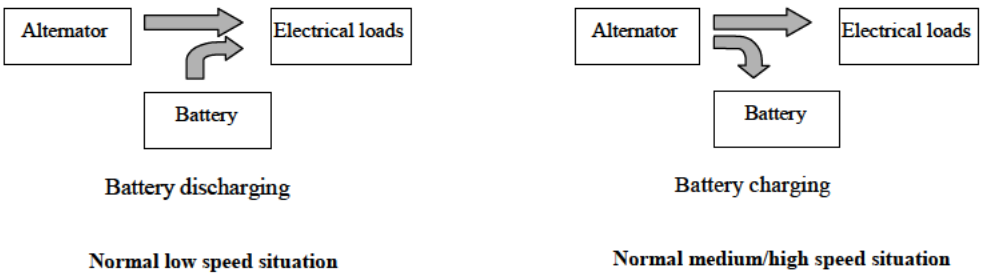

Figure C.1. Normal situations for low, medium and high speeds

C.2 Ultracapacitors

C.2.1 Principle of energy storage

Electrochemical capacitors store the electric energy in an electrochemical double layer (Helmholtz Layer) formed at a solid/electrolyte interface. Positive and negative ions within the electrolyte accumulate at the surface of the solid electrode and compensate for the electronic charge at the electrode surface (Grbovic 2013). The thickness of the double layer depends on the concentration of the electrolyte and on the size of the ions and is in the order of 5-10 Armstrong for concentrated electrolytes. The double layer capacitance is about 10-20μF/cm^2 for a smooth electrode in concentrated electrolyte solution and can be estimated according to equation (Grbovic 2013).:

$$\frac{C}{A} = \frac{\varepsilon_o \varepsilon_r}{d} \tag{C.1}$$

where:

ε_o = dielectric permittivity of free space

ε_r = relative dielectric constant

A = surface area

d = thickness of double layer

In order to achieve a higher capacitance the electrode surface area is additionally increased by using porous electrodes with an extremely large internal effective surface. Combination of two such electrodes gives an electrochemical capacitor of high capacitance.

The maximum energy stored in such a capacitor is given by:

$$W = \frac{1}{2} C V_o^{\,2} \tag{C.2}$$

where:

C = cell capacitance

Vo=cell voltage

C.2.2 Classification of electrochemical capacitors

All capacitors consist of two metallic electrode plates separated by an insulating medium called the capacitor's dielectric layer. Some types of capacitors also require a solid or liquid electrolyte. These are three main classifications of capacitors: electrostatic, electrolytic and electrochemical. In this study electrochemical capacitors will be analysed since are the usual for automotive applications. Electrochemical capacitors may be distinguished by several criteria such as the electrode material, the electrolyte or the cell design. With respect to electrode materials there are three main categories:

- Carbon based
- Metal oxides
- Polymeric materials

With respect to the electrolyte there are two categories:

- Organic electrolyte
- Aqueous electrolyte

More details of these technologies may be found in (Grbovic 2013).

C.2.2.1 Carbon based electrode

Electrochemical capacitors (EC) have a dielectric layer that forms naturally in the electrolyte with applied voltage. This dielectric forms in a very thin double layer on the surface of the capacitor's electrodes. Because of this effect, these capacitors are also known as double layer capacitors.

By using a very high surface area substance for the capacitor electrode, EC capacitors can reach 5000 farads (F) in a single cell. Activated carbon is a common electrode material due to its high surface area (1000 m^2 /g and more), availability, chemical stability and relatively low cost. More details on carbon-based capacitors may be found in (Grbovic 2013).

C.2.2.2 Organic electrolyte

The advantage of an organic electrolyte is the higher achievable voltage. According equation (C.2) the square of the unit-cell voltage determines the maximum stored energy. Organic electrolytes allow for a unit cell voltage above 2V. Typically the cell voltage is 2.3V-2.7V. The cell voltage probably is

limited by the water content of the electrolyte. Some companies plan to increase the float voltage at 3.2V with extreme purification procedures of special electrolyte and corrosion reduction of the carbon-based electrodes by special protective coatings.

On the other hand organic electrolytes have a significantly higher specific resistance. The higher electrolyte resistance affects the equivalent distributed resistance of the porous layer and consequently reduces the maximum usable power which is calculated by:

$$P = VI = \frac{U^2}{4R} \tag{C.3}$$

where R is the total equivalent series resistance (ESR). However, part of the reduction in power is compensated by the higher cell voltage that is achieved with an organic electrolyte.

C.2.4 Voltage balancing

Most ECs have an operating voltage limit of around 2.3-2.7V, which some manufacturers are working to extend (Grbovic 2013). When ultracapacitors are used for automotive applications, it is necessary to stack the cells in series. The total ultracapacitors's effective capacity will be decreased. But when you connect in series capacitors, any mismatch between the individual cells will affect the distributed voltage across them. There is the danger of exceeding the rated voltage on any of the stacks. Most of the manufacturers do not indicate any catastrophic failure mechanism for an ultracapacitor over exceeding its operating voltage but a reduction of its life cycle is possible.

In order to avoid overvoltage across the terminals of an individual cell or a complete stack of cells, voltage balancing circuits are introduced. There two techniques of balancing the voltage: a passive or an active technique. Passive balancing involves a resistor in parallel with the capacitors, the so-called 'bleed resistor' (R_{bypass}), setting the voltage levels across the capacitors by the voltage divider rule. Active balancing uses semiconductor switches to hold the voltage across the capacitor terminals within the specified voltage limits. An example of an active balancing circuit is shown in Figure C2.1:

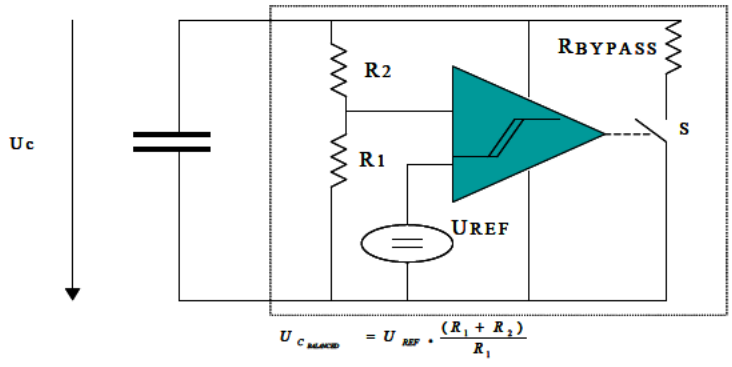

Figure C.2.1 Active voltage balancing circuit (EPCOS)

C.2.5 Ultracapacitors vs automotive batteries

EC capacitors can be used in applications where batteries are employed. They can be used in voltage back up applications where the voltage must be held a certain level for a few seconds. High power capability is also an advantage for EC capacitors. Although batteries exceed in energy storage, EC capacitors provide high power levels. The ideal applications for ECs are all those demanding energy for a duration in the time range of $10^{-2}s < t < 10^{2}s$ (Grbovic 2013; Pavlov 2017). For those applications, for both batteries and EC capacitors, the ratio of stored energy to available power is not very good and the devices have to be over-dimensioned due to the increased demand of power or energy.

The power density of EC capacitors can reach several kW/kg instead of lead acid batteries that only reach from 0.1kW/kg to 0.5kW/kg (Grbovic 2013; Pavlov 2017). This, in combination with the extremely low internal resistance (ESR) characteristic enables ultracapacitors to supply large amounts of instantaneous peak power, when demanded by the load. EC capacitors can be operated in a wider range of temperature than batteries. The reason is that a battery uses a chemical system to supply energy instead of EC capacitors that store their energy electrostatically, so they still work efficiently up to $-55^{0}C$.

Another important advantage of ECs is that in general, they do not contain toxic materials and are easy to dispose. They do not need any servicing during their life and have large life cycle. Their efficiency can reach 95%. Also, short-term overvoltages (in ms or even s), is not critical for the devices. If the applied voltage exceeds the nominal voltage for longer duration, the lifetime of the EC will be shorted. Gas may be produced which can cause leakage of the device. Self-discharge is not an issue since the characteristic time is in the order of days to months.

An EC capacitor can recharged quickly and easily unlike batteries that require that may take up to 10hr to recharge. EC capacitors are easily recharged in seconds or minutes with simple charging

systems. Rather than operate as a main battery, EC capacitors are more commonly used a memory backup or load levelling. An EC capacitor can be connected in parallel to the battery terminal and provides current boost on high load demands.

Most EC capacitors are short circuit proven. The larger internal resistance in comparison with conventional capacitors limits the peak power the smaller amount of energy stored in comparison to batteries allows only a limited heating (self-ignition has to be avoided).

Finally, the basic technology of EC capacitors with carbon electrodes is independent of polarity. However, present EC capacitors are not suitable for AC applications and high ripple current. The internal resistance is higher than that of the conventional capacitors and thermal degradation may occur (Grbovic 2013; Pavlov 2017). Another disadvantage of EC capacitors compared with the lead-acid batteries is the lower energy density capability than that of the lead-acid batteries. The large EC devices can reach up to 1/3 the energy of the batteries.

C.3 Photovoltaic (PV) panels

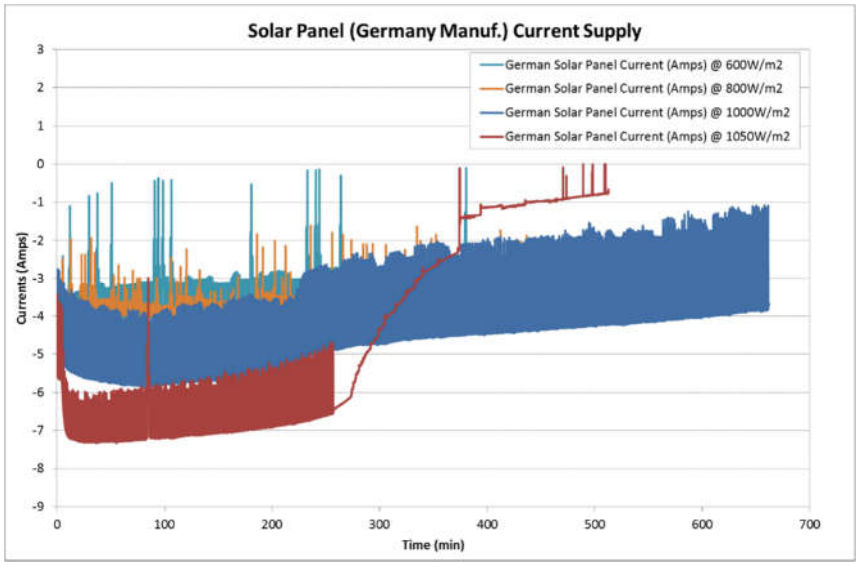

Figure C.3.1 Current output achieved during different solar loading levels ($W.m^{-2}$) (Enecom PV panel manufactured in Germany)

The current output of the PV panel manufactured in Germany is slightly different to that shown at Figure C3.1. As a 12-volt battery used for a load, its initial SoC was higher than expected therefore after several hours of charging reached its maximum level of SoC and based on the voltage level achieved the MPPT controller reduced the output as expected.

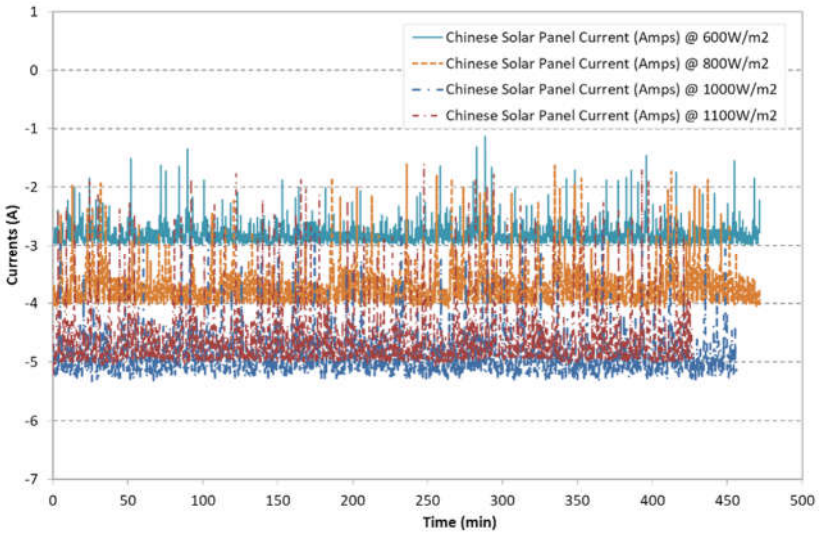

Figure C.4.2 Current output achieved during different solar loading levels ($W.m^{-2}$)
(Enecom PV panel manufactured in Germany)

The current output of the PV panel manufactured in China is slightly different to that shown at Figure C3.1. As a 12-volt battery used for a load, its initial SoC was lower therefore a continues charging was accepted without achieving maximum level of SoC, MPPT controller didn't reduced the output as expected.

Appendix D MATLAB®/Simulink™ test suite

The study carried out has led to the design and implementation of a MATLAB®/Simulink™ test suite for the modular implementation and investigation of the individual components. The following screenshots illustrate the user-friendly test suite. Figure D1.1 depicts the graphical user interface for choosing a combination of vehicle configuration with regards driving cycles, battery parameters, alternator parameters, ultracapacitor parameters, and graphical results. Depending on the user choice, the corresponding input files are loaded.

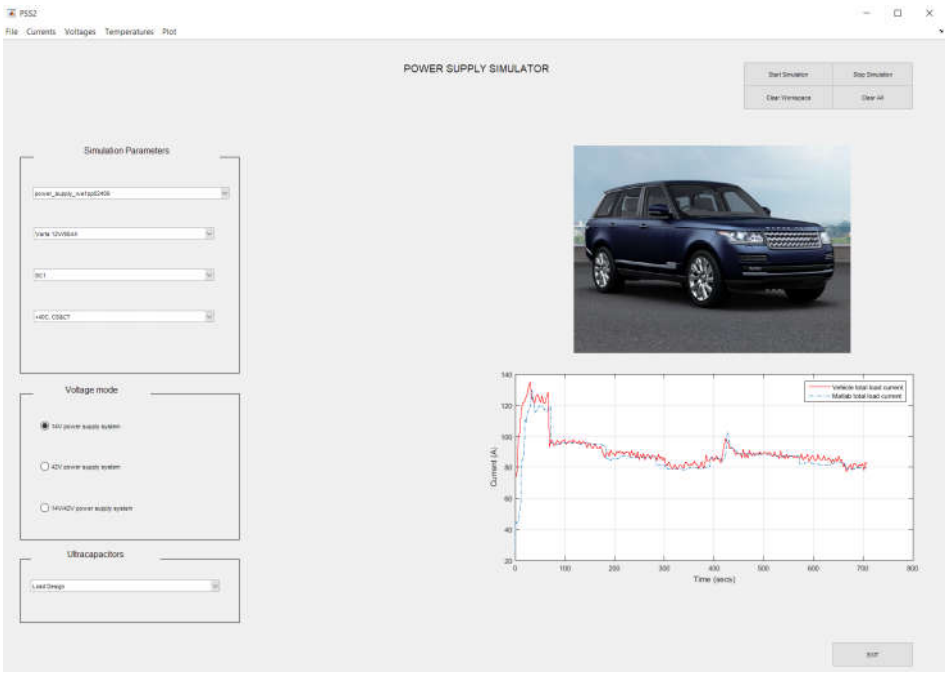

Figure D.1. Screenshot of the developed intuitive GUI

D.1 MATLAB®/Simulink™ battery model

According to the large variety of vehicles and power supply systems, differently sized batteries exploiting the same basic technology are available. To reduce the parameterisation effort, all the parameters of the model are defined with respect to the battery's nominal current and the number of cells connected in series. Adopting a linear up or downscaling of the battery quantities still yields reasonable results and is an easy adaptation of the models. Furthermore, the model has then been scaled down to 12-volt and nominal capacities of 95/90/80/70 to represent the 12-volt AGM lead-acid batteries for the purpose of the simulation. This model will be used to simulate voltage responses during highly dynamic current profiles. Figure D.2 shows the Simulink layout of the battery model:

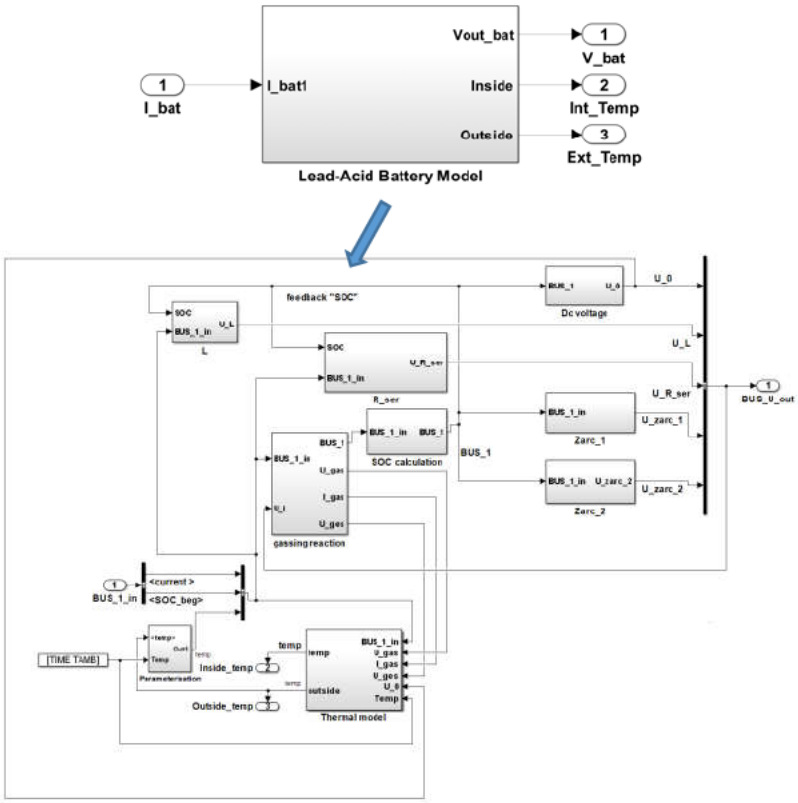

Figure D.2. The Simulink layout of the battery model

The input quantities of the model are battery current, initial state of charge (SoC), initial battery ambient temperature and charging voltage from the alternator. The outputs of the battery model are terminal voltage, internal predicted temperature and external predicted temperature of the battery model. The SoC input doesn't appear at the block since it has been included at the initial parameters window. The user can set up the initial parameters prior to the simulation by double click on the Simulink block.

D.2 Alternator model based on empirical data

Figure D.3 shows the final Simulink layout of the developed alternator model including the voltage regulation block, the current estimation block and the alternator estimation block. It is worth noting that the boost function is included within the current estimation block:

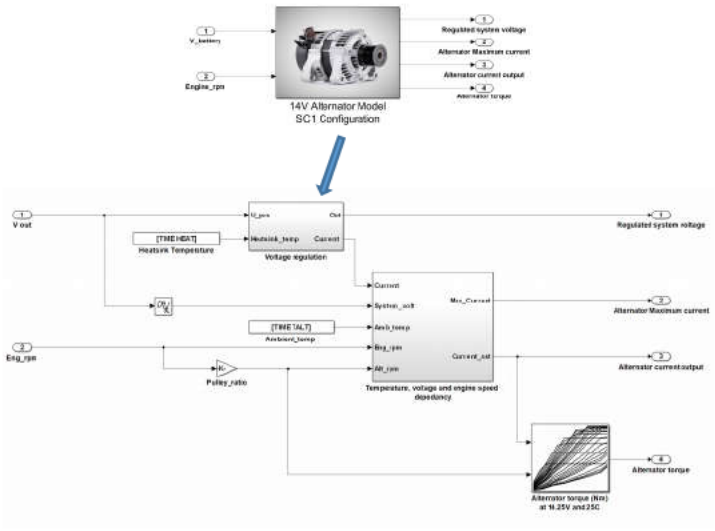

Figure D.3. The Simulink layout of the alternator model

Table D.1 shows the average current output of an SC1 alternator (note that the average is based on 10 sampled values):

	Average Alternator Current (Ampere) at given speed and temperature									
Ambient (^{0}C)	1500 (rpm)	2000 (rpm)	2500 (rpm)	3000 (rpm)	3500 (rpm)	4000 (rpm)	4500 (rpm)	5000 (rpm)	5500 (rpm)	6000 (rpm)
100	58.5	84.4	97.2	102.5	105.0	106.6	107.5	108.2	109.1	109.6
80	62.6	89.8	103.7	110.2	113.9	116.1	117.6	118.7	119.9	120.6
60	65.1	94.5	109.2	115.3	119.5	122.1	123.5	124.6	125.6	126.5
40	67.6	98.0	113.2	120.8	124.8	127.4	128.4	129.5	130.5	131.2
20	71.1	103.1	118.4	126.3	130.5	133.3	135.3	136.7	137.9	138.7
0	73.6	106.9	122.9	131.2	135.6	138.3	140.5	141.9	143.0	144.0
-20	76.9	109.9	126.7	135.7	140.6	143.8	145.6	147.2	148.4	149.6

Table D.1. Average current output of an SC1 alternator at different temperatures

Table D.2 shows the corrections needed at the output of an SC1 alternator according system voltage:

Current output corrections according system voltage								
Voltage (V) / Engine speed(rpm)	10.5	11	11.5	12	12.5	13	13.5	14
600	4	3	2	1	0	-1	-2	-4
750	-9	-7	-6	-4	-3	0	1.5	2
1500	-9	-7	-6	-4	-3	0	1.5	2
3000	-9	-7	-6	-4	-3	0	1.5	2

Table D.2. Corrections of maximum current output of an SC1 alternator

Table D.3 shows the torque of the alternator as a function of alternator speed and electrical load applied at the alternator:

Average Drive Torque @25degC (Nm)											
Alt_rpm	0 Amp	10 Amp	20 Amp	30 Amp	40 Amp	50 Amp	60 Amp	80 Amp	100 Amp	120 Amp	Full Output
1300	0	1.69	3.13	3.89	3.89	3.89	3.89	3.89	3.89	3.89	3.89
1400	0	1.54	2.78	4.1	5.42	5.42	5.42	5.42	5.42	5.42	5.42
1500	0	1.41	2.52	3.75	5	6.34	6 55	6.55	6.55	6.55	6.55
1600	0	1.33	2.34	3.44	4.64	5.85	7 22	7.22	7.22	7.22	7.22
1700	0	1.25	2.17	3.21	4.33	5.46	6.8	7.72	7.72	7.72	7.72
1800	0	1.18	2.05	3.02	4.1	5.2	6 29	8.13	8.13	8.13	8.13
1900	0	1.1	1.94	2.83	3.89	4.92	6	8.26	8.26	8.35	8.35
2000	0	1.03	1.85	2.71	3.7	4.67	5.71	7.76	8.59	8.59	8.59
2100	0	0.98	1.75	2.61	3.52	4.42	5.4	7.45	8.66	8.66	8.66
2200	0	0.93	1.7	2.49	3.36	4.24	5 13	7.09	8.72	8.72	8.72
2400	0	0.84	1.55	2.28	3.08	3.86	4.73	6.45	8.35	8.69	8.69
2500	0	0.82	1.5	2.19	3	3.71	4 55	6.21	7.98	8.63	8.63
2600	0	0.79	1.45	2.1	2.87	3.58	4 39	5.97	7.65	8.52	8.52
2800	0	0.77	1.36	1.98	2.65	3.32	4.05	5.58	7.18	8.33	8.33
3000	0	0.71	1.26	1.9	2.52	3.19	3.8	5.17	6.7	8.02	8.02
3500	0	0.69	1.1	1.61	2.19	2.75	3 25	4.44	5.74	7.31	7.34
4000	0	0.65	0.97	1.43	1.95	2.41	2 9	3.95	5.11	6.4	6.67
4000	0	0.59	0.88	1.27	1.79	2.12	2.65	3.55	4.6	5.7	6 2
5000	0	0.57	0.81	1.19	1.61	2.01	2 11	3.23	4.22	5.15	5 9
5500	0	0.55	0.74	1.1	1.53	1.88	2 21	2.99	3.95	4.68	5.42
6000	0	0.55	0.7	1.03	1.45	1.76	2 1	2.83	3.7	4.4	5.12
8000	0	0.55	0.68	0.97	1.27	1.51	1.74	2.35	2.94	3.68	4.31
10000	0	0.55	0.68	0.98	1.26	1.42	1 58	2.12	2.63	3.24	3.78
12000	0	0.55	0.68	0.98	1.21	1.38	1 55	2.03	2.47	3.02	3.64

Table D.3. SC1 alternator torque data measured at 14.25V and 25^0C

D.3 Ultracapacitors MATLAB®/Simulink™ model

Figure 5.22. Each model is parameterised according the above characteristics. The inputs of the models are current, and temperature and the outputs are total voltage and peak power.

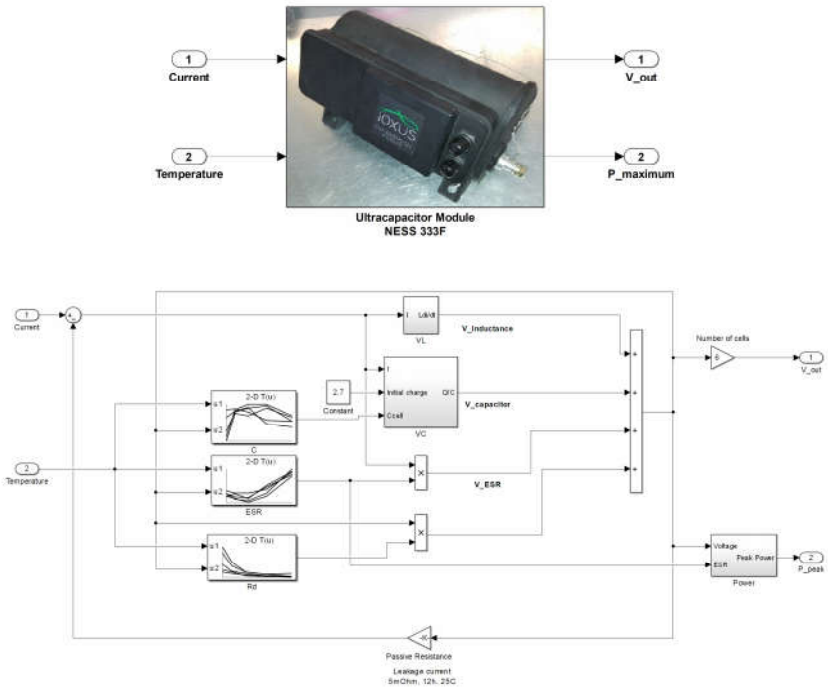

Figure D3.1. Simulink layout of the ultracapacitors models

D.4 Solar panel MATLAB®/Simulink™ model

D.4.1 Solar panel model based on empirical data

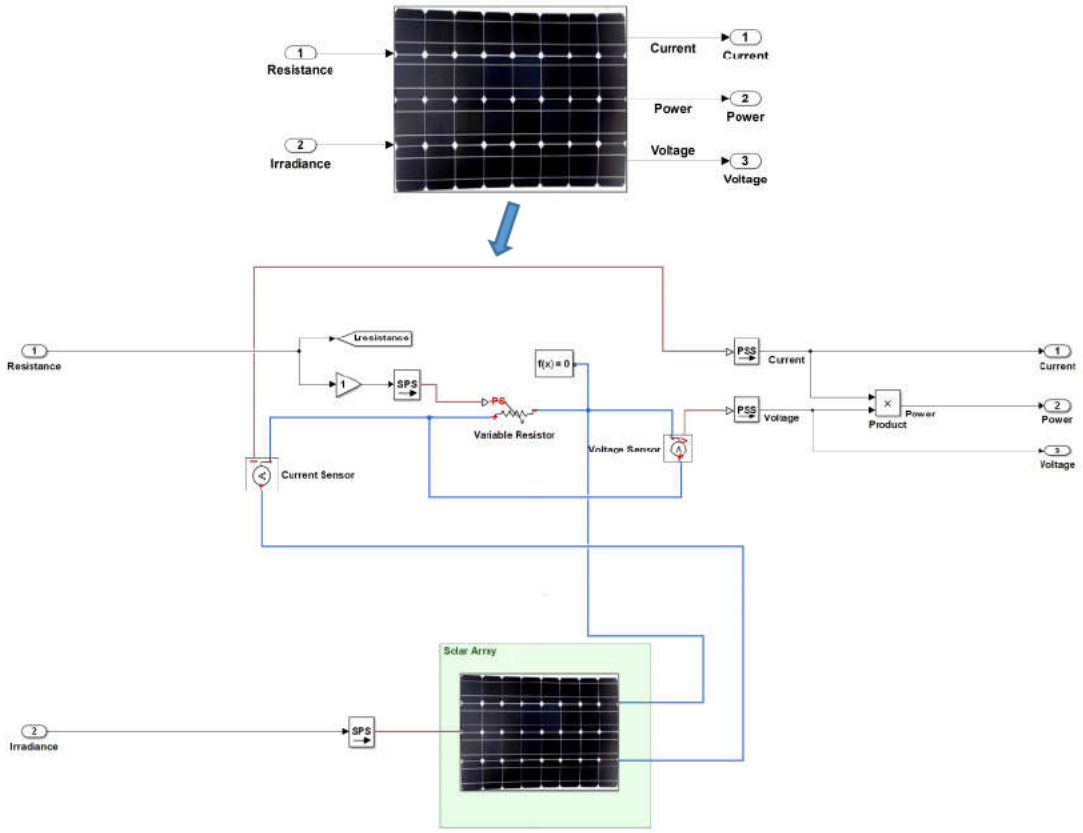

Figure D4.1. Simulink layout of the developed Solar Panel

D.5 Electrical Loads MATLAB®/Simulink™ model

D.5.1 Vehicle Electrical features/loads Model representation

The developed model representing the above described vehicle electrical features have been separated into different subsystems as shown in Figure 5.29, including the engine base load subsystem, electrical lighting subsystem, heating/comfort cabin subsystem, and finally the infotainment and the chassis subsystems respectively. The operation of the electrical loads was fully customisable based on either manual or automatic mode.

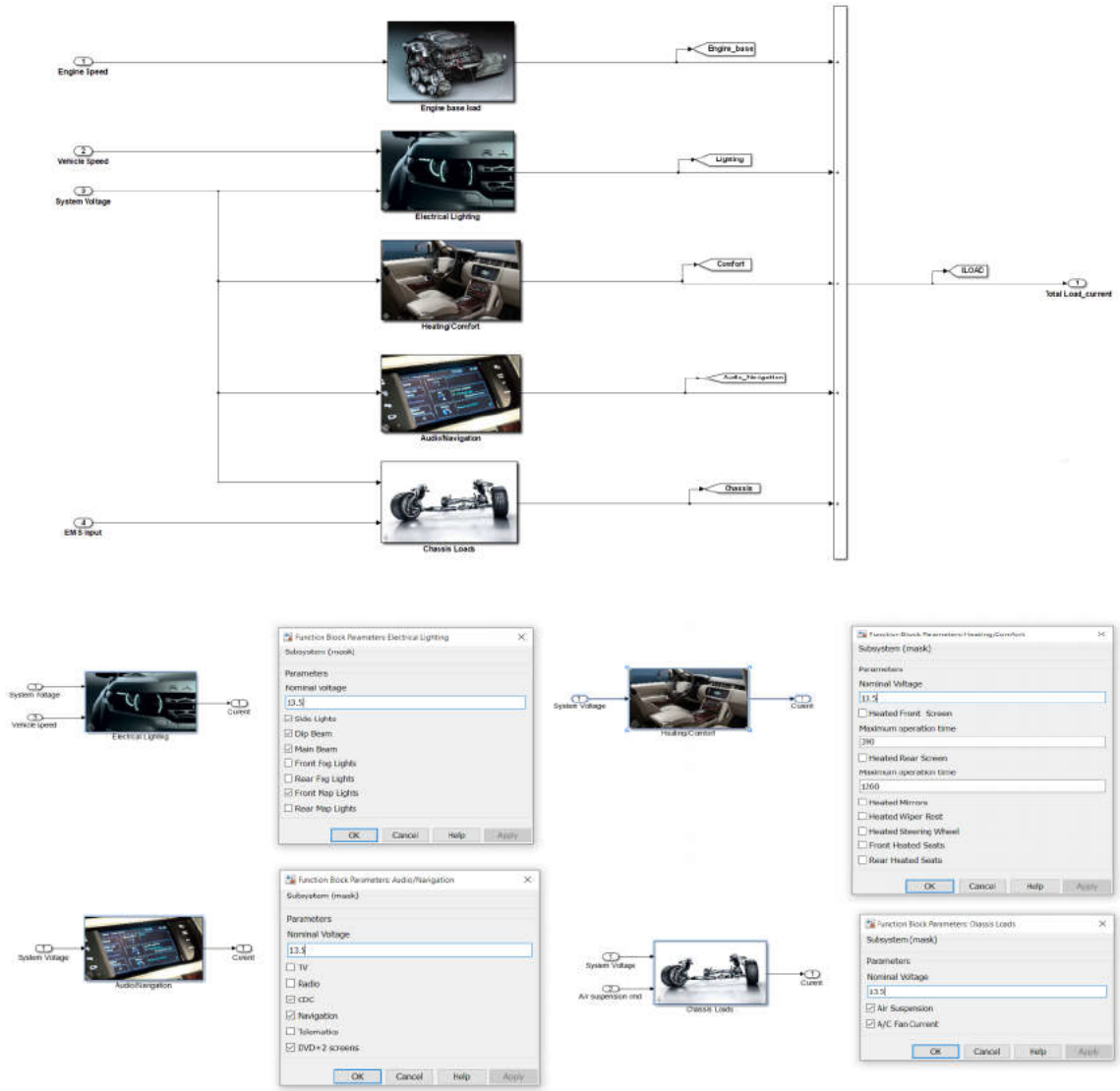

Figure D5.1. MATLAB®/Simulink™ model of vehicle's electrical features.

Appendix E Model validation

E.1 Driving Cycles

Suburban traffic cycle-Cold Climate Use:

Time Period (Minutes)	Speed (MPH/KPH)
0-3	0
3-6	28/45
6-8	9/14
8-10	0
10-14	18/28
14-15	0
15-18	28/45
18-20	9/14
20-22	0
22-24	18/28
24-25	0
25-28	28/45
28-30	9/14
30-32	0
32-34	18/28
34-35	0

Table E3.1. Suburban Traffic cycle – Cold Climate Use

Time Period (Minutes)	Speed (MPH/KPH)
0-3	0
3-6	28/45
6-8	9/14
8-10	0
10-14	18/28
14-15	0
15-18	28/45
18-20	9/14
20-22	0
22-24	18/28
24-25	0
25-28	28/45
28-30	9/14
30-32	0
32-34	18/28
34-35	0

Table E3.2. Suburban Traffic cycle – Hot Climate Use

Time Period (Seconds)	Acceleration Rate (MPH/sec or KPH/sec)	Target Road Speed (MPH/KPH)
0 - 0.71	3.5 or 11.1	25/40
7.1 - 13.6	0	25/40
13.6 - 22.6	-2.7 or -4.4	0
22.6 - 42.6	0	0

Table E3.3. City Traffic Cycle Format

To complete a full CSCT cycle, suburban cycle given in tables E3.1-2 and City Traffic cycle in E3.3 are combined together. City Traffic cycle in E3.3 is performed a total of 35 times. The rate of positive acceleration may be reduced by up to 30% if it is found that the vehicle is not capable of matching the required profile.

Time Period (Minutes)	Speed (MPH/KPH)
0 - 15	30/48
15 - 45	0
45 - 60	30/48
60 - 70	40/64
70 - 75	50/80

Table E3.4. Drive Idle Drive cycle

When at zero speed, there must be no air flow over the front of the vehicle. When testing in an environment chamber, the shutters covering the fan nozzle must be lowered to block the direct air flow to the vehicle. When testing in an external environment, the vehicle shall be stopped facing an obstruction, such as, for example, a building or a wall.

E.2 MATLAB®/Simulink™ model performance

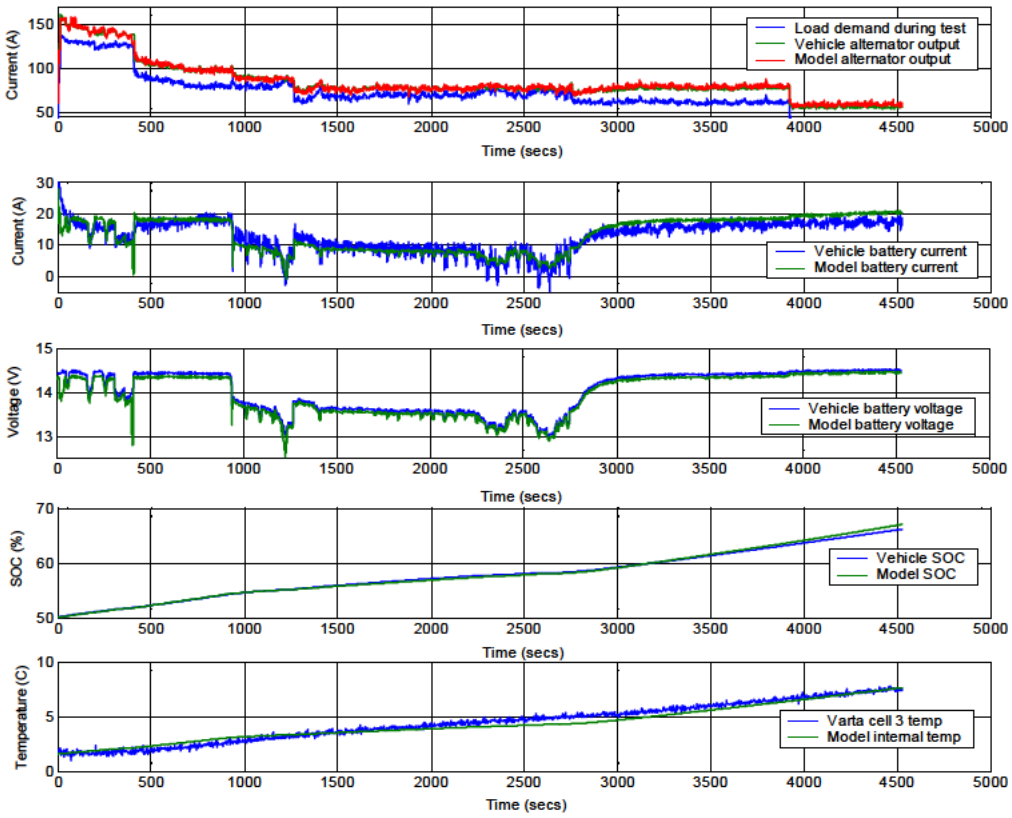

Figure E2.1. Ambient +0^{0}C, DID test

Figure E2.1 shows that the developed system meets the design criteria (described in section 4.1.2) throughout the test. In particular:

Subplot 1. Alternator output vs load demand. The absolute error of the model alternator current output is 5A underestimated comparing that of the vehicle's alternator current output throughout the test (idle-drive-idle period).

Subplot 2. Battery current. The absolute error on the battery model current level is less than 5A throughout the test.

Subplot 3. Battery voltage. The error of the battery voltage is within the range of $\pm$ 0.5V. It is worth noting that 'simulation spikes' occurs throughout the test.

Subplot 4. SoC. The battery model SoC indicates a similar trend to the measured data with almost identical final state of charge.

Subplot 5. Internal temperature. The model internal temperature estimation is within the range of $\pm$ 0.2^{0}C relatively good with that of the actual cell 3 temperature and the final result is almost identical.

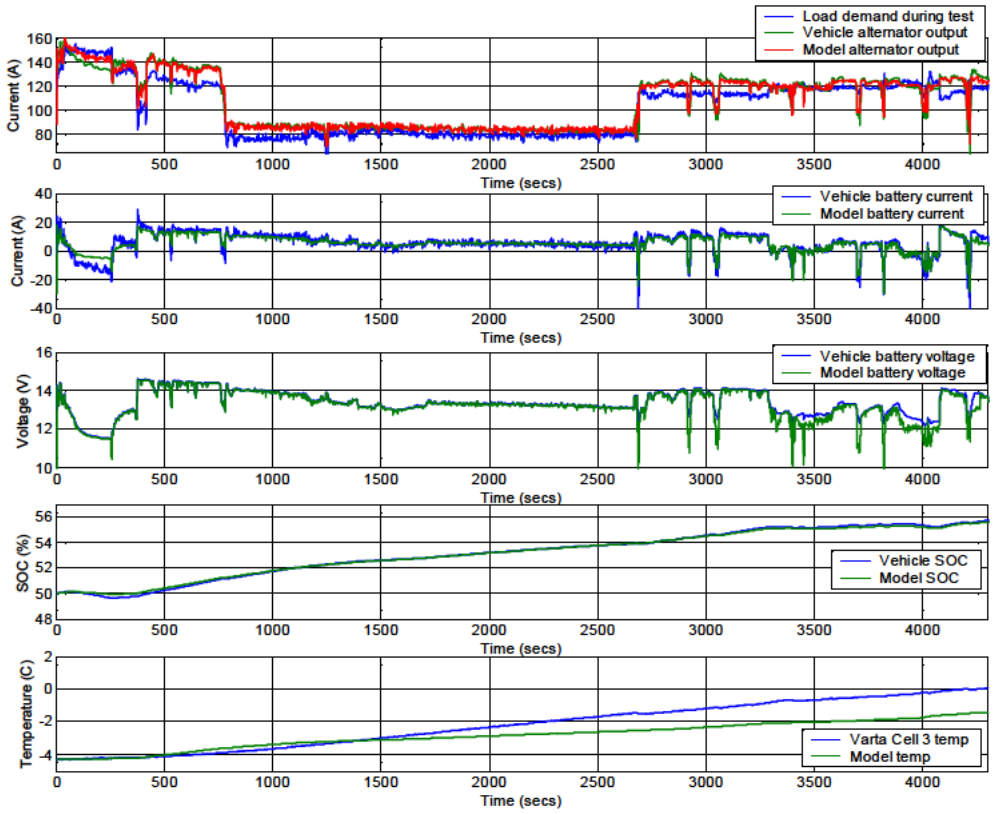

Figure E2.2. Ambient –5.5^{0}C, DID test

Figure E2.2 shows that the developed simulation model does perform well and meet the desired design criteria. It is worth noting that some discrepancies occur at the end of the test. In particular:

Subplot 1. Alternator output vs load demand. The absolute error of the model alternator current output is 1-3A comparing that of the vehicle's alternator current output. At the final period of the test, rapid changes of load demand and system voltage level occur.

Subplot 2. Battery current. The absolute error on the battery model current level is 1-3A. The maximum absolute error occurs at the end of the second 'drive' period of the test.

Subplot 3. Battery voltage. The absolute error of the battery model voltage is 0.1-0.7 and occurs at the end of the test (at the second ‘drive’ period). It is worth noting that inaccuracies are introduced at the end of the test when frequent changes on load demand occur.

Subplot 4. SoC. The model SoC indicates a quite similar trend to the measured data with an underestimation of 2% of the battery's SoC.

Subplot 5. Internal temperature. The model internal temperature estimation is underestimated by 0.8 ^{0}C of the vehicle's battery cell 3 temperature at the end of the test.

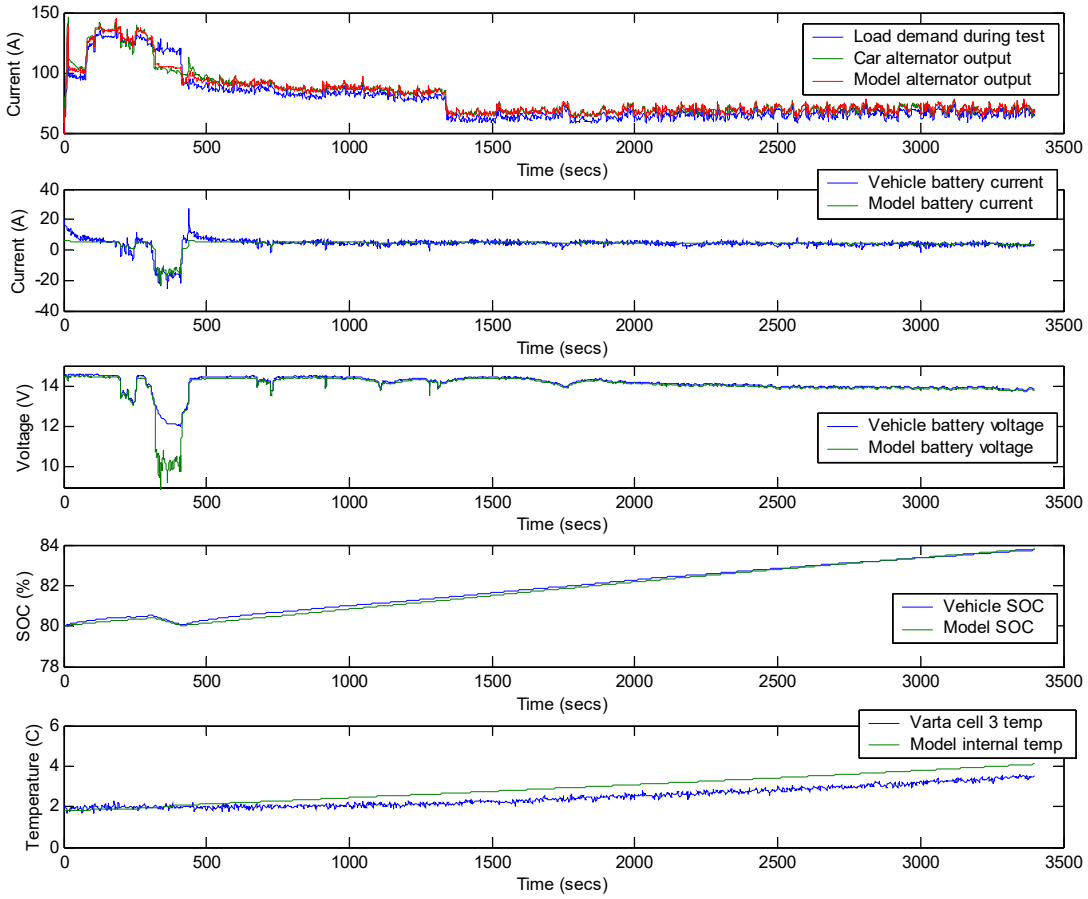

Figure E2.3. Ambient +0^{0}C, CSCT test

Figure E2.3. Ambient +0^{0}C, CSCT test, using x100 2003 MY U74a cooling fan map, dip beam used + front fogs, Defrost for 3mins then a/c auto 23^{0}C. recirc mode. Heated rear screen on.

Simulated loads: side marker lights (4x5W) = Map lights x 2

Adaptive cruise control = 1.5A = HMSL on all time

Heated front screen = 32.2A- OFF @ 6.5mins

Heated seats x 2 = adaptive damping = 6.9A

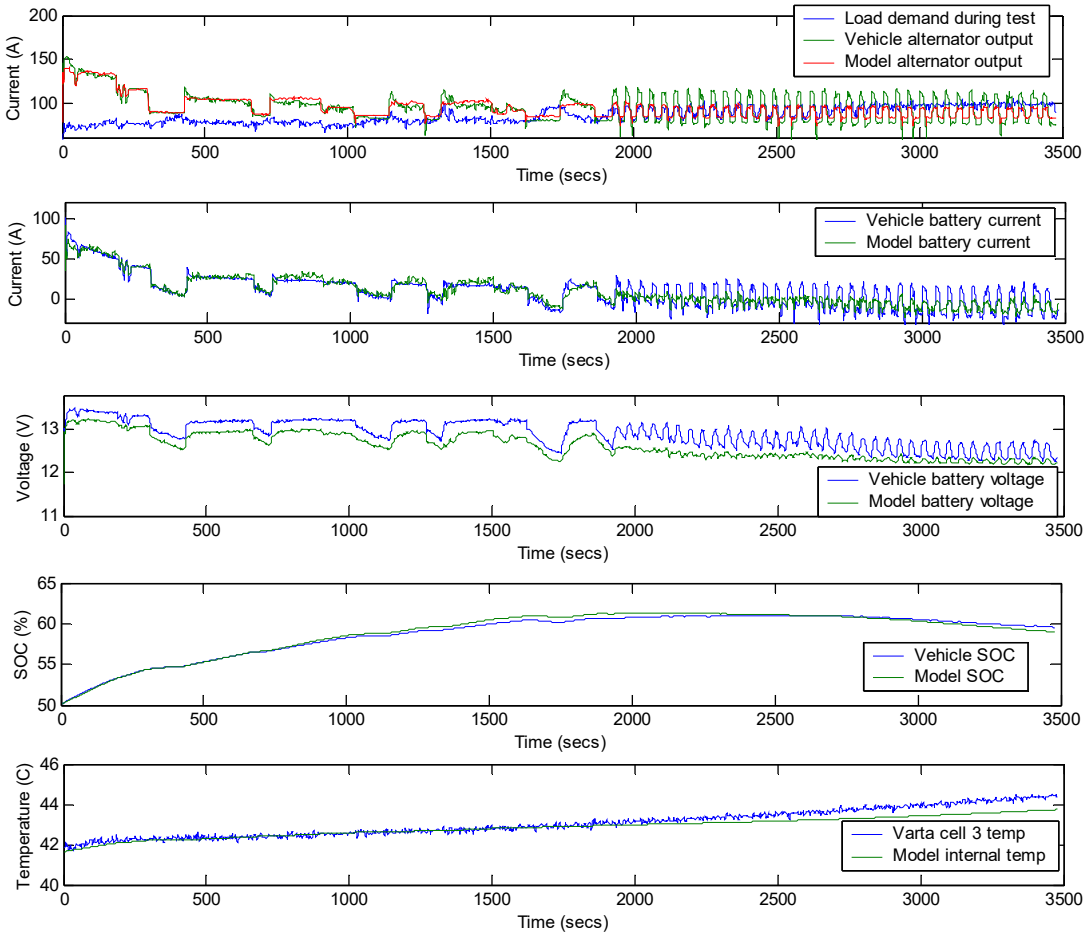

Figure E2.4. Ambient +40^{0}C, CSCT test

Figure E2.4. Ambient +40^{0}C, CS&CT test, using x100 2003 MY U74a cooling fan map, dip beam used, a/c auto 23^{0}C. recirc mode.

Simulated loads: side marker lights (4x5W) = Map lights x 2 (on until light off @ 65min)

Adaptive cruise control = 1.5A = HMSL on all time

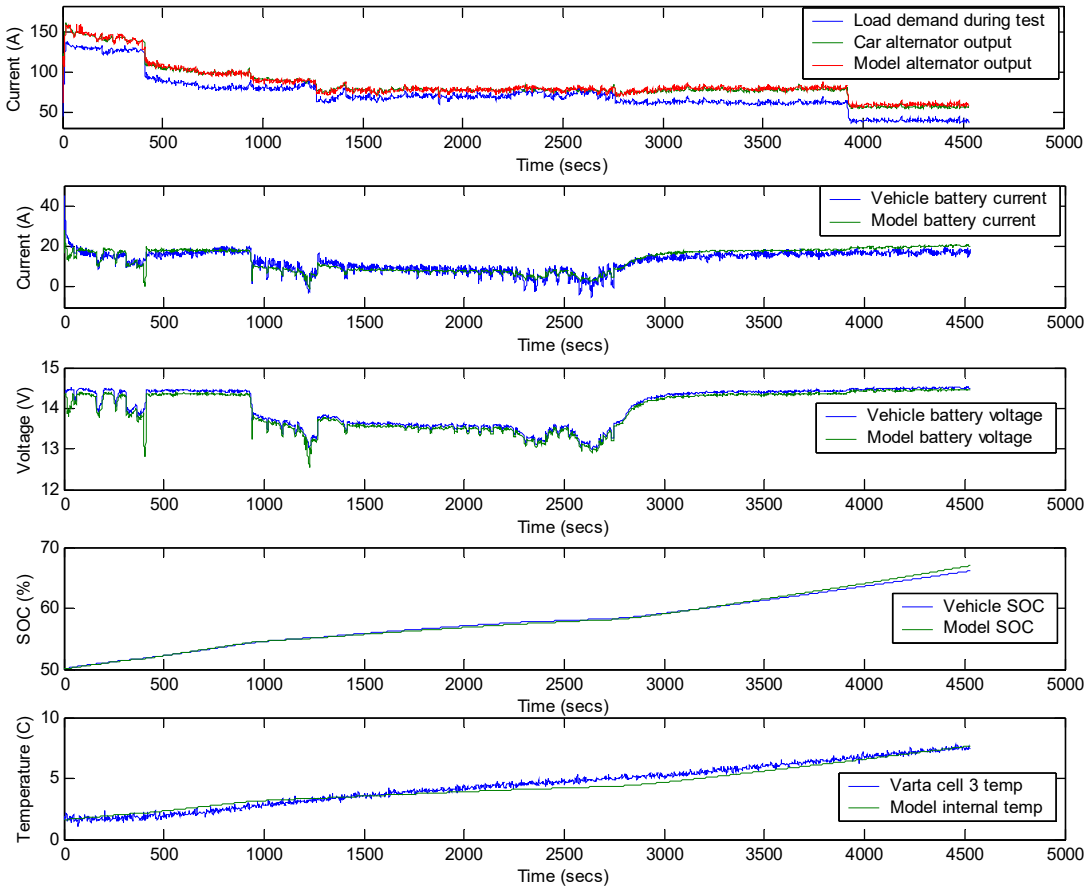

Figure E2.5. Ambient +0^{0}C, DID test

Figure E2.5. Ambient +0^{0}C, CS&CT test, using base x100 2003 MY U74a cooling fan map, dip beam used + front fogs, Defrost for 3mins then a/c auto 23^{0}C. recirc mode.

Heated rear screen on.

Simulated loads: side marker lights (4x5W) =1.6A= Map lights x 2 (on until light off@65min)

Adaptive cruise control = 1.5A = HMSL on all time

Heated front screen OFF @ 6.5mins

Heated seats x 2 simulated using adaptive damping = 6.9A

Battery 07/2001/90/10 @ 50%

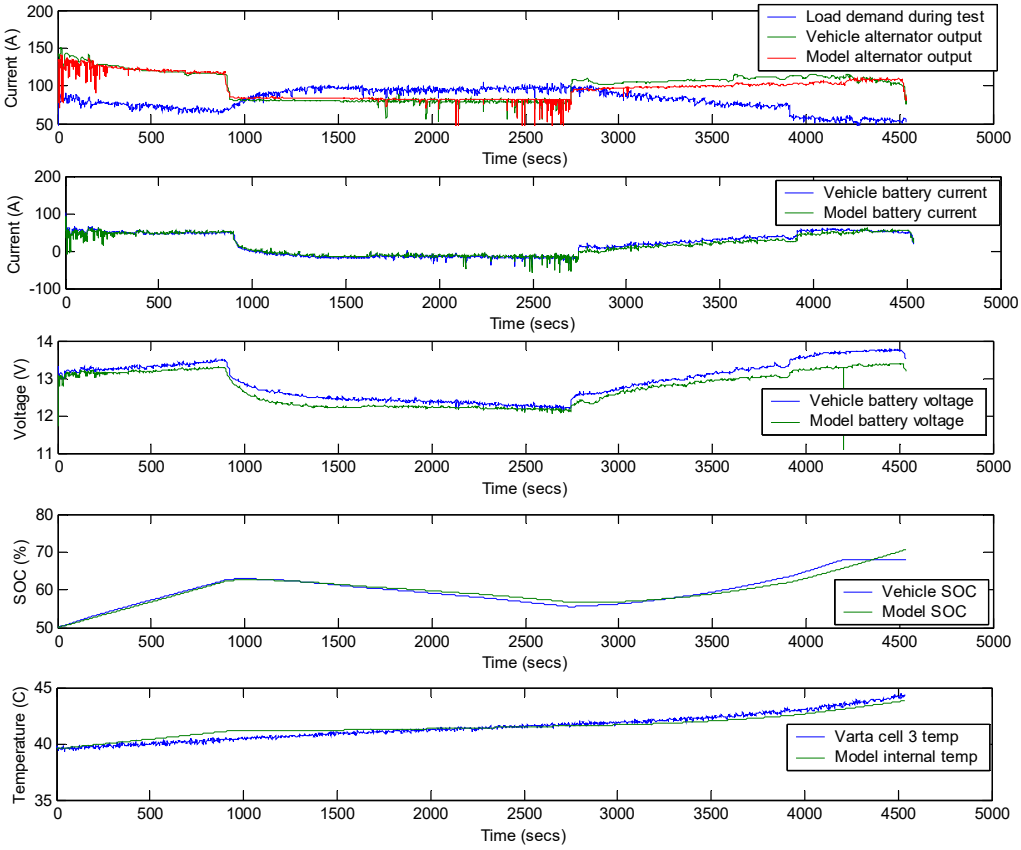

Figure E2.6. Ambient +40^{0}C, DID test

Figure E2.6. Ambient +40^{0}C, DID test, using x100 2003 MY U74a cooling fan map, dip beam used, a/c auto 23^{0}C. recirc mode.

Simulated loads: side marker lights (4x5W) = Map lights x 2

(on until light off @ 65min)

Adaptive cruise control = 1.5A = HMSL on all time

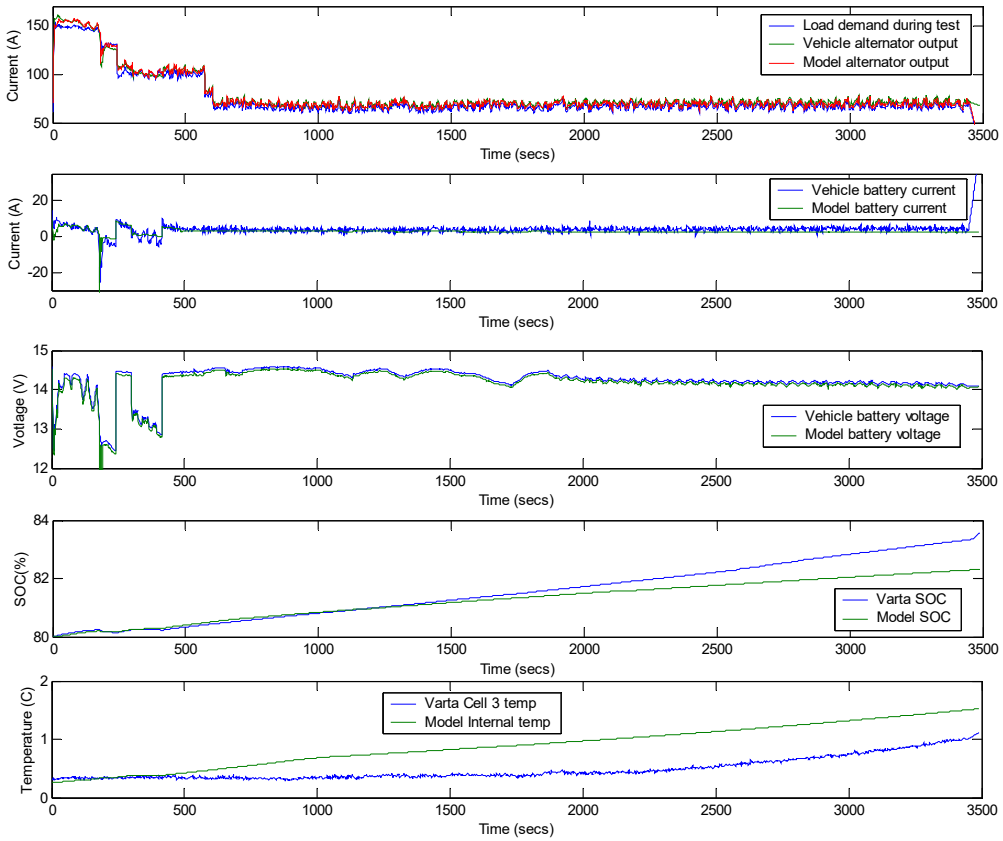

Figure E2.7. Ambient 0^0C, CSCT Test

Subplot 1. Alternator output vs load demand. The performance of the model alternator output is good throughout the test. The absolute error here is 5-7A.

Subplot2. Battery current. The absolute error on the battery model current level is within 5A for the suburban phase. The error in the 'city traffic' period is underestimated 2-5A.

Subplot3. Battery voltage. The absolute error of the battery voltage is within the range of 0.5V throughout the test.

Subplot4. SoC. The model SoC indicates a quite similar trend to the measured data with an underestimated final state of charge 1.1%.

Subplot5. Internal temperature. The model internal temperature estimation is quite good throughout the test. The final result is underestimated 0.4 ^{0}C of the actual battery's cell 3 temp.

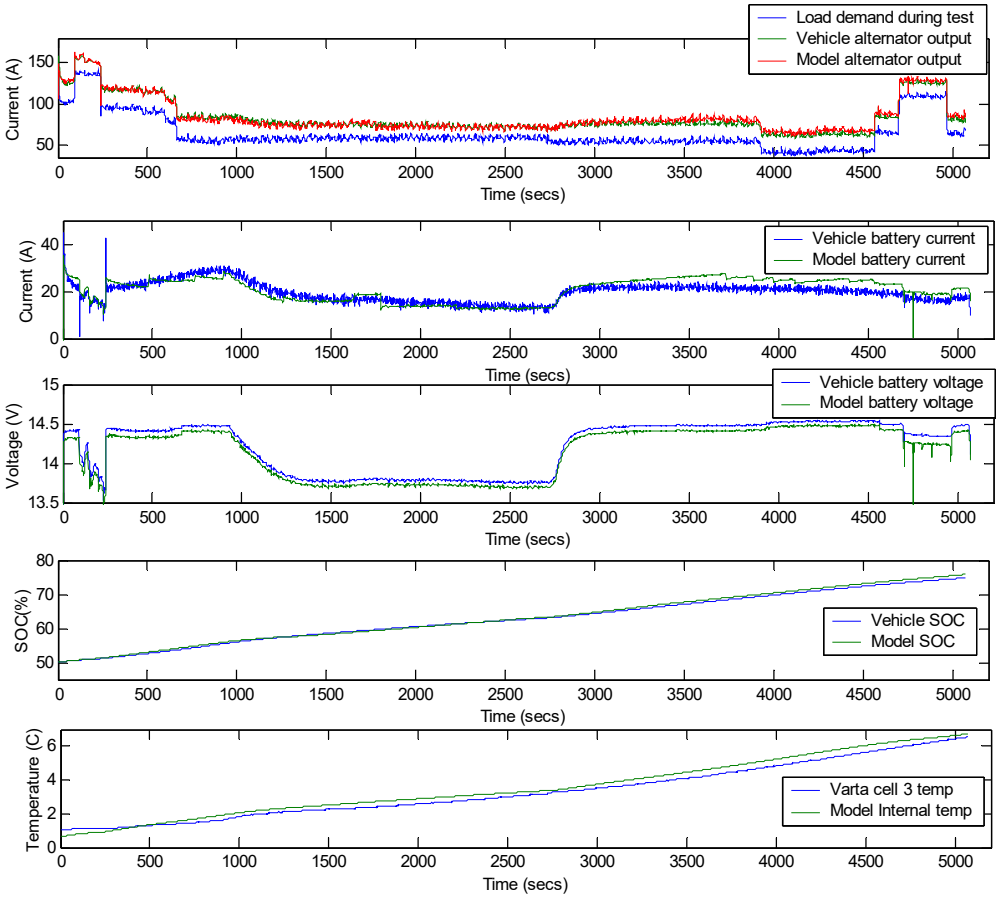

Figure E2.8. Ambient 0^0C, DID Test

Subplot 1. Alternator output vs load demand. The performance of the model alternator output is quite good during 'the drive-idle-drive' test. The absolute error that occurs here is 5-10A (during the second 'drive' period.

Subplot 2. Battery current. The absolute error on the battery model current level is 5-8A while the maximum error occurs in both 'drive' phases of the test.

Subplot 3. Battery voltage. The absolute error of the battery voltage is within the range of 0.5V throughout the test. Simulation spikes are generated again on the last phases of the test.

Subplot 4. SoC. The model SoC indicates a quite similar trend to the measured data with an overestimated final state of charge 1% of the battery's SoC.

Subplot 5. Internal temperature. The model internal temperature estimation is good throughout the test. The final result is overestimated 0.1 ^{0}C of the actual battery's cell 3 temp.

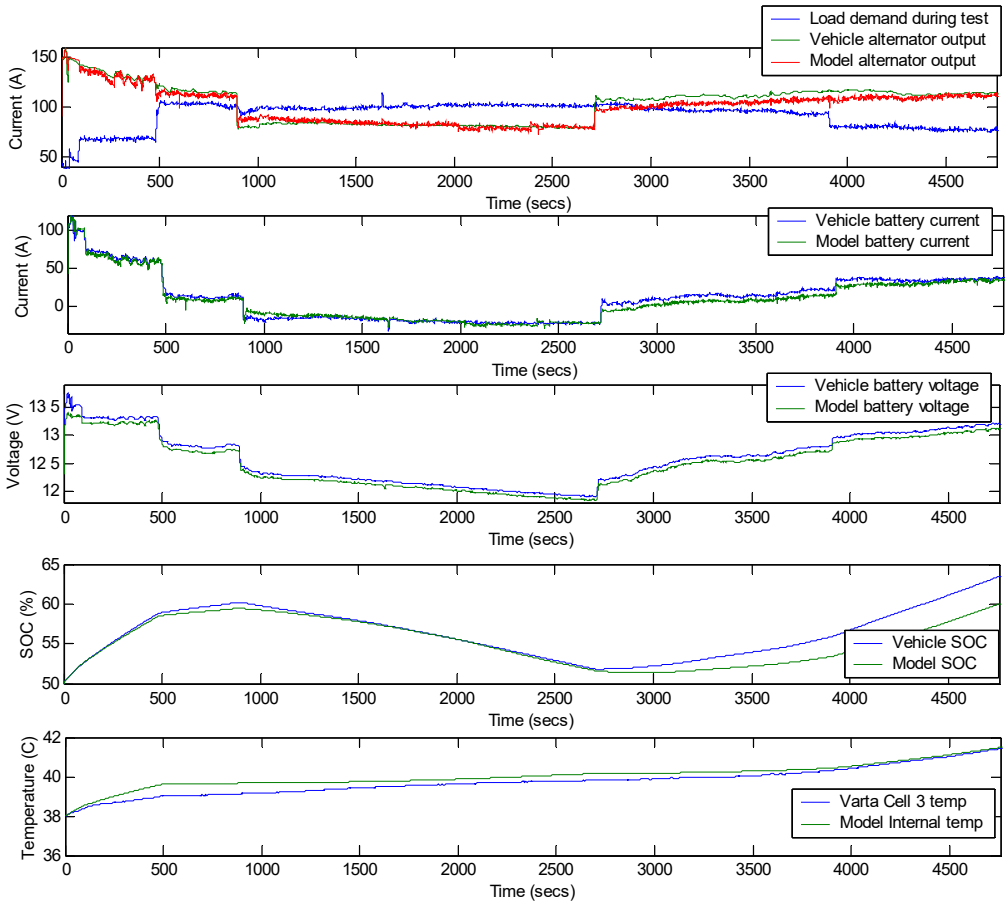

Figure E2.9. Ambient +40^{0}C, DID Test

Subplot 1. Alternator output vs load demand. The performance of the model alternator output is good during the test. The absolute error that occurs here is 5-8A (during the second 'drive' period) and the maximum output is underestimated of the vehicle alternator's output.

Subplot 2. Battery current. The absolute error on the battery model current level is 5-8A while the maximum error occurs in both 'drive' phases of the test and is underestimated of the vehicle battery's current.

Subplot 3. Battery voltage. The absolute error of the battery voltage is 0.2V throughout the test.

Subplot 4. SoC. The model SoC indicates a quite similar trend to the measured data with an underestimated final state of charge of 3.5% of the battery's SoC.

Subplot 5. Internal temperature. The model internal temperature estimation is relatively good with an almost identical final result of the actual battery's cell 3 temp.

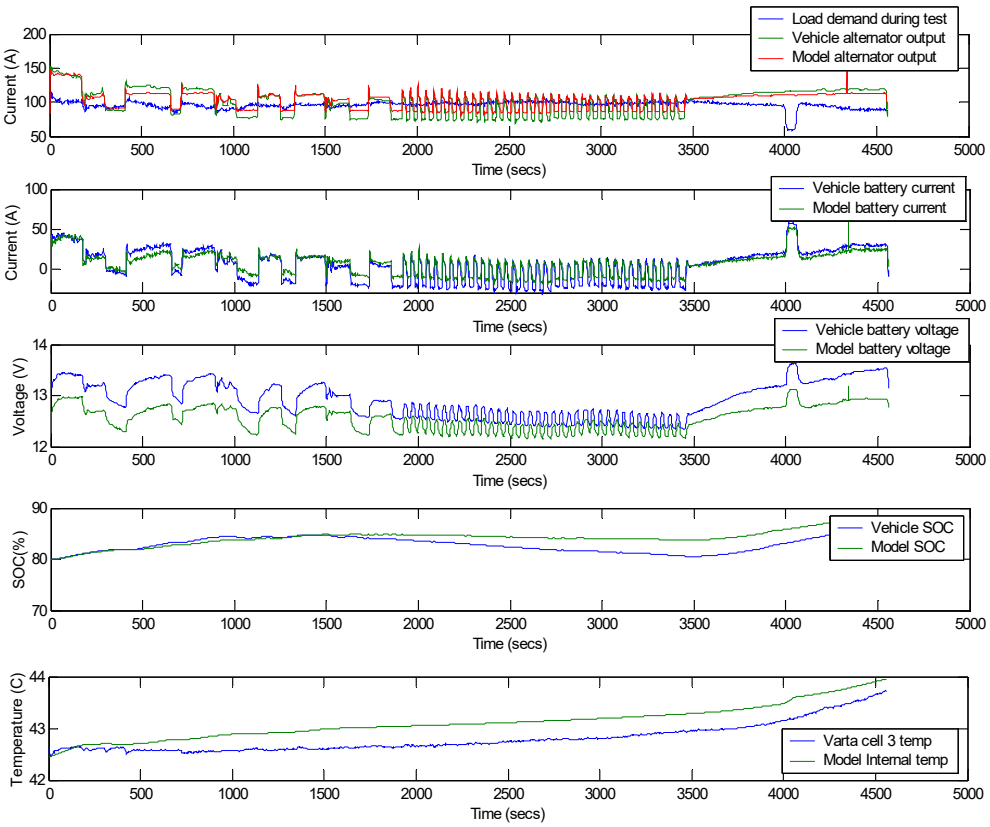

Figure E2.10. Ambient +40^{0}C, CSCT Test

Subplot 1. Alternator output vs load demand. The performance of the model alternator output is relatively good during the test. The absolute error that occurs here is 5-20A during the test.

Subplot 2. Battery current. The absolute error on the battery model current level is 5-20A and doesn't meet the design criteria of 5A accuracy. The maximum absolute error occurs in both phases of the test with an underestimation of the model battery current at the end of the test.

Subplot 3. Battery voltage. The absolute error of the battery voltage is 0.2-0.6V throughout the test.

Subplot 4. SoC. The model SoC indicates a quite similar trend to the measured data with an underestimated final state of charge of 2% of the battery's SoC.

Subplot 5. Internal temperature. The model internal temperature estimation is quite good with an absolute error of 0.1-0.5 ^{0}C throughout the test.

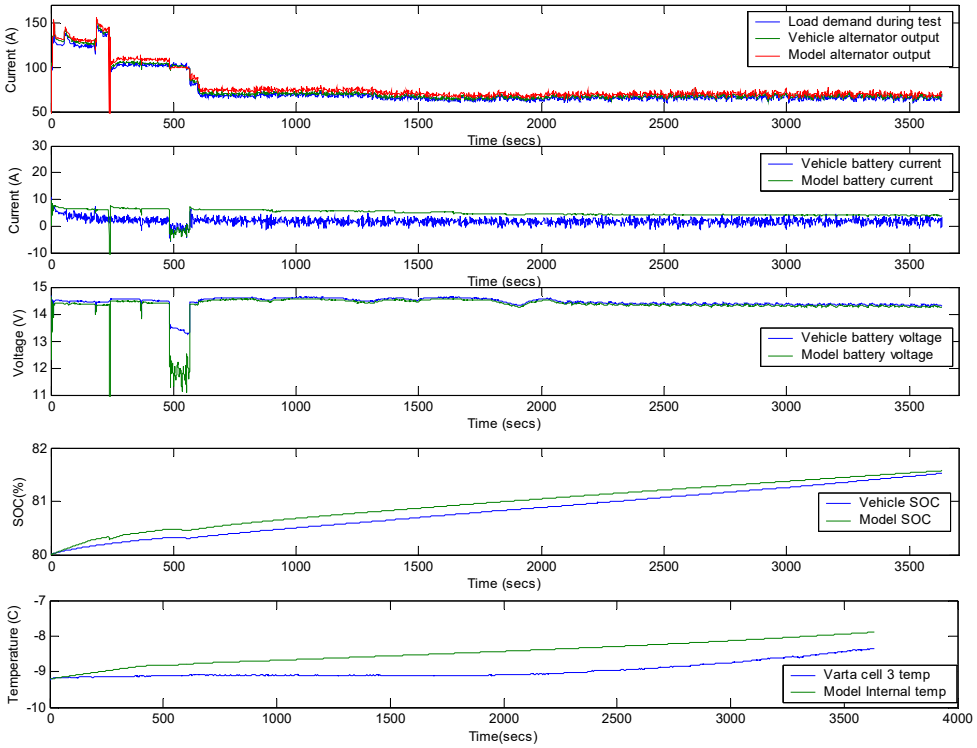

Figure E2.11. Ambient -10^{0}C, CSCT

Subplot 1. Alternator output vs load demand. The performance of the model alternator output is good during that test. The absolute error that occurs here is 1-5A during the test.

Subplot 2. Battery current. The absolute error on the battery model current level is 1-5A and does meet the design criteria of 5A accuracy. The maximum absolute error occurs in the first phase of the test while it reduces during the end of the test.

Subplot 3. Battery voltage. The absolute error of the battery voltage is 0.2-0.3V throughout the test. It is important to note that in an overload situation that occurs after 500secs the battery voltage discharge is steeper than the actual vehicle's battery voltage.

Subplot 4. SoC. The model SoC indicates a quite similar trend to the measured data with an overestimated final state of charge of 0.1% of the battery's SoC.

Subplot 5. Internal temperature. The model internal temperature estimation is overestimated during the test by 0.1-0.5 ^{0}C throughout the test.

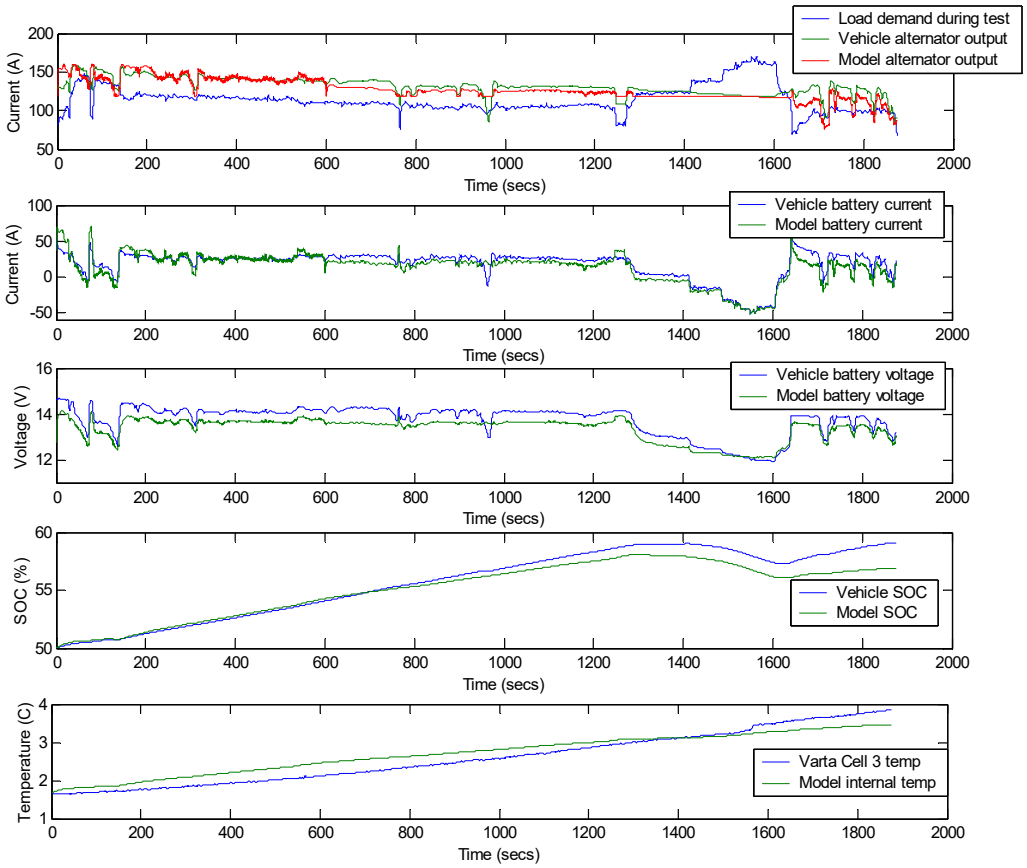

Figure E2.12. Ambient $+0^0$C, Drive at 40mph

Subplot 1. Alternator output vs load demand. The performance of the model alternator output is quite good throughout the duration of the test. The absolute error that occurs in some instance during the test is of the range 5-10A.

Subplot 2. Battery current. The battery current level is of the same trend of the alternator's performance. The overall battery current estimation during the test is quite good despite some inaccuracies that occurs of 5-10A in short periods throughout the test

Subplot 3. Battery voltage. The absolute error of the battery voltage is of the range of 0.2-0.5V throughout the test and does meet the design criteria.

Subplot 4. SoC. The model SoC indicates a quite similar trend to the measured data with an overestimation in the beginning of the test and underestimation at the final stage of the test with 2% higher of the actual battery's SoC.

Subplot 5. Internal temperature. The model internal temperature estimation is overestimated initially and underestimated at the final stage of the test. The final estimated temperature is 0.3^0C less than the actual cell 3 temperature.

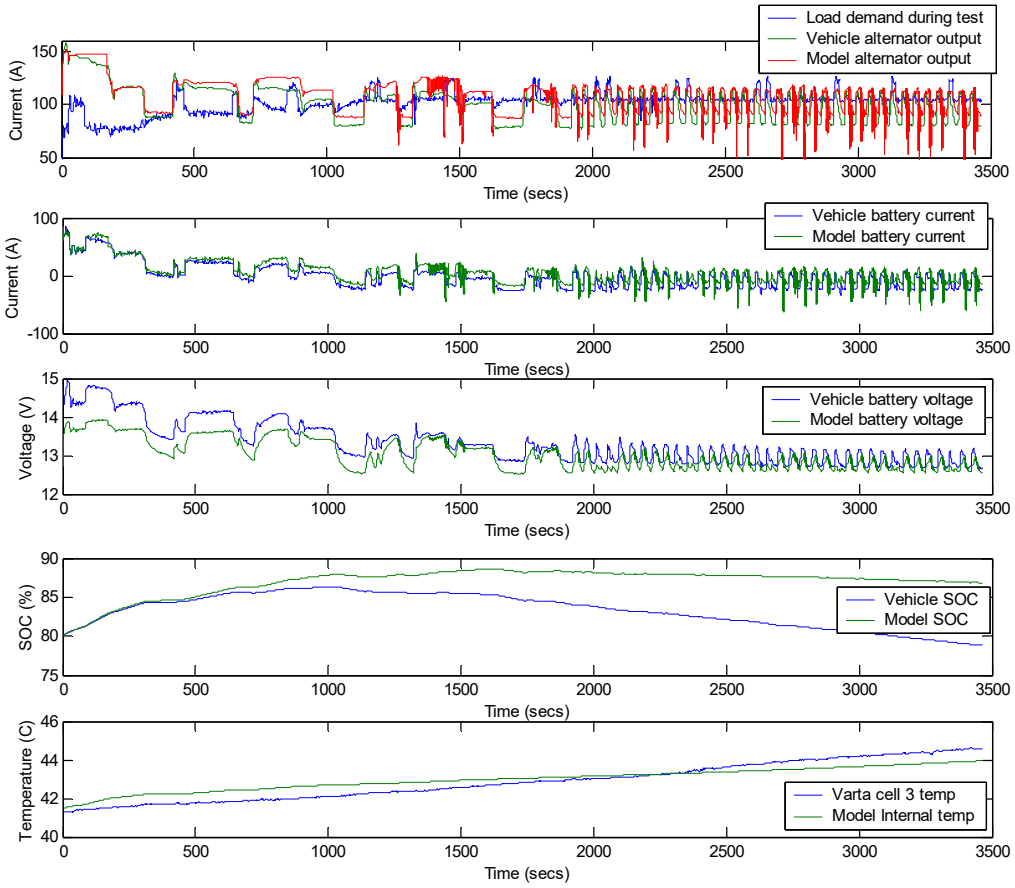

Figure E2.13. Ambient +40^{0}C, CS&CT test

Subplot 1. Alternator output vs load demand. The performance of the model alternator output is overestimated during the test. The absolute error that occurs here is 8-12A during the test. It is also shown that the battery model discharge less than the actual battery and this affect the overall SOC.

Subplot 2. Battery current. The absolute error on the battery model current level is 8-12A and does not meet the design criteria of 5A accuracy.

Subplot 3. Battery voltage. The absolute error of the battery voltage is 0.5-0.7V throughout the test. Despite the overestimation of the battery current the model voltage system is lower level than the actual system voltage.

Subplot 4. SoC. The model SoC indicates a quite similar trend to the measured data with an overestimated final state of charge of 6% of the battery's SoC.

Subplot 5. Internal temperature. The model internal temperature estimation is again overestimated since the battery model draws more current throughout the test. Since less charge occurs during the city traffic cycle the final estimated temperature is 0.2^{0}C less than the actual cell 3 temperature.

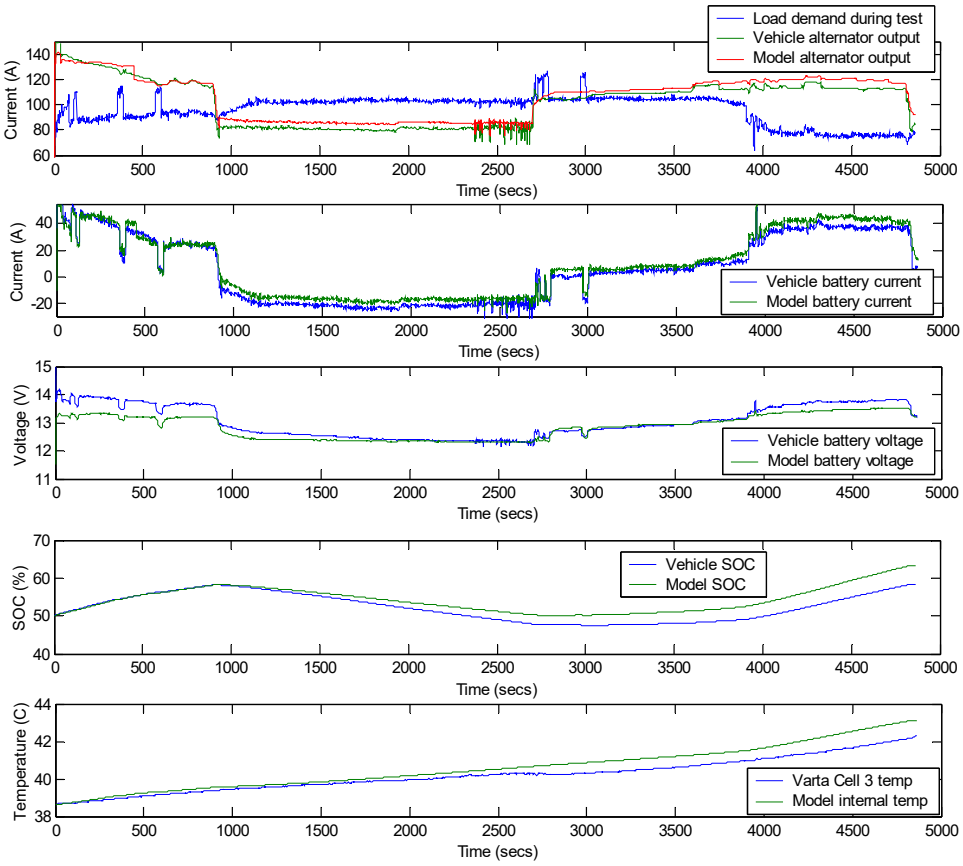

Figure E2.14. Ambient +40^{0}C, DID test

Subplot 1. Alternator output vs load demand. The performance of the model alternator output is overestimated throughout the test with an absolute error 5-8A during the test.

Subplot 2. Battery current. The absolute error on the battery model current level is 5-8A. The maximum absolute error occurs in the 'idle' period of the test and at the end of the second 'drive' period of the test.

Subplot 3. Battery voltage. The absolute error of the battery voltage is 0.1-0.6V throughout the test. It is important to note that in the overload situation of the idle period of the test the battery voltage level is quite good and matches the level of the vehicle's battery voltage.

Subplot 4. SoC. The model SoC indicates a quite similar trend to the measured data with an overestimated final state of charge of 4% of the battery's SoC.

Subplot 5. Internal temperature. The model internal temperature estimation is overestimated during the test by 0.8 ^{0} C throughout the test.

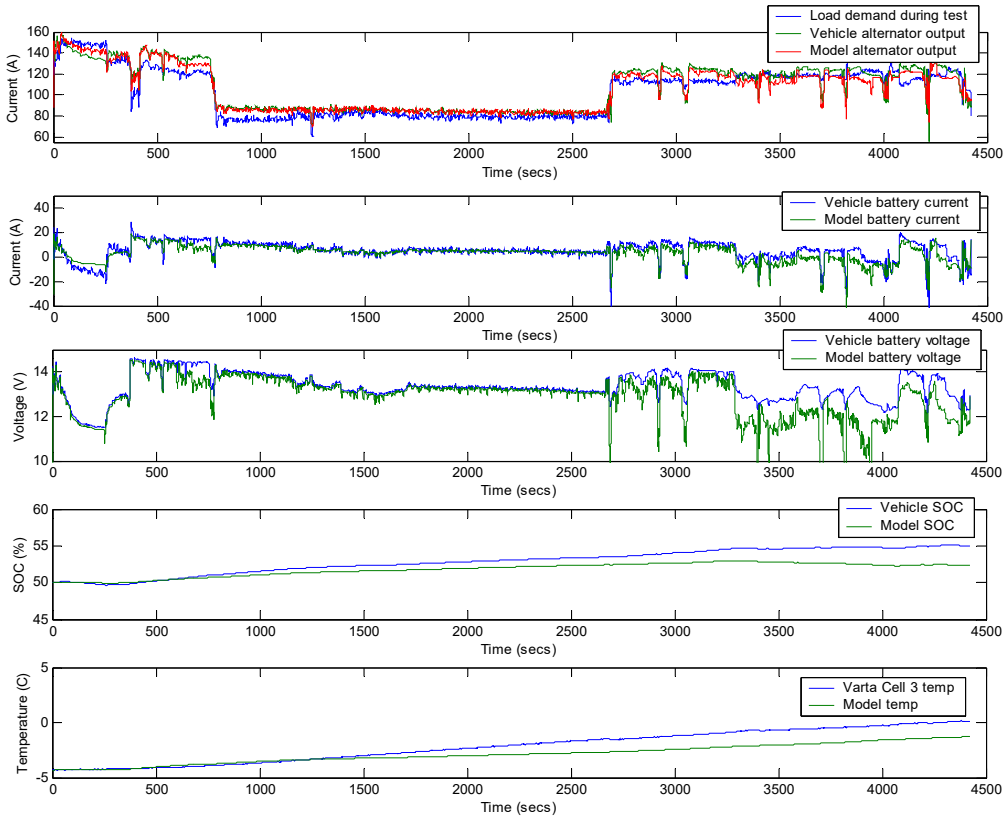

Figure E2.15. Ambient –5.5^{0}C, DID test

Subplot 1. Alternator output vs load demand. The performance of the model alternator output is good throughout the test. The estimation of the maximum alternator current is almost identical of the actual alternator's output. At the final period of the test which rapid changes of load demand and system voltage level, an absolute error of 7A occurs and the alternator output is underestimated.

Subplot 2. Battery current. The battery current estimation is good throughout the test. The absolute error on the battery model current level is 2-7A. The maximum absolute error occurs at the end of the second 'drive' period of the test.

Subplot 3. Battery voltage. The absolute error of the battery voltage is 0.1-0.7 and occurs at the end of the test (second 'drive' period). It is important to note that inaccuracies are introduced during the end of the test with frequent changes on load demand.

Subplot 4. SoC. The model SoC indicates a quite similar trend to the measured data with an underestimation of 2% of the battery's SoC.

Subplot 5. Internal temperature. The model internal temperature estimation is underestimated of 0.8 ^{0}C of the actual battery's cell 3 temperature at the end of the test.

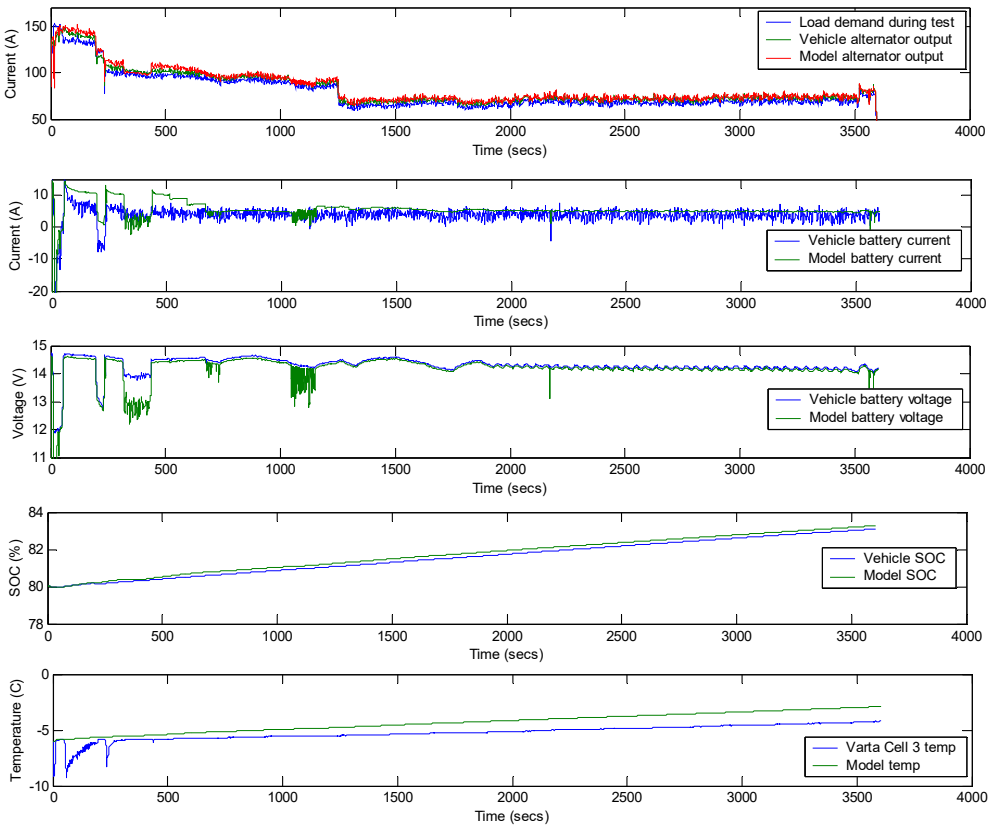

Figure E2.16. Ambient -10^{0}C, CSCT test

Subplot 1. Alternator output vs load demand. The performance of the model alternator output is good throughout the test. The estimation of the maximum alternator current is almost identical of the actual alternator's output. The absolute error is 2-4A and meets the design criteria.

Subplot 2. Battery current. The battery current estimation is good throughout the test. The absolute error on the battery model current level is 2-4A. It is worth to note the rapid discharges occurs at the actual system (similar rapid temperature changes occurs) at the beginning of the test while the battery model discharges less than the actual battery.

Subplot 3. Battery voltage. The absolute error of the battery voltage is 0.1-0.2V throughout the test. At the overload situations the inaccuracies are introduced with an absolute error of 1V.

Subplot 4. SoC. The model SoC indicates a quite similar trend to the measured data with a slight overestimation of the battery's SoC.

Subplot 5. Internal temperature. The model internal temperature estimation is good with an overall 0.5 ^{0}C of the actual battery's cell 3 temperature at the end of the test.

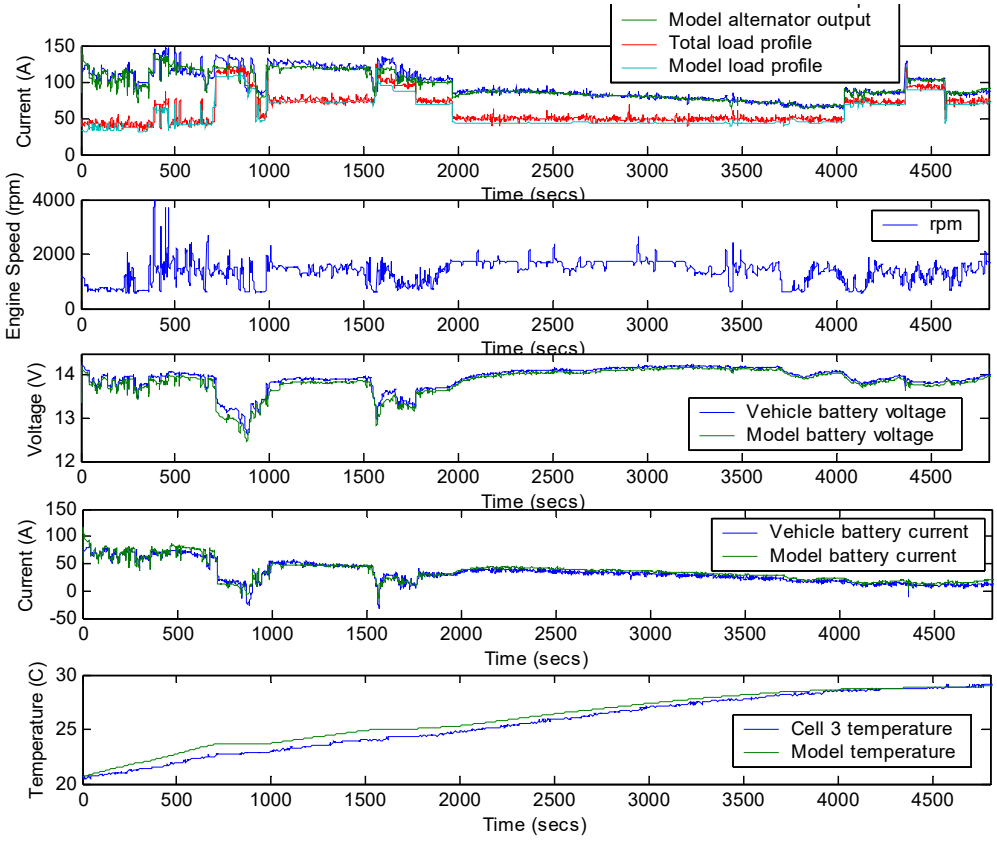

Figure E2.17. Initial SOC of the battery @ 50%. Description of the test: M6J12 50% SoC

Subplot 1. Alternator output vs estimated load demand. The performance of the model alternator output is good throughout the test. The estimation of the maximum alternator current is almost identical of the actual alternator's output. The absolute error is 2-4A and meets the design criteria. The plot also shows the performance of the load estimation model against the experimental load demand.

Subplot 2. Engine speed. This plot shows the engine speed profile throughout the test. Since that test is not an actual combined cycle or a drive-idle-drive test it is worth to include the engine speed in order to correlate the alternator maximum current output.

Subplot 3. Battery voltage. The absolute error of the battery voltage is 0.1-0.3V throughout the test. At the overload situations the inaccuracies are introduced with an absolute error of 0.3V.

Subplot 4. Battery current. The battery current estimation is relatively good throughout the test and the absolute error on the battery model current level is low 2-4A.

Subplot 5. SoC. The overall temperature estimation indicates a quite similar trend to the measured data with a slight overestimation comparing the actual battery's SoC.

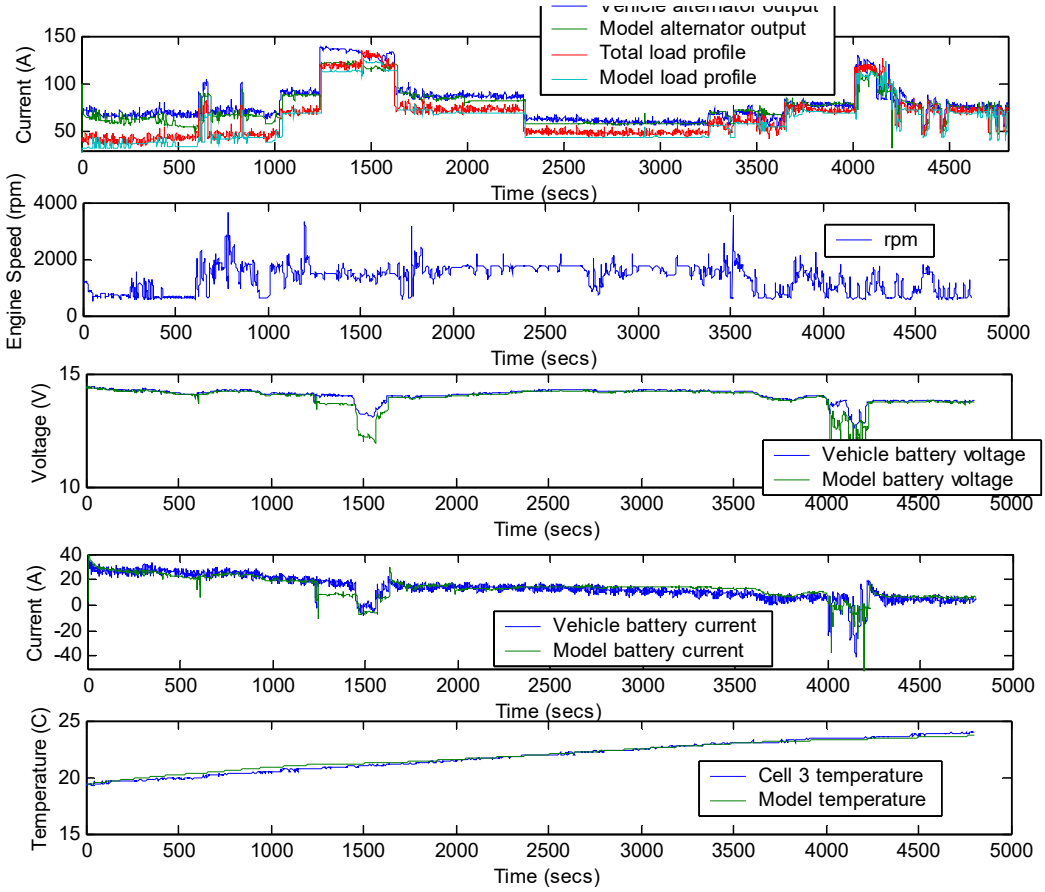

Figure E2.18. Initial SoC of the battery @80%. Description of the test: M6J12 80% SoC

Subplot 1. Alternator output vs load demand. The performance of the model alternator output is promising throughout the test. The estimation of the maximum alternator current is almost identical of the actual alternator's output. The absolute error is 2-4A and meets the design criteria.

Subplot 2. Battery current. The battery current estimation is good throughout the test. The absolute error on the battery model current level is 2-4A. It is worth to note the rapid discharges occurs at the actual system (similar rapid temperature changes occurs) at the beginning of the test while the battery model discharges less than the actual battery.

Subplot 3. Battery voltage. The absolute error of the battery voltage is 0.1-0.2V throughout the test. At the overload situations the inaccuracies are introduced with an absolute error of 0.5V.

Subplot 4. Internal temperature. The model internal temperature estimation is overall very good with an absolute error of 0.1 ^{0}C of the actual battery's cell 3 temperature during the tests.

E.3 Ultracapacitors model performance

The developed MATLAB®/Simulink™ models have been correlated against the experimental current profiles. The Simulink models have been tested for different initial cell voltages (2.5V) and different temperatures (-10^{0}C, 25^{0}C). The voltage responses of the ultracapacitor were measured and simulations with the above described current profiles as input signal were performed. Figures E3.1 and E3.2 show the correlation of the developed Simulink model against experimental results:

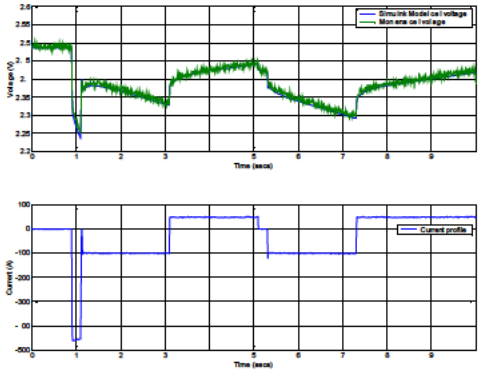

Figure E3.1. Measured current profile representing ISG operation, initial voltage at 2.5V and at 25^{0}C

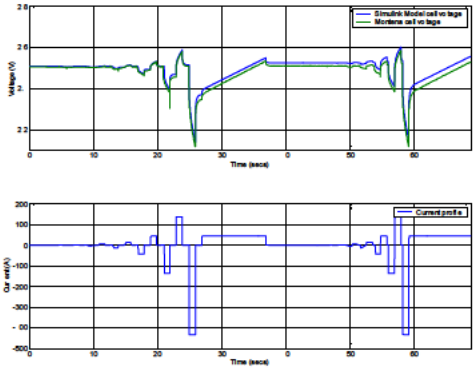

Figure E3.2. Measured current profile, alternating charge and discharge, initial voltage at 2.5V and 25^{0}C

Figures E3.1-E3.2 show a good correlation of the developed MATLAB®/SimulinkTM model comparing experimental data. The voltage absolute error was within 0.05V (design criteria target) for all different current profiles. By achieving a good agreement of the developed Simulink model and that of the real ultracapacitors it could give us an advantage to investigate ultracapacitors capability to support various applications (such as support critical loads, engine starting etc.).

Appendix F Fuzzy Logic Theory

F.1 Basic concepts of fuzzy sets theory

Until fuzzy sets were first introduced by Zadeh (1965) probability theory had been the main framework that used to cope with the uncertainty aspect in mathematical models. Since then, fuzzy sets have been complementary to the probability theory (Zadeh 1965; Dubois and Prade 1986). The probability theory deals with the uncertainty attributed to the random outcome of a precisely defined event. Fuzzy sets theory provides a formal framework that models uncertainty related to vague, imprecise and gradual information that cannot be evaluated, into real world applications. The following definitions are presented that define fuzzy sets and fuzzy numbers (Zadeh 1965; Pedrycz and Gomide 1998):

Definition F.1 (Zadeh, 1965): A fuzzy set A is characterised by a generalised characteristic function $\mu_A: X \rightarrow [0,1]$, called membership function of A and defined over a universe of discourse X. The membership function $\mu_A(x)$ denotes the degree of membership of each $x \in X$ to A. The fuzzy set A in a classical set X is defined as follows:

$$A = \{(x\mu_A(x)) \mid x \in X\} \tag{F.1}$$

The closer the degree of $\mu_A(x)$ to unity is, the higher the membership degree of x in A is. It should be noted that a fuzzy set is an extension of a classical crisp set. In classical set theory, an object is either an element of a set or not therefore there is a step transition from membership to non-membership. While this can be represented with a fuzzy set by assigning membership degree 1 to represent full membership and 0 to full non-membership, in the same fuzzy set, a gradual representation of membership is also feasible by assigning membership degrees to the elements from the interval $[0,1]$.

Definition F.2 (Zadeh 1965): The support of the fuzzy set A, $supp(A)$, is the crisp set of all arguments of the membership function of A, $\mu_A(x)$, which correspond to a nonzero value:

$$supp(A) = \{x \in X \mid \mu_A(x) > 0\} \tag{F.2}$$

Definition F.3 (Zadeh 1965): The crisp set of elements that belongs to the fuzzy set A at least to the degree α is called the α-level set, defined for each $\alpha \in I = [0,1]$ as:

$$A^{>\alpha} = \{x \in X \,|\mu_A(x) > \alpha\} \tag{F.3}$$

$A^{>\alpha}$ is called strong level α or strong α cut.

Definition F.4 (Zadeh 1965): A fuzzy set is convex if:

$$\mu_A(\lambda_{X_1} + (1 - \lambda)x_2) \geq \min\{\mu_A(x_1)\mu_A(x_2)\} \text{ for } x_1 x_2 \in X, \lambda \in [0,1] \tag{F.4}$$

Alternatively, a fuzzy set is convex if all α-level sets are convex.

Definition F.5 (Zadeh 1965): A finite fuzzy set A has as a further characteristic value its cardinality (i.e. its number of membership degrees). Formally this number can be found out by adding up all values of the characteristic function, sum of the membership degrees:

$$card(A) = \sum_{x \in X} \mu_A(x) \tag{F.5}$$

A relative cardinality of a fuzzy set is given by $card_x(A) = card(A)/N$, with N the number of elements of the universe of discourse X.

Figure F1.1 displays an example of a type-1 fuzzy set, the support of a fuzzy set as the set of all points x in X such that $\mu_A(x) > 0$, and a singleton fuzzy set, where a singleton is a fuzzy set whose support is a single point in where $\mu_A = 1.0$ (Kassem 2012, Gottwald et al. 1995).

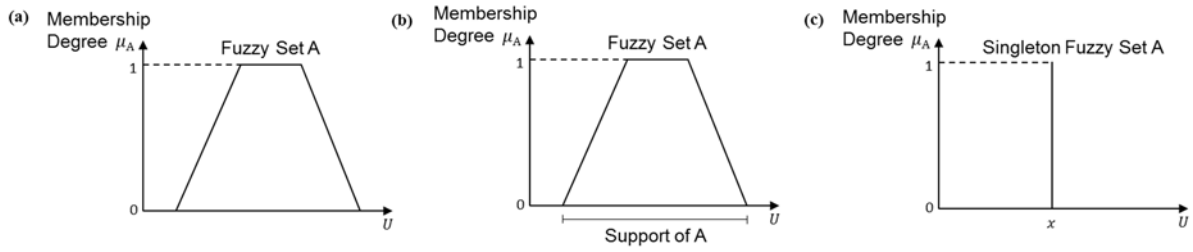

Figure F1.1. a) Type-1 fuzzy set, b) Support of a fuzzy set, c) A Singleton Fuzzy Set

F.2 Standard operation of fuzzy sets

The most elementary operations for usual sets are the *union* as well as the *intersection* of any two sets and the complement of any set with respect to some superset of it. For the basic set algebraic operations (Zadeh, 1965) has already given such extensions. Let us have two fuzzy sets A and B with the membership functions $\mu_A(x)$ and $\mu_B(x)$. The union operation $A \cup B$ of fuzzy sets AB , according to Zadeh is:

$$\mu_{A\cup B}(x) = \max\{\mu_A(x)\mu_{\ B}(x)\} \text{ for all } x \in X \tag{F.6}$$

Membership function of the intersection $A \cap B$ of fuzzy sets A, B is the minimum of their membership functions $\mu_A(x)$ and $\mu_B(x)$ and is defined as:

$$\mu_{A\cap B}(x) = \min\{\mu_A(x)\mu_{\ B}(x)\} \text{ for all } x \in X \tag{F.7}$$

Membership function of the complement A^c of a fuzzy set A (relative to the universe of discourse X) with a membership function $\mu_A(x)$, is defined as:

$$\mu_{A^c}(x) = 1 - \mu_A(x) \text{ for all } x \in X \tag{F.8}$$

Figure F2.1 illustrates the operations of the fuzzy sets as described above:

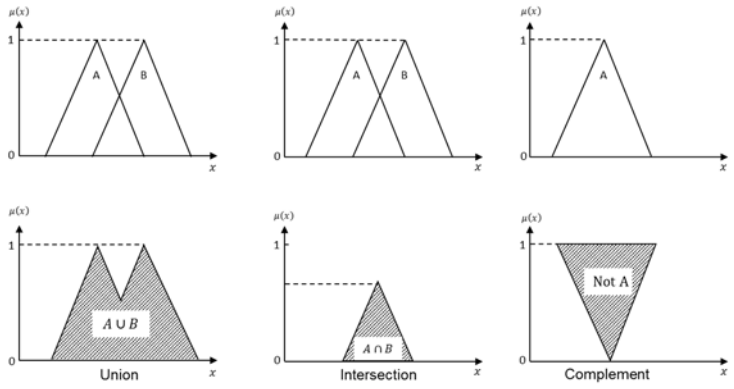

Figure F2.1. Union, Intersection and Complement of a fuzzy set

All these operations on fuzzy sets are straightforward generalisations of the corresponding operations on usual sets. Regarding the α-cuts, a simple definition which relates the union and intersection of crisp sets is:

$$(A \cup B)^{>\alpha} = A^{>\alpha} \cup B^{>\alpha}, (A \cap B)^{>\alpha} = A^{>\alpha} \cap B^{>\alpha} \tag{F.9}$$

For the complement on the other hand we have:

$$(A^c)^{>\alpha} = A^{<1-\alpha} = \{x \in X \,|\mu_A(x) < 1 - \alpha\} \tag{F.10}$$

which applies for strong α-cuts as well (Gottwald et al. 1995).

F.3 Membership functions

As described in definition (6.1) (Zadeh 1965), a fuzzy set A is characterised by a generalised characteristic function $\mu_A: X \to [0,1]$, called membership function of A. There are various membership functions (Gottwald et al. 1995; Zadeh 1965) including the following specific three:

- *Gaussian membership function* represented as:

$$\mu_A(x; c, \delta) = e^{\left(-\frac{(x-c)^2}{2\delta^2}\right)} \tag{F.11}$$

where c specifies the center of a function and δ determines its dispersion.

- *Trapezoidal membership function* represented by four parameters p, q, r, s:

$$\mu_A(x; p, q, r, s) = \begin{cases} 0, & x \le p, \\ \frac{x-p}{q-p}, & x \le q, \\ 1, & x \le r, \\ \frac{s-x}{s-r}, & x \le s, \\ 0, & x > s \end{cases} \tag{F.12}$$

A special case of a trapezoidal function (for $q = r$) is a triangular function.

- *Singleton membership function* represented as:

$$\mu_A(x; x_0) = \begin{cases} 1, & x = x_0 \\ 0, & x \ne x_0 \end{cases} \tag{F.13}$$

where parameter x_0 specifies the location of the singleton, the single value of x which belongs to a set A (with a membership degree equal to 1). An example of the Gaussian, trapezoidal and singleton membership functions are illustrated in Figure F3.1:

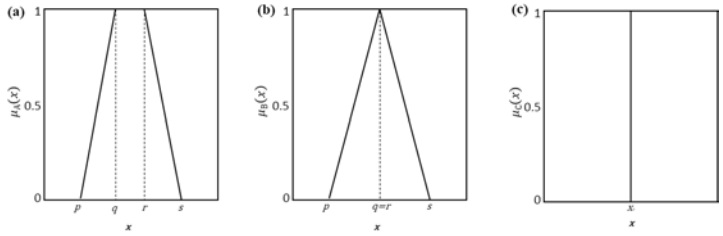

Figure F3.1. Examples of membership functions: a) trapezoidal, b) triangular, c) singleton

F.4 Fuzzy Logic Rules

As described in definition (6.1) (Zadeh 1965), a fuzzy set A is characterised by a generalised characteristic function $\mu_A: X \rightarrow [0,1]$, called membership function of A. There are various membership functions (Gottwald et al. 1995; Zadeh 1965) including the following specific three:

No. Rules	Rule Base for Fuzzy PMS Cabin 2
1	If (HSW is LP) and (FS_loading is LP) and (RS_loading is LP) and (Cabin_Blower is LP) and (FCI is VL) and (CSI is Low) then (Electrical_Load is VL) (1)
2	If (HSW is LP) and (FS_loading is LP) and (RS_loading is LP) and (Cabin_Blower is LP) and (FCI is L) and (CSI is Low) then (Electrical_Load is VL) (1)
3	If (HSW is LP) and (FS_loading is LP) and (RS_loading is LP) and (Cabin_Blower is LP) and (FCI is M) and (CSI is Low) then (Electrical_Load is VL) (1)
4	If (HSW is LP) and (FS_loading is LP) and (RS_loading is LP) and (Cabin_Blower is LP) and (FCI is MH) and (CSI is Low) then (Electrical_Load is VL) (1)
5	If (HSW is LP) and (FS_loading is LP) and (RS_loading is LP) and (Cabin_Blower is LP) and (FCI is LM) and (CSI is Low) then (Electrical_Load is VL) (1)
6	If (HSW is LP) and (FS_loading is LP) and (RS_loading is LP) and (Cabin_Blower is LP) and (FCI is H) and (CSI is Low) then (Electrical_Load is VL) (1)
7	If (HSW is LP) and (FS_loading is LP) and (RS_loading is LP) and (Cabin_Blower is LP) and (FCI is VH) and (CSI is Low) then (Electrical_Load is VL) (1)
8	If (HSW is HP) and (FS_loading is HP) and (RS_loading is HP) and (Cabin_Blower is LP) and (FCI is VL) and (CSI is Low) then (Electrical_Load is M) (1)
9	If (HSW is HP) and (FS_loading is HP) and (RS_loading is HP) and (Cabin_Blower is LP) and (FCI is L) and (CSI is Low) then (Electrical_Load is M) (1)
10	If (HSW is HP) and (FS_loading is HP) and (RS_loading is HP) and (Cabin_Blower is LP) and (FCI is M) and (CSI is Low) then (Electrical_Load is L) (1)
11	If (HSW is HP) and (FS_loading is HP) and (RS_loading is HP) and (Cabin_Blower is LP) and (FCI is MH) and (CSI is Low) then (Electrical_Load is VL) (1)
12	If (HSW is HP) and (FS_loading is HP) and (RS_loading is HP) and (Cabin_Blower is LP) and (FCI is LM) and (CSI is Low) then (Electrical_Load is L) (1)
13	If (HSW is HP) and (FS_loading is HP) and (RS_loading is HP) and (Cabin_Blower is LP) and (FCI is H) and (CSI is Low) then (Electrical_Load is VL) (1)
14	If (HSW is HP) and (FS_loading is HP) and (RS_loading is HP) and (Cabin_Blower is LP) and (FCI is VH) and (CSI is Low) then (Electrical_Load is VL) (1)
15	If (HSW is LP) and (FS_loading is LP) and (RS_loading is LP) and (Cabin_Blower is MP) and (FCI is VL) and (CSI is Low) then (Electrical_Load is L) (1)
16	If (HSW is LP) and (FS_loading is LP) and (RS_loading is LP) and (Cabin_Blower is MP) and (FCI is L) and (CSI is Low) then (Electrical_Load is L) (1)
17	If (HSW is LP) and (FS_loading is LP) and (RS_loading is LP) and (Cabin_Blower is MP) and (FCI is LM) and (CSI is Low) then (Electrical_Load is L) (1)
18	If (HSW is LP) and (FS_loading is LP) and (RS_loading is LP) and (Cabin_Blower is MP) and (FCI is M) and (CSI is Low) then (Electrical_Load is L) (1)
19	If (HSW is LP) and (FS_loading is LP) and (RS_loading is LP) and (Cabin_Blower is MP) and (FCI is MH) and (CSI is Low) then (Electrical_Load is L) (1)
20	If (HSW is LP) and (FS_loading is LP) and (RS_loading is LP) and (Cabin_Blower is MP) and (FCI is H) and (CSI is Low) then (Electrical_Load is VL) (1)
21	If (HSW is LP) and (FS_loading is LP) and (RS_loading is LP) and (Cabin_Blower is MP) and (FCI is VH) and (CSI is Low) then (Electrical_Load is VL) (1)
22	If (HSW is HP) and (FS_loading is HP) and (RS_loading is HP) and (Cabin_Blower is MP) and (FCI is VL) and (CSI is Low) then (Electrical_Load is M) (1)
23	If (HSW is HP) and (FS_loading is HP) and (RS_loading is HP) and (Cabin_Blower is MP) and (FCI is L) and (CSI is Low) then (Electrical_Load is M) (1)
24	If (HSW is HP) and (FS_loading is HP) and (RS_loading is HP) and (Cabin_Blower is MP) and (FCI is LM) and (CSI is Low) then (Electrical_Load is L) (1)
25	If (HSW is HP) and (FS_loading is HP) and (RS_loading is HP) and (Cabin_Blower is MP) and (FCI is M) and (CSI is Low) then (Electrical_Load is VL) (1)
26	If (HSW is HP) and (FS_loading is HP) and (RS_loading is HP) and (Cabin_Blower is MP) and (FCI is H) and (CSI is Low) then (Electrical_Load is VL) (1)
27	If (HSW is HP) and (FS_loading is HP) and (RS_loading is HP) and (Cabin_Blower is MP) and (FCI is VH) and (CSI is Low) then (Electrical_Load is VL) (1)
28	If (HSW is LP) and (FS_loading is LP) and (RS_loading is LP) and (Cabin_Blower is HP) and (FCI is L) and (CSI is Low) then (Electrical_Load is M) (1)
29	If (HSW is LP) and (FS_loading is LP) and (RS_loading is LP) and (Cabin_Blower is HP) and (FCI is LM) and (CSI is Low) then (Electrical_Load is L) (1)
30	If (HSW is LP) and (FS_loading is LP) and (RS_loading is LP) and (Cabin_Blower is HP) and (FCI is M) and (CSI is Low) then (Electrical_Load is L) (1)
31	If (HSW is LP) and (FS_loading is LP) and (RS_loading is LP) and (Cabin_Blower is HP) and (FCI is MH) and (CSI is Low) then (Electrical_Load is VL) (1)
32	If (HSW is LP) and (FS_loading is LP) and (RS_loading is LP) and (Cabin_Blower is HP) and (FCI is H) and (CSI is Low) then (Electrical_Load is VL) (1)

33	If (HSW is LP) and (FS_loading is LP) and (RS_loading is LP) and (Cabin_Blower is HP) and (FCI is VH) and (CSI is Low) then (Electrical_Load is VL) (1)
34	If (HSW is LP) and (FS_loading is LP) and (RS_loading is LP) and (Cabin_Blower is HP) and (FCI is VL) and (CSI is Low) then (Electrical_Load is M) (1)
35	If (HSW is HP) and (FS_loading is HP) and (RS_loading is HP) and (Cabin_Blower is MP) and (FCI is MH) and (CSI is Low) then (Electrical_Load is VL) (1)
36	If (HSW is HP) and (FS_loading is HP) and (RS_loading is HP) and (Cabin_Blower is HP) and (FCI is VL) and (CSI is Low) then (Electrical_Load is MH) (1)
37	If (HSW is HP) and (FS_loading is HP) and (RS_loading is HP) and (Cabin_Blower is HP) and (FCI is L) and (CSI is Low) then (Electrical_Load is MH) (1)
38	If (HSW is HP) and (FS_loading is HP) and (RS_loading is HP) and (Cabin_Blower is HP) and (FCI is LM) and (CSI is Low) then (Electrical_Load is M) (1)
39	If (HSW is HP) and (FS_loading is HP) and (RS_loading is HP) and (Cabin_Blower is HP) and (FCI is M) and (CSI is Low) then (Electrical_Load is M) (1)
40	If (HSW is HP) and (FS_loading is HP) and (RS_loading is HP) and (Cabin_Blower is HP) and (FCI is MH) and (CSI is Low) then (Electrical_Load is VL) (1)
41	If (HSW is HP) and (FS_loading is HP) and (RS_loading is HP) and (Cabin_Blower is HP) and (FCI is H) and (CSI is Low) then (Electrical_Load is VL) (1)
42	If (HSW is HP) and (FS_loading is HP) and (RS_loading is HP) and (Cabin_Blower is HP) and (FCI is VH) and (CSI is Low) then (Electrical_Load is VL) (1)
43	If (HSW is LP) and (FS_loading is LP) and (RS_loading is LP) and (Cabin_Blower is LP) and (FCI is VL) and (CSI is Normal) then (Electrical_Load is VL) (1)
44	If (HSW is LP) and (FS_loading is LP) and (RS_loading is LP) and (Cabin_Blower is LP) and (FCI is L) and (CSI is Normal) then (Electrical_Load is VL) (1)
45	If (HSW is LP) and (FS_loading is LP) and (RS_loading is LP) and (Cabin_Blower is LP) and (FCI is M) and (CSI is Normal) then (Electrical_Load is VL) (1)
46	If (HSW is LP) and (FS_loading is LP) and (RS_loading is LP) and (Cabin_Blower is LP) and (FCI is MH) and (CSI is Normal) then (Electrical_Load is VL) (1)
47	If (HSW is LP) and (FS_loading is LP) and (RS_loading is LP) and (Cabin_Blower is LP) and (FCI is LM) and (CSI is Normal) then (Electrical_Load is VL) (1)
48	If (HSW is LP) and (FS_loading is LP) and (RS_loading is LP) and (Cabin_Blower is LP) and (FCI is H) and (CSI is Normal) then (Electrical_Load is VL) (1)
49	If (HSW is LP) and (FS_loading is LP) and (RS_loading is LP) and (Cabin_Blower is LP) and (FCI is VH) and (CSI is Normal) then (Electrical_Load is VL) (1)
50	If (HSW is HP) and (FS_loading is HP) and (RS_loading is HP) and (Cabin_Blower is LP) and (FCI is VL) and (CSI is Normal) then (Electrical_Load is MH) (1)
51	If (HSW is HP) and (FS_loading is HP) and (RS_loading is HP) and (Cabin_Blower is LP) and (FCI is L) and (CSI is Normal) then (Electrical_Load is MH) (1)
52	If (HSW is HP) and (FS_loading is HP) and (RS_loading is HP) and (Cabin_Blower is LP) and (FCI is LM) and (CSI is Normal) then (Electrical_Load is M) (1)
53	If (HSW is HP) and (FS_loading is HP) and (RS_loading is HP) and (Cabin_Blower is LP) and (FCI is M) and (CSI is Normal) then (Electrical_Load is M) (1)
54	If (HSW is HP) and (FS_loading is HP) and (RS_loading is HP) and (Cabin_Blower is LP) and (FCI is MH) and (CSI is Normal) then (Electrical_Load is L) (1)
55	If (HSW is HP) and (FS_loading is HP) and (RS_loading is HP) and (Cabin_Blower is LP) and (FCI is H) and (CSI is Normal) then (Electrical_Load is L) (1)
56	If (HSW is HP) and (FS_loading is HP) and (RS_loading is HP) and (Cabin_Blower is LP) and (FCI is VH) and (CSI is Normal) then (Electrical_Load is L) (1)
57	If (HSW is LP) and (FS_loading is LP) and (RS_loading is LP) and (Cabin_Blower is MP) and (FCI is VL) and (CSI is Normal) then (Electrical_Load is L) (1)
58	If (HSW is LP) and (FS_loading is LP) and (RS_loading is LP) and (Cabin_Blower is MP) and (FCI is L) and (CSI is Normal) then (Electrical_Load is L) (1)
59	If (HSW is LP) and (FS_loading is LP) and (RS_loading is LP) and (Cabin_Blower is MP) and (FCI is LM) and (CSI is Normal) then (Electrical_Load is L) (1)
60	If (HSW is LP) and (FS_loading is LP) and (RS_loading is LP) and (Cabin_Blower is MP) and (FCI is M) and (CSI is Normal) then (Electrical_Load is L) (1)
61	If (HSW is LP) and (FS_loading is LP) and (RS_loading is LP) and (Cabin_Blower is MP) and (FCI is MH) and (CSI is Normal) then (Electrical_Load is L) (1)
62	If (HSW is LP) and (FS_loading is LP) and (RS_loading is LP) and (Cabin_Blower is MP) and (FCI is H) and (CSI is Normal) then (Electrical_Load is L) (1)
63	If (HSW is LP) and (FS_loading is LP) and (RS_loading is LP) and (Cabin_Blower is MP) and (FCI is VH) and (CSI is Normal) then (Electrical_Load is VL) (1)
64	If (HSW is HP) and (FS_loading is HP) and (RS_loading is HP) and (Cabin_Blower is MP) and (FCI is VL) and (CSI is Normal) then (Electrical_Load is MH) (1)
65	If (HSW is HP) and (FS_loading is HP) and (RS_loading is HP) and (Cabin_Blower is MP) and (FCI is L) and (CSI is Normal) then (Electrical_Load is MH) (1)
66	If (HSW is HP) and (FS_loading is HP) and (RS_loading is HP) and (Cabin_Blower is MP) and (FCI is LM) and (CSI is Normal) then (Electrical_Load is M) (1)
67	If (HSW is HP) and (FS_loading is HP) and (RS_loading is HP) and (Cabin_Blower is MP) and (FCI is M) and (CSI is Normal) then (Electrical_Load is M) (1)
68	If (HSW is HP) and (FS_loading is HP) and (RS_loading is HP) and (Cabin_Blower is MP) and (FCI is MH) and (CSI is Normal) then (Electrical_Load is L) (1)
69	If (HSW is HP) and (FS_loading is HP) and (RS_loading is HP) and (Cabin_Blower is MP) and (FCI is H) and (CSI is Normal) then (Electrical_Load is L) (1)
70	If (HSW is HP) and (FS_loading is HP) and (RS_loading is HP) and (Cabin_Blower is MP) and (FCI is VH) and (CSI is Normal) then (Electrical_Load is VL) (1)
71	If (HSW is LP) and (FS_loading is LP) and (RS_loading is LP) and (Cabin_Blower is HP) and (FCI is VL) and (CSI is Normal) then (Electrical_Load is M) (1)
72	If (HSW is LP) and (FS_loading is LP) and (RS_loading is LP) and (Cabin_Blower is HP) and (FCI is L) and (CSI is Normal) then (Electrical_Load is M) (1)
73	If (HSW is LP) and (FS_loading is LP) and (RS_loading is LP) and (Cabin_Blower is HP) and (FCI is LM) and (CSI is Normal) then (Electrical_Load is M) (1)
74	If (HSW is LP) and (FS_loading is LP) and (RS_loading is LP) and (Cabin_Blower is HP) and (FCI is M) and (CSI is Normal) then (Electrical_Load is M) (1)

75	If (HSW is LP) and (FS_loading is LP) and (RS_loading is LP) and (Cabin_Blower is HP) and (FCI is MH) and (CSI is Normal) then (Electrical_Load is L) (1)
76	If (HSW is LP) and (FS_loading is LP) and (RS_loading is LP) and (Cabin_Blower is HP) and (FCI is H) and (CSI is Normal) then (Electrical_Load is L) (1)
77	If (HSW is LP) and (FS_loading is LP) and (RS_loading is LP) and (Cabin_Blower is HP) and (FCI is VH) and (CSI is Normal) then (Electrical_Load is L) (1)
78	If (HSW is HP) and (FS_loading is HP) and (RS_loading is HP) and (Cabin_Blower is HP) and (FCI is VL) and (CSI is Normal) then (Electrical_Load is MH) (1)
79	If (HSW is HP) and (FS_loading is HP) and (RS_loading is HP) and (Cabin_Blower is HP) and (FCI is L) and (CSI is Normal) then (Electrical_Load is MH) (1)
80	If (HSW is HP) and (FS_loading is HP) and (RS_loading is HP) and (Cabin_Blower is HP) and (FCI is LM) and (CSI is Normal) then (Electrical_Load is M) (1)
81	If (HSW is HP) and (FS_loading is HP) and (RS_loading is HP) and (Cabin_Blower is HP) and (FCI is M) and (CSI is Normal) then (Electrical_Load is M) (1)
82	If (HSW is HP) and (FS_loading is HP) and (RS_loading is HP) and (Cabin_Blower is HP) and (FCI is MH) and (CSI is Normal) then (Electrical_Load is L) (1)
83	If (HSW is HP) and (FS_loading is HP) and (RS_loading is HP) and (Cabin_Blower is HP) and (FCI is H) and (CSI is Normal) then (Electrical_Load is L) (1)
84	If (HSW is HP) and (FS_loading is HP) and (RS_loading is HP) and (Cabin_Blower is HP) and (FCI is VH) and (CSI is Normal) then (Electrical_Load is VL) (1)
85	If (HSW is LP) and (FS_loading is LP) and (RS_loading is LP) and (Cabin_Blower is LP) and (FCI is VL) and (CSI is High) then (Electrical_Load is VL) (1)
86	If (HSW is LP) and (FS_loading is LP) and (RS_loading is LP) and (Cabin_Blower is LP) and (FCI is L) and (CSI is High) then (Electrical_Load is VL) (1)
87	If (HSW is LP) and (FS_loading is LP) and (RS_loading is LP) and (Cabin_Blower is LP) and (FCI is M) and (CSI is High) then (Electrical_Load is VL) (1)
88	If (HSW is LP) and (FS_loading is LP) and (RS_loading is LP) and (Cabin_Blower is LP) and (FCI is MH) and (CSI is High) then (Electrical_Load is VL) (1)
89	If (HSW is LP) and (FS_loading is LP) and (RS_loading is LP) and (Cabin_Blower is LP) and (FCI is LM) and (CSI is High) then (Electrical_Load is VL) (1)
90	If (HSW is LP) and (FS_loading is LP) and (RS_loading is LP) and (Cabin_Blower is LP) and (FCI is H) and (CSI is High) then (Electrical_Load is VL) (1)
91	If (HSW is LP) and (FS_loading is LP) and (RS_loading is LP) and (Cabin_Blower is LP) and (FCI is VH) and (CSI is High) then (Electrical_Load is VL) (1)
92	If (HSW is HP) and (FS_loading is HP) and (RS_loading is HP) and (Cabin_Blower is LP) and (FCI is VL) and (CSI is High) then (Electrical_Load is MH) (1)
93	If (HSW is HP) and (FS_loading is HP) and (RS_loading is HP) and (Cabin_Blower is LP) and (FCI is L) and (CSI is High) then (Electrical_Load is MH) (1)
94	If (HSW is HP) and (FS_loading is HP) and (RS_loading is HP) and (Cabin_Blower is LP) and (FCI is LM) and (CSI is High) then (Electrical_Load is MH) (1)
95	If (HSW is HP) and (FS_loading is HP) and (RS_loading is HP) and (Cabin_Blower is LP) and (FCI is M) and (CSI is High) then (Electrical_Load is M) (1)
96	If (HSW is HP) and (FS_loading is HP) and (RS_loading is HP) and (Cabin_Blower is LP) and (FCI is MH) and (CSI is High) then (Electrical_Load is M) (1)
97	If (HSW is HP) and (FS_loading is HP) and (RS_loading is HP) and (Cabin_Blower is LP) and (FCI is H) and (CSI is High) then (Electrical_Load is L) (1)
98	If (HSW is HP) and (FS_loading is HP) and (RS_loading is HP) and (Cabin_Blower is LP) and (FCI is VH) and (CSI is High) then (Electrical_Load is L) (1)
99	If (HSW is LP) and (FS_loading is LP) and (RS_loading is LP) and (Cabin_Blower is MP) and (FCI is VL) and (CSI is High) then (Electrical_Load is L) (1)
100	If (HSW is LP) and (FS_loading is LP) and (RS_loading is LP) and (Cabin_Blower is MP) and (FCI is L) and (CSI is High) then (Electrical_Load is L) (1)
101	If (HSW is LP) and (FS_loading is LP) and (RS_loading is LP) and (Cabin_Blower is MP) and (FCI is M) and (CSI is High) then (Electrical_Load is L) (1)
102	If (HSW is LP) and (FS_loading is LP) and (RS_loading is LP) and (Cabin_Blower is MP) and (FCI is MH) and (CSI is High) then (Electrical_Load is L) (1)
103	If (HSW is LP) and (FS_loading is LP) and (RS_loading is LP) and (Cabin_Blower is MP) and (FCI is LM) and (CSI is High) then (Electrical_Load is L) (1)
104	If (HSW is LP) and (FS_loading is LP) and (RS_loading is LP) and (Cabin_Blower is MP) and (FCI is H) and (CSI is High) then (Electrical_Load is L) (1)
105	If (HSW is LP) and (FS_loading is LP) and (RS_loading is LP) and (Cabin_Blower is MP) and (FCI is VH) and (CSI is High) then (Electrical_Load is VL) (1)
106	If (HSW is HP) and (FS_loading is HP) and (RS_loading is HP) and (Cabin_Blower is MP) and (FCI is VL) and (CSI is High) then (Electrical_Load is MH) (1)
107	If (HSW is HP) and (FS_loading is HP) and (RS_loading is HP) and (Cabin_Blower is MP) and (FCI is L) and (CSI is High) then (Electrical_Load is MH) (1)
108	If (HSW is HP) and (FS_loading is HP) and (RS_loading is HP) and (Cabin_Blower is MP) and (FCI is LM) and (CSI is High) then (Electrical_Load is MH) (1)
109	If (HSW is HP) and (FS_loading is HP) and (RS_loading is HP) and (Cabin_Blower is MP) and (FCI is M) and (CSI is High) then (Electrical_Load is M) (1)
110	If (HSW is HP) and (FS_loading is HP) and (RS_loading is HP) and (Cabin_Blower is MP) and (FCI is MH) and (CSI is High) then (Electrical_Load is M) (1)
111	If (HSW is HP) and (FS_loading is HP) and (RS_loading is HP) and (Cabin_Blower is MP) and (FCI is H) and (CSI is High) then (Electrical_Load is L) (1)
112	If (HSW is HP) and (FS_loading is HP) and (RS_loading is HP) and (Cabin_Blower is MP) and (FCI is VH) and (CSI is High) then (Electrical_Load is L) (1)
113	If (HSW is LP) and (FS_loading is LP) and (RS_loading is LP) and (Cabin_Blower is HP) and (FCI is VL) and (CSI is High) then (Electrical_Load is M) (1)
114	If (HSW is LP) and (FS_loading is LP) and (RS_loading is LP) and (Cabin_Blower is HP) and (FCI is L) and (CSI is High) then (Electrical_Load is M) (1)
115	If (HSW is LP) and (FS_loading is LP) and (RS_loading is LP) and (Cabin_Blower is HP) and (FCI is M) and (CSI is High) then (Electrical_Load is M) (1)
116	If (HSW is LP) and (FS_loading is LP) and (RS_loading is LP) and (Cabin_Blower is HP) and (FCI is MH) and (CSI is High) then (Electrical_Load is M) (1)

117	If (HSW is LP) and (FS_loading is LP) and (RS_loading is LP) and (Cabin_Blower is HP) and (FCI is LM) and (CSI is High) then (Electrical_Load is M) (1)
118	If (HSW is LP) and (FS_loading is LP) and (RS_loading is LP) and (Cabin_Blower is HP) and (FCI is H) and (CSI is High) then (Electrical_Load is M) (1)
119	If (HSW is LP) and (FS_loading is LP) and (RS_loading is LP) and (Cabin_Blower is HP) and (FCI is VH) and (CSI is High) then (Electrical_Load is L) (1)
120	If (HSW is HP) and (FS_loading is HP) and (RS_loading is HP) and (Cabin_Blower is HP) and (FCI is VL) and (CSI is High) then (Electrical_Load is MH) (1)
121	If (HSW is HP) and (FS_loading is HP) and (RS_loading is HP) and (Cabin_Blower is HP) and (FCI is L) and (CSI is High) then (Electrical_Load is MH) (1)
122	If (HSW is HP) and (FS_loading is HP) and (RS_loading is HP) and (Cabin_Blower is HP) and (FCI is LM) and (CSI is High) then (Electrical_Load is MH) (1)
123	If (HSW is HP) and (FS_loading is HP) and (RS_loading is HP) and (Cabin_Blower is HP) and (FCI is M) and (CSI is High) then (Electrical_Load is MH) (1)
124	If (HSW is HP) and (FS_loading is HP) and (RS_loading is HP) and (Cabin_Blower is HP) and (FCI is MH) and (CSI is High) then (Electrical_Load is M) (1)
125	If (HSW is HP) and (FS_loading is HP) and (RS_loading is HP) and (Cabin_Blower is HP) and (FCI is H) and (CSI is High) then (Electrical_Load is M) (1)
126	If (HSW is HP) and (FS_loading is HP) and (RS_loading is HP) and (Cabin_Blower is HP) and (FCI is VH) and (CSI is High) then (Electrical_Load is L) (1)
127	If (HSW is HP) and (FS_loading is LP) and (RS_loading is LP) and (Cabin_Blower is LP) and (FCI is VL) and (CSI is Low) then (Electrical_Load is L) (1)
128	If (HSW is HP) and (FS_loading is LP) and (RS_loading is LP) and (Cabin_Blower is LP) and (FCI is L) and (CSI is Low) then (Electrical_Load is L) (1)
129	If (HSW is HP) and (FS_loading is LP) and (RS_loading is LP) and (Cabin_Blower is LP) and (FCI is M) and (CSI is Low) then (Electrical_Load is L) (1)
130	If (HSW is HP) and (FS_loading is LP) and (RS_loading is LP) and (Cabin_Blower is LP) and (FCI is LM) and (CSI is Low) then (Electrical_Load is L) (1)
131	If (HSW is HP) and (FS_loading is LP) and (RS_loading is LP) and (Cabin_Blower is LP) and (FCI is MH) and (CSI is Low) then (Electrical_Load is L) (1)
132	If (HSW is HP) and (FS_loading is LP) and (RS_loading is LP) and (Cabin_Blower is LP) and (FCI is H) and (CSI is Low) then (Electrical_Load is VL) (1)
133	If (HSW is HP) and (FS_loading is LP) and (RS_loading is LP) and (Cabin_Blower is LP) and (FCI is VH) and (CSI is Low) then (Electrical_Load is VL) (1)
134	If (HSW is HP) and (FS_loading is LP) and (RS_loading is LP) and (Cabin_Blower is MP) and (FCI is VL) and (CSI is Low) then (Electrical_Load is L) (1)
135	If (HSW is HP) and (FS_loading is LP) and (RS_loading is LP) and (Cabin_Blower is MP) and (FCI is L) and (CSI is Low) then (Electrical_Load is L) (1)
136	If (HSW is HP) and (FS_loading is LP) and (RS_loading is LP) and (Cabin_Blower is MP) and (FCI is M) and (CSI is Low) then (Electrical_Load is L) (1)
137	If (HSW is HP) and (FS_loading is LP) and (RS_loading is LP) and (Cabin_Blower is MP) and (FCI is LM) and (CSI is Low) then (Electrical_Load is L) (1)
138	If (HSW is HP) and (FS_loading is LP) and (RS_loading is LP) and (Cabin_Blower is MP) and (FCI is MH) and (CSI is Low) then (Electrical_Load is L) (1)
139	If (HSW is HP) and (FS_loading is LP) and (RS_loading is LP) and (Cabin_Blower is MP) and (FCI is H) and (CSI is Low) then (Electrical_Load is VL) (1)
140	If (HSW is HP) and (FS_loading is LP) and (RS_loading is LP) and (Cabin_Blower is MP) and (FCI is VH) and (CSI is Low) then (Electrical_Load is VL) (1)
141	If (HSW is HP) and (FS_loading is LP) and (RS_loading is LP) and (Cabin_Blower is HP) and (FCI is VL) and (CSI is Low) then (Electrical_Load is M) (1)
142	If (HSW is HP) and (FS_loading is LP) and (RS_loading is LP) and (Cabin_Blower is HP) and (FCI is L) and (CSI is Low) then (Electrical_Load is M) (1)
143	If (HSW is HP) and (FS_loading is LP) and (RS_loading is LP) and (Cabin_Blower is HP) and (FCI is LM) and (CSI is Low) then (Electrical_Load is M) (1)
144	If (HSW is HP) and (FS_loading is LP) and (RS_loading is LP) and (Cabin_Blower is HP) and (FCI is M) and (CSI is Low) then (Electrical_Load is M) (1)
145	If (HSW is HP) and (FS_loading is LP) and (RS_loading is LP) and (Cabin_Blower is HP) and (FCI is MH) and (CSI is Low) then (Electrical_Load is L) (1)
146	If (HSW is HP) and (FS_loading is LP) and (RS_loading is LP) and (Cabin_Blower is HP) and (FCI is H) and (CSI is Low) then (Electrical_Load is VL) (1)
147	If (HSW is HP) and (FS_loading is LP) and (RS_loading is LP) and (Cabin_Blower is HP) and (FCI is VH) and (CSI is Low) then (Electrical_Load is VL) (1)
148	If (HSW is HP) and (FS_loading is LP) and (RS_loading is LP) and (Cabin_Blower is LP) and (FCI is VL) and (CSI is Normal) then (Electrical_Load is L) (1)
149	If (HSW is HP) and (FS_loading is LP) and (RS_loading is LP) and (Cabin_Blower is LP) and (FCI is L) and (CSI is Normal) then (Electrical_Load is L) (1)
150	If (HSW is HP) and (FS_loading is LP) and (RS_loading is LP) and (Cabin_Blower is LP) and (FCI is LM) and (CSI is Normal) then (Electrical_Load is L) (1)
151	If (HSW is HP) and (FS_loading is LP) and (RS_loading is LP) and (Cabin_Blower is LP) and (FCI is M) and (CSI is Normal) then (Electrical_Load is L) (1)
152	If (HSW is HP) and (FS_loading is LP) and (RS_loading is LP) and (Cabin_Blower is LP) and (FCI is MH) and (CSI is Normal) then (Electrical_Load is L) (1)
153	If (HSW is HP) and (FS_loading is LP) and (RS_loading is LP) and (Cabin_Blower is LP) and (FCI is H) and (CSI is Normal) then (Electrical_Load is VL) (1)
154	If (HSW is HP) and (FS_loading is LP) and (RS_loading is LP) and (Cabin_Blower is LP) and (FCI is VH) and (CSI is Normal) then (Electrical_Load is VL) (1)
155	If (HSW is HP) and (FS_loading is LP) and (RS_loading is LP) and (Cabin_Blower is MP) and (FCI is VL) and (CSI is Normal) then (Electrical_Load is L) (1)
156	If (HSW is HP) and (FS_loading is LP) and (RS_loading is LP) and (Cabin_Blower is MP) and (FCI is L) and (CSI is Normal) then (Electrical_Load is L) (1)
157	If (HSW is HP) and (FS_loading is LP) and (RS_loading is LP) and (Cabin_Blower is MP) and (FCI is LM) and (CSI is Normal) then (Electrical_Load is L) (1)
158	If (HSW is HP) and (FS_loading is LP) and (RS_loading is LP) and (Cabin_Blower is MP) and (FCI is M) and (CSI is Normal) then (Electrical_Load is L) (1)

159	If (HSW is HP) and (FS_loading is LP) and (RS_loading is LP) and (Cabin_Blower is MP) and (FCI is MH) and (CSI is Normal) then (Electrical_Load is L) (1)
160	If (HSW is HP) and (FS_loading is LP) and (RS_loading is LP) and (Cabin_Blower is MP) and (FCI is H) and (CSI is Normal) then (Electrical_Load is VL) (1)
161	If (HSW is HP) and (FS_loading is LP) and (RS_loading is LP) and (Cabin_Blower is MP) and (FCI is VH) and (CSI is Normal) then (Electrical_Load is VL) (1)
162	If (HSW is HP) and (FS_loading is LP) and (RS_loading is LP) and (Cabin_Blower is HP) and (FCI is VL) and (CSI is Normal) then (Electrical_Load is M) (1)
163	If (HSW is HP) and (FS_loading is LP) and (RS_loading is LP) and (Cabin_Blower is HP) and (FCI is L) and (CSI is Normal) then (Electrical_Load is M) (1)
164	If (HSW is HP) and (FS_loading is LP) and (RS_loading is LP) and (Cabin_Blower is HP) and (FCI is LM) and (CSI is Normal) then (Electrical_Load is M) (1)
165	If (HSW is HP) and (FS_loading is LP) and (RS_loading is LP) and (Cabin_Blower is HP) and (FCI is M) and (CSI is Normal) then (Electrical_Load is M) (1)
166	If (HSW is HP) and (FS_loading is LP) and (RS_loading is LP) and (Cabin_Blower is HP) and (FCI is MH) and (CSI is Normal) then (Electrical_Load is L) (1)
167	If (HSW is HP) and (FS_loading is LP) and (RS_loading is LP) and (Cabin_Blower is HP) and (FCI is H) and (CSI is Normal) then (Electrical_Load is L) (1)
168	If (HSW is HP) and (FS_loading is LP) and (RS_loading is LP) and (Cabin_Blower is HP) and (FCI is VH) and (CSI is Normal) then (Electrical_Load is VL) (1)
169	If (HSW is HP) and (FS_loading is LP) and (RS_loading is LP) and (Cabin_Blower is LP) and (FCI is VL) and (CSI is High) then (Electrical_Load is L) (1)
170	If (HSW is HP) and (FS_loading is LP) and (RS_loading is LP) and (Cabin_Blower is LP) and (FCI is L) and (CSI is High) then (Electrical_Load is L) (1)
171	If (HSW is HP) and (FS_loading is LP) and (RS_loading is LP) and (Cabin_Blower is LP) and (FCI is LM) and (CSI is High) then (Electrical_Load is L) (1)
172	If (HSW is HP) and (FS_loading is LP) and (RS_loading is LP) and (Cabin_Blower is LP) and (FCI is M) and (CSI is High) then (Electrical_Load is L) (1)
173	If (HSW is HP) and (FS_loading is LP) and (RS_loading is LP) and (Cabin_Blower is LP) and (FCI is MH) and (CSI is High) then (Electrical_Load is L) (1)
174	If (HSW is HP) and (FS_loading is LP) and (RS_loading is LP) and (Cabin_Blower is LP) and (FCI is H) and (CSI is High) then (Electrical_Load is VL) (1)
175	If (HSW is HP) and (FS_loading is LP) and (RS_loading is LP) and (Cabin_Blower is LP) and (FCI is VH) and (CSI is High) then (Electrical_Load is VL) (1)
176	If (HSW is HP) and (FS_loading is LP) and (RS_loading is LP) and (Cabin_Blower is MP) and (FCI is VL) and (CSI is High) then (Electrical_Load is M) (1)
177	If (HSW is HP) and (FS_loading is LP) and (RS_loading is LP) and (Cabin_Blower is MP) and (FCI is L) and (CSI is High) then (Electrical_Load is M) (1)
178	If (HSW is HP) and (FS_loading is LP) and (RS_loading is LP) and (Cabin_Blower is MP) and (FCI is LM) and (CSI is High) then (Electrical_Load is M) (1)
179	If (HSW is HP) and (FS_loading is LP) and (RS_loading is LP) and (Cabin_Blower is MP) and (FCI is M) and (CSI is High) then (Electrical_Load is L) (1)
180	If (HSW is HP) and (FS_loading is LP) and (RS_loading is LP) and (Cabin_Blower is MP) and (FCI is MH) and (CSI is High) then (Electrical_Load is L) (1)
181	If (HSW is HP) and (FS_loading is LP) and (RS_loading is LP) and (Cabin_Blower is MP) and (FCI is H) and (CSI is High) then (Electrical_Load is L) (1)
182	If (HSW is HP) and (FS_loading is LP) and (RS_loading is LP) and (Cabin_Blower is MP) and (FCI is VH) and (CSI is High) then (Electrical_Load is VL) (1)
183	If (HSW is HP) and (FS_loading is LP) and (RS_loading is LP) and (Cabin_Blower is HP) and (FCI is VL) and (CSI is High) then (Electrical_Load is M) (1)
184	If (HSW is HP) and (FS_loading is LP) and (RS_loading is LP) and (Cabin_Blower is HP) and (FCI is L) and (CSI is High) then (Electrical_Load is M) (1)
185	If (HSW is HP) and (FS_loading is LP) and (RS_loading is LP) and (Cabin_Blower is HP) and (FCI is LM) and (CSI is High) then (Electrical_Load is M) (1)
186	If (HSW is HP) and (FS_loading is LP) and (RS_loading is LP) and (Cabin_Blower is HP) and (FCI is M) and (CSI is High) then (Electrical_Load is M) (1)
187	If (HSW is HP) and (FS_loading is LP) and (RS_loading is LP) and (Cabin_Blower is HP) and (FCI is MH) and (CSI is High) then (Electrical_Load is L) (1)
188	If (HSW is HP) and (FS_loading is LP) and (RS_loading is LP) and (Cabin_Blower is HP) and (FCI is H) and (CSI is High) then (Electrical_Load is L) (1)
189	If (HSW is HP) and (FS_loading is LP) and (RS_loading is LP) and (Cabin_Blower is HP) and (FCI is VH) and (CSI is High) then (Electrical_Load is VL) (1)
190	If (HSW is LP) and (FS_loading is HP) and (RS_loading is LP) and (Cabin_Blower is LP) and (FCI is VL) and (CSI is Low) then (Electrical_Load is L) (1)
191	If (HSW is LP) and (FS_loading is HP) and (RS_loading is LP) and (Cabin_Blower is LP) and (FCI is L) and (CSI is Low) then (Electrical_Load is L) (1)
192	If (HSW is LP) and (FS_loading is HP) and (RS_loading is LP) and (Cabin_Blower is LP) and (FCI is LM) and (CSI is Low) then (Electrical_Load is L) (1)
193	If (HSW is LP) and (FS_loading is HP) and (RS_loading is LP) and (Cabin_Blower is LP) and (FCI is M) and (CSI is Low) then (Electrical_Load is L) (1)
194	If (HSW is LP) and (FS_loading is HP) and (RS_loading is LP) and (Cabin_Blower is LP) and (FCI is MH) and (CSI is Low) then (Electrical_Load is VL) (1)
195	If (HSW is LP) and (FS_loading is HP) and (RS_loading is LP) and (Cabin_Blower is LP) and (FCI is H) and (CSI is Low) then (Electrical_Load is VL) (1)
196	If (HSW is LP) and (FS_loading is HP) and (RS_loading is LP) and (Cabin_Blower is LP) and (FCI is VH) and (CSI is Low) then (Electrical_Load is VL) (1)
197	If (HSW is LP) and (FS_loading is HP) and (RS_loading is LP) and (Cabin_Blower is MP) and (FCI is VL) and (CSI is Low) then (Electrical_Load is M) (1)
198	If (HSW is LP) and (FS_loading is HP) and (RS_loading is LP) and (Cabin_Blower is MP) and (FCI is L) and (CSI is Low) then (Electrical_Load is M) (1)
199	If (HSW is LP) and (FS_loading is HP) and (RS_loading is LP) and (Cabin_Blower is MP) and (FCI is LM) and (CSI is Low) then (Electrical_Load is M) (1)
200	If (HSW is LP) and (FS_loading is HP) and (RS_loading is LP) and (Cabin_Blower is MP) and (FCI is M) and (CSI is Low) then (Electrical_Load is M) (1)

201	If (HSW is LP) and (FS_loading is HP) and (RS_loading is LP) and (Cabin_Blower is MP) and (FCI is MH) and (CSI is Low) then (Electrical_Load is L) (1)
202	If (HSW is LP) and (FS_loading is HP) and (RS_loading is LP) and (Cabin_Blower is MP) and (FCI is H) and (CSI is Low) then (Electrical_Load is VL) (1)
203	If (HSW is LP) and (FS_loading is HP) and (RS_loading is LP) and (Cabin_Blower is MP) and (FCI is VH) and (CSI is Low) then (Electrical_Load is VL) (1)
204	If (HSW is LP) and (FS_loading is HP) and (RS_loading is LP) and (Cabin_Blower is HP) and (FCI is VL) and (CSI is Low) then (Electrical_Load is M) (1)
205	If (HSW is LP) and (FS_loading is HP) and (RS_loading is LP) and (Cabin_Blower is HP) and (FCI is L) and (CSI is Low) then (Electrical_Load is M) (1)
206	If (HSW is LP) and (FS_loading is HP) and (RS_loading is LP) and (Cabin_Blower is HP) and (FCI is LM) and (CSI is Low) then (Electrical_Load is M) (1)
207	If (HSW is LP) and (FS_loading is HP) and (RS_loading is LP) and (Cabin_Blower is HP) and (FCI is M) and (CSI is Low) then (Electrical_Load is M) (1)
208	If (HSW is LP) and (FS_loading is HP) and (RS_loading is LP) and (Cabin_Blower is HP) and (FCI is MH) and (CSI is Low) then (Electrical_Load is L) (1)
209	If (HSW is LP) and (FS_loading is HP) and (RS_loading is LP) and (Cabin_Blower is HP) and (FCI is H) and (CSI is Low) then (Electrical_Load is VL) (1)
210	If (HSW is LP) and (FS_loading is HP) and (RS_loading is LP) and (Cabin_Blower is HP) and (FCI is VH) and (CSI is Low) then (Electrical_Load is VL) (1)
211	If (HSW is LP) and (FS_loading is HP) and (RS_loading is LP) and (Cabin_Blower is LP) and (FCI is VL) and (CSI is Normal) then (Electrical_Load is M) (1)
212	If (HSW is LP) and (FS_loading is HP) and (RS_loading is LP) and (Cabin_Blower is LP) and (FCI is L) and (CSI is Normal) then (Electrical_Load is M) (1)
213	If (HSW is LP) and (FS_loading is HP) and (RS_loading is LP) and (Cabin_Blower is LP) and (FCI is LM) and (CSI is Normal) then (Electrical_Load is M) (1)
214	If (HSW is LP) and (FS_loading is HP) and (RS_loading is LP) and (Cabin_Blower is LP) and (FCI is M) and (CSI is Normal) then (Electrical_Load is L) (1)
215	If (HSW is LP) and (FS_loading is HP) and (RS_loading is LP) and (Cabin_Blower is LP) and (FCI is MH) and (CSI is Normal) then (Electrical_Load is L) (1)
216	If (HSW is LP) and (FS_loading is HP) and (RS_loading is LP) and (Cabin_Blower is LP) and (FCI is H) and (CSI is Normal) then (Electrical_Load is VL) (1)
217	If (HSW is LP) and (FS_loading is HP) and (RS_loading is LP) and (Cabin_Blower is LP) and (FCI is VH) and (CSI is Normal) then (Electrical_Load is VL) (1)
218	If (HSW is LP) and (FS_loading is HP) and (RS_loading is LP) and (Cabin_Blower is MP) and (FCI is VL) and (CSI is Normal) then (Electrical_Load is M) (1)
219	If (HSW is LP) and (FS_loading is HP) and (RS_loading is LP) and (Cabin_Blower is MP) and (FCI is L) and (CSI is Normal) then (Electrical_Load is M) (1)
220	If (HSW is LP) and (FS_loading is HP) and (RS_loading is LP) and (Cabin_Blower is MP) and (FCI is LM) and (CSI is Normal) then (Electrical_Load is M) (1)
221	If (HSW is LP) and (FS_loading is HP) and (RS_loading is LP) and (Cabin_Blower is MP) and (FCI is M) and (CSI is Normal) then (Electrical_Load is M) (1)
222	If (HSW is LP) and (FS_loading is HP) and (RS_loading is LP) and (Cabin_Blower is MP) and (FCI is MH) and (CSI is Normal) then (Electrical_Load is L) (1)
223	If (HSW is LP) and (FS_loading is HP) and (RS_loading is LP) and (Cabin_Blower is MP) and (FCI is H) and (CSI is Normal) then (Electrical_Load is L) (1)
224	If (HSW is LP) and (FS_loading is HP) and (RS_loading is LP) and (Cabin_Blower is MP) and (FCI is VH) and (CSI is Normal) then (Electrical_Load is VL) (1)
225	If (HSW is LP) and (FS_loading is HP) and (RS_loading is LP) and (Cabin_Blower is HP) and (FCI is VL) and (CSI is Normal) then (Electrical_Load is MH) (1)
226	If (HSW is LP) and (FS_loading is HP) and (RS_loading is LP) and (Cabin_Blower is HP) and (FCI is L) and (CSI is Normal) then (Electrical_Load is MH) (1)
227	If (HSW is LP) and (FS_loading is HP) and (RS_loading is LP) and (Cabin_Blower is HP) and (FCI is LM) and (CSI is Normal) then (Electrical_Load is M) (1)
228	If (HSW is LP) and (FS_loading is HP) and (RS_loading is LP) and (Cabin_Blower is HP) and (FCI is M) and (CSI is Normal) then (Electrical_Load is M) (1)
229	If (HSW is LP) and (FS_loading is HP) and (RS_loading is LP) and (Cabin_Blower is HP) and (FCI is MH) and (CSI is Normal) then (Electrical_Load is L) (1)
230	If (HSW is LP) and (FS_loading is HP) and (RS_loading is LP) and (Cabin_Blower is HP) and (FCI is H) and (CSI is Normal) then (Electrical_Load is L) (1)
231	If (HSW is LP) and (FS_loading is HP) and (RS_loading is LP) and (Cabin_Blower is HP) and (FCI is VH) and (CSI is Normal) then (Electrical_Load is VL) (1)
232	If (HSW is LP) and (FS_loading is HP) and (RS_loading is LP) and (Cabin_Blower is LP) and (FCI is VL) and (CSI is High) then (Electrical_Load is M) (1)
233	If (HSW is LP) and (FS_loading is HP) and (RS_loading is LP) and (Cabin_Blower is LP) and (FCI is L) and (CSI is High) then (Electrical_Load is M) (1)
234	If (HSW is LP) and (FS_loading is HP) and (RS_loading is LP) and (Cabin_Blower is LP) and (FCI is LM) and (CSI is High) then (Electrical_Load is M) (1)
235	If (HSW is LP) and (FS_loading is HP) and (RS_loading is LP) and (Cabin_Blower is LP) and (FCI is M) and (CSI is High) then (Electrical_Load is M) (1)
236	If (HSW is LP) and (FS_loading is HP) and (RS_loading is LP) and (Cabin_Blower is LP) and (FCI is MH) and (CSI is High) then (Electrical_Load is L) (1)
237	If (HSW is LP) and (FS_loading is HP) and (RS_loading is LP) and (Cabin_Blower is LP) and (FCI is H) and (CSI is High) then (Electrical_Load is L) (1)
238	If (HSW is LP) and (FS_loading is HP) and (RS_loading is LP) and (Cabin_Blower is LP) and (FCI is VH) and (CSI is High) then (Electrical_Load is L) (1)
239	If (HSW is LP) and (FS_loading is HP) and (RS_loading is LP) and (Cabin_Blower is MP) and (FCI is VL) and (CSI is High) then (Electrical_Load is MH) (1)
240	If (HSW is LP) and (FS_loading is HP) and (RS_loading is LP) and (Cabin_Blower is MP) and (FCI is L) and (CSI is High) then (Electrical_Load is MH) (1)
241	If (HSW is LP) and (FS_loading is HP) and (RS_loading is LP) and (Cabin_Blower is MP) and (FCI is LM) and (CSI is High) then (Electrical_Load is MH) (1)
242	If (HSW is LP) and (FS_loading is HP) and (RS_loading is LP) and (Cabin_Blower is MP) and (FCI is M) and (CSI is High) then (Electrical_Load is M) (1)

243	If (HSW is LP) and (FS_loading is HP) and (RS_loading is LP) and (Cabin_Blower is MP) and (FCI is MH) and (CSI is High) then (Electrical_Load is M) (1)
244	If (HSW is LP) and (FS_loading is HP) and (RS_loading is LP) and (Cabin_Blower is MP) and (FCI is H) and (CSI is High) then (Electrical_Load is L) (1)
245	If (HSW is LP) and (FS_loading is HP) and (RS_loading is LP) and (Cabin_Blower is MP) and (FCI is VH) and (CSI is High) then (Electrical_Load is L) (1)
246	If (HSW is LP) and (FS_loading is HP) and (RS_loading is LP) and (Cabin_Blower is HP) and (FCI is VL) and (CSI is High) then (Electrical_Load is MH) (1)
247	If (HSW is LP) and (FS_loading is HP) and (RS_loading is LP) and (Cabin_Blower is HP) and (FCI is L) and (CSI is High) then (Electrical_Load is MH) (1)
248	If (HSW is LP) and (FS_loading is HP) and (RS_loading is LP) and (Cabin_Blower is HP) and (FCI is LM) and (CSI is High) then (Electrical_Load is MH) (1)
249	If (HSW is LP) and (FS_loading is HP) and (RS_loading is LP) and (Cabin_Blower is HP) and (FCI is M) and (CSI is High) then (Electrical_Load is MH) (1)
250	If (HSW is LP) and (FS_loading is HP) and (RS_loading is LP) and (Cabin_Blower is HP) and (FCI is MH) and (CSI is High) then (Electrical_Load is MH) (1)
251	If (HSW is LP) and (FS_loading is HP) and (RS_loading is LP) and (Cabin_Blower is HP) and (FCI is H) and (CSI is High) then (Electrical_Load is M) (1)
252	If (HSW is LP) and (FS_loading is HP) and (RS_loading is LP) and (Cabin_Blower is HP) and (FCI is VH) and (CSI is High) then (Electrical_Load is M) (1)
253	If (HSW is LP) and (FS_loading is LP) and (RS_loading is HP) and (Cabin_Blower is LP) and (FCI is VL) and (CSI is Low) then (Electrical_Load is L) (1)
254	If (HSW is LP) and (FS_loading is LP) and (RS_loading is HP) and (Cabin_Blower is LP) and (FCI is L) and (CSI is Low) then (Electrical_Load is L) (1)
255	If (HSW is LP) and (FS_loading is LP) and (RS_loading is HP) and (Cabin_Blower is LP) and (FCI is LM) and (CSI is Low) then (Electrical_Load is L) (1)
256	If (HSW is LP) and (FS_loading is LP) and (RS_loading is HP) and (Cabin_Blower is LP) and (FCI is M) and (CSI is Low) then (Electrical_Load is L) (1)
257	If (HSW is LP) and (FS_loading is LP) and (RS_loading is HP) and (Cabin_Blower is LP) and (FCI is MH) and (CSI is Low) then (Electrical_Load is VL) (1)
258	If (HSW is LP) and (FS_loading is LP) and (RS_loading is HP) and (Cabin_Blower is LP) and (FCI is H) and (CSI is Low) then (Electrical_Load is VL) (1)
259	If (HSW is LP) and (FS_loading is LP) and (RS_loading is HP) and (Cabin_Blower is LP) and (FCI is VH) and (CSI is Low) then (Electrical_Load is VL) (1)
260	If (HSW is LP) and (FS_loading is LP) and (RS_loading is HP) and (Cabin_Blower is MP) and (FCI is VL) and (CSI is Low) then (Electrical_Load is M) (1)
261	If (HSW is LP) and (FS_loading is LP) and (RS_loading is HP) and (Cabin_Blower is MP) and (FCI is L) and (CSI is Low) then (Electrical_Load is M) (1)
262	If (HSW is LP) and (FS_loading is LP) and (RS_loading is HP) and (Cabin_Blower is MP) and (FCI is LM) and (CSI is Low) then (Electrical_Load is M) (1)
263	If (HSW is LP) and (FS_loading is LP) and (RS_loading is HP) and (Cabin_Blower is MP) and (FCI is M) and (CSI is Low) then (Electrical_Load is M) (1)
264	If (HSW is LP) and (FS_loading is LP) and (RS_loading is HP) and (Cabin_Blower is MP) and (FCI is MH) and (CSI is Low) then (Electrical_Load is L) (1)
265	If (HSW is LP) and (FS_loading is LP) and (RS_loading is HP) and (Cabin_Blower is MP) and (FCI is H) and (CSI is Low) then (Electrical_Load is VL) (1)
266	If (HSW is LP) and (FS_loading is LP) and (RS_loading is HP) and (Cabin_Blower is MP) and (FCI is VH) and (CSI is Low) then (Electrical_Load is VL) (1)
267	If (HSW is LP) and (FS_loading is LP) and (RS_loading is HP) and (Cabin_Blower is HP) and (FCI is VL) and (CSI is Low) then (Electrical_Load is M) (1)
268	If (HSW is LP) and (FS_loading is LP) and (RS_loading is HP) and (Cabin_Blower is HP) and (FCI is L) and (CSI is Low) then (Electrical_Load is M) (1)
269	If (HSW is LP) and (FS_loading is LP) and (RS_loading is HP) and (Cabin_Blower is HP) and (FCI is LM) and (CSI is Low) then (Electrical_Load is M) (1)
270	If (HSW is LP) and (FS_loading is LP) and (RS_loading is HP) and (Cabin_Blower is HP) and (FCI is M) and (CSI is Low) then (Electrical_Load is M) (1)
271	If (HSW is LP) and (FS_loading is LP) and (RS_loading is HP) and (Cabin_Blower is HP) and (FCI is MH) and (CSI is Low) then (Electrical_Load is L) (1)
272	If (HSW is LP) and (FS_loading is LP) and (RS_loading is HP) and (Cabin_Blower is HP) and (FCI is H) and (CSI is Low) then (Electrical_Load is VL) (1)
273	If (HSW is LP) and (FS_loading is LP) and (RS_loading is HP) and (Cabin_Blower is HP) and (FCI is VH) and (CSI is Low) then (Electrical_Load is VL) (1)
274	If (HSW is LP) and (FS_loading is LP) and (RS_loading is HP) and (Cabin_Blower is LP) and (FCI is VL) and (CSI is Normal) then (Electrical_Load is M) (1)
275	If (HSW is LP) and (FS_loading is LP) and (RS_loading is HP) and (Cabin_Blower is LP) and (FCI is L) and (CSI is Normal) then (Electrical_Load is M) (1)
276	If (HSW is LP) and (FS_loading is LP) and (RS_loading is HP) and (Cabin_Blower is LP) and (FCI is LM) and (CSI is Normal) then (Electrical_Load is M) (1)
277	If (HSW is LP) and (FS_loading is LP) and (RS_loading is HP) and (Cabin_Blower is LP) and (FCI is M) and (CSI is Normal) then (Electrical_Load is L) (1)
278	If (HSW is LP) and (FS_loading is LP) and (RS_loading is HP) and (Cabin_Blower is LP) and (FCI is MH) and (CSI is Normal) then (Electrical_Load is L) (1)
279	If (HSW is LP) and (FS_loading is LP) and (RS_loading is HP) and (Cabin_Blower is LP) and (FCI is VH) and (CSI is Normal) then (Electrical_Load is VL) (1)
280	If (HSW is LP) and (FS_loading is LP) and (RS_loading is HP) and (Cabin_Blower is LP) and (FCI is H) and (CSI is Normal) then (Electrical_Load is VL) (1)
281	If (HSW is LP) and (FS_loading is LP) and (RS_loading is HP) and (Cabin_Blower is MP) and (FCI is VL) and (CSI is Normal) then (Electrical_Load is M) (1)
282	If (HSW is LP) and (FS_loading is LP) and (RS_loading is HP) and (Cabin_Blower is MP) and (FCI is L) and (CSI is Normal) then (Electrical_Load is M) (1)
283	If (HSW is LP) and (FS_loading is LP) and (RS_loading is HP) and (Cabin_Blower is MP) and (FCI is LM) and (CSI is Normal) then (Electrical_Load is M) (1)
284	If (HSW is LP) and (FS_loading is LP) and (RS_loading is HP) and (Cabin_Blower is MP) and (FCI is M) and (CSI is Normal) then (Electrical_Load is M) (1)

285	If (HSW is LP) and (FS_loading is LP) and (RS_loading is HP) and (Cabin_Blower is MP) and (FCI is MH) and (CSI is Normal) then (Electrical_Load is L) (1)
286	If (HSW is LP) and (FS_loading is LP) and (RS_loading is HP) and (Cabin_Blower is MP) and (FCI is H) and (CSI is Normal) then (Electrical_Load is L) (1)
287	If (HSW is LP) and (FS_loading is LP) and (RS_loading is HP) and (Cabin_Blower is MP) and (FCI is VH) and (CSI is Normal) then (Electrical_Load is VL) (1)
288	If (HSW is LP) and (FS_loading is LP) and (RS_loading is HP) and (Cabin_Blower is HP) and (FCI is VL) and (CSI is Normal) then (Electrical_Load is MH) (1)
289	If (HSW is LP) and (FS_loading is LP) and (RS_loading is HP) and (Cabin_Blower is HP) and (FCI is L) and (CSI is Normal) then (Electrical_Load is MH) (1)
290	If (HSW is LP) and (FS_loading is LP) and (RS_loading is HP) and (Cabin_Blower is HP) and (FCI is LM) and (CSI is Normal) then (Electrical_Load is M) (1)
291	If (HSW is LP) and (FS_loading is LP) and (RS_loading is HP) and (Cabin_Blower is HP) and (FCI is M) and (CSI is Normal) then (Electrical_Load is M) (1)
292	If (HSW is LP) and (FS_loading is LP) and (RS_loading is HP) and (Cabin_Blower is HP) and (FCI is MH) and (CSI is Normal) then (Electrical_Load is L) (1)
293	If (HSW is LP) and (FS_loading is LP) and (RS_loading is HP) and (Cabin_Blower is HP) and (FCI is H) and (CSI is Normal) then (Electrical_Load is L) (1)
294	If (HSW is LP) and (FS_loading is LP) and (RS_loading is HP) and (Cabin_Blower is HP) and (FCI is VH) and (CSI is Normal) then (Electrical_Load is VL) (1)
295	If (HSW is LP) and (FS_loading is LP) and (RS_loading is HP) and (Cabin_Blower is LP) and (FCI is VL) and (CSI is High) then (Electrical_Load is M) (1)
296	If (HSW is LP) and (FS_loading is LP) and (RS_loading is HP) and (Cabin_Blower is LP) and (FCI is L) and (CSI is High) then (Electrical_Load is M) (1)
297	If (HSW is LP) and (FS_loading is LP) and (RS_loading is HP) and (Cabin_Blower is LP) and (FCI is LM) and (CSI is High) then (Electrical_Load is M) (1)
298	If (HSW is LP) and (FS_loading is LP) and (RS_loading is HP) and (Cabin_Blower is LP) and (FCI is M) and (CSI is High) then (Electrical_Load is M) (1)
299	If (HSW is LP) and (FS_loading is LP) and (RS_loading is HP) and (Cabin_Blower is LP) and (FCI is MH) and (CSI is High) then (Electrical_Load is L) (1)
300	If (HSW is LP) and (FS_loading is LP) and (RS_loading is HP) and (Cabin_Blower is LP) and (FCI is H) and (CSI is High) then (Electrical_Load is L) (1)
301	If (HSW is LP) and (FS_loading is LP) and (RS_loading is HP) and (Cabin_Blower is LP) and (FCI is VH) and (CSI is High) then (Electrical_Load is L) (1)
302	If (HSW is LP) and (FS_loading is LP) and (RS_loading is HP) and (Cabin_Blower is MP) and (FCI is VL) and (CSI is High) then (Electrical_Load is MH) (1)
303	If (HSW is LP) and (FS_loading is LP) and (RS_loading is HP) and (Cabin_Blower is MP) and (FCI is L) and (CSI is High) then (Electrical_Load is MH) (1)
304	If (HSW is LP) and (FS_loading is LP) and (RS_loading is HP) and (Cabin_Blower is MP) and (FCI is LM) and (CSI is High) then (Electrical_Load is MH) (1)
305	If (HSW is LP) and (FS_loading is LP) and (RS_loading is HP) and (Cabin_Blower is MP) and (FCI is M) and (CSI is High) then (Electrical_Load is M) (1)
306	If (HSW is LP) and (FS_loading is LP) and (RS_loading is HP) and (Cabin_Blower is MP) and (FCI is MH) and (CSI is High) then (Electrical_Load is M) (1)
307	If (HSW is LP) and (FS_loading is LP) and (RS_loading is HP) and (Cabin_Blower is MP) and (FCI is H) and (CSI is High) then (Electrical_Load is L) (1)
308	If (HSW is LP) and (FS_loading is LP) and (RS_loading is HP) and (Cabin_Blower is MP) and (FCI is VH) and (CSI is High) then (Electrical_Load is L) (1)
309	If (HSW is LP) and (FS_loading is LP) and (RS_loading is HP) and (Cabin_Blower is HP) and (FCI is VL) and (CSI is High) then (Electrical_Load is MH) (1)
310	If (HSW is LP) and (FS_loading is LP) and (RS_loading is HP) and (Cabin_Blower is HP) and (FCI is L) and (CSI is High) then (Electrical_Load is MH) (1)
311	If (HSW is LP) and (FS_loading is LP) and (RS_loading is HP) and (Cabin_Blower is HP) and (FCI is LM) and (CSI is High) then (Electrical_Load is MH) (1)
312	If (HSW is LP) and (FS_loading is LP) and (RS_loading is HP) and (Cabin_Blower is HP) and (FCI is M) and (CSI is High) then (Electrical_Load is MH) (1)
313	If (HSW is LP) and (FS_loading is LP) and (RS_loading is HP) and (Cabin_Blower is HP) and (FCI is MH) and (CSI is High) then (Electrical_Load is MH) (1)
314	If (HSW is LP) and (FS_loading is LP) and (RS_loading is HP) and (Cabin_Blower is HP) and (FCI is H) and (CSI is High) then (Electrical_Load is M) (1)
315	If (HSW is LP) and (FS_loading is LP) and (RS_loading is HP) and (Cabin_Blower is HP) and (FCI is VH) and (CSI is High) then (Electrical_Load is M) (1)
316	If (HSW is HP) and (FS_loading is HP) and (RS_loading is LP) and (Cabin_Blower is LP) and (FCI is VL) and (CSI is Low) then (Electrical_Load is M) (1)
317	If (HSW is HP) and (FS_loading is HP) and (RS_loading is LP) and (Cabin_Blower is LP) and (FCI is L) and (CSI is Low) then (Electrical_Load is M) (1)
318	If (HSW is HP) and (FS_loading is HP) and (RS_loading is LP) and (Cabin_Blower is LP) and (FCI is LM) and (CSI is Low) then (Electrical_Load is M) (1)
319	If (HSW is HP) and (FS_loading is HP) and (RS_loading is LP) and (Cabin_Blower is LP) and (FCI is M) and (CSI is Low) then (Electrical_Load is M) (1)
320	If (HSW is HP) and (FS_loading is HP) and (RS_loading is LP) and (Cabin_Blower is LP) and (FCI is MH) and (CSI is Low) then (Electrical_Load is L) (1)
321	If (HSW is HP) and (FS_loading is HP) and (RS_loading is LP) and (Cabin_Blower is LP) and (FCI is VH) and (CSI is Low) then (Electrical_Load is VL) (1)
322	If (HSW is HP) and (FS_loading is HP) and (RS_loading is LP) and (Cabin_Blower is MP) and (FCI is VL) and (CSI is Low) then (Electrical_Load is M) (1)
323	If (HSW is HP) and (FS_loading is HP) and (RS_loading is LP) and (Cabin_Blower is MP) and (FCI is L) and (CSI is Low) then (Electrical_Load is M) (1)
324	If (HSW is HP) and (FS_loading is HP) and (RS_loading is LP) and (Cabin_Blower is MP) and (FCI is LM) and (CSI is Low) then (Electrical_Load is M) (1)
325	If (HSW is HP) and (FS_loading is HP) and (RS_loading is LP) and (Cabin_Blower is MP) and (FCI is M) and (CSI is Low) then (Electrical_Load is L) (1)
326	If (HSW is HP) and (FS_loading is HP) and (RS_loading is LP) and (Cabin_Blower is MP) and (FCI is MH) and (CSI is Low) then (Electrical_Load is L) (1)

327	If (HSW is HP) and (FS_loading is HP) and (RS_loading is LP) and (Cabin_Blower is MP) and (FCI is H) and (CSI is Low) then (Electrical_Load is VL) (1)
328	If (HSW is HP) and (FS_loading is HP) and (RS_loading is LP) and (Cabin_Blower is MP) and (FCI is VH) and (CSI is Low) then (Electrical_Load is VL) (1)
329	If (HSW is HP) and (FS_loading is HP) and (RS_loading is LP) and (Cabin_Blower is HP) and (FCI is VL) and (CSI is Low) then (Electrical_Load is M) (1)
330	If (HSW is HP) and (FS_loading is HP) and (RS_loading is LP) and (Cabin_Blower is HP) and (FCI is L) and (CSI is Low) then (Electrical_Load is M) (1)
331	If (HSW is HP) and (FS_loading is HP) and (RS_loading is LP) and (Cabin_Blower is HP) and (FCI is LM) and (CSI is Low) then (Electrical_Load is M) (1)
332	If (HSW is HP) and (FS_loading is HP) and (RS_loading is LP) and (Cabin_Blower is HP) and (FCI is M) and (CSI is Low) then (Electrical_Load is M) (1)
333	If (HSW is HP) and (FS_loading is HP) and (RS_loading is LP) and (Cabin_Blower is HP) and (FCI is MH) and (CSI is Low) then (Electrical_Load is L) (1)
334	If (HSW is HP) and (FS_loading is HP) and (RS_loading is LP) and (Cabin_Blower is HP) and (FCI is H) and (CSI is Low) then (Electrical_Load is VL) (1)
335	If (HSW is HP) and (FS_loading is HP) and (RS_loading is LP) and (Cabin_Blower is HP) and (FCI is VH) and (CSI is Low) then (Electrical_Load is VL) (1)
336	If (HSW is HP) and (FS_loading is HP) and (RS_loading is LP) and (Cabin_Blower is LP) and (FCI is VL) and (CSI is Normal) then (Electrical_Load is M) (1)
337	If (HSW is HP) and (FS_loading is HP) and (RS_loading is LP) and (Cabin_Blower is LP) and (FCI is L) and (CSI is Normal) then (Electrical_Load is M) (1)
338	If (HSW is HP) and (FS_loading is HP) and (RS_loading is LP) and (Cabin_Blower is LP) and (FCI is LM) and (CSI is Normal) then (Electrical_Load is M) (1)
339	If (HSW is HP) and (FS_loading is HP) and (RS_loading is LP) and (Cabin_Blower is LP) and (FCI is M) and (CSI is Normal) then (Electrical_Load is M) (1)
340	If (HSW is HP) and (FS_loading is HP) and (RS_loading is LP) and (Cabin_Blower is LP) and (FCI is MH) and (CSI is Normal) then (Electrical_Load is M) (1)
341	If (HSW is HP) and (FS_loading is HP) and (RS_loading is LP) and (Cabin_Blower is LP) and (FCI is H) and (CSI is Normal) then (Electrical_Load is L) (1)
342	If (HSW is HP) and (FS_loading is HP) and (RS_loading is LP) and (Cabin_Blower is LP) and (FCI is VH) and (CSI is Normal) then (Electrical_Load is VL) (1)
343	If (HSW is HP) and (FS_loading is HP) and (RS_loading is LP) and (Cabin_Blower is MP) and (FCI is VL) and (CSI is Normal) then (Electrical_Load is M) (1)
344	If (HSW is HP) and (FS_loading is HP) and (RS_loading is LP) and (Cabin_Blower is MP) and (FCI is L) and (CSI is Normal) then (Electrical_Load is M) (1)
345	If (HSW is HP) and (FS_loading is HP) and (RS_loading is LP) and (Cabin_Blower is MP) and (FCI is LM) and (CSI is Normal) then (Electrical_Load is M) (1)
346	If (HSW is HP) and (FS_loading is HP) and (RS_loading is LP) and (Cabin_Blower is MP) and (FCI is M) and (CSI is Normal) then (Electrical_Load is M) (1)
347	If (HSW is HP) and (FS_loading is HP) and (RS_loading is LP) and (Cabin_Blower is MP) and (FCI is MH) and (CSI is Normal) then (Electrical_Load is L) (1)
348	If (HSW is HP) and (FS_loading is HP) and (RS_loading is LP) and (Cabin_Blower is MP) and (FCI is H) and (CSI is Normal) then (Electrical_Load is L) (1)
349	If (HSW is HP) and (FS_loading is HP) and (RS_loading is LP) and (Cabin_Blower is MP) and (FCI is VH) and (CSI is Normal) then (Electrical_Load is VL) (1)
350	If (HSW is HP) and (FS_loading is HP) and (RS_loading is LP) and (Cabin_Blower is HP) and (FCI is VL) and (CSI is Normal) then (Electrical_Load is MH) (1)
351	If (HSW is HP) and (FS_loading is HP) and (RS_loading is LP) and (Cabin_Blower is HP) and (FCI is L) and (CSI is Normal) then (Electrical_Load is MH) (1)
352	If (HSW is HP) and (FS_loading is HP) and (RS_loading is LP) and (Cabin_Blower is HP) and (FCI is LM) and (CSI is Normal) then (Electrical_Load is MH) (1)
353	If (HSW is HP) and (FS_loading is HP) and (RS_loading is LP) and (Cabin_Blower is HP) and (FCI is M) and (CSI is Normal) then (Electrical_Load is M) (1)
354	If (HSW is HP) and (FS_loading is HP) and (RS_loading is LP) and (Cabin_Blower is HP) and (FCI is MH) and (CSI is Normal) then (Electrical_Load is L) (1)
355	If (HSW is HP) and (FS_loading is HP) and (RS_loading is LP) and (Cabin_Blower is HP) and (FCI is H) and (CSI is Normal) then (Electrical_Load is L) (1)
356	If (HSW is HP) and (FS_loading is HP) and (RS_loading is LP) and (Cabin_Blower is HP) and (FCI is VH) and (CSI is Normal) then (Electrical_Load is VL) (1)
357	If (HSW is HP) and (FS_loading is HP) and (RS_loading is LP) and (Cabin_Blower is LP) and (FCI is H) and (CSI is Low) then (Electrical_Load is VL) (1)
358	If (HSW is HP) and (FS_loading is HP) and (RS_loading is LP) and (Cabin_Blower is LP) and (FCI is VL) and (CSI is High) then (Electrical_Load is MH) (1)
359	If (HSW is HP) and (FS_loading is HP) and (RS_loading is LP) and (Cabin_Blower is LP) and (FCI is L) and (CSI is High) then (Electrical_Load is MH) (1)
360	If (HSW is HP) and (FS_loading is HP) and (RS_loading is LP) and (Cabin_Blower is LP) and (FCI is LM) and (CSI is High) then (Electrical_Load is MH) (1)
361	If (HSW is HP) and (FS_loading is HP) and (RS_loading is LP) and (Cabin_Blower is LP) and (FCI is M) and (CSI is High) then (Electrical_Load is MH) (1)
362	If (HSW is HP) and (FS_loading is HP) and (RS_loading is LP) and (Cabin_Blower is LP) and (FCI is MH) and (CSI is High) then (Electrical_Load is M) (1)
363	If (HSW is HP) and (FS_loading is HP) and (RS_loading is LP) and (Cabin_Blower is LP) and (FCI is H) and (CSI is High) then (Electrical_Load is M) (1)
364	If (HSW is HP) and (FS_loading is HP) and (RS_loading is LP) and (Cabin_Blower is LP) and (FCI is VH) and (CSI is High) then (Electrical_Load is L) (1)
365	If (HSW is HP) and (FS_loading is HP) and (RS_loading is LP) and (Cabin_Blower is MP) and (FCI is VL) and (CSI is High) then (Electrical_Load is MH) (1)
366	If (HSW is HP) and (FS_loading is HP) and (RS_loading is LP) and (Cabin_Blower is MP) and (FCI is L) and (CSI is High) then (Electrical_Load is MH) (1)
367	If (HSW is HP) and (FS_loading is HP) and (RS_loading is LP) and (Cabin_Blower is MP) and (FCI is LM) and (CSI is High) then (Electrical_Load is MH) (1)
368	If (HSW is HP) and (FS_loading is HP) and (RS_loading is LP) and (Cabin_Blower is MP) and (FCI is M) and (CSI is High) then (Electrical_Load is MH) (1)

369	If (HSW is HP) and (FS_loading is HP) and (RS_loading is LP) and (Cabin_Blower is MP) and (FCI is MH) and (CSI is High) then (Electrical_Load is M) (1)
370	If (HSW is HP) and (FS_loading is HP) and (RS_loading is LP) and (Cabin_Blower is MP) and (FCI is H) and (CSI is High) then (Electrical_Load is M) (1)
371	If (HSW is HP) and (FS_loading is HP) and (RS_loading is LP) and (Cabin_Blower is MP) and (FCI is VH) and (CSI is High) then (Electrical_Load is L) (1)
372	If (HSW is HP) and (FS_loading is HP) and (RS_loading is LP) and (Cabin_Blower is HP) and (FCI is VL) and (CSI is High) then (Electrical_Load is MH) (1)
373	If (HSW is HP) and (FS_loading is HP) and (RS_loading is LP) and (Cabin_Blower is HP) and (FCI is L) and (CSI is High) then (Electrical_Load is MH) (1)
374	If (HSW is HP) and (FS_loading is HP) and (RS_loading is LP) and (Cabin_Blower is HP) and (FCI is LM) and (CSI is High) then (Electrical_Load is MH) (1)
375	If (HSW is HP) and (FS_loading is HP) and (RS_loading is LP) and (Cabin_Blower is HP) and (FCI is M) and (CSI is High) then (Electrical_Load is MH) (1)
376	If (HSW is HP) and (FS_loading is HP) and (RS_loading is LP) and (Cabin_Blower is HP) and (FCI is MH) and (CSI is High) then (Electrical_Load is M) (1)
377	If (HSW is HP) and (FS_loading is HP) and (RS_loading is LP) and (Cabin_Blower is HP) and (FCI is H) and (CSI is High) then (Electrical_Load is M) (1)
378	If (HSW is HP) and (FS_loading is HP) and (RS_loading is LP) and (Cabin_Blower is HP) and (FCI is VH) and (CSI is High) then (Electrical_Load is M) (1)
379	If (HSW is LP) and (FS_loading is HP) and (RS_loading is HP) and (Cabin_Blower is LP) and (FCI is VL) and (CSI is Low) then (Electrical_Load is M) (1)
380	If (HSW is LP) and (FS_loading is HP) and (RS_loading is HP) and (Cabin_Blower is LP) and (FCI is L) and (CSI is Low) then (Electrical_Load is M) (1)
381	If (HSW is LP) and (FS_loading is HP) and (RS_loading is HP) and (Cabin_Blower is LP) and (FCI is LM) and (CSI is Low) then (Electrical_Load is M) (1)
382	If (HSW is LP) and (FS_loading is HP) and (RS_loading is HP) and (Cabin_Blower is LP) and (FCI is M) and (CSI is Low) then (Electrical_Load is L) (1)
383	If (HSW is LP) and (FS_loading is HP) and (RS_loading is HP) and (Cabin_Blower is LP) and (FCI is MH) and (CSI is Low) then (Electrical_Load is L) (1)
384	If (HSW is LP) and (FS_loading is HP) and (RS_loading is HP) and (Cabin_Blower is LP) and (FCI is H) and (CSI is Low) then (Electrical_Load is VL) (1)
385	If (HSW is LP) and (FS_loading is HP) and (RS_loading is HP) and (Cabin_Blower is LP) and (FCI is VH) and (CSI is Low) then (Electrical_Load is VL) (1)
386	If (HSW is LP) and (FS_loading is HP) and (RS_loading is HP) and (Cabin_Blower is MP) and (FCI is VL) and (CSI is Low) then (Electrical_Load is M) (1)
387	If (HSW is LP) and (FS_loading is HP) and (RS_loading is HP) and (Cabin_Blower is MP) and (FCI is L) and (CSI is Low) then (Electrical_Load is M) (1)
388	If (HSW is LP) and (FS_loading is HP) and (RS_loading is HP) and (Cabin_Blower is MP) and (FCI is LM) and (CSI is Low) then (Electrical_Load is M) (1)
389	If (HSW is LP) and (FS_loading is HP) and (RS_loading is HP) and (Cabin_Blower is MP) and (FCI is M) and (CSI is Low) then (Electrical_Load is L) (1)
390	If (HSW is LP) and (FS_loading is HP) and (RS_loading is HP) and (Cabin_Blower is MP) and (FCI is MH) and (CSI is Low) then (Electrical_Load is L) (1)
391	If (HSW is LP) and (FS_loading is HP) and (RS_loading is HP) and (Cabin_Blower is MP) and (FCI is H) and (CSI is Low) then (Electrical_Load is VL) (1)
392	If (HSW is LP) and (FS_loading is HP) and (RS_loading is HP) and (Cabin_Blower is MP) and (FCI is VH) and (CSI is Low) then (Electrical_Load is VL) (1)
393	If (HSW is LP) and (FS_loading is HP) and (RS_loading is HP) and (Cabin_Blower is HP) and (FCI is VL) and (CSI is Low) then (Electrical_Load is MH) (1)
394	If (HSW is LP) and (FS_loading is HP) and (RS_loading is HP) and (Cabin_Blower is HP) and (FCI is L) and (CSI is Low) then (Electrical_Load is MH) (1)
395	If (HSW is LP) and (FS_loading is HP) and (RS_loading is HP) and (Cabin_Blower is HP) and (FCI is LM) and (CSI is Low) then (Electrical_Load is M) (1)
396	If (HSW is LP) and (FS_loading is HP) and (RS_loading is HP) and (Cabin_Blower is HP) and (FCI is M) and (CSI is Low) then (Electrical_Load is M) (1)
397	If (HSW is LP) and (FS_loading is HP) and (RS_loading is HP) and (Cabin_Blower is HP) and (FCI is MH) and (CSI is Low) then (Electrical_Load is L) (1)
398	If (HSW is LP) and (FS_loading is HP) and (RS_loading is HP) and (Cabin_Blower is HP) and (FCI is H) and (CSI is Low) then (Electrical_Load is L) (1)
399	If (HSW is LP) and (FS_loading is HP) and (RS_loading is HP) and (Cabin_Blower is HP) and (FCI is VH) and (CSI is Low) then (Electrical_Load is VL) (1)
400	If (HSW is LP) and (FS_loading is HP) and (RS_loading is HP) and (Cabin_Blower is LP) and (FCI is VL) and (CSI is Normal) then (Electrical_Load is M) (1)
401	If (HSW is LP) and (FS_loading is HP) and (RS_loading is HP) and (Cabin_Blower is LP) and (FCI is L) and (CSI is Normal) then (Electrical_Load is M) (1)
402	If (HSW is LP) and (FS_loading is HP) and (RS_loading is HP) and (Cabin_Blower is LP) and (FCI is LM) and (CSI is Normal) then (Electrical_Load is M) (1)
403	If (HSW is LP) and (FS_loading is HP) and (RS_loading is HP) and (Cabin_Blower is LP) and (FCI is M) and (CSI is Normal) then (Electrical_Load is M) (1)
404	If (HSW is LP) and (FS_loading is HP) and (RS_loading is HP) and (Cabin_Blower is LP) and (FCI is MH) and (CSI is Normal) then (Electrical_Load is L) (1)
405	If (HSW is LP) and (FS_loading is HP) and (RS_loading is HP) and (Cabin_Blower is LP) and (FCI is H) and (CSI is Normal) then (Electrical_Load is L) (1)
406	If (HSW is LP) and (FS_loading is HP) and (RS_loading is HP) and (Cabin_Blower is LP) and (FCI is VH) and (CSI is Normal) then (Electrical_Load is VL) (1)
407	If (HSW is LP) and (FS_loading is HP) and (RS_loading is HP) and (Cabin_Blower is MP) and (FCI is VL) and (CSI is Normal) then (Electrical_Load is M) (1)
408	If (HSW is LP) and (FS_loading is HP) and (RS_loading is HP) and (Cabin_Blower is MP) and (FCI is L) and (CSI is Normal) then (Electrical_Load is M) (1)
409	If (HSW is LP) and (FS_loading is HP) and (RS_loading is HP) and (Cabin_Blower is MP) and (FCI is LM) and (CSI is Normal) then (Electrical_Load is M) (1)
410	If (HSW is LP) and (FS_loading is HP) and (RS_loading is HP) and (Cabin_Blower is MP) and (FCI is M) and (CSI is Normal) then (Electrical_Load is M) (1)

411	If (HSW is LP) and (FS_loading is HP) and (RS_loading is HP) and (Cabin_Blower is MP) and (FCI is MH) and (CSI is Normal) then (Electrical_Load is M) (1)
412	If (HSW is LP) and (FS_loading is HP) and (RS_loading is HP) and (Cabin_Blower is MP) and (FCI is H) and (CSI is Normal) then (Electrical_Load is L) (1)
413	If (HSW is LP) and (FS_loading is HP) and (RS_loading is HP) and (Cabin_Blower is MP) and (FCI is VH) and (CSI is Normal) then (Electrical_Load is VL) (1)
414	If (HSW is LP) and (FS_loading is HP) and (RS_loading is HP) and (Cabin_Blower is HP) and (FCI is VL) and (CSI is Normal) then (Electrical_Load is MH) (1)
415	If (HSW is LP) and (FS_loading is HP) and (RS_loading is HP) and (Cabin_Blower is HP) and (FCI is L) and (CSI is Normal) then (Electrical_Load is MH) (1)
416	If (HSW is LP) and (FS_loading is HP) and (RS_loading is HP) and (Cabin_Blower is HP) and (FCI is LM) and (CSI is Normal) then (Electrical_Load is MH) (1)
417	If (HSW is LP) and (FS_loading is HP) and (RS_loading is HP) and (Cabin_Blower is HP) and (FCI is M) and (CSI is Normal) then (Electrical_Load is MH) (1)
418	If (HSW is LP) and (FS_loading is HP) and (RS_loading is HP) and (Cabin_Blower is HP) and (FCI is MH) and (CSI is Normal) then (Electrical_Load is M) (1)
419	If (HSW is LP) and (FS_loading is HP) and (RS_loading is HP) and (Cabin_Blower is HP) and (FCI is H) and (CSI is Normal) then (Electrical_Load is M) (1)
420	If (HSW is LP) and (FS_loading is HP) and (RS_loading is HP) and (Cabin_Blower is HP) and (FCI is VH) and (CSI is Normal) then (Electrical_Load is L) (1)
421	If (HSW is LP) and (FS_loading is HP) and (RS_loading is HP) and (Cabin_Blower is LP) and (FCI is VL) and (CSI is High) then (Electrical_Load is MH) (1)
422	If (HSW is LP) and (FS_loading is HP) and (RS_loading is HP) and (Cabin_Blower is LP) and (FCI is L) and (CSI is High) then (Electrical_Load is M) (1)
423	If (HSW is LP) and (FS_loading is HP) and (RS_loading is HP) and (Cabin_Blower is LP) and (FCI is LM) and (CSI is High) then (Electrical_Load is M) (1)
424	If (HSW is LP) and (FS_loading is HP) and (RS_loading is HP) and (Cabin_Blower is LP) and (FCI is M) and (CSI is High) then (Electrical_Load is M) (1)
425	If (HSW is LP) and (FS_loading is HP) and (RS_loading is HP) and (Cabin_Blower is LP) and (FCI is MH) and (CSI is High) then (Electrical_Load is M) (1)
426	If (HSW is LP) and (FS_loading is HP) and (RS_loading is HP) and (Cabin_Blower is LP) and (FCI is H) and (CSI is High) then (Electrical_Load is L) (1)
427	If (HSW is LP) and (FS_loading is HP) and (RS_loading is HP) and (Cabin_Blower is LP) and (FCI is VH) and (CSI is High) then (Electrical_Load is L) (1)
428	If (HSW is LP) and (FS_loading is HP) and (RS_loading is HP) and (Cabin_Blower is MP) and (FCI is VL) and (CSI is High) then (Electrical_Load is MH) (1)
429	If (HSW is LP) and (FS_loading is HP) and (RS_loading is HP) and (Cabin_Blower is MP) and (FCI is L) and (CSI is High) then (Electrical_Load is MH) (1)
430	If (HSW is LP) and (FS_loading is HP) and (RS_loading is HP) and (Cabin_Blower is MP) and (FCI is LM) and (CSI is High) then (Electrical_Load is MH) (1)
431	If (HSW is LP) and (FS_loading is HP) and (RS_loading is HP) and (Cabin_Blower is MP) and (FCI is M) and (CSI is High) then (Electrical_Load is MH) (1)
432	If (HSW is LP) and (FS_loading is HP) and (RS_loading is HP) and (Cabin_Blower is MP) and (FCI is MH) and (CSI is High) then (Electrical_Load is M) (1)
433	If (HSW is LP) and (FS_loading is HP) and (RS_loading is HP) and (Cabin_Blower is MP) and (FCI is H) and (CSI is High) then (Electrical_Load is M) (1)
434	If (HSW is LP) and (FS_loading is HP) and (RS_loading is HP) and (Cabin_Blower is MP) and (FCI is VH) and (CSI is High) then (Electrical_Load is L) (1)
435	If (HSW is LP) and (FS_loading is HP) and (RS_loading is HP) and (Cabin_Blower is HP) and (FCI is VL) and (CSI is High) then (Electrical_Load is H) (1)
436	If (HSW is LP) and (FS_loading is HP) and (RS_loading is HP) and (Cabin_Blower is HP) and (FCI is L) and (CSI is High) then (Electrical_Load is H) (1)
437	If (HSW is LP) and (FS_loading is HP) and (RS_loading is HP) and (Cabin_Blower is HP) and (FCI is LM) and (CSI is High) then (Electrical_Load is MH) (1)
438	If (HSW is LP) and (FS_loading is HP) and (RS_loading is HP) and (Cabin_Blower is HP) and (FCI is M) and (CSI is High) then (Electrical_Load is MH) (1)
439	If (HSW is LP) and (FS_loading is HP) and (RS_loading is HP) and (Cabin_Blower is HP) and (FCI is MH) and (CSI is High) then (Electrical_Load is MH) (1)
440	If (HSW is LP) and (FS_loading is HP) and (RS_loading is HP) and (Cabin_Blower is HP) and (FCI is H) and (CSI is High) then (Electrical_Load is M) (1)
441	If (HSW is LP) and (FS_loading is HP) and (RS_loading is HP) and (Cabin_Blower is HP) and (FCI is VH) and (CSI is High) then (Electrical_Load is M) (1)
442	If (HSW is HP) and (FS_loading is LP) and (RS_loading is HP) and (Cabin_Blower is LP) and (FCI is VL) and (CSI is Low) then (Electrical_Load is L) (1)
443	If (HSW is HP) and (FS_loading is LP) and (RS_loading is HP) and (Cabin_Blower is LP) and (FCI is L) and (CSI is Low) then (Electrical_Load is L) (1)
444	If (HSW is HP) and (FS_loading is LP) and (RS_loading is HP) and (Cabin_Blower is LP) and (FCI is LM) and (CSI is Low) then (Electrical_Load is VL) (1)
445	If (HSW is HP) and (FS_loading is LP) and (RS_loading is HP) and (Cabin_Blower is LP) and (FCI is M) and (CSI is Low) then (Electrical_Load is VL) (1)
446	If (HSW is HP) and (FS_loading is LP) and (RS_loading is HP) and (Cabin_Blower is LP) and (FCI is MH) and (CSI is Low) then (Electrical_Load is VL) (1)
447	If (HSW is HP) and (FS_loading is LP) and (RS_loading is HP) and (Cabin_Blower is LP) and (FCI is H) and (CSI is Low) then (Electrical_Load is VL) (1)
448	If (HSW is HP) and (FS_loading is LP) and (RS_loading is HP) and (Cabin_Blower is LP) and (FCI is VH) and (CSI is Low) then (Electrical_Load is VL) (1)
449	If (HSW is HP) and (FS_loading is LP) and (RS_loading is HP) and (Cabin_Blower is MP) and (FCI is VL) and (CSI is Low) then (Electrical_Load is M) (1)
450	If (HSW is HP) and (FS_loading is LP) and (RS_loading is HP) and (Cabin_Blower is MP) and (FCI is L) and (CSI is Low) then (Electrical_Load is M) (1)
451	If (HSW is HP) and (FS_loading is LP) and (RS_loading is HP) and (Cabin_Blower is MP) and (FCI is LM) and (CSI is Low) then (Electrical_Load is L) (1)
452	If (HSW is HP) and (FS_loading is LP) and (RS_loading is HP) and (Cabin_Blower is MP) and (FCI is M) and (CSI is Low) then (Electrical_Load is L) (1)

453	If (HSW is HP) and (FS_loading is LP) and (RS_loading is HP) and (Cabin_Blower is MP) and (FCI is MH) and (CSI is Low) then (Electrical_Load is VL) (1)
454	If (HSW is HP) and (FS_loading is LP) and (RS_loading is HP) and (Cabin_Blower is MP) and (FCI is H) and (CSI is Low) then (Electrical_Load is VL) (1)
455	If (HSW is HP) and (FS_loading is LP) and (RS_loading is HP) and (Cabin_Blower is MP) and (FCI is VH) and (CSI is Low) then (Electrical_Load is VL) (1)
456	If (HSW is HP) and (FS_loading is LP) and (RS_loading is HP) and (Cabin_Blower is HP) and (FCI is VL) and (CSI is Low) then (Electrical_Load is MH) (1)
457	If (HSW is HP) and (FS_loading is LP) and (RS_loading is HP) and (Cabin_Blower is HP) and (FCI is L) and (CSI is Low) then (Electrical_Load is MH) (1)
458	If (HSW is HP) and (FS_loading is LP) and (RS_loading is HP) and (Cabin_Blower is HP) and (FCI is LM) and (CSI is Low) then (Electrical_Load is M) (1)
459	If (HSW is HP) and (FS_loading is LP) and (RS_loading is HP) and (Cabin_Blower is HP) and (FCI is M) and (CSI is Low) then (Electrical_Load is L) (1)
460	If (HSW is HP) and (FS_loading is LP) and (RS_loading is HP) and (Cabin_Blower is HP) and (FCI is MH) and (CSI is Low) then (Electrical_Load is L) (1)
461	If (HSW is HP) and (FS_loading is LP) and (RS_loading is HP) and (Cabin_Blower is HP) and (FCI is H) and (CSI is Low) then (Electrical_Load is VL) (1)
462	If (HSW is HP) and (FS_loading is LP) and (RS_loading is HP) and (Cabin_Blower is HP) and (FCI is VH) and (CSI is Low) then (Electrical_Load is VL) (1)
463	If (HSW is HP) and (FS_loading is LP) and (RS_loading is HP) and (Cabin_Blower is LP) and (FCI is VL) and (CSI is Normal) then (Electrical_Load is L) (1)
464	If (HSW is HP) and (FS_loading is LP) and (RS_loading is HP) and (Cabin_Blower is LP) and (FCI is L) and (CSI is Normal) then (Electrical_Load is L) (1)
465	If (HSW is HP) and (FS_loading is LP) and (RS_loading is HP) and (Cabin_Blower is LP) and (FCI is LM) and (CSI is Normal) then (Electrical_Load is L) (1)
466	If (HSW is HP) and (FS_loading is LP) and (RS_loading is HP) and (Cabin_Blower is LP) and (FCI is M) and (CSI is Normal) then (Electrical_Load is L) (1)
467	If (HSW is HP) and (FS_loading is LP) and (RS_loading is HP) and (Cabin_Blower is LP) and (FCI is MH) and (CSI is Normal) then (Electrical_Load is VL) (1)
468	If (HSW is HP) and (FS_loading is LP) and (RS_loading is HP) and (Cabin_Blower is LP) and (FCI is H) and (CSI is Normal) then (Electrical_Load is VL) (1)
469	If (HSW is HP) and (FS_loading is LP) and (RS_loading is HP) and (Cabin_Blower is LP) and (FCI is VH) and (CSI is Normal) then (Electrical_Load is VL) (1)
470	If (HSW is HP) and (FS_loading is LP) and (RS_loading is HP) and (Cabin_Blower is MP) and (FCI is VL) and (CSI is Normal) then (Electrical_Load is M) (1)
471	If (HSW is HP) and (FS_loading is LP) and (RS_loading is HP) and (Cabin_Blower is MP) and (FCI is L) and (CSI is Normal) then (Electrical_Load is M) (1)
472	If (HSW is HP) and (FS_loading is LP) and (RS_loading is HP) and (Cabin_Blower is MP) and (FCI is LM) and (CSI is Normal) then (Electrical_Load is M) (1)
473	If (HSW is HP) and (FS_loading is LP) and (RS_loading is HP) and (Cabin_Blower is MP) and (FCI is M) and (CSI is Normal) then (Electrical_Load is L) (1)
474	If (HSW is HP) and (FS_loading is LP) and (RS_loading is HP) and (Cabin_Blower is MP) and (FCI is MH) and (CSI is Normal) then (Electrical_Load is L) (1)
475	If (HSW is HP) and (FS_loading is LP) and (RS_loading is HP) and (Cabin_Blower is MP) and (FCI is H) and (CSI is Normal) then (Electrical_Load is VL) (1)
476	If (HSW is HP) and (FS_loading is LP) and (RS_loading is HP) and (Cabin_Blower is MP) and (FCI is VH) and (CSI is Normal) then (Electrical_Load is VL) (1)
477	If (HSW is HP) and (FS_loading is LP) and (RS_loading is HP) and (Cabin_Blower is HP) and (FCI is VL) and (CSI is Normal) then (Electrical_Load is MH) (1)
478	If (HSW is HP) and (FS_loading is LP) and (RS_loading is HP) and (Cabin_Blower is HP) and (FCI is L) and (CSI is Normal) then (Electrical_Load is MH) (1)
479	If (HSW is HP) and (FS_loading is LP) and (RS_loading is HP) and (Cabin_Blower is HP) and (FCI is LM) and (CSI is Normal) then (Electrical_Load is MH) (1)
480	If (HSW is HP) and (FS_loading is LP) and (RS_loading is HP) and (Cabin_Blower is HP) and (FCI is M) and (CSI is Normal) then (Electrical_Load is M) (1)
481	If (HSW is HP) and (FS_loading is LP) and (RS_loading is HP) and (Cabin_Blower is HP) and (FCI is MH) and (CSI is Normal) then (Electrical_Load is L) (1)
482	If (HSW is HP) and (FS_loading is LP) and (RS_loading is HP) and (Cabin_Blower is HP) and (FCI is H) and (CSI is Normal) then (Electrical_Load is VL) (1)
483	If (HSW is HP) and (FS_loading is LP) and (RS_loading is HP) and (Cabin_Blower is HP) and (FCI is VH) and (CSI is Normal) then (Electrical_Load is VL) (1)
484	If (HSW is HP) and (FS_loading is LP) and (RS_loading is HP) and (Cabin_Blower is LP) and (FCI is VL) and (CSI is High) then (Electrical_Load is L) (1)
485	If (HSW is HP) and (FS_loading is LP) and (RS_loading is HP) and (Cabin_Blower is LP) and (FCI is L) and (CSI is High) then (Electrical_Load is L) (1)
486	If (HSW is HP) and (FS_loading is LP) and (RS_loading is HP) and (Cabin_Blower is LP) and (FCI is LM) and (CSI is High) then (Electrical_Load is L) (1)
487	If (HSW is HP) and (FS_loading is LP) and (RS_loading is HP) and (Cabin_Blower is LP) and (FCI is M) and (CSI is High) then (Electrical_Load is L) (1)
488	If (HSW is HP) and (FS_loading is LP) and (RS_loading is HP) and (Cabin_Blower is LP) and (FCI is MH) and (CSI is High) then (Electrical_Load is L) (1)
489	If (HSW is HP) and (FS_loading is LP) and (RS_loading is HP) and (Cabin_Blower is LP) and (FCI is H) and (CSI is High) then (Electrical_Load is L) (1)
490	If (HSW is HP) and (FS_loading is LP) and (RS_loading is HP) and (Cabin_Blower is LP) and (FCI is VH) and (CSI is High) then (Electrical_Load is VL) (1)
491	If (HSW is HP) and (FS_loading is LP) and (RS_loading is HP) and (Cabin_Blower is MP) and (FCI is VL) and (CSI is High) then (Electrical_Load is M) (1)
492	If (HSW is HP) and (FS_loading is LP) and (RS_loading is HP) and (Cabin_Blower is MP) and (FCI is L) and (CSI is High) then (Electrical_Load is M) (1)
493	If (HSW is HP) and (FS_loading is LP) and (RS_loading is HP) and (Cabin_Blower is MP) and (FCI is LM) and (CSI is High) then (Electrical_Load is M) (1)
494	If (HSW is HP) and (FS_loading is LP) and (RS_loading is HP) and (Cabin_Blower is MP) and (FCI is M) and (CSI is High) then (Electrical_Load is M) (1)

495	If (HSW is HP) and (FS_loading is LP) and (RS_loading is HP) and (Cabin_Blower is MP) and (FCI is MH) and (CSI is High) then (Electrical_Load is L) (1)
496	If (HSW is HP) and (FS_loading is LP) and (RS_loading is HP) and (Cabin_Blower is MP) and (FCI is H) and (CSI is High) then (Electrical_Load is L) (1)
497	If (HSW is HP) and (FS_loading is LP) and (RS_loading is HP) and (Cabin_Blower is MP) and (FCI is VH) and (CSI is High) then (Electrical_Load is VL) (1)
498	If (HSW is HP) and (FS_loading is LP) and (RS_loading is HP) and (Cabin_Blower is HP) and (FCI is VL) and (CSI is High) then (Electrical_Load is MH) (1)
499	If (HSW is HP) and (FS_loading is LP) and (RS_loading is HP) and (Cabin_Blower is HP) and (FCI is L) and (CSI is High) then (Electrical_Load is MH) (1)
500	If (HSW is HP) and (FS_loading is LP) and (RS_loading is HP) and (Cabin_Blower is HP) and (FCI is LM) and (CSI is High) then (Electrical_Load is MH) (1)
501	If (HSW is HP) and (FS_loading is LP) and (RS_loading is HP) and (Cabin_Blower is HP) and (FCI is M) and (CSI is High) then (Electrical_Load is M) (1)
502	If (HSW is HP) and (FS_loading is LP) and (RS_loading is HP) and (Cabin_Blower is HP) and (FCI is MH) and (CSI is High) then (Electrical_Load is L) (1)
503	If (HSW is HP) and (FS_loading is LP) and (RS_loading is HP) and (Cabin_Blower is HP) and (FCI is H) and (CSI is High) then (Electrical_Load is L) (1)
504	If (HSW is HP) and (FS_loading is LP) and (RS_loading is HP) and (Cabin_Blower is HP) and (FCI is VH) and (CSI is High) then (Electrical_Load is L) (1)

Table F.1. Rule base for Fuzzy_*Cabin* controller

No. Rules	Rule Base for Fuzzy PMS Glazing 4
1	If (HFS is LP) and (HRW is LP) and (HRM is LP) and (HWP is LP) and (FCI is VL) then (Electrical_Load is VVL) (1)
2	If (HFS is LP) and (HRW is LP) and (HRM is LP) and (HWP is LP) and (FCI is L) then (Electrical_Load is VVL) (1)
3	If (HFS is LP) and (HRW is LP) and (HRM is LP) and (HWP is LP) and (FCI is LM) then (Electrical_Load is VVL) (1)
4	If (HFS is LP) and (HRW is LP) and (HRM is LP) and (HWP is LP) and (FCI is M) then (Electrical_Load is VVL) (1)
5	If (HFS is LP) and (HRW is LP) and (HRM is LP) and (HWP is LP) and (FCI is MH) then (Electrical_Load is VVL) (1)
6	If (HFS is LP) and (HRW is LP) and (HRM is LP) and (HWP is LP) and (FCI is H) then (Electrical_Load is VVL) (1)
7	If (HFS is LP) and (HRW is LP) and (HRM is LP) and (HWP is LP) and (FCI is VH) then (Electrical_Load is VVL) (1)
8	If (HFS is HP) and (HRW is HP) and (HRM is HP) and (HWP is HP) and (FCI is VL) then (Electrical_Load is MH) (1)
9	If (HFS is HP) and (HRW is HP) and (HRM is HP) and (HWP is HP) and (FCI is L) then (Electrical_Load is MH) (1)
10	If (HFS is HP) and (HRW is HP) and (HRM is HP) and (HWP is HP) and (FCI is LM) then (Electrical_Load is MH) (1)
11	If (HFS is HP) and (HRW is HP) and (HRM is HP) and (HWP is HP) and (FCI is M) then (Electrical_Load is M) (1)
12	If (HFS is HP) and (HRW is HP) and (HRM is HP) and (HWP is HP) and (FCI is MH) then (Electrical_Load is M) (1)
13	If (HFS is HP) and (HRW is HP) and (HRM is HP) and (HWP is HP) and (FCI is H) then (Electrical_Load is L) (1)
14	If (HFS is HP) and (HRW is HP) and (HRM is HP) and (HWP is HP) and (FCI is VH) then (Electrical_Load is L) (1)
15	If (HFS is HP) and (HRW is LP) and (HRM is LP) and (HWP is LP) and (FCI is VL) then (Electrical_Load is MH) (1)
16	If (HFS is HP) and (HRW is LP) and (HRM is LP) and (HWP is LP) and (FCI is L) then (Electrical_Load is MH) (1)
17	If (HFS is HP) and (HRW is LP) and (HRM is LP) and (HWP is LP) and (FCI is LM) then (Electrical_Load is MH) (1)
18	If (HFS is HP) and (HRW is LP) and (HRM is LP) and (HWP is LP) and (FCI is M) then (Electrical_Load is M) (1)
19	If (HFS is HP) and (HRW is LP) and (HRM is LP) and (HWP is LP) and (FCI is MH) then (Electrical_Load is M) (1)
20	If (HFS is HP) and (HRW is LP) and (HRM is LP) and (HWP is LP) and (FCI is H) then (Electrical_Load is L) (1)
21	If (HFS is HP) and (HRW is LP) and (HRM is LP) and (HWP is LP) and (FCI is VH) then (Electrical_Load is L) (1)
22	If (HFS is HP) and (HRW is HP) and (HRM is LP) and (HWP is LP) and (FCI is VL) then (Electrical_Load is M) (1)
23	If (HFS is HP) and (HRW is HP) and (HRM is LP) and (HWP is LP) and (FCI is L) then (Electrical_Load is M) (1)
24	If (HFS is HP) and (HRW is HP) and (HRM is LP) and (HWP is LP) and (FCI is LM) then (Electrical_Load is M) (1)
25	If (HFS is HP) and (HRW is HP) and (HRM is LP) and (HWP is LP) and (FCI is M) then (Electrical_Load is L) (1)
26	If (HFS is HP) and (HRW is HP) and (HRM is LP) and (HWP is LP) and (FCI is MH) then (Electrical_Load is L) (1)
27	If (HFS is HP) and (HRW is HP) and (HRM is LP) and (HWP is LP) and (FCI is H) then (Electrical_Load is L) (1)
28	If (HFS is HP) and (HRW is HP) and (HRM is LP) and (HWP is LP) and (FCI is VH) then (Electrical_Load is L) (1)
29	If (HFS is HP) and (HRW is HP) and (HRM is HP) and (HWP is LP) and (FCI is VL) then (Electrical_Load is MH) (1)
30	If (HFS is HP) and (HRW is HP) and (HRM is HP) and (HWP is LP) and (FCI is L) then (Electrical_Load is MH) (1)
31	If (HFS is HP) and (HRW is HP) and (HRM is HP) and (HWP is LP) and (FCI is LM) then (Electrical_Load is M) (1)
32	If (HFS is HP) and (HRW is HP) and (HRM is HP) and (HWP is LP) and (FCI is M) then (Electrical_Load is M) (1)
33	If (HFS is HP) and (HRW is HP) and (HRM is HP) and (HWP is LP) and (FCI is MH) then (Electrical_Load is M) (1)
34	If (HFS is HP) and (HRW is HP) and (HRM is HP) and (HWP is LP) and (FCI is H) then (Electrical_Load is L) (1)
35	If (HFS is HP) and (HRW is HP) and (HRM is HP) and (HWP is LP) and (FCI is VH) then (Electrical_Load is L) (1)
36	If (HFS is LP) and (HRW is HP) and (HRM is LP) and (HWP is LP) and (FCI is VL) then (Electrical_Load is L) (1)
37	If (HFS is LP) and (HRW is HP) and (HRM is LP) and (HWP is LP) and (FCI is L) then (Electrical_Load is L) (1)
38	If (HFS is LP) and (HRW is HP) and (HRM is LP) and (HWP is LP) and (FCI is LM) then (Electrical_Load is VL) (1)
39	If (HFS is LP) and (HRW is HP) and (HRM is LP) and (HWP is LP) and (FCI is M) then (Electrical_Load is VL) (1)
40	If (HFS is LP) and (HRW is HP) and (HRM is LP) and (HWP is LP) and (FCI is MH) then (Electrical_Load is VL) (1)
41	If (HFS is LP) and (HRW is HP) and (HRM is LP) and (HWP is LP) and (FCI is H) then (Electrical_Load is VL) (1)
42	If (HFS is LP) and (HRW is HP) and (HRM is LP) and (HWP is LP) and (FCI is VH) then (Electrical_Load is VL) (1)
43	If (HFS is LP) and (HRW is HP) and (HRM is HP) and (HWP is LP) and (FCI is VL) then (Electrical_Load is L) (1)
44	If (HFS is LP) and (HRW is HP) and (HRM is HP) and (HWP is LP) and (FCI is L) then (Electrical_Load is L) (1)
45	If (HFS is LP) and (HRW is HP) and (HRM is HP) and (HWP is LP) and (FCI is LM) then (Electrical_Load is L) (1)
46	If (HFS is LP) and (HRW is HP) and (HRM is HP) and (HWP is LP) and (FCI is M) then (Electrical_Load is L) (1)
47	If (HFS is LP) and (HRW is HP) and (HRM is HP) and (HWP is LP) and (FCI is MH) then (Electrical_Load is VL) (1)

48	If (HFS is LP) and (HRW is HP) and (HRM is HP) and (HWP is LP) and (FCI is H) then (Electrical_Load is VL) (1)
49	If (HFS is LP) and (HRW is HP) and (HRM is HP) and (HWP is LP) and (FCI is VH) then (Electrical_Load is VL) (1)
50	If (HFS is LP) and (HRW is HP) and (HRM is HP) and (HWP is HP) and (FCI is VL) then (Electrical_Load is M) (1)
51	If (HFS is LP) and (HRW is HP) and (HRM is HP) and (HWP is HP) and (FCI is L) then (Electrical_Load is M) (1)
52	If (HFS is LP) and (HRW is HP) and (HRM is HP) and (HWP is HP) and (FCI is LM) then (Electrical_Load is L) (1)
53	If (HFS is LP) and (HRW is HP) and (HRM is HP) and (HWP is HP) and (FCI is M) then (Electrical_Load is L) (1)
54	If (HFS is LP) and (HRW is HP) and (HRM is HP) and (HWP is HP) and (FCI is MH) then (Electrical_Load is L) (1)
55	If (HFS is LP) and (HRW is HP) and (HRM is HP) and (HWP is HP) and (FCI is H) then (Electrical_Load is L) (1)
56	If (HFS is LP) and (HRW is HP) and (HRM is HP) and (HWP is HP) and (FCI is VH) then (Electrical_Load is L) (1)
57	If (HFS is LP) and (HRW is LP) and (HRM is HP) and (HWP is LP) and (FCI is VL) then (Electrical_Load is VL) (1)
58	If (HFS is LP) and (HRW is LP) and (HRM is HP) and (HWP is LP) and (FCI is L) then (Electrical_Load is VL) (1)
59	If (HFS is LP) and (HRW is LP) and (HRM is HP) and (HWP is LP) and (FCI is LM) then (Electrical_Load is VL) (1)
60	If (HFS is LP) and (HRW is LP) and (HRM is HP) and (HWP is LP) and (FCI is M) then (Electrical_Load is VL) (1)
61	If (HFS is LP) and (HRW is LP) and (HRM is HP) and (HWP is LP) and (FCI is MH) then (Electrical_Load is VL) (1)
62	If (HFS is LP) and (HRW is LP) and (HRM is HP) and (HWP is LP) and (FCI is H) then (Electrical_Load is VL) (1)
63	If (HFS is LP) and (HRW is LP) and (HRM is HP) and (HWP is LP) and (FCI is VH) then (Electrical_Load is VL) (1)
64	If (HFS is LP) and (HRW is LP) and (HRM is LP) and (HWP is HP) and (FCI is VL) then (Electrical_Load is VL) (1)
65	If (HFS is LP) and (HRW is LP) and (HRM is LP) and (HWP is HP) and (FCI is L) then (Electrical_Load is VL) (1)
66	If (HFS is LP) and (HRW is LP) and (HRM is LP) and (HWP is HP) and (FCI is LM) then (Electrical_Load is VL) (1)
67	If (HFS is LP) and (HRW is LP) and (HRM is LP) and (HWP is HP) and (FCI is M) then (Electrical_Load is VL) (1)
68	If (HFS is LP) and (HRW is LP) and (HRM is LP) and (HWP is HP) and (FCI is MH) then (Electrical_Load is VL) (1)
69	If (HFS is LP) and (HRW is LP) and (HRM is LP) and (HWP is HP) and (FCI is H) then (Electrical_Load is VL) (1)
70	If (HFS is LP) and (HRW is LP) and (HRM is LP) and (HWP is HP) and (FCI is VH) then (Electrical_Load is VL) (1)
71	If (HFS is HP) and (HRW is HP) and (HRM is LP) and (HWP is HP) and (FCI is VL) then (Electrical_Load is H) (1)
72	If (HFS is HP) and (HRW is HP) and (HRM is LP) and (HWP is HP) and (FCI is L) then (Electrical_Load is H) (1)
73	If (HFS is HP) and (HRW is HP) and (HRM is LP) and (HWP is HP) and (FCI is LM) then (Electrical_Load is MH) (1)
74	If (HFS is HP) and (HRW is HP) and (HRM is LP) and (HWP is HP) and (FCI is M) then (Electrical_Load is MH) (1)
75	If (HFS is HP) and (HRW is HP) and (HRM is LP) and (HWP is HP) and (FCI is MH) then (Electrical_Load is M) (1)
76	If (HFS is HP) and (HRW is HP) and (HRM is LP) and (HWP is HP) and (FCI is H) then (Electrical_Load is M) (1)
77	If (HFS is HP) and (HRW is HP) and (HRM is LP) and (HWP is HP) and (FCI is VH) then (Electrical_Load is L) (1)
78	If (HFS is HP) and (HRW is LP) and (HRM is HP) and (HWP is LP) and (FCI is VL) then (Electrical_Load is MH) (1)
79	If (HFS is HP) and (HRW is LP) and (HRM is HP) and (HWP is LP) and (FCI is L) then (Electrical_Load is MH) (1)
80	If (HFS is HP) and (HRW is LP) and (HRM is HP) and (HWP is LP) and (FCI is LM) then (Electrical_Load is M) (1)
81	If (HFS is HP) and (HRW is LP) and (HRM is HP) and (HWP is LP) and (FCI is M) then (Electrical_Load is M) (1)
82	If (HFS is HP) and (HRW is LP) and (HRM is HP) and (HWP is LP) and (FCI is MH) then (Electrical_Load is L) (1)
83	If (HFS is HP) and (HRW is LP) and (HRM is HP) and (HWP is LP) and (FCI is H) then (Electrical_Load is L) (1)
84	If (HFS is HP) and (HRW is LP) and (HRM is HP) and (HWP is LP) and (FCI is VH) then (Electrical_Load is VL) (1)
85	If (HFS is HP) and (HRW is LP) and (HRM is HP) and (HWP is HP) and (FCI is VL) then (Electrical_Load is MH) (1)
86	If (HFS is HP) and (HRW is LP) and (HRM is HP) and (HWP is HP) and (FCI is L) then (Electrical_Load is MH) (1)
87	If (HFS is HP) and (HRW is LP) and (HRM is HP) and (HWP is HP) and (FCI is LM) then (Electrical_Load is M) (1)
88	If (HFS is HP) and (HRW is LP) and (HRM is HP) and (HWP is HP) and (FCI is M) then (Electrical_Load is M) (1)
89	If (HFS is HP) and (HRW is LP) and (HRM is HP) and (HWP is HP) and (FCI is MH) then (Electrical_Load is L) (1)
90	If (HFS is HP) and (HRW is LP) and (HRM is HP) and (HWP is HP) and (FCI is H) then (Electrical_Load is L) (1)
91	If (HFS is HP) and (HRW is LP) and (HRM is HP) and (HWP is HP) and (FCI is VH) then (Electrical_Load is VL) (1)
92	If (HFS is HP) and (HRW is LP) and (HRM is LP) and (HWP is HP) and (FCI is VL) then (Electrical_Load is MH) (1)
93	If (HFS is HP) and (HRW is LP) and (HRM is LP) and (HWP is HP) and (FCI is L) then (Electrical_Load is MH) (1)
94	If (HFS is HP) and (HRW is LP) and (HRM is LP) and (HWP is HP) and (FCI is LM) then (Electrical_Load is M) (1)
95	If (HFS is HP) and (HRW is LP) and (HRM is LP) and (HWP is HP) and (FCI is M) then (Electrical_Load is M) (1)
96	If (HFS is HP) and (HRW is LP) and (HRM is LP) and (HWP is HP) and (FCI is MH) then (Electrical_Load is L) (1)
97	If (HFS is HP) and (HRW is LP) and (HRM is LP) and (HWP is HP) and (FCI is H) then (Electrical_Load is L) (1)
98	If (HFS is HP) and (HRW is LP) and (HRM is LP) and (HWP is HP) and (FCI is VH) then (Electrical_Load is VL) (1)
99	If (HFS is LP) and (HRW is HP) and (HRM is LP) and (HWP is HP) and (FCI is VL) then (Electrical_Load is L) (1)
100	If (HFS is LP) and (HRW is HP) and (HRM is LP) and (HWP is HP) and (FCI is L) then (Electrical_Load is L) (1)
101	If (HFS is LP) and (HRW is HP) and (HRM is LP) and (HWP is HP) and (FCI is LM) then (Electrical_Load is L) (1)
102	If (HFS is LP) and (HRW is HP) and (HRM is LP) and (HWP is HP) and (FCI is M) then (Electrical_Load is L) (1)
103	If (HFS is LP) and (HRW is HP) and (HRM is LP) and (HWP is HP) and (FCI is MH) then (Electrical_Load is VL) (1)
104	If (HFS is LP) and (HRW is HP) and (HRM is LP) and (HWP is HP) and (FCI is H) then (Electrical_Load is VL) (1)
105	If (HFS is LP) and (HRW is HP) and (HRM is LP) and (HWP is HP) and (FCI is VH) then (Electrical_Load is VL) (1)
106	If (HFS is LP) and (HRW is LP) and (HRM is HP) and (HWP is HP) and (FCI is VL) then (Electrical_Load is L) (1)
107	If (HFS is LP) and (HRW is LP) and (HRM is HP) and (HWP is HP) and (FCI is L) then (Electrical_Load is L) (1)
108	If (HFS is LP) and (HRW is LP) and (HRM is HP) and (HWP is HP) and (FCI is LM) then (Electrical_Load is L) (1)
109	If (HFS is LP) and (HRW is LP) and (HRM is HP) and (HWP is HP) and (FCI is M) then (Electrical_Load is VL) (1)
110	If (HFS is LP) and (HRW is LP) and (HRM is HP) and (HWP is HP) and (FCI is MH) then (Electrical_Load is VL) (1)
111	If (HFS is LP) and (HRW is LP) and (HRM is HP) and (HWP is HP) and (FCI is H) then (Electrical_Load is VL) (1)
112	If (HFS is LP) and (HRW is LP) and (HRM is HP) and (HWP is HP) and (FCI is VH) then (Electrical_Load is VL) (1)

Table F.2. Rule base for Fuzzy_*Glazing* controller

Appendix G Low Emissions Vehicle experimental data

Alternator Loading (A)	Fuel (ml)	Distance (miles)	MPG (CAN)	MPG (Trip)	Avg MPG	Avg Speed (mph)	ml per km	g/km of CO2	g/km per Amp	Test conditions
71 3	3157 3125	22 3	32 109	31	31 554	39	87 97592	234 016	3 2821311	As per customer scenario
63 7	2471 75	23 1	42 486	42 9	42 693	38	66 48806	176 858	2 7764246	As per customer scenario
73 41	2684 4375	18 7	31 668	39 9	35 784	48	89 19958	237 271	3 232133	As per customer scenario
63 25	2847 375	22 5	35 923	37 3	36 612	39	78 63452	209 168	3 3070013	As per customer scenario
106	945 125	6 7	32 227	27 7	29 964	21	87 65275	233 156	2 199588	As per customer scenario
62 9	2724 25	22 1	36 879	28 7	32 79	30	76 59595	203 745	3 2391928	As per customer scenario
85 94	2649 875	21 9	37 571	38 8	38 186	50	75 1852	199 993	2 3271194	As per customer scenario
55	1969 4375	20 5	47 321	37 3	42 31	30	59 69521	158 789	2 8870772	As per customer scenario
75 6	2754	21 7	35 821	38	36 91	57	78 85974	209 767	2 7746944	As per customer scenario
55 2	2688 375	23 3	39 401	40 9	40 15	42	71 69437	190 707	3 4548373	As per customer scenario
69 23	2112 9375	16 2	34 855	35 9	35 378	31	81 04435	215 578	3 1139387	As per customer scenario
94 7	2425 0625	16 5	30 931	39	34 966	32 2	91 32509	242 925	2 5652031	As per customer scenario
72 3	2135 8125	16 1	34 269	36 2	35 234	32	82 43058	219 265	3 0327157	As per customer scenario
80 61	1781 625	13 1	33 427	45	39 213	39	84 50767	224 79	2 7886168	As per customer scenario
81 25	2595 8125	16 6	29 072	31	30 036	27	97 16645	258 463	3 1810802	As per customer scenario
88	1982 875	16 3	37 371	42 9	40 135	47	75 58904	201 067	2 2848506	As per customer scenario
85 3	2429 375	16 9	31 625	32 6	32 113	49	89 32211	237 597	2 7854257	As per customer scenario
51 1	2952 25	22 3	34 339	37	35 67	46	82 26202	218 817	4 2821327	As per customer scenario
70 1	2523 1875	21 5	38 737	40 2	39 469	50	72 92261	193 974	2 767106	As per customer scenario
88 1	3099 5	22 5	33 001	34 9	33 951	50	85 59733	227 689	2 5844371	As per customer scenario
71	2596 75	21 9	38 34	39 7	39 02	46	73 67788	195 983	2 7603263	As per customer scenario
74 1	2820 5625	23 5	37 877	39 5	38 688	42	74 57942	198 381	2 6772098	As per customer scenario
85 5	2989 875	22 6	34 363	34 7	34 532	47	82 20452	218 664	2 557474	As per customer scenario
93 1	3028 3125	22 8	34 227	34 8	34 514	45	82 53097	219 532	2 3580278	As per customer scenario
69	2500 875	21 3	38 719	39 9	39 31	42	72 95642	194 064	2 8125227	As per customer scenario
98	3284 375	22 6	31 282	33 3	32 291	52	90 30159	240 202	2 4510432	As per customer scenario
69 3	2920	22 6	35 186	36	35 593	48	80 28336	213 554	3 0815834	As per customer scenario
95 6	3470 9375	26 8	35 102	36 2	35 651	53	80 47539	214 065	2 2391689	As per customer scenario
82 9	2467 375	19 1	35 191	37 5	36 346	41	80 26993	213 518	2 5756095	As per customer scenario
88 8	2693 375	22 1	37 302	38 7	38 001	45	75 72786	201 436	2 2684245	As per customer scenario
99 79	2868	18 7	29 642	31 2	30 421	35	95 29907	253 496	2 5402898	As per customer scenario
72 6	2780 625	23 6	38 584	39 9	39 242	44	73 21188	194 744	2 6824186	As per customer scenario
90 4	3239 875	22 6	31 712	32 9	32 306	51	89 0781	236 948	2 6211033	As per customer scenario
107 86	3298 1875	29	39 972	39 972	39 972	45	70 66892	187 979	1 7428085	As per customer scenario
126 6	4095 25	29 7	32 97	29 6	31 285	40	85 67914	227 907	1 8002094	As per customer scenario
72 5	2125 4375	18 2	38 928	39 9	39 414	46	72 56514	193 023	2 6623901	As per customer scenario
69 2	9851 4	71 6	33 041	34 2	33 621	49	85 49408	227 414	3 2863332	As per customer scenario
89 8	3185 6875	21 9	31 252	31 252	31 252	39	90 38787	240 432	2 6774136	As per customer scenario
85 3	2612 875	21 9	38 103	40 1	39 102	51	74 1354	197 2	2 3118425	As per customer scenario
85 6	2886	20 7	32 607	40 2	36 404	57	86 63175	230 44	2 6920614	As per customer scenario
83 65	2506 5625	22 6	40 989	41 6	41 295	43	68 91618	183 317	2 1914769	As per customer scenario
70 3	3393 5	22 5	30 142	31 4	30 771	24	93 71658	249 286	3 5460329	As per customer scenario
74 8	2861 9375	23 7	37 647	39 1	38 373	50	75 03483	199 593	2 668351	As per customer scenario
99 39	3305 5625	22 6	31 081	32 2	31 641	49	90 88413	241 752	2 4323552	As per customer scenario
46 3	2862 0625	22 3	35 421	36 4	35 911	53	79 74902	212 132	4 5816933	As per customer scenario
81 2	3280 25	22 4	31 044	32 1	31 572	51	90 99343	242 043	2 9808193	As per customer scenario
83 48	2512 75	23 1	41 793	37 9	39 846	34	67 59093	179 792	2 1537119	As per customer scenario
81 2	3153 5625	22 6	32 58	33 7	33 14	43	86 705	230 635	2 840336	As per customer scenario
45 44	1896 375	17 1	40 993	37 8	39 397	35 2	68 90952	183 299	4 033876	As per customer scenario
93 96	3274 4375	22 6	31 377	33 2	32 288	49	90 02837	239 475	2 5486958	As per customer scenario

Alternator Loading (A)	Fuel (ml)	Distance (miles)	MPG (CAN)	MPG (Trip)	Avg MPG	Avg Speed (mph)	ml per km	g/km of CO2	g/km per Amp	Test conditions
37 21	2642 875	21 5	36 983	38 4	37 691	52	76 38169	203 175	5 4602339	Alternator Loading low
98 18	3144 625	22 6	32 672	33 8	33 236	49	86 45926	229 982	2 342449	As per customer scenario
69 2	2537 75	22	39 411	40 4	39 905	51	71 67658	190 66	2 755198	As per customer scenario
109 4	2892 8125	22 6	35 516	34 5	35 008	51	79 53586	211 565	1 93387	As per customer scenario
6	2408 25	22 1	41 719	42 16	41 939	45	67 71118	180 112	30 018625	Alternator OFF,AC ON+minimum blower
92 35	3202 375	22 6	32 083	33 3	32 691	52	88 04706	234 205	2 5360604	As per customer scenario
6	2627 25	21 6	37 376	39 1	38 238	44	75 57859	201 039	33 506507	Alternator OFF,AC ON+minimum blower
77 9	3282 6875	22 6	31 298	32 5	31 899		90 2552	240 079	3 0818848	As per customer scenario
6	2401 8125	21 4	40 505	42 1	41 303	48	69 73912	185 506	30 917675	Alternator OFF,AC ON+minimum blower
106 6	3154 3125	22 6	32 572	33 8	33 186	46	86 72562	230 69	2 1640726	As per customer scenario
6	2602 3125	21 6	37 734	39 1	38 417	54	74 8612	199 131	33 188467	Alternator OFF,AC ON+minimum blower
92 8	3025 125	22 6	33 963	35 3	34 631	52	83 1737	221 242	2 3840736	As per customer scenario
59 7	2613 125	21 8	37 926	39 4	38 663	42	74 4826	198 124	3 318655	Alternator Loading Low Lights and AC on Auto
55	2837 1875	21 8	34 931	36 4	35 665	55	80 86911	215 112	3 9111242	Alternator Loading Low Lights and AC on Auto
6	2536 0625	22 6	40 512	41 8	41 156	65	69 72726	185 475	30 912421	Alternator OFF,AC ON+minimum blower
52	2955	22 3	34 307	36 5	35 404	47	82 33865	219 021	4 2119386	Failed
45	2352 4375	19 2	37 104	38 5	37 802	43	76 13213	202 511	4 5002548	As per customer scenario
83	3740 0625	29 7	36 101	37 5	36 8	37	78 24805	208 14	2 5077086	As per customer scenario
88 8	3147 1875	21 9	31 634	35 8	33 717	55	89 29551	237 526	2 674843	As per customer scenario
46 98	2418 125	19 7	37 036	39 4	38 218	37	76 27174	202 883	4 3184934	As per customer scenario
57 3	2658	22 2	37 97	38 6	38 285	50	74 3966	197 895	3 4536644	As per customer scenario
84 5	2997 5	22 6	34 276	35	34 638	50	82 41417	219 222	2 5943394	As per customer scenario
34 8	2716	21 9	36 657	38 2	37 428	51	77 06138	204 983	5 8903237	As per customer scenario
68 9	2900	22 3	34 958		17 479		80 80612	214 944	3 1196557	As per customer scenario
52 1	2950	22 6	34 828	47	40 914	46	81 10819	215 748	4 1410322	As per customer scenario
18	3102	22 6	33 121	34 4	33 761	52	85 28732	226 864	12 603571	Alternator OFF after 4 min
6	2680 3125	22 1	37 484	38 2	37 842	56	75 36059	200 459	33 40986	Alternator OFF,AC ON+minimum blower
80 4	3273 5625	22	30 552	33 1	31 826	27	92 45897	245 941	3 0589661	Heavy traffic
56	1708 3125	16 4	43 643	44 8	44 222	34	64 72538	172 17	3 0744554	16miles journey only
87 04	2889 375	22 6	35 558	36 4	35 979	46	79 44134	211 314	2 4277801	As per customer scenario
85 6	3081 125	22 6	33 346	34 5	33 923	49	84 71338	225 338	2 6324484	As per customer scenario
82 5	3371 5	22 6	30 474	32 2	31 337	38	92 69703	246 574	2 9887771	As per customer scenario
50	2765 5	22 1	36 329	37	36 665	40	77 75575	206 83	4 1366058	As per customer scenario
38	2886	22	34 655	37 4	36 027	52	81 5126	216 824	5 7058822	As per customer scenario
40 1	2531	22 1	39 695	41 5	40 598	50	71 16247	189 292	4 7205027	As per customer scenario
75 7	3224	22 6	31 868	33 3	32 584	39	88 64162	235 787	3 1147519	As per customer scenario
38 8	2520	21 8	39 327	41 1	40 214	44	71 82823	191 063	4 9243065	As per customer scenario
9	2423	22 1	41 465	43 4	42 432	48	68 1259	181 215	20 134988	Alternator OFF, AC OFF
55 7	3100	22 6	33 142	34 5	33 821	52	85 23233	226 718	4 0703412	As per customer scenario
6	2314	22 1	43 418	44 1	43 759	41	65 06122	173 063	28 843807	Alternator OFF, AC OFF
51 5	2950	22 6	34 828	47 1	40 964	47	81 10819	215 748	4 1892772	AC OFF, Base load
7 4	2228 5	20 5	41 82	45 7	43 76	49	67 5476	179 677	24 280622	AC OFF
95 8	2800 6	22 6	36 686	38 4	37 543	54	77 00054	204 821	2 1380108	AC ON, Base Load
8 73	2453	20 9	38 734	42 2	40 467	48	72 92936	193 992	22 221316	Alternator OFF,AC OFF
60	3021	22 6	34 009	35 6	34 805	36	83 06028	220 94	3 6823392	As per customer scenario
10	2477	21 8	40 01	41 8	40 905	40	70 60259	187 803	18 780289	Alternator OFF,AC OFF
78 7	2890	22 6	35 551	37 2	36 375	51	79 45853	211 36	2 6856377	Cold climate loads
41 9	2346	21 3	41 275	43 1	42 188	47	68 43835	182 046	4 3447734	Base load, AC off
68 2	2920	22 1	34 407	35 3	34 854	48	82 09972	218 385	3 20213	As per customer scenario
60 7	3070	22 6	33 466	34 7	34 083	52	84 4075	224 524	3 698912	As per customer scenario
44 7	2927	22 6	35 101	36 3	35 701	44	80 47582	214 066	4 7889413	As per customer scenario
29 2	2720	22 1	36 937	39 5	38 219	39	76 47645	203 427	6 9666907	As per customer scenario
32 7	3472	22 6	29 592	32 1	30 846	44	95 46021	253 924	7 7652649	As per customer scenario
52 2	2892	22 1	34 74	38 8	36 77	55	81 31247	216 291	4 1435088	As per customer scenario
60 7	3140	22 6	32 72	33 9	33 31	44	86 3321	229 643	3 783252	As per customer scenario

Table G.3. Summary of real world fuel consumption under various loading levels